Increasing renewable energy penetration on LV networks using intelligent control of virtual power plants

LA Jansen

orcid.org/0000-0002-0961-2025

Dissertation accepted in fulfilment of the requirements for the degree *Master of Engineering in Electrical and Electronic Engineering* at the North-West University

Supervisor:	Dr MG Botha
Co-supervisor:	Prof G van Schoor
Co-supervisor:	Prof KR Uren

Graduation:	May 2022
Student number:	27064972

Abstract

The global rise in energy consumption has ushered in a new era of technological advancements dictating how energy is generated, distributed and utilised. The surge in the distributed energy resources (DER) penetration and the continuous strive towards a competitive energy market requires new policies and technologies to accommodate the emerging technical and economic hurdles generated by DER implementation. The management and intensification of DER on the national grid have brought forth the idea of a technical virtual power plant (T-VPP) which is utilised by various researchers. The T-VPP aggregates an array of SSEG units that can act as a single virtual generation unit. The VPP presents the opportunity to increase the renewable energy penetration on the grid while simultaneously providing ancillary services to the grid and controlling the network parameters to remain within the regulatory standards.

The aim of this study is to develop an intelligent VPP algorithm that will prove its implementation on South African LV residential networks not only supports the network but to also enhances the network's capabilities. The primary objective of this study is to safely increase the renewable energy penetration limit on an LV network irrespective of the network topology existent in South Africa. Numerous objectives have been identified as performance measures supporting the primary objective.

The literature has identified and highlighted the current regulatory control strategies incorporated into renewable energy technology and future energy management strategies. An LV network simulation model is developed in MATLAB Simulink® to simulate the effect of renewable energy on the network and the implementation of the various regulatory strategies. The model is verified to accurately represent the real-world system and mimics the necessary functionalities with the highest accuracy. The final control structure is developed, modelled, and finally verified by an iterative design process that analyses and improves on the various existing regulatory control structures. The exact control strategy is designed to achieve the set objectives and provide grounds on which the current regulatory specification needs to be adapted to pave the way for a more inclusive generation scheme.

The final T-VPP control architecture is implemented over a longer run time on the reference network and subsequently on a different network typology. The simulation data is then collected and compared to the reference control data to validate that the VPP control scheme is not implementation-specific and can be a generic energy management implementation.

The emphasis of this study lies in the importance of regulating vital network parameters to improve renewable energy utilisation and penetration in the national grid. The study also indicates how the renewable energy penetration can be improved if the incentive is in place for

prosumers to work together, improving grid stability and reducing the capital and operational expenditure of state-owned entities. This study also highlights the versatility that MATLAB and Simulink® provide in power system and control based simulations. The results indicate that intelligent VPP's have promising potential to set a precedent in how energy is generated, transmitted and consumed.

Keywords: Renewable energy, intelligent control, virtual power plant (VPP), small scale embedded generation(SSEG), energy aggregation.

Acknowledgements

I would firstly like to thank the Lord Almighty for giving me the strength and perseverance to finish my thesis during these trying times.

I would secondly like to thank Merseta for funding my research, and I would also like to thank Energy Supremacy Inc. for providing me with the necessary data for my experiments.

I would also like to acknowledge the following people for their contributions during my years of study.

- My supervisors Dr MG. Botha, Prof. G. van Schoor and Prof. K.R. Uren for their positivity, guidance and inputs. I would especially like to thank Dr Botha for proposing this study, taking me under his wing, and guiding me through this process.

- My partner, Andrea Fourie, for her unwavering love and support throughout the study.

- My parents (Frik and Elize Jansen) for their unconditional love and support through my years of study.

Contents

List of Figures

List of Tables

Acronyms

AC	alternating current.
ADMD	after diversity maximum demand.
AGC	automatic generator control.
ANN	artificial neural network.
BMS	battery management system.
COHDA	combinatorial optimisation metaheuristic for distributed agents.
CPP	conventional power plant.
DAC	distributed sverage consensus.
DC	direct current.
DEG	distributed energy generation.
DER	distributed energy resources.
DES	distributed energy storage.
DG	distributed generation.
DOD	depth of discharge.
EG	embedded generation.
EMS	energy management system.
ESS	energy etorage system.
GAM	generalised addative model.
GCRPP	Grid Code for Renewable Power Producers.
HB method	Herman-Beta method.
IPS	interconnected power systems.
kWh	kilowatt-hour.
kWp	kilowatt peak.
LCOE	levelised cost of energy.
LSM	living standard measure.
LSTM	long-short term memory.
LV	low voltage.
MAS	multi agent system.
MCB	main circuit breaker.
MCS	Monte Carlo simulation.
MD	maximum demand.
MILP	Mixed integer linear programming.
MINLP	Mixed-integer non-linear programming.
MPC	model predictive control.
MV	medium voltage.
NERSA	national energy regulator of South Africa.
NMD	notified maximum demand.
NRS	National Regulatory Specificaion.
PCC	Point of Common Coupling.
PDF	probability density function.
pf	power factor.
PFC	Power Factor correction.
PHSP	pumped hydro storage plant.

POC	Point of Connection.
PV	photovoltaic.
PV-EG	photovoltaic embedded generation.
PV-DG	photovoltaic distributed generation.
RES	renewable energy sources.
rms	root mean squared.
SAGC	South African grid code.
SO	system operator.
SOC	state of charge.
SSEG	small scale embedded generator.
STC	Standard Test Conditions.
STLF	short term load forecasting.
TS	transmission system.
T-VPP	technical virtual power plant.
VPP	virtual power plant.
VR	voltage regulation.
WPP	wind power plant.

Chapter 1

Introduction

1.1 Introduction

The fundamental role of the background is to bring forth critical information on the role that energy generation plays in our lives. This chapter discusses the concept of a microgrid as an enhancement of traditional ageing grids. The challenges and opportunities are briefly discussed to identify the key research objective of increasing renewable energy penetration on LV networks. At the end of this chapter, the conclusion will illuminate all the vital issues to be investigated in the research study.

1.2 Background

The pollution brought forth by fossil fuel-based energy generation and the deterioration of the ageing electrical infrastructure has led to a shift in the way researchers think about energy generation and distribution. The rolling blackouts and deteriorating state-owned electrical infrastructure maintained by Eskom has resulted in the South African homeowner opting for the more reliable green alternatives in the form of small scale embedded generator (SSEG).

The implementation of SSEG has resulted in the rise in generation uncertainty. The stochastic nature of SSEG has caused the energy regulators to limit the amount of renewable energy that a homeowner is allowed to install without prior approval. This has inhibited homeowners with higher consumption profiles to service a larger portion of their loads with renewable energy.

PV generation is a cost-effective and popular alternative energy source that has significantly reduced carbon emissions at the cost of introducing more uncertainty into the network. The

stochastic variations in energy generation are the limiting factor of DERs. Renewable energy generation variations can induce variations in fossil fuel-based power generation. This variation has directly increased ancillary service requirements. The need for spinning reserves, frequency regulation and reactive power compensation, has increased exponentially because of this.

In order to limit any uncontrolled increase in renewable energy penetration and attempt to protect the deteriorating infrastructure in a third world country such as South Africa, the NRS 097-2 was implemented to limit the maximum installed generation capacity. The regulations specified that the maximum allowable capacity of photovoltaic (PV) generation to be installed equals 3.81 kW. A more concise measurement would amount to 25% of the main breaker size when the Point of Connection (POC) is on a shared feeder and 75% of the main breaker size when the POC is on a dedicated feeder.

An example of what could happen when renewable energy penetration is unregulated is displayed in figure 1.1. The graph exhibits a duck curve of the energy demand as viewed by centralised generation plants of California over the years, with a renewable generation capacity increase every year.

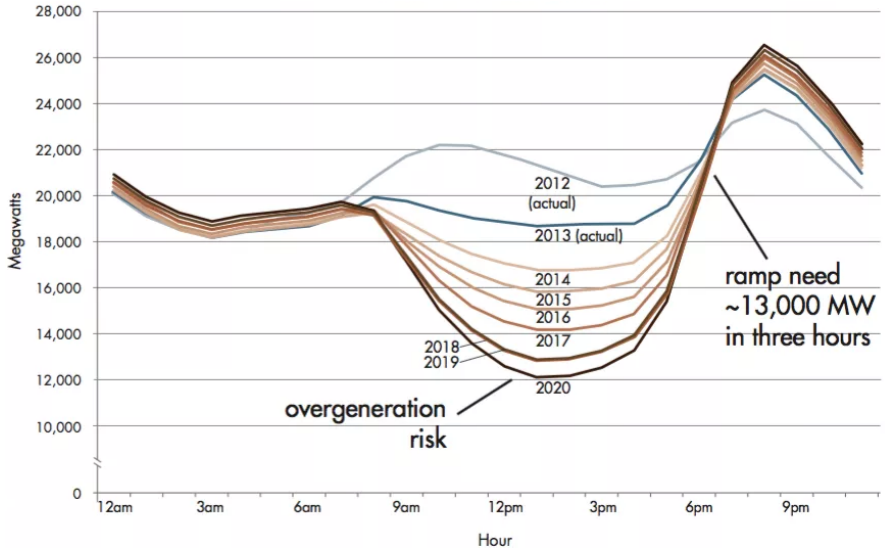

Figure 1.1: Energy generation yearly comparison in the state of California[1]

The data denotes that as renewable energy penetration increases, so does the variation in the duck curve. This is due to the PV energy being generated during periods of high irradiance. However, generation and consumption do not coincide, resulting in a duck-like energy curve which could lead to overgeneration as the renewable energy penetration increases. In order to solve this problem, grid-level energy storage has been implemented to store excess energy

and redistribute the stored energy when demand is high.

Renewable energy penetration is not the only problem when it comes to SSEG. The policing of SSEG installations are complicated since wealthy communities install the systems and do not register them with their municipality. As a deterrent, prepaid meters limit power export through financial penalties or brute force. On the other hand, analogue meters tend to reverse the units on the meter. Unbeknown to the municipality, credit their bill by illegally feeding energy back into the network unregulated. A centralised control structure and energy as a service can solve most of the problems associated with renewable energy, including the policing of SSEG systems. This can be accomplished through the implementation of microgrids or power aggregators.

Microgrids utilise coordination and control to manage the DER's efficiency. This form of integrated control is what separates microgrids from standard distributed feeders with DERs incorporated into them. Microgrids, therefore, require an advanced control structure in order to function at optimal efficiency [2]. As distributed energy generation (DEG)'s are becoming ever increasingly popular, people are not just limiting their use to isolated electrical systems that are not capable of connecting to the main grid or places with low power supply security. SSEG has evolved with the evolution of technology and have become a cost-effective way of lowering grid energy dependence. This is as a result of the drop in the levelised cost of energy (LCOE) of solar and wind-based energy generation [3].

Power aggregation is a concept similar to a microgrid in the sense that aggregators also utilise and combine various forms of DER's and energy management system (EMS) in order to generate and store energy from which various loads are powered. However, the difference between a microgrid and a power aggregator is that a microgrid can connect to and disconnect from the grid. In contrast, an aggregator is permanently connected to the grid to provide ancillary services to the grid with the DER's in the aggregator's portfolio. Energy aggregation approaches include cells, smart grids, active distribution networks and virtual utilities. Energy aggregators are a vital component utilised in smart grid networks where communication and information technology bind the systems together.

An aggregator combines the various SSEG resources to collectively produce excess power to be injected into the network to assist with core network functions and sell power back into the network. One of the aggregation typologies already utilised by Tesla is called a virtual power plant (VPP). VPPs combine single and multi-unit SSEG sources seen by the network as one large power plant capable of injecting energy into the network or absorbing energy from the network to regulate the stability of the network. Which in effect leads to a system that provides a reliable power supply. VPP's are capable of providing power more efficiently

with high flexibility.

In addition to the aforementioned capabilities, VPPs provide ancillary services previously only provided by large scale generators that run at a high cost and low efficiency. VPPs also operate with low operational costs compared to centralised generation. VPPs are utilised to integrate aggregated renewable resources such as SSEG into the energy market as a single market participant. This provides flexible participation. However, as renewable energy utilisation increases, renewable generation and load demand uncertainties increase. The accurate modelling and control of these uncertainties are crucial to the implementation of VPPs to assist the ancillary service market. The improvement of VPPs for commercial implementation requires new and innovative control techniques to mitigate uncertainties whilst handling and processing the large data volumes associated with VPPs. An intelligent control algorithm will increase renewable energy penetration in the network and make centralised energy generation obsolete.

1.3 Problem statement

The increase in renewable energy penetration presents a unique set of problems, as discussed in the background. These problems include aggregated controllability of PV systems as well as energy etorage system (ESS) with the mitigation of uncertainty paired with DEG. The increased amounts of renewable energy need to be modularly controllable to improve the voltage regulation on the network while protecting network components such as transformers or substations. The aggregation and control of the various energy sources raise the concern of dealing with large data volumes that need to be processed to control each system independently. The controllability of the system needs to be dynamic, scalable and unaffected by any anomalies. This means that if additional SSEG is added, it will seamlessly integrate with the VPP and aid in the everyday operation of the system.

The research proposes to model a representative network of a small residential neighbourhood or gated community with generation and ESS capable of being independently or collectively controlled to support the prosumers (both power consumer and producer) on the LV network. This will be done through power-sharing and active power-based voltage regulation. Various intelligent algorithms will control the system. The results and methodologies will be compared to determine the maximum safe percentage of renewable energy penetration and, in turn, the most effective control scheme. Once the simulation data is favourable, the intelligent algorithm will be implemented on a different network to validate the control scheme. The results of the various simulations will be compared to each other to validate that the chosen intelligent

control scheme can safely and efficiently increase the renewable energy penetration above the regulatory specifications without violating the network parameters. This will prove that the National Regulatory Specificaion (NRS) 097-2-3 can be rewritten to safely accommodate larger renewable energy systems.

1.4 Research objective

The objectives are divided into two ranking categories: primary and secondary objectives. The study's main aim is encapsulated in the primary objective, whereas the secondary objectives are to complete the primary objective.

1.4.1 Main objective

The main objective is to evaluate the impact of increasing renewable (PV) energy penetration on LV networks above the NRS 097-2-3 simplified criteria by implementing an appropriate controller. The result would be improved voltage regulation, energy management, storage, distribution and ancillary services.

1.4.2 Secondary objective

The primary objectives will be accomplished by means of completing the following secondary objectives:

1.4.2.1 Model of the representative network

The research study will be applied to a virtual residential complex consisting of up to 40 units with unique load profiles. The units will consist of identical SSEGs. The tests will be divided into four different combination types. The implementations consist of a feeder without PV to form a baseline and then a feeder with only unregulated PV, followed by a feeder with regulated PV and finally PV plus storage with control. This will allow for the network model to accurately represent the different conditions. The reason for utilising different variations of PV plus storage is to consider the limitations of the units at different renewable energy penetration levels. The model will be utilised to measure PV power production, load power consumption, ESS state of charge, ESS energy flow, power flow to and from each node to determine power distribution within the network.

The power flow between the low voltage (LV) and medium voltage (MV) network will be measured for active power support. The voltage at each POC will be measured to control the voltage level at every node within the system to allow for a higher energy penetration within the network.

1.4.2.2 Simulation environment

The simulation environment will be developed in MATLAB Simulink® to better understand the fundamental characteristics of the common distributed LV energy network typically implemented in residential settings. The simulation environment has to provide load flow data in the form of power flow at specific key points and voltage levels at every POC, including the Point of Common Coupling (PCC). This will provide a basis that can be utilised in order to develop a truth table control structure. The truth table control structure will show how the network reacts to increased DER penetration and rudimentary control schemes.

1.4.2.3 Control strategy

The control strategy will commence once the model has been verified and validated. In order to implement an intelligent strategy, the baseline characteristics of the model must first be established. The simulation will initially be evaluated in its natural transient state without any form of control. The implementation of manual control will follow in which parameters will manually be changed during the simulation to improve the simulation outcome. The monitoring will be implemented on the power flow at the PCC and the POC. The ESS state of charge (SOC) and capacity will also be monitored along with PV production and node voltage at each unit on the feeder. Control will be implemented on the charging or discharging of the batteries and the curtailment of the PV system.

The rule-based control strategy will be implemented before any form of intelligence is introduced into the simulation. The strategy regarding intelligent control is to initially implement a basic algorithm that mimics the voltage regulation methods currently approved by the regulations. The control will then increase in complexity and functionality. With each implementation, the capabilities of the controller and system alike will expand. The final control algorithm will then be implemented in order to display the true potential of aggregated energy systems on LV feeders, after which all the algorithms will be evaluated in terms of performance.

1.4.2.4 Evaluation of control strategies

The evaluation of the different control strategies is dependent on a set of criteria against which the algorithms will be compared. The algorithms will be compared to one another to determine which of the algorithms best fulfil the requirements set out by the criteria. The determining factor for the performance evaluation of each algorithm is as follows

- The level of renewable energy penetration safely and successfully reached by each algorithm.
- The number of regulatory violations that occurred during each control implementation.
- The controllers' capability to minimise unbalance.
- The algorithm's capability to maintain control over extended periods of time.
- The algorithms capability to be implemented on different network topologies.
- The effective energy management of each controller where the controller utilises as much renewable energy as possible while remaining within the regulatory limits .

1.4.2.5 Verification and validation

This research proposes an intelligent control scheme to control a virtual power plant to effectively increase the renewable energy penetration in an LV network. In order to verify that intelligent control is the correct method for safely increasing renewable penetration, it has to first be demonstrated that intelligent control algorithms can manage and control the system with higher efficiency than that of a linear control algorithm or no collective control at all.

The intelligent control algorithm will be validated by implementing control on the system in the simulation environment. Once refined, the algorithm can then be implemented on different network topologies, bringing forth new challenges due to the topology change. The algorithm must overcome these challenges to be validated as a generic algorithm that can be implemented on any network.

1.5 Research methodology

The research methodology to be followed in this research study can be encapsulated and closely correlate to the research objectives.

1.5.1 Model development

The accurate modelling of a battery is dependent on the characterisation of the battery type. For this dissertation, the battery chemistry will be limited to lithium iron phosphate. The parameters that will be considered are each battery's capacity, state of charge, and chemical efficiencies associated with the chosen units. As opposed to the mathematical modelling of the battery, the load and PV generation will be modelled with real-time data extracted from a lookup table and implemented in the system. The electrical network will be modelled with series RL circuits in order to represent the line parameters and simulate voltage deviations between the nodes in the system. The power source will be modelled as either a single or a three-phase power source susceptible to network disturbances.

1.5.2 Simulation development

The model will be implemented in the MATLAB Simulink® simulation environment. The load, PV, and ESS system will interface with the grid by means of utilising controlled current sources as the power production or consumption medium. This is due to the fact that the distributed energy system synchronises to the grid and injects or absorbs only current, which in turn affects the voltage level. The power source will be simulated through a three-phase Alternating Current (AC) energy source and will feed into a step-down transformer used to step down the voltage from 11 kV to 400 V.

1.5.3 Control development

The intelligent control will be implemented in a ladder control scheme where a central controller will dictate the actions of the entire system in order to effectively control the overhead power management of the entire system based on the general parameters. A second controller will be implemented on each unit to manage the balance of power between the ESS, the PV system and the network. The unit-based control schemes will first and foremost monitor its internal parameters to determine if it has sufficient power to provide voltage regulation support if instructed by the central controller.

Once all algorithms have met the deliverables, the renewable energy penetration will be increased by a factor of 25%, to the point where the network parameters are continuously violated. The simulation will be re-run without altering any control algorithm parameters, and the results will be compared.

1.5.4 Performance analysis

The various energy management algorithms, be it active or passive, will be evaluated based on performance, speed, and reliability. Performance indicates how accurately the algorithm will control the system to possibly eliminate any disturbances in the network due to the increased penetration of renewable sources whilst ensuring that enough reserve capacity is available for any unforeseen circumstances. Speed refers to each algorithm's processing time, which might cause the system to fail or put additional strain on the network due to a delayed reaction. Reliability will evaluate how well the algorithms cope with the increased sources of renewable energy and storage.

1.5.5 Verification and validation

The verification of the intelligent algorithms will be conducted by means of initially running the system with no form of control, regulatory control and then intelligent control. The results will be compared in order to verify that the intelligent control algorithms will dynamically manage the energy flow within the system.

The validation process will consist of implementing the proposed control algorithms on the simulation, determining if the system functions as predicted. Once verified that the results are as expected and correlated with the data present in the literature, the algorithm can then be implemented on a different network topology to correlate the results and validate that the algorithm is correctly designed.

1.6 Outline of dissertation

Chapter 1 highlights the limitations of increasing renewable energy penetration and how a VPP will provide a possible solution to the problem. The problem is clearly defined in this chapter. The research objectives are then clearly outlined. The objectives will serve as the steps that need to be taken to develop the simulation environment and control structure to safely increase the renewable energy penetration on an LV network. The literature review in chapter 2 will provide insight into the work that has already been completed and published in the field of VPP research. Chapter 3 will see the development of the mathematical model, establish the parameters that the model development needs to adhere to, and verify the calculations with that found in the literature.

Chapter 4 will see the transference from the mathematical model to the simulation model, where chapter 5 will implement the model validation techniques and evaluate the effect of different network topologies to implement the control on.

Chapter 6 is the development and implementation of the different control algorithms on the chosen simulation model, where the results will be reviewed and compared to determine the effectiveness of the different control implementations in order to verify the VPP algorithm. Chapter 7 will validate the VPP algorithm by exposing the control algorithm to different scenarios and a different feeder topology. The verification process will ensure that the proposed algorithm is the optimal algorithm for the intended application and can present recognisable improvement in the penetration levels of renewable energy in an LV network. Chapter 8 will see a conclusion drawn regarding the findings of this dissertation, and possible future work will be suggested.

Chapter 2

Literature review

2.1 Introduction

The purpose of this chapter is to provide the reader with an overview of the research already conducted and provide insight into the different technical aspects required for the EMS of the VPP. The energy management objectives will be thoroughly discussed, followed by the methodologies utilised to model the virtual power plant and integrate it with the national grid.

In order to realise an increase in renewable energy penetration through the implementation of a VPP, a thorough literature review first needs to be conducted. The literature review will dive deep into some of the vital factors in a virtual power plant operation. These factors are denoted in the literature review diagram displayed in figure 2.1. The first research component will consist of the policies, standards and guidelines to review their impact on the solution. Subsequently, the possibility of load aggregation will be investigated. In order to effectively control the entire system, the effectiveness of control needs to be high, which could only be achieved with a suitable intelligent controller. Finally, the different types of ancillary services will be investigated, and the applicable services will be selected.

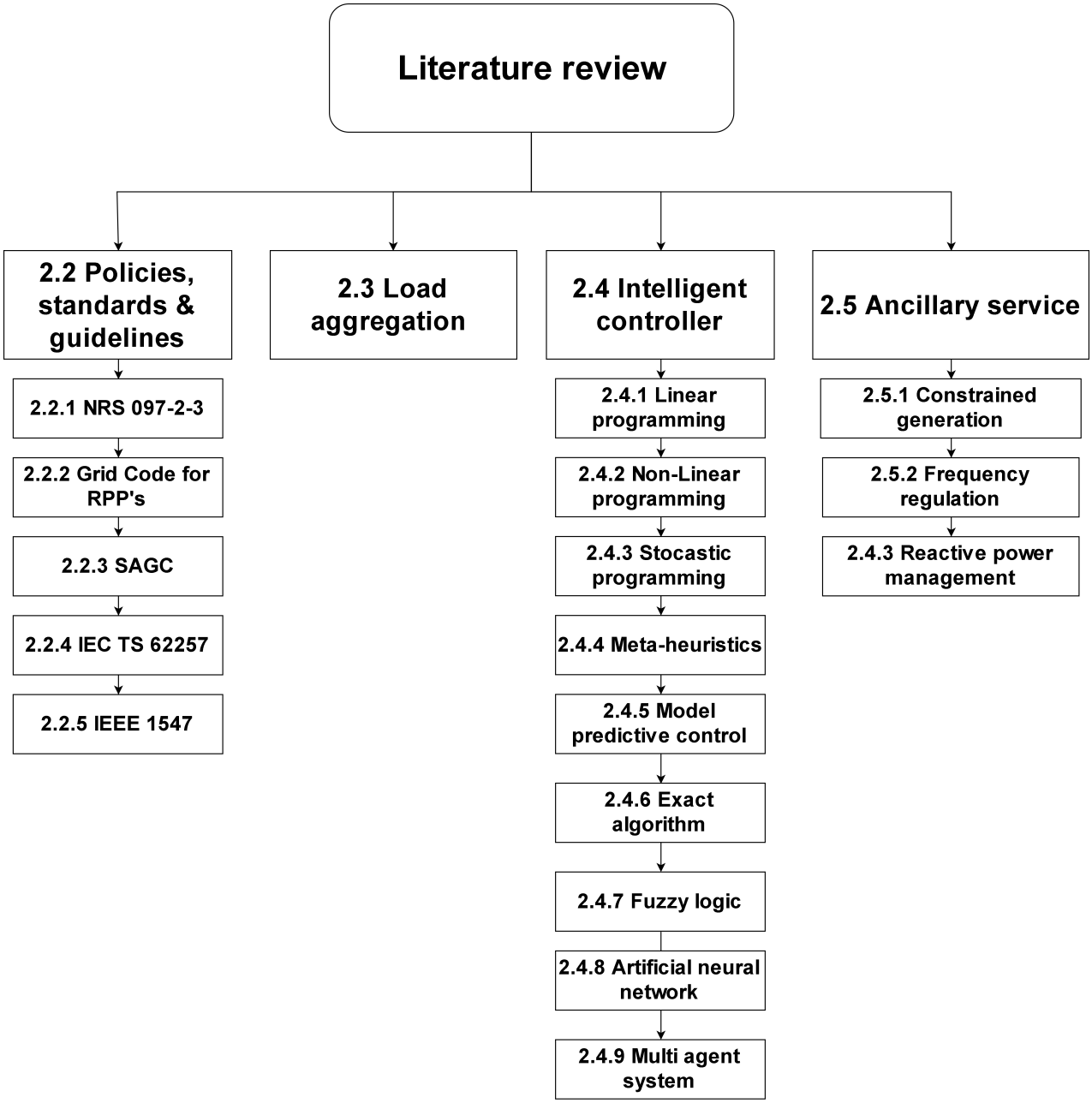

Figure 2.1: Literature review research organogram

2.2 Policies, standards and guidelines

The policies, standards and guidelines are written to serve as a form of law in their relevant industries. The policies, standards and guidelines are written for the renewable energy industry to ensure that all involved parties within the industry have specific guidelines to work with. This promotes competition within the industry that drives market prices down, enforces safety regarding installation, and develops compatibility with other interacting in-

dustries. Renewable energy standards ensure that all renewable energy systems worldwide conform to strict rules when developing uniformity in the system. Renewable energy policies encourage players to follow specific guidelines to optimise functionality. There are a variety of regulatory standards applicable at different levels of governance. Among these regulatory standards, the national level and international level standards will be looked at. International standards are written so that the regulations apply to all countries. In contrast, national regulatory standards are derived from international standards and are written to conform to the operation conditions adopted by the relevant country.

2.2.1 NRS 097-2-3

The NRS 097-2-3 serves as an elementary guideline for South African distributors to assess LV-connected embedded generation. The content of the 097-2-3 097-2-3 indicates how the SSEG needs to be connected to the grid and the safeguards that need to be implemented to ensure the safe implementation and operation of distributed energy sources without the need for detailed network analysis. These regulations are derived from a wide variety of different standards and regulations. These documents include the South African Grid Connection Code for Renewable Power Producers, the NRS 048-2 and the NRS 048-4.

The NRS 097-2 is compiled to simplify the implementation of SSEG. If these regulatory procedures and guidelines are not followed, an alternative process can be followed. This will, however, lead to the requirement of additional network studies. The NRS 097-2 applies to customers supplied by dedicated or shared LV networks but exclude customers with a living standard measure of six or less.

The NRS 097-2-3 guideline indicates that the renewable energy penetration of customers on a shared feeder equals a maximum of 25% of their notified maximum demand (NMD) and 75% on a dedicated feeder. This creates a grey area since batteries are able to absorb any excess energy and redistribute the energy at a later stage [4]. The curtailment of renewable energy is not considered to limit grid feed-in, and the regulations do not accommodate SSEG clients' aggregation to participate in grid activities such as ancillary services. Ancillary services would significantly benefit the network when provided by renewable energy generators.

A renewable energy incentive scheme for the private sector (residential and commercial) will lead to a just transition from fossil fuel-based generation to renewable energy generation. This transition by the private sector will alleviate the burden on Eskom to undergo the costly exercise of procuring their own renewable energy generation. The energy generated by these prosumers can then be utilised to provide ancillary services to the grid when aggregated with

one another. This will increase renewable energy penetration in a safe and viable manner. The main problem is that the NRS 097 regulations do not cater to hybrid systems in the way they should. The NRS 097-2-3 only specifies that the presence of storage reduces the relative active power output in relation to the grid. However, the specifications do not quantify the relation of generation to storage.

2.2.2 Grid Connection Code for Renewable Power Plants

The Grid Connection Code for Renewable Power Plants is a regulatory standard that dictates all technical aspects of RPP's connecting to the transmission network or distribution network. The size classifications of RPP's can be divided into three categories, namely category A, B and C, with category A consisting of 3 subcategories namely A1, A2 and A3. The purpose of dividing the RPP's into production-specific categories is to dictate the network participation of each category. The categories are as follows:

Category A: 0 – 1 MVA

All RPP's that fall under this category are typically connected to an LV feeder and are viewed by the national energy regulator of South Africa (NERSA) as private producers and are not obligated to be licenced as independent power producers but have to register with NERSA [5]. The three generation subcategories are as follows:

Category A1: 0 – 13.8 kVA

This category is typically reserved for residential systems, mainly made up of micro wind turbines or solar PV systems. The systems are mandated to maintain a minimum power factor of 0.98 and are prohibited from participating in the network ancillary services unless instructed otherwise by the system operator. This is due to the system's size and the chaos it will cause when all of these systems attempt to participate in network activities independently. This category of RPP has to withstand and fulfil stipulated voltage ride through conditions at the POC.

Category A2: 13.8 kVA – 100 kVA

Small industrial and commercial installations typically fall under this category and consist of micro wind turbines and solar PV plants. This category of RPP is also mandated to maintain

a constant power factor of 0.98 or greater and is not allowed to independently participate in network activities such as reactive power control or frequency regulation unless otherwise instructed by the system operator. All PV inverters are mandated to have droop control capabilities to curtail the PV production if grid frequency rises above 50.5 Hz due to excess power generation.

Category A3: 100 kVA – 1 MVA

Large-scale commercial, industrial, and free field PV and wind power plants typically fall under this RPP category. Category A3, B and C RPP's are designed to withstand and fulfil extremely low voltage ride through conditions at the POC. RPP's of category A3 shall remain connected to the grid in the event of a symmetrical fault sequence. The RPP is prohibited from injecting reactive power into the network at any moment of the fault's occurrence. The RPP will vary its reactive power between 0.95 leading and lagging. This power factor regulation will be available from 20% to 100% power output. The RPP shall curtail its power output when instructed by the system operator (SO) per the absolute production constraint regulation.

Category B: 1 MVA – 20 MVA

Category B RPP's are viewed as independent power producers by the national energy regulator of South Africa and therefore have to be licenced with NERSA [5]. These power plants have to conform to the same regulations applicable to fossil fuel-based power plants, and category B RPP's will not be considered in the scope of this study.

Category C: 20 MVA and greater

Category C RPP's are viewed as independent power producers by the national energy regulator of South Africa and therefore have to be licenced with NERSA [5]. These power plants have to conform to the same regulations applicable to fossil fuel-based power plants, and category C RPP's will not be considered in the scope of this study. The Grid Code for Renewable Power Producers (GCRPP) is a standard set out by national control for the interconnection and participation of RPP's in the energy network. With the increasing renewable energy penetration and energy forecasting capabilities, a plea is made to the national energy regulators to allow for better network participation of small renewable energy generators.

2.2.3 South African Grid Code

The South African grid code (SAGC) is developed to establish mutual obligations of industry participants concerning the use of the transmission system (TS) and the operation of interconnected power systems. The purpose of the grid code is to ensure that all party accountabilities are defined for the provision to easily access the TS. The SAGC ensures that customers connecting to the transmission system understand the minimum technical requirements that must be satisfied to utilise its services. Service providers, too, have to be made aware of the technical requirements for connecting to the TS. The SO has to adhere to the obligations defined by the SAGC to ensure the integrity of the interconnected power system. All the rules set out by the grid code are done to guarantee the safe and efficient operation of the TS. Suppose a participant of the TS wishes to obtain any relevant information of the TS. In that case, they may do so from the information made available to and by industry participants. The pricing principles of services provided and technical cost drivers possess a sense of transparency towards the participants.

The SAGC is divided into different sections to isolate the different aspects of the grid code. The aspects include the governance code, which details all possible aspects of grid code governance and the network code, which sets a standard of operation for all customers connecting to the TS. The network code defines the technical design requirements applicable to the network's service and defines the TS development process and methodology. The system operation code defines the rights and obligations of participants regarding the operation of the interconnected power systems (IPS). The system operation code will serve as a guideline to which the VPP will be designed. The metering code serves as a specification for the tariff metering at the TS interface level. The transmission tariff code represents the objectives and structure of the transmission tariff structure and the employed methodologies.

The SAGC preamble defines a set of terms applicable to the implementation of a VPP. The preamble states that the use of demand-side load management is allowed. This indicates that the load power draw with respect to the point of common coupling may be increased or decreased in response to a signal from the system operator. This is very similar to load curtailment. The only difference between demand-side load management and load curtailment is that the user can curtail their loads with load curtailment and is therefore compensated for the curtailment. The use of embedded generators is allowed in the system but must be connected to the distribution network.

2.2.4 IEC TS 62257

The IEC TS 62257 series are presented as technical specifications. They are viewed as guidelines and recommendations for implementing small scale renewable energy resources and hybrid systems for the electrification of distributed customers and not as standards that must be followed to the letter. The TS 62257 is developed to assist renewable energy engineers, system designers, project managers and operators in accurately pairing the correct implementation with the correct application. This is to accurately design the system to suit the project's critical needs and efficiently operate and maintain the system according to the system specifications. The following subsections of the TS 62257 and the IEC 62898 are both, directly and indirectly, part of the microgrid and, in turn, VPP implementation. We will only look at the standards that influence microgrids and power aggregation.

- IEC 62257-9-1: Micro power plants
- IEC 62257-9-2: Micro Grids
- IEC 62898-2: Technical Requirements for the operation and control of microgrids*
- IEC 62898-3-2: Technical requirements for a Micro Grid EMS *
- IEC 62898-3-3: The technical requirements for self-regulation of dispatchable loads in microgrids

The technical requirements for both the operation and control of microgrids and the microgrid energy management system will be used to interact with the VPP and the microgrid in the form of dominant control. The technical requirements for the self-regulation of dispatchable loads in the microgrid will provide a baseline for the implementation of demand-side load management of aggregated loads in the VPP.

2.2.5 IEEE 1547

The IEEE 1547 is a vital document for the interconnection of DERs with the power grid. The IEEE 1547 has laid the foundation for the future involvement of renewable energy within energy networks worldwide. The IEEE 1547 is written to promote grid modernisation and DER advancements, of which renewable energy interconnections are one facet. The IEEE 1547 has positively altered how the energy industry can conduct business with the incorporation of DER's. The purpose of the IEEE 1547 is to provide the mandatory functional requirements, technical requirements and specifications, and the flexibility and choices that go along with these types of standards. The requirements provided in the standards are relevant to the safety, performance, operation, testing, and maintenance of the interconnected DER systems.

The national grid in its entirety is viewed to be a technically and operationally complex system. As a result, the grid structure in a traditional sense is viewed as a top-down power generation scheme with a centralised power plant situated at the top of the structure and generating power in the megawatt or gigawatt range. This energy is then transmitted and finally distributed to the customers. The power tends to only flow from the power station to the customer and not the other way around. The deregulation of electricity led to the increase in the implementation of DERs, which led to a more cost-effective manner of providing electricity. Consumers were able to install systems and generate their own electricity. Specific consumers then became generators, which disrupted the traditional operation of the electrical infrastructure. SSEG started to affect the distribution grid circuits because various circuits experienced a bidirectional flow of electricity, which caused the protective equipment to be rendered useless due to their inability to detect fault conditions in systems with bi-directional energy flow. The increased renewable energy penetration also affected the distribution grid ancillary equipment operation.

The GCRPP and the NRS 097-2-3, among others, are all local regulations and standards derived from the IEEE 1547. The IEEE 1547 has revolutionised the implementation and operation of microgrids worldwide. This, as a result, will have a net positive effect on the further implementation of new advanced smart grids and aggregated DERs of which VPPs are a subset. As time marches on and technology becomes highly sophisticated, and the levels of renewable energy penetration continue to increase, so does the regulations of the IEEE 1547 improve.

The recently revised version of the IEEE 1547 addresses distribution level DER interconnections which consist of generation and storage systems with storage, the advanced functionalities of both modern grid and DER equipment. The document also discusses the adequate inertia that DER needs to supply to the grid, distribution and transmission impacts, and the cross harmonisation of requirements. The subject of high renewable energy penetration also arises in the IEEE 1547. The intermittence of the renewable energy supply is one of the key topics of discussion regarding the reliability of supply that DER's need to provide.

The IEEE 1547, in conjunction with the IEEE 2030.2, will provide the groundwork for building a fully operational, integral and easily scalable VPP capable of increasing the renewable energy penetration to the maximum capable amount.

2.3 Virtual power plant load aggregation

A VPP is used to aggregate renewable energy resources to promote the goal of achieving a 100% renewable dependent national grid. The main focus of aggregation typically lies with the generation and not with the consumption. This is because there is a particular social inconvenience associated with the external control of shiftable loads, not to mention the difficulty associated with scheduling these shiftable loads. However, the main dilemma is that to have a VPP functioning at its optimal best. All assets are required to participate in the operation of the VPP. Therefore, the aggregation of shiftable loads must be incorporated into the functionality of the VPP. This can be coupled to a compensation structure that compensates the owner based on the amount of discomfort the load's absence inflicts. The main objectives that the implementation of demand-side management needs to satisfy are as follows:

- Minimising the electricity bill
- Minimising operational cost
- Levelling the demand curve
- Improving the overall network reliability
- Social welfare maximisation
- Assisting with ancillary service provision

The objectives can only be solved by means of implementing shiftable loads. Therefore, it is crucial to identify and categorise these shiftable loads to efficiently aggregate the respective loads. The loads can be divided into different categories. The first category consists of purely resistive loads. Purely resistive loads include water heaters and space heaters, and underfloor heating. The second category of loads can be viewed as inductive loads. These loads typically consist of motors that perform specific tasks such as borehole pumps on a farm or residential area, swimming pool pumps, large blowers and air compressors. The power consumption of an electric motor can be varied by implementing a device called a variable frequency drive. Controlling shiftable loads are simple yet effective. This allows for the load operations to be aggregated to assist with the functionality of the VPP.

2.4 Virtual power plant control strategies

The objectives of a VPP EMS are achievable through means of implementing techniques such as artificial intelligence or by means of solving an objective function critical to the system.

This section provides a plethora of methods that can be utilised in order to achieve the aforementioned objectives. This section aims to provide insight on how some of the most commonly used techniques work and how they were implemented in order to improve the VPP's functionality.

2.4.1 Linear programming

Linear programming is deemed a mathematical programming method utilised to optimise a linear objective function that is subjected to linear inequality constraints and linear equality. The authors in [6] discussed a single objective problem where minimising the virtual power plant cost is achieved by means of efficiently minimising the conventional power plants production cost through the implementation of the mixed-integer linear programming method. Research indicates that the problem can be solved by commercial optimisation software such as CPLEX. In [7], the authors discussed a multi-objective problem in which maximising the number of connections to be restored based on a priority model, maximising system profits and minimising curtailment costs is achieved by means of utilising a Mixed integer linear programming (MILP) method. The optimisation was applied by means of utilising a MATLAB based modelling program called CVX. Typical examples of linear control include PID control, feed-forward control and feedback control.

2.4.2 Non-Linear programming

Mixed-integer non-linear programming (MINLP) can be viewed as the method for solving optimisation problems containing non-linear constraints or objective functions. In [8], a two-stage multi-objective programming method is proposed for the optimal allocation of distributed generation. The first stage is to minimise the total cost function by means of determining the optimal installed capacity of various types of DG and decreasing the payback time of the investment. The second stage will maximise the all-encompassing system benefit function to identify the optimal investment payback time by determining the optimal energy price. Equation 2.1 expresses the continuous cost minimisation function:

$$cost(\$/h) = C_{(InDG)} + C_{(OMDG)} + C_{(InSC)} + C_{(OMSC)} + C_E + C_{loss} + C_{ENS} \tag{2.1}$$

Where $C_{(InDG)}$ is the annualised investment cost of the DG, $C_{(OMDG)}$ is the DG operation and maintenance cost, $C_{(InSC)}$ is the SC annualised investment cost, $C_{(OMSC)}$ is the SC operation maintenance cost, C_E is the cost of purchasing additional power form other utility companies,

C_{loss} is the cost of any energy losses in the system and lastly C_{ENS} being the energy not supplied within the system, an example of a non-linear equation would be the equation for the lifetime of the synchronous condenser denoted by A_{sc} as displayed in (2.2):

$$A_{sc} = ((1 - (1 + d)^{(-T_{sc})}))/d \tag{2.2}$$

Where d indicates the distance and T_{sc} indicates the period of operation. This equation is a simple example of a non-linear function that can be solved with mixed-integer non-linear programming by means of utilising an optimisation software package. The aforementioned literature serves as one example of many on how MINLP can be integrated into the VPP management systems to optimise the system [9].

2.4.3 Stochastic programming

Stochastic programming is a programming method developed for use in model optimisation problems containing uncertainty elements. The dependence of renewable energy on natural elements has caused renewable energy to be highly unpredictable and stochastic. Although stochastic programming possesses the capability of dealing with uncertainties, it does not possess the ability to adapt with human-like precision. Stochastic programming is defined by splitting the control up into different stages based on whether the variables within the system are made known to the control architecture. The initial control stage will cater to independent variable conditions, whereas the second stage will be responsible for variable dependant conditions.

The VPP in [10] consists of a wind power plant (WPP), conventional power plant (CPP), and a pumped hydro storage plant (PHSP) has two identified sources of uncertainty, with one being the renewable energy production and the other being the market price. The uncertainties will have to be addressed when partaking in the day-ahead market. The first stage variable problem indicates that the VPP control system has to submit its predicted offering curve in the day ahead market without knowing the wind power output or market price at the time of submission. The uncertainty of the WPP is dependent on the weather of the following day. The second stage variable problem, such as the electrical market price, will be dependent on the remaining capacity of the PHSP and the production of the WPP. This method allows for optimal CPP scheduling by means of taking any future uncertainties into account.

2.4.4 Metaheuristic approach

Metaheuristic optimisation methods are typically faster than traditional optimisation methods. The metaheuristic method sacrifices accuracy, precision, and completeness for speed. The difference between heuristic and metaheuristic approaches is that heuristic approaches exploit the problem-dependent information to find an adequate solution to a specific problem. In contrast, metaheuristics act like design patterns that can be applied to an extensive set of problems since metaheuristics do not require any information about the problem. This is due to the fact that the control structure evolves its control scheme as it acquires more information. Metaheuristic algorithms are developed in order to quickly reach a short-term goal by whatever means necessary. Metaheuristic methods can be viewed as non-optimal, although a sufficient approach is required to reach the immediate goal. The metaheuristic approach is present in a multitude of optimisation categories. These categories include genetic algorithms, tabu search, particle swarm optimisation, ant colony optimisation, artificial bee colony, cat swarm optimisation, big bang big crunch and the firefly algorithm. In [11], the authors present a bio-inspired metaheuristic for the predictive scheduling of fully distributed energy resources.

The authors' objective is to make the approach scalable and preserve the evolving autonomy of individual DER operators by means of implementing a combinatorial optimisation metaheuristic for distributed agents (COHDA). The COHDA algorithm is an asynchronous approximate best response behaviour. This means that each DER agent reacts to updated information from other agents by means of adapting its selected schedule with respect to the target profile. The algorithm's behaviour is based on the biomimicry of a school of fish, where each fish reacts to developments in its vicinity by altering its travelling direction and velocity. This creates an equilibrium because the agents constantly strive to reach the optimal position, which keeps all the actors together. At the same time, the agents are repulsed by one another, which causes them to maintain their distance. The general algorithm is commonly referred to as particle swarm optimisation. The swarm utilises DER generation to determine their position in the swarm. It reacts to the generation of other actors to optimally schedule generation so that the entire system remains in optimal condition. The system was simulated in three steps. In the first step, it became clear that after an elapsed period from the start of the metaheuristic, the actors gained some knowledge about the participating players, enabling the agents to generate valuable solution possibilities for the optimisation problem. In the second step, the actors were more aware of their surroundings, which eventually led to the actual solution of the metaheuristic. In the final step, all agents were aware of their surroundings, which led to the final solution candidate being known by all agents, resulting in the termination of the metaheuristic.

2.4.5 Model predictive control

Model predictive control is defined as an advanced process control method used to control a specific process while still satisfying a series of constraints [12]. Immediate objectives are achieved by means of utilising a dynamic system model. The control structure is also able to take certain future events into account. VPPs have to adhere to a strict set of guidelines in order to not cause an inconvenience to the electrical network. Therefore, it is of vital importance for the control structure to adhere to these guidelines. In [13], a distributed model predictive control method is proposed in order to optimise DER coordination. The authors stated that the model predictive control (MPC) would serve as a control benchmark in the low voltage system. The coordinated MPC regulators have successfully steered towards the successful VPP operation plan.

2.4.6 Exact algorithm

An exact algorithm produces the desired outputs by means of running the input through a series of states or rules. These rules determine if the input is worthy of an output and can induce a safe state if the input is not favourable. Exact algorithms are commonly referred to as deterministic algorithms. These algorithms are robust and can be implemented on any application and implementation. Deterministic algorithms are diverse in that they can be combined with heuristic approaches, resulting in non-exact outputs but would be more dynamic in the decision-making process and do not rely heavily on the knowledge of the algorithm creator. Developing an exact algorithm requires the developer to consider the input possibilities or software conditions. Common examples of exact algorithms include truth tables and state machines. Some of the applications of a deterministic algorithm include industrial control and automation.

2.4.7 Fuzzy logic

Fuzzy logic control utilises a distinct set of user-defined rules to approximate the characteristics of human logic. Fuzzy logic relies on a degree of truth structure instead of a Boolean logic structure, otherwise known as on-off logic, consisting of only 1 and 0 as outputs. This indicates that an output can be partially true, wholly true or otherwise viewed as entirely false. Fuzzy logic control is developed with the intent of mitigating any uncertainties within a control system that computers are not naturally excellent at doing. If a select amount of professional knowledge of a virtual power plant or microgrid is available to the designer, a

collection of rules can then be introduced in order to dictate how the system reacts when faced with specialised scenarios [14]. Fuzzy logic is a considerably popular control method in the microgrid environment. This, as a result, has led to it also becoming a widespread implementation within the virtual power plant control structure [9].In [15] a fuzzy-logic based particle swarm optimisation algorithm is prosed in order to maintain complete control over the charge and discharge rates of the battery ESS. The PSO algorithm mimics the sociological nature of a flock of birds.

The control strategy is obligated to store energy at the correct time and location within the VPP to balance the generation and consumption to maintain system stability. This strategy, in turn, will assist in the reduction of lost power. Both the charging and discharging trigger signals are dependent on the demand gap, state of charge and the maximum power. The system's overall goal is to mitigate the risks of energy trading with a high penetration of renewable energy. The authors in [16] have presented a combined control architecture that utilises fuzzy logic along with a human-based novel insecurity metric in order to automate the decision making process of a VPP. The insecurity factor generated by the collected data represents the operational flexibility of the DERs in the VPP translated into a numerical value. This method of control allows the VPP to create a fully functional internal VPP market, where all generators can trade energy autonomously according to their own needs and external pricing signals. In [17], a multiple block fuzzy logic control algorithm was proposed for the implementation of a demand-side management strategy of an electric water heater in order to level the distribution feeder demand profile. The water heater's power consumption depended upon a wide variety of environmental factors. The fuzzy logic control inputs include the energy demand on the feeder, the current temperature of the water, the consumer's comfort level, the demand trajectory, and lastly, the percentage of power provided to the geyser. The effective management of water heater energy consumption will result in the high loads during peak periods being shifted to off-peak periods.

The previous paragraph contained detailed information on how type-1 fuzzy logic works and example implementations of fuzzy logic control in the VPP environment. Type-1 fuzzy logic is limited to the uncertainties of the linguistic values with fixed weighted membership functions. Zadeh introduced a newer concept of fuzzy logic in 1975, which serves as an extension of the popular type-1 fuzzy logic system [18]. The new control scheme is known as type-2 fuzzy logic control or otherwise known as fuzzy-fuzzy control. The type-2 control structure also allows for uncertainties in the weight of the membership function. This type of control compensates for more uncertainties in the data and allows for crisper outputs. Fuzzy logic type-2 control structures are relatively new, and there are no implementations on virtual power plants. There is, however, a limited number of implementations on microgrid control platforms.

In [19], a protection strategy is proposed for fault detection within a microgrid. The protection strategy utilises interval type-2 fuzzy logic control to detect, classify and locate faults that might occur within the microgrid in less than one cycle of the test system. The fault direction is detected by means of utilising the phase angle between the modal voltage and the modal current as input for the fuzzy controller. The controller protects the microgrid in a single-phase tripping event. A simulation of the control structure and system is performed in MATLAB Simulink®. The system is redundant because the controller provides backup protection if the primary protection fails.

Although fuzzy logic control is viral in the microgrid environment, it is still relatively scarce within a VPP setting. This is possibly due to the limited amount of research conducted on fuzzy logic applications in VPPs.

2.4.8 Artificial neural network

An artificial neural network (ANN) is a computing system based on the biological neural network that constitutes a living brain. An ANN utilises artificial neurons, which act like synapses in a natural brain, transmitting signals to surrounding artificial neurons. The interconnect ability of the neurons provides the ability to learn from one another. The signal present at the connection between the neurons is considered a real number. The outputs of each neuron are computed by means of a non-linear function of the sum of its inputs. The outputs of each neuron are connected to edges that interconnect the neurons to one another. Both neurons and edges are weighted. These weights are adjusted as the learning progresses [20]. The application of an ANN is typically wide-ranging. However, ANNs are commonly used to study situations and detect patterns. This functionality is of immense advantage to those who seek to predict situations and forecast patterns [21]. Using an ANN in a microgrid is beneficial for load forecasting, weather forecasting, and generation forecasting scenarios. ANN's are typically complemented by other control strategies in order to interpret the data more accurately and better control the system.

The authors of [22] employ a long-short term memory network in order to develop a distributed decentralised prediction method for managing the power output of the VPP by means of forecasting the generation of the PV production plant. The authors have joined three variations of the long-short term memory (LSTM) neural network with a distributed sverage consensus (DAC) protocol. The three different LSTM ANN's consisted of a centralised LSTM, a local LSTM, and a distributed LSTM. The numerical results stated that the test was carried out for six days with variable weather conditions. The prediction algorithm provided both a one

day and a three-day forecast. The data obtained from the training session indicated that the global performance of the distributed algorithm always performed better than the local algorithm with a general root mean squared (rms) error of 23%. At times the value improved to 35%.

In [23] an ANN-based methodology for scheduling distributed energy resources is proposed. The goal of the ANN is to train on the data accumulated from day to day operation and then accurately schedule both generation and loads according to the systems set demands. The ANN methodology is compared to a reference methodology that utilises MILP to calculate the optimal scheduling parameters. The article states that the financial results produced by the reference approach are superior to those produced by the ANN. However, the reaction time of the ANN is significantly faster than that of the reference approach. The conclusion is that the ANN approach can be advantageous to small players that have to manage their resources with a limited amount of computational power. In [24], the authors utilised a feed-forward neural network technique in order to accurately forecast wind speed and solar irradiation of the immediate environment. The forecasting is conducted to complement the algorithm utilised to determine the optimal ESS connected to the microgrid based on the cost-benefit analysis of the algorithm.

2.4.9 Multi agent system

A multi agent system (MAS) is considered a system consisting of a wide array of interdependent intelligent agents. The multi-agent system is an aggregation of individual systems which is capable of solving problems that are frequently difficult or impossible for an individual agent or a monolithic system to solve [25]. The authors of [26] proposed a multi-agent control system for the advanced distributed energy management of an array of distributed energy storage (DES). The resources consist of two PV plants, two wind turbines with two local consumers, each possessing their own solar PV system and energy storage medium. All of the aforementioned resources are bundled together in a grid interconnected microgrid.

A diesel power plant complements renewable energy resources. The agent-based framework expedites energy management within the microgrid and assists with selling energy to the market and managing different resources within the VPP. The MAS identifies the optimal operating environment and then steers the system towards the determined goal. The MAS, therefore, leads to an optimal environmental and economic state. The benefit of the MAS is that it reduced timings in the system due to its efficiency. The MAS, therefore, provides higher operational efficiencies than a convention DER system. However, a MAS requires a

high bandwidth rate that directly relates to the development of modern infrastructure.

2.5 Ancilary services

Ancillary services as set out by the SAGC will be managed by the SO. The scheduling of generation and ancillary services will be provided by the SO a day ahead of activation. The SO shall provide a day ahead demand forecast for the power system with which the ancillary service providers can plan their generation and service provision tenders. The VPP system operator will receive a daily 24-hour ancillary service and energy schedule before two o'clock in the afternoon each day. Ancillary service provision is vital in the journey to a net-zero carbon emission future. Renewable energy penetration can only increase if SSEG is allowed to participate in ancillary services. The development of accurate load and energy generation forecasting methods have provided renewable energy with the competitive edge required to dominate fossil fuel-based energy generation in the energy market. Incorporating DEG in ancillary service provision has reduced the operational expenditure of peaking power plants and has also resulted in lower capital expenditure for the maintenance of ancillary services. The following categories define the different types of ancillary services to be provided.

2.5.1 Constrained generation

Constrained generation is typically a service supplied to the national transmission network by a power station, which could be a virtual power plant by constraining the VPP's power output at the unconstrained schedule level. This is done to ensure the power system remains optimal in thermal regulation, voltage and stability. The main downfall of constraining generation in favour of system equilibrium is that owners tend to lose out on potential profit from selling energy to the power system. Therefore, a compensation scheme is of utmost importance. If a power producer constrains its generation, it will be compensated by the National Transmission Corporation. This is stipulated in the rules set out by NERSA.

2.5.2 Frequency regulation

Frequency regulation ancillary services consist of both upward and downward frequency regulation. This is done by automatically matching the supply and demand in real-time by increasing or decreasing the active power of the generation unit. The control system implemented to control the generation is called automatic generator control (AGC). The AGC can

send commands to increase or decrease the real power output when signalled to do so. This, however, is a tad challenging to do with renewable energy or, more specifically, wind and PV energy.

There are two different frequency regulation stages with renewable energy: upwards frequency regulation and downwards frequency regulation. Upwards frequency regulation is a complex task since renewable energy is stochastic and operates at maximum capacity continuously. For renewable energy systems to possess the ability to implement upwards frequency regulation, the systems need to operate with a spinning reserve. This, however, is inefficient and costly since RPP's pay for themselves with the energy they sell. If they do not sell all the energy they utilise, the system will deliver an atrocious return on investment. Downwards frequency regulation is quite simple to achieve with DERs since all certified grid-tied inverters have failsafe protocols and are grid compliant. This means that if generation exceeds the demand, the frequency rises, which is a clear indicator to the inverters that there is an excess amount of energy on the network, which leads to the systems curtailing the energy production or even ceasing generation completely when the frequency exceeds the predefined limits.

2.5.3 Reactive power management

Reactive power is a critical part of the electrical network because the reactive power balance affects the system's stability. Reactive power is mainly consumed by inductive loads and generated by capacitive loads. The main dilemma is that the supply and consumption of reactive power and voltage control are related to one another because the changes in reactive power flow generate a change in the voltage. Reactive power can be consumed or generated by static VAr compensators. The problem, however, is that reactive power needs to be generated or consumed close to the loads because reactive power dissipates when transmitted over long distances. DERs are capable of generating or consuming reactive power instantaneously. This makes DERs versatile because they are already close to the load and require no additional capital expenditure. The aggregation of DERs provides the capability of generating or absorbing reactive power in different regions as needed all at the same time.

2.6 Conclusion

The literature review brought to light a wide variety of factors that were not initially anticipated to play a role in the development of a VPP. The analysis of the different renewable energy policies, standards and guidelines indicated that there was still information lacking

which could benefit the renewable energy industry and the national energy infrastructure. The different control schemes provided the promising potential to control the aggregated energy resources. The control algorithm with the most potential for this application is the exact control algorithm. The reason is that the researcher has predetermined knowledge on the workings of renewable energy and can therefore program the controller with the specific requirements. The ancillary services that were chosen are voltage regulation and constrained generation support. With the review phase complete, the next step is to model a representative network on which the controller would be designed and tested.

Chapter 3

Model of a representative network

3.1 Introduction

Modelling is the mathematical simulation of a process, concept, or system operation, commonly aided by computer software implementation. In order to test and simulate the performance of the VPP, a specific model is required to accurately represent real-world characteristics of the VPP. This enables the developer of the stability controller to verify the controller's performance before implementing the controller in a real-world application. The two main methods with which an intelligent electrical network can be modelled are dynamic and data-driven modelling. When testing an intelligent energy controller succeeding simulation verification, the conventional approach commonly referred to in literature is to conduct hardware-in-the-loop testing. This, however, will not be possible due to resource limitations. Therefore, other methods for validating the simulation model and control architecture will be considered.

3.1.1 Dynamic modelling

Studies revolving around intelligent network control, where the controller is responsible for voltage and frequency stability control, rely heavily on the use of dynamic modelling in order to gauge the effects that the control algorithms have on component level performance in a SSEG system. A dynamic model can assist in proving regulatory compliance to specific standards such as the IEEE 1547 or local standards such as the NRS097-2 or the GCRPP. Dynamic modelling can be conducted by utilising existing software packages to create unique intelligent network models. Additionally, the network can be modelled by utilising traditional

mathematical modelling techniques. Traditional mathematical modelling allows for systems to be modelled from first principles.

3.1.2 Data-driven modelling

The DER in microgrids commonly possess measurement devices integrated into their physical architecture or acquire data from within the system. These devices are capable of acquiring system data over time. This provides researchers with the capability of designing and developing data-driven microgrid models. The data can either represent a transient condition or represent the network in steady-state conditions signifying normal operational conditions. In order to test the functionality of the control algorithm, a fault can be injected into the data, and the reaction of the control system can then be documented. Data-driven modelling can be viewed as the more popular modelling method of the two since in today's day and age, data can be acquired from almost anywhere as a result of the pre-existing metering infrastructure [27, 28, 29, 30].

Mathematical models of controllable dynamic components are incorporated into data-driven models where these components need to act independently of the system to stabilise the system. The most common example of such a system is the battery bank. Other examples include reticulation lines, generators and transformers. These types of loads generally react passively to parameters in a system. The charge and discharge rates and the scheduling of the battery operation are single-handedly controlled by the system controller. This is due to the fact that the PV systems produce power under nominal conditions, irrespective of the rest of the system. Therefore, the system controller can control the power flow within the system by means of charging and discharging the ESS. However, this method is limited to the battery's state of charge. If the battery reaches a high SOC, the potential to keep charging the battery decreases and if the battery reaches a low SOC, then the potential to discharge decreases. Data-driven modelling can also be incorporated into dynamic models in the sense that accurate load data would simulate the load interaction with the dynamic models of both the PV energy system and the ESS instead of modelling individual appliances or loads.

3.2 Power source

A distribution network requires some form of power source to provide electricity to the loads situated within the network. The national grid will fulfil the synchronising power source in this study. According to the SABS 1019:1985, low voltage is any voltage up to 1 kV, and

medium voltage ranges between 1 kV and 44 kV. Since the study will mainly be conducted on the low voltage network, a medium voltage power source will be required, typically equal to a medium-voltage substation with a nominal voltage of 11 kV. The reason for this is to utilise the 11 kV feeder and step down the voltage through a step-down transformer to 400 V at a nominal frequency of 50Hz. The reason for following this approach is to analyse the power flow through the transformer while providing power to the LV network. As previously mentioned, the power source will provide 11kV alternating current (AC) 3-phase power due to the fact that the most common distribution transformers being fed from the substation are 11 kV to 0.4 kV step-down transformers. The three-phase voltages are generated in a positive sequence, meaning phase A will have a phase angle of zero, whereas phase B and phase C will lag phase A by 120 degrees and 240 degrees distinctively.

3.3 ADMD of residential participants

Residential sectors will be the main focus of this network study with the possible incorporation of commercial loads at times. Residential sectors are, amongst other things, classified based on the living standards of the community in which they reside. This is known as the living standard measure (LSM). For example, a family living in an informal settlement that collectively generates an income of R7000 or less will have a smaller effect on the utility infrastructure than a family generating a collective minimum income of R24000 and living in gated communities and estates. This is due to the different living standards that they are accustomed to as a result of their income. Utility planners can utilise this living standard measurement to accurately plan and predict the consumption of load within various distribution networks.

Table 3.1 exhibits the physical classification of domestic consumers based on their dwelling. These classifications are also matched with the after diversity maximum demand (ADMD). The ADMD is utilised in the design of electrical distribution grids in which the consumer demand is aggregated over a large number of customers. The ADMD is robust in its development that it accounts for any coincidental peaks load that the network may experience in its lifetime, which in effect means that the ADMD is an over-estimation of the typical network demand. The focal point of this study is on upmarket consumers with a typical LSM of 8 and higher. This is due to the fact that the economics of renewable energy mainly favours high earning families due to the easily affordable price of installing PV. These families typically live in urban complexes or residential estates. These pristine estates in the concrete jungle typically consist of 40 or more units. Residential units that fall under the LSM 8+ category have a present ADMD of 4.3 kW [31]. The ADMD is expected to increase to 5.3 kW within the

next fifteen years [31]. This needs to be taken into account when sizing the transformer. The high concentration of renewable energy in residential complexes is perfect for implementing a virtual power plant, and that is the exact reason this setting was chosen.

Table 3.1: Classification of domestic consumers — Description of consumer load classes [31]

1	2	3	4	5
Consumer load class	Derivation of income	Description of dwelling	Type of road	Water reticulation
Rural settlment	Mainly from pensions and subsistence farming. Some breadwinners work far away in cities.	Mainly based on traditional construction methods	Normally tracks with diffcult access	Normally none
Rural village	From pensions and subsistence farming. Some breadwinners are employed in nearby industrialised areas and commute daily.	Mixture of modern and traditional construction methods	Mainly gravel with main roads tarred	Some communal standpipes
Informal settlement	From work in a nearby town or city - largely from the informal sector	A range, from shacks to newer "government subsidy" houses made from blocks. Self-build schemes fall into this category. Built area of dwellings generally less than 40 m^2.	A range, from tracks in informal areas to gravel in planned areas.	None in informal areas. Planned areas generally have water piped to a tap in the yard of each dwelling.
Township area	From work in cities or towns, pensions, and some informal employment	A range, from low-income flats to old township houses and newer government scheme houses (mid-range), to small semi-detached houses. Built area of dwellings generally from 50 m^2 to 80 m^2.	Mostly tarred	Piped to most houses - half of which eventually have working electrical hot water cylinders.
Urban residential	From blue-collar jobs in cities	Houses that range in size from 80 m^2 to 170 m^2. Most houses have some visible repair or maintenance work in progress.	All tarred	Piped to all houses.
Urban residential	From formal employment in cities, mostly white-collar jobs	The built area of main dwellings is typically 190 m^2. None of the houses are multi-story.	All tarred	Piped to all houses, all of which have electrical hot water cylinders.
Urban township complex	Mainly from professional jobs in cities, level of employment is high.	Normally very high density, in complexes that incorporate security or other shared services. Dwellings are single or multi-storey. Floor area in the range from 80 m^2 to 150 m^2 per unit.	All tarred	Piped to all houses. A high percentage of such houses have multiple electrical hot-water cylinders.
Urban multi-story/ estate	Mainly from professional jobs in cities, level of employment is very high.	Large, constructed of brick or concrete, oor area from 250 m^2 to 500 m^2. In regions with some desirable natural feature (e.g. a view).		

3.4 MV/LV transformer sizing

The medium voltage to low voltage transformer must step the 11 kV medium voltage down to 400 V low voltage. However, to determine the sizing of the transformer, a set of requirements first needs to be established. The requirement for the transformer providing power to the low voltage network will be to provide power to 40 units at most. The ADMD will affect the sizing of the specified transformer, and for that reason, a higher rated transformer will be selected in order to account for possible future load increases. This is done based on the guidelines for human settlement planning and design. Each node within the network will be limited to a maximum of three units [31]. The standard desired reticulation line length will be a total distance of 500m from the point of common coupling to the end of the feeder.

The SANS 60076 stipulates that all power transformers have to adhere to a certain standard derived from the IEC 60076-1 [32]. The standards specify that the minimum short circuit impedance of transformers with rated power between 25 kVA and 630 kVA equals 4% at rated load. The standards indicate that the transformer's primary winding resistance has to be between 0.8Ω and 1Ω due to the fact that thinner conductors are used, and the number of turns is also higher on the primary side as opposed to the secondary side of the transformer. The secondary side requires a winding resistance between 1.1 mΩ and 0.4 mΩ since the windings on the secondary side have fewer turns than the primary side, and the amount of current passing through is significantly higher when compared to the primary side. This is because the losses need to be lower, and the conductor winding on the secondary side is thicker than the primary windings. The inductance in the primary and secondary winding is induced by the AC travelling through the windings and inducing a magnetic field. The magnetising resistance and inductance within the transformer core are mutually specific to the manufacturer and client. Therefore, the magnetising resistance will be averaged based on the MV/LV transformer supplied by Actom with a magnetising resistance of 226.78 kΩ and a magnetising impedance of 722.17 H.

The diversified maximum demand determines the number of units sharing a feeder. The number of units typically ranges from 20 to 160 units depending on the transformer sizing. This is a general rule of thumb based on the standards set out by the NRS 034-1, which operates on a prudent ADMD of 4.16 kVA. This value is obtained by means of dividing the transformer power rating by the number of units sharing the transformer as displayed in table 3.2. Therefore, the determined minimum energy capacity for the transformer is equal to 167 kW for the 40 units in the network. The closest rated transformer is 200 kVA. However, to accommodate future expansion due to additions to the network, the transformer has to be oversized, and

the subsequent possible sizing is 315 kVA which is also a widespread implementation in most distribution networks.

Table 3.2: Distribution network transformer parameters

TRF rating [kVA]	Impedance [%]	Load losses [%]	No load loss [%]	# Units sharing
100	4.5	1.70	0.30	24
200	4.5	1.35	0.26	50
315	4.5	1.21	0.23	81
400	4.5	1.13	0.23	104
500	5	1.08	0.22	131
630	5	1.02	0.21	167

3.5 Conductor sizing

The conductor sizing of a low voltage distribution network is critical to both the network's capacity and the budget. Network planners typically design the network to be close to maximum capacity to drive down cost. Various factors affect the design of the network, such as conducting material, network load, cable position and cable length. The network infrastructure is designed to make the cables leading from the transformer to the first feeder the thickest. As the network progresses, the lines tend to become thinner and thinner due to the decreased line loading at the end of the network. The NRS 034-1 stipulates that a conductor's line losses have to be 10% or less. Therefore, a conductor thickness has to be chosen that correlates with these parameters while being capable of carrying the network load without failing.

Displayed within the NRS 034-1 is a graph with the conductor sizing utilised within a distribution network and the voltage drop of each conductor at a specific length. The maximum line length chosen for this study is 500 meters from the transformer to the end of the feeder. Therefore, the 25 mm^2 and the 35 mm^2 are not considered solely based on their voltage drop characteristics. This means that the only two possible options that satisfy the 10% voltage drop limit at a range of 500 meters are the 50 mm^2 and the 75 mm^2 wires as displayed in Figure 3.1 below. However, according to Aberdare cables, 75 mm^2 are not made anymore. The closest diameter is 70 mm^2

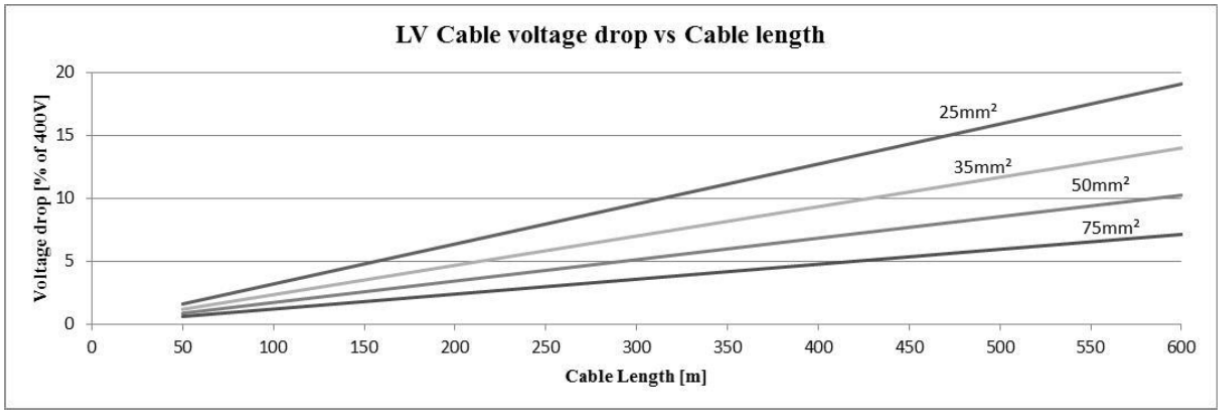

Figure 3.1: LV cable voltage dorp vs cable length for determining the appropriate cable size[31]

The determination of the cable sizing lies in the calculation of the full load current of the 315 kVA transformer. In order to determine the full load current of the transformer, (3.1) will need to be utilised:

$$I = \frac{S}{\sqrt{3} \times V \cos \phi} \tag{3.1}$$

From the (3.1), it is evident that I is a representation of the full load current flowing through the transformer, which is determined by means of utilising the apparent power symbolised by S and dividing it by the line to line voltage symbolised by V and $\cos \phi$ is a representation of the power factor. The assumption is made that all calculations are to be done at unity power factor [31].

The rated apparent power is deduced from the manufacturer's specifications as 315 kVA with the nominal line to neutral voltage being $230V$ the correct values we are able to calculate the full load current:

$$I = \frac{315000}{\sqrt{3} \times 400}$$

$$I = 454.67A$$

Table 3.3: LV copper conductor electrical properties [33]

Cable size	Electrical properties					
	Current rating			Impedance	Volt drop	1 Sec short circuit rating
	Ground	Duct	Air			
(mm^2)	(A)	(A)	(A)	(Ω/km)	(mV/A/m	(kA)
1.5	24	20	19	14.48	25.080	0.17
2.5	32	26	26	8.87	15.363	0.28
4	42	34	35	5.52	9.561	0.46
6	53	43	45	3.69	6.391	0.69
10	70	58	62	2.19	3.793	1.15
16	91	75	83	1.38	2.390	1.84
25	119	96	110	0.8749	1.515	2.87
35	143	116	135	0.6335	1.097	4.02
50	169	138	163	0.4718	0.817	5.75
70	210	171	207	0.3325	0.576	8.05
95	251	205	251	0.246	0.427	10.92
120	285	234	290	0.2012	0.348	13.8
150	320	263	332	0.1698	0.294	17.25
185	361	298	378	0.1445	0.25	21.27
240	416	344	445	0.1220	0.211	27.6
300	465	385	510	0.109	0.189	34.5

The assumption is that the conductor will be placed underground, with ground temperature equal to 25 ℃. Based on these parameters and the copper conductor electrical property graph, it is evident that when utilising a single conductor, the optimal wire size with a current-carrying capacity equal to that of the full load current is the 300 mm^2 conductor.This conductor has an in-ground current rating of 465 A. However, the issue is that a cable of this magnitude is not widely used within a distribution network. The aim would therefore be to distribute the load amongst smaller conductors. Thus, in the event that the transformer directly feeds two conductors, the current carrying capacity of the conductors can be divided by two, which will then equal a maximum current of 221.79 A. This current requirement can be satisfied by a conductor with a size of 95 mm^2. In the event that the full load will be divided between three conductors, the current carrying capacity of each conductor will be equivalent to 147.86 A. The conductor that is capable of handling a current draw of this magnitude is 50 mm^2.

3.6 Conductor length

The conductor length between nodes in the network is predetermined to be equal to 40 m. In order to accurately model the effects of the reticulation lines on the low voltage network, the line impedance of the 50 mm^2 reticulation line first needs to be calculated. The first calculation will be the line resistance per meter. The line resistance per meter is calculated by means of utilising (3.2).

$$R = \frac{\rho L}{A} \tag{3.2}$$

In (3.2) displayed above R is the line resistance in $\Omega \cdot mm^2/m$ and ρ is the electrical resistivity of the conducting material, annealed copper has an electrical resistivity of 1.72×10^{-2} $\Omega \cdot mm^2/m$ at an environmental temperature of 20 °C. L is the length of the conductor in meters, and A is the surface area of the conductor in mm^2 which has previously been decided to be 50 mm^2. In order to correctly calculate the line resistance, the resistivity constant at the line operating temperature needs to be calculated. The operating line temperature is equal to 60 °C. The formula for calculating the difference in electrical resistivity is as follows in (3.3):

$$\Delta\rho = \alpha \times \Delta T \times \rho_0 \tag{3.3}$$

From (3.3), it is evident that $\Delta\rho$ is the difference in electrical resistivity at different temperature points. A is the temperature coefficient of the material, ΔT is the temperature difference between the reference temperature and the operating temperature, and finally, ρ_0 is the initial electrical resistivity of the conducting material. The temperature coefficient of copper is equal to $0.00393k^{-1}$, the difference in electrical resistivity is therefore calculated as follows [34]:

$$\Delta\rho = 0.00393 \times (60 - 20) \times 2.7038 \times 10^{-3}$$

$$\Delta\rho = 2.7038 \times 10^{-3} A$$

$$\rho_n ew = 2.7038 \times 10^{-3} + 2.7038 \times 10^{-3} = 1.99 \times \Omega \cdot mm^2/m$$

The new electrical resistivity can be utilised in order to determine the line resistance per meter of a cable with a surface area of 50 mm^2

$$R = \frac{1.99 \times 10^{-2} \times 1}{50} = 398\mu\Omega$$

Each 40 m conductor will possess a line resistance of 15.8 $m\Omega$.The inductance and, in turn, the reactance of an AC cable is dependent upon many factors, which include but are not limited to the axial spacing between the conductors and the proximity and magnetic properties of surrounding steelwork. These dependencies are mainly applicable to multicore cables utilised in distribution networks. The cable's inductance needs to be calculated based on the spacing between the conductors. For this study, the inductance will be derived from the manufacturer table. The manufacturer, Aberdare cables, specifies that the reactance of a 50 mm^2 cable equals 0.101Ω per km. However, this is only the reactance. In order to determine the inductance, the reactance needs to be reverted by means of utilising (3.4) as stipulated by the IEC 60092-352:

$$\begin{aligned} X &= 2 \cdot f \times \pi \times L \times l \\ L &= \frac{X}{2 \times f \times \pi \times l} \end{aligned} \tag{3.4}$$

Equation 3.4 represents a formula for acquiring the inductance of a conductor. The reactance supplied in the cable datasheet is represented by X, which is a component of the nominal network frequency represented by f and the length of the conductor represented by l, which is kept standard at 1 m. The product of the aforementioned variables will produce the inductance present within the conductor represented by L and measured in $H \cdot m$. In order to convert the impedance from kilometer to meter, the reactance must first be divided by 1000, which will result in a value of 0.101 $m\Omega$ per meter. The line reactance will be utilised to calculate the line impedance as follows:

$$L = \frac{0.101 \times 10^{-3}}{2 \times 50 \times \pi \times 1} = 0.322\mu H/m$$

The 40 m reticulation cable's inductance, which spans two nodes, will equate to 12.88 μH. A series RL circuit will model the transmission line to model the voltage drop of the reticulation line and the line loading in the system. The capacitance component will be negated due to the negligible effect that the capacitance has on the reticulation lines.

3.7 Maximum allowable branches

The units situated within the electrical network will be the determining factor when deciding on the number of network branchings. When the network is operating at full load, the minimum number of branches are restricted to three branches. This is due to the fact that the current-carrying capacity of the specified reticulation line will be exceeded in the event that only a single reticulation line is utilised for energy distribution. The various network configurations determine the maximum number of branches. The extreme conditions will result in a set of three houses on each feeder connected to the transformer, adding up to 14 branches from the transformer for a maximum of 40 houses.

The variation in branches will affect the balancing of the network and, in turn, affect the voltage deviation disproportionally between feeders. However, the maximum length of each feeder will be limited to 500 m to accurately define and control the network parameters and simultaneously limit the voltage drop to 10% of the nominal voltage. The branch lengths will be equal to the difference between the maximum line length and the length from the transformer to the branch. Variations in the number of units per node are also tolerable but restricted to a maximum of three units per node to limit drastic loading on the feeder.

3.8 Network typologies

The network typologies laid out in this section will be utilised to determine which electrical network topology will be best suited for implementing an intelligent VPP. The parameters that will be evaluated to determine the effect on the line voltage are as follows:

- the units on the line
- the length of the line
- the loading on the line
- the branches situated in the network.

The network displayed in figure 3.2 consists of three single-phase reticulation lines feeding a total of 12 nodes per phase. This summates to 36 units connected to the reticulation line. The purpose of a reticulation line without branches is to determine the effect that the number of loads sharing a single reticulation line has on the line voltage at the various nodes within the system. The basic model will also indicate the effect of the increase in the line impedance from the feeder to each node.

The total line length from the start of the feeder to the end is equal to 240 m. As stated in the test specifications, this line length can be increased to 500 m. The basic model will also provide a good indication of the line loading magnitude and transformer magnitude. The prediction would be that the basic model will violate the nominal state of the feeder on over or under voltage before exceeding the line and transformer power limits. The number of units on the line model is close to the maximum specified units. This is because we are attempting to determine the effect of the number of units on the feeder.

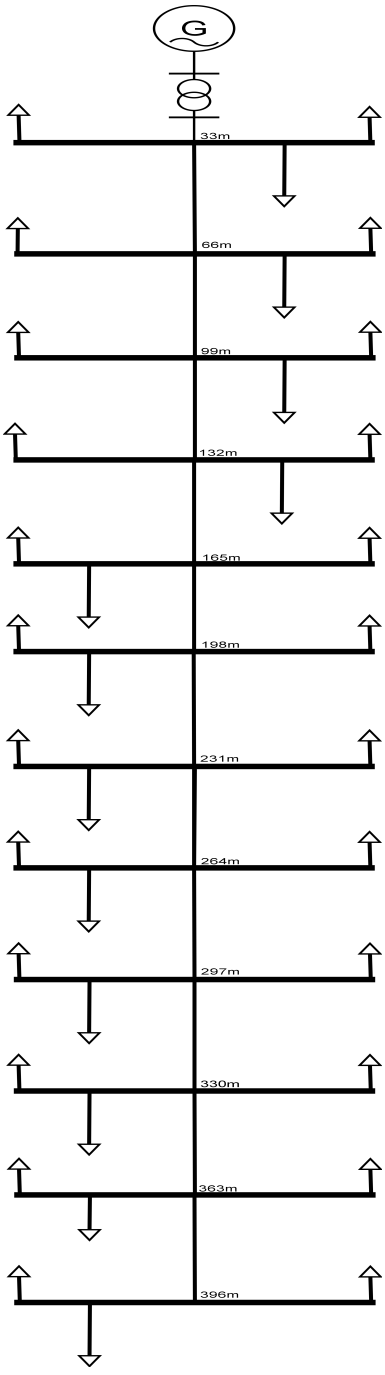

Figure 3.2: Single feeder extended three phase network

The line diagram displayed in figure 3.3 represents a short feeder with a single branch housing a total of 20 units on the feeder. The layout of this feeder is random at best due to the goal of implementing uneven load distribution in the network. The branching is situated at the start of the line to determine the effect of a branch network on the line voltage at the POC and on the nodes along the line without being affected by the line impedance. The feeder is limited to 20 units dispersed between the branches to evaluate the effect of light loading on the network.

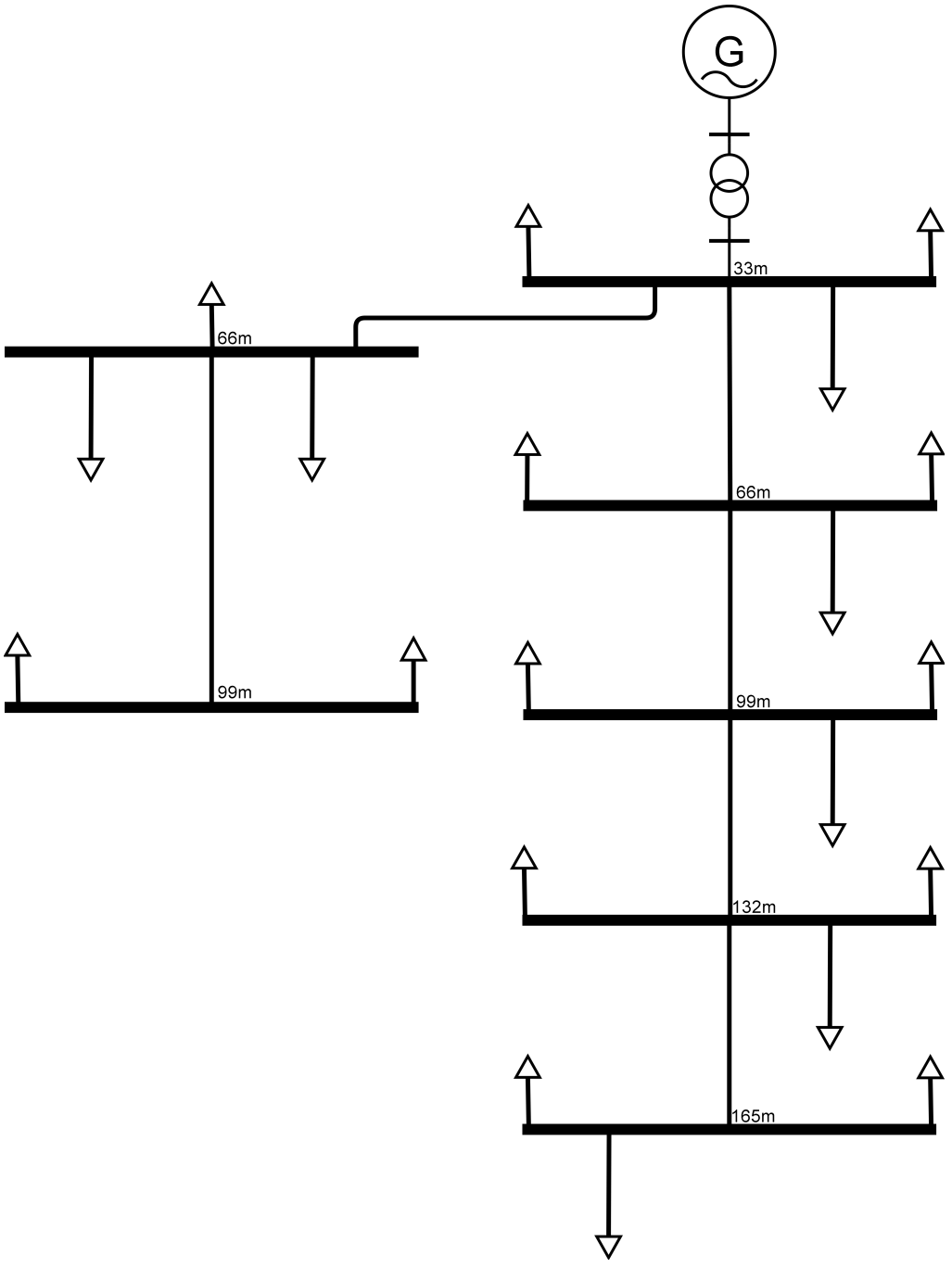

Figure 3.3: Single feeder dual branch network

The line diagram displayed in figure 3.4 exhibits that of a spider feeder consisting of 5 branches and at the farthest end of the feeder a node with only two units attached to it. The spider feeder is not very long, consisting of only one node per branch. The reason for this is that the network configuration will be used to test the effect of the loading on the transformer due to the low line impedance resulting from the short line lengths. This means that there will be a minimal increase in the node voltage while the possibility of transformer overloading is relatively high. The unbalanced bus will also indicate the effect of unbalance within the network. The units on the network remain constant at 20 units equally divided across phases.

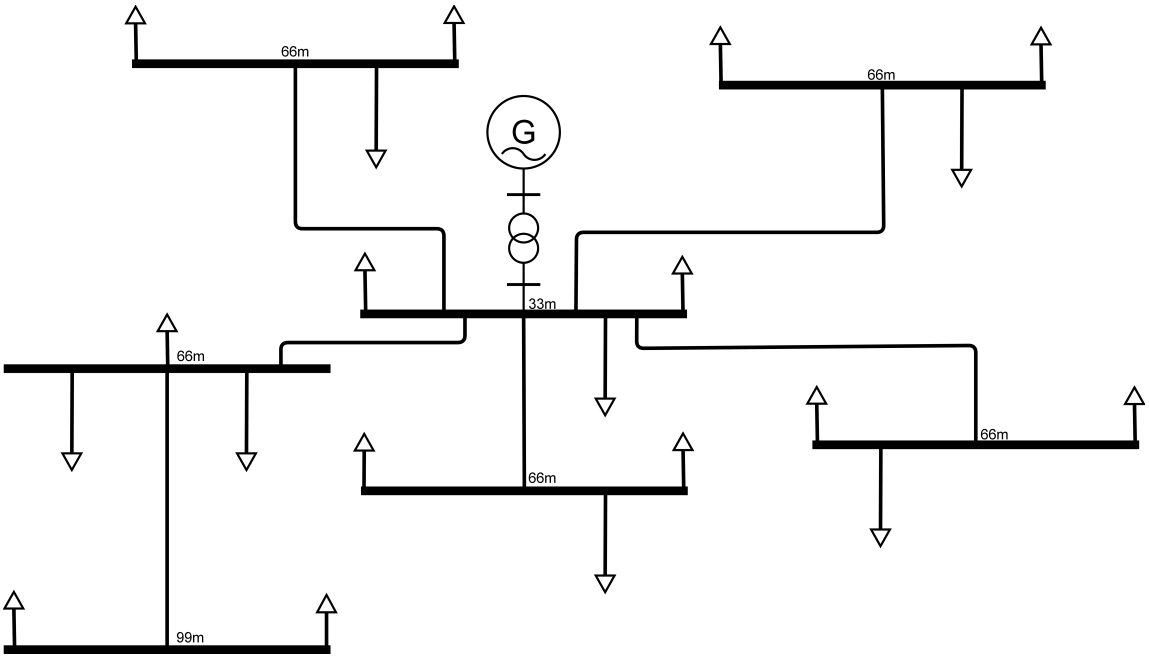

Figure 3.4: Spider feeder network

The line diagram displayed in figure 3.5 represents a combination between the spider network and the basic network. The purpose of this network is to test a wide variety of factors. One factor includes testing the combined effect of the increased line impedance at a single point in the system due to the cascade connection of specific nodes on the feeder. In addition to testing the voltage variation with respect to the line impedance, a test will be conducted in parallel on the transformer loading effects of this configuration. The number of units on the feeder has also been increased due to the fact that when designing this feeder layout, the goal was to create the most unstable configuration for a specific transformer capacity.

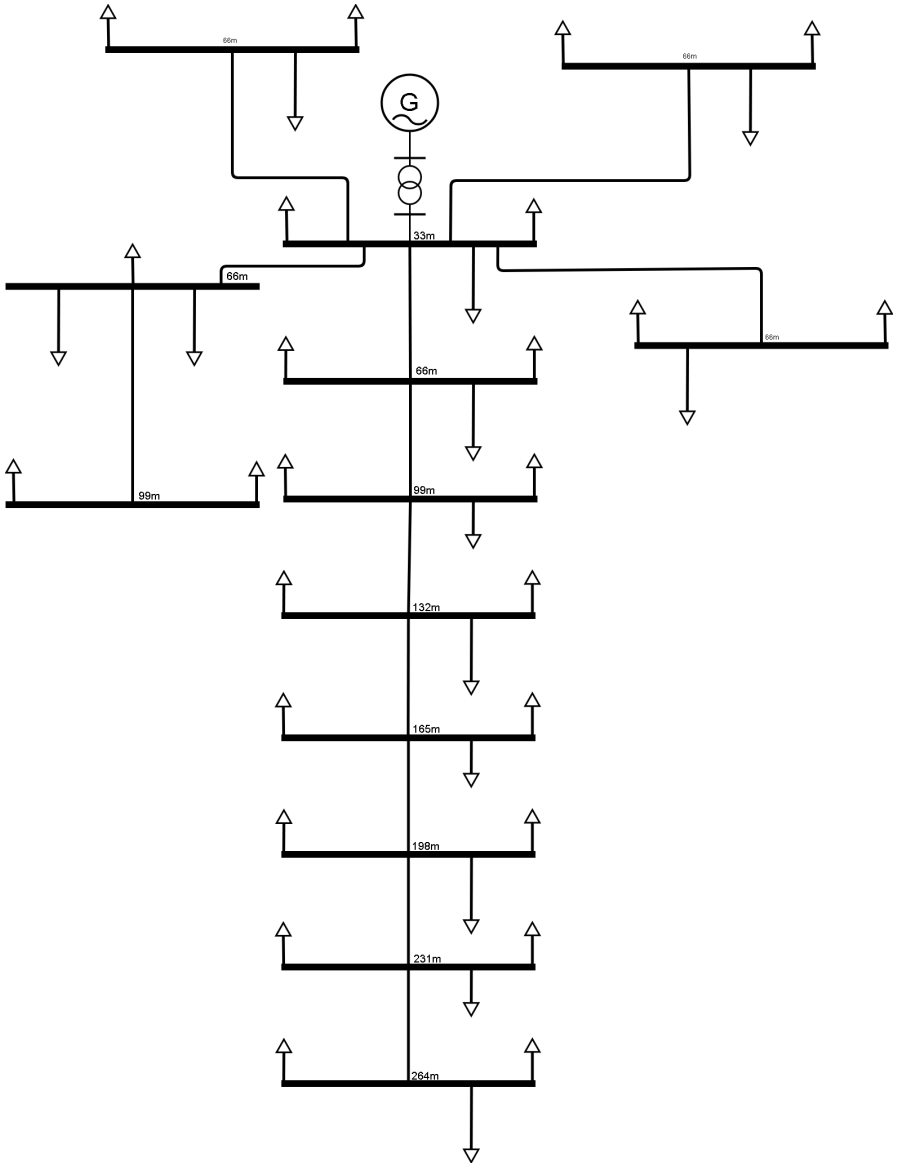

Figure 3.5: Spider feeder network with an extended shared feeder

The line diagram displayed in figure 3.6 represents a Three feeder network with varying unit quantities. Each branch contains a row of nodes connected in cascade with the feeder. The design of this configuration determines the effect of many units on a network where two of the feeders are disproportional to the third branch, with 15 units connected to the two branches. The unequal distribution of loads will be used to determine if the uneven loading on the feeder has any effect on the line voltage. The Three branches will also determine the effect of high loading on the network at lower line impedance levels due to the cascade connection. One would assume that the reticulation lines situated at each branch will exhibit a behaviour similar to the base model displayed in figure 3.2.

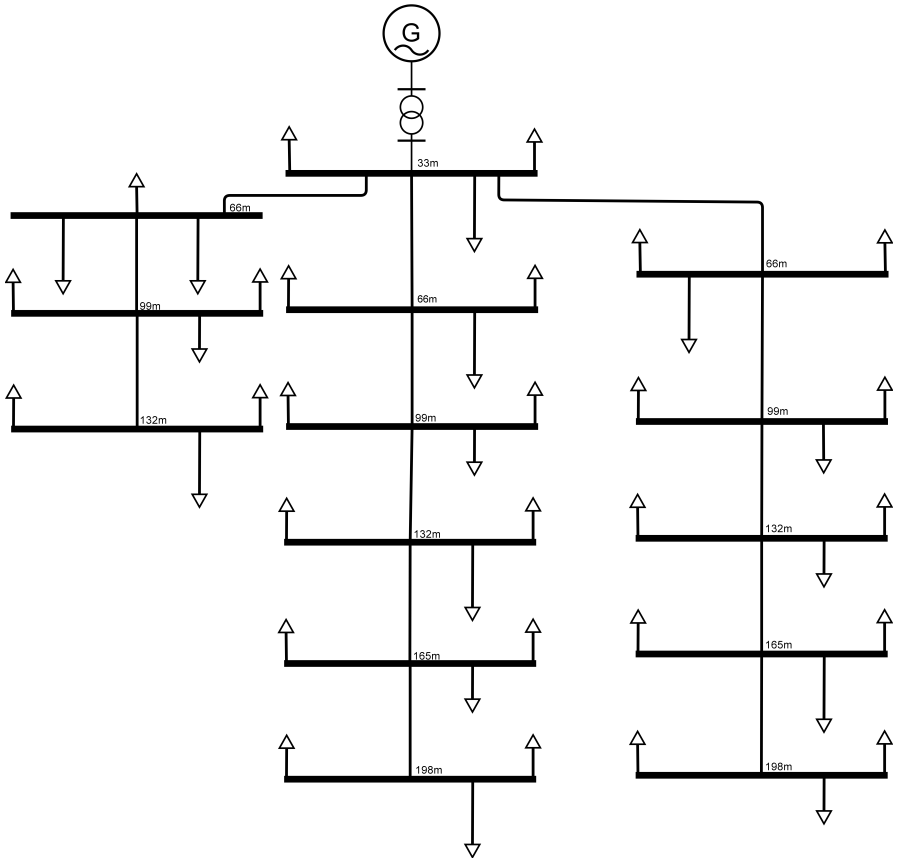

Figure 3.6: Three feeder network with varying unit quantities

The line diagram displayed in figure 3.7 represents a network with five branches, each connected to a specific node on the feeder. This design is to determine how the distance between the branching and the POC affects the line voltage. The feeder houses 33 units evenly distributed across the three phases. The layout of the feeder will also provide information as to how the renewable energy distribution and penetration will affect the voltage stability within the network. The difference in node voltage between the branching and the next node will also be analysed. The configuration will bring to light how a network of this configuration will increase or decrease power stability as well as line loading on the network.

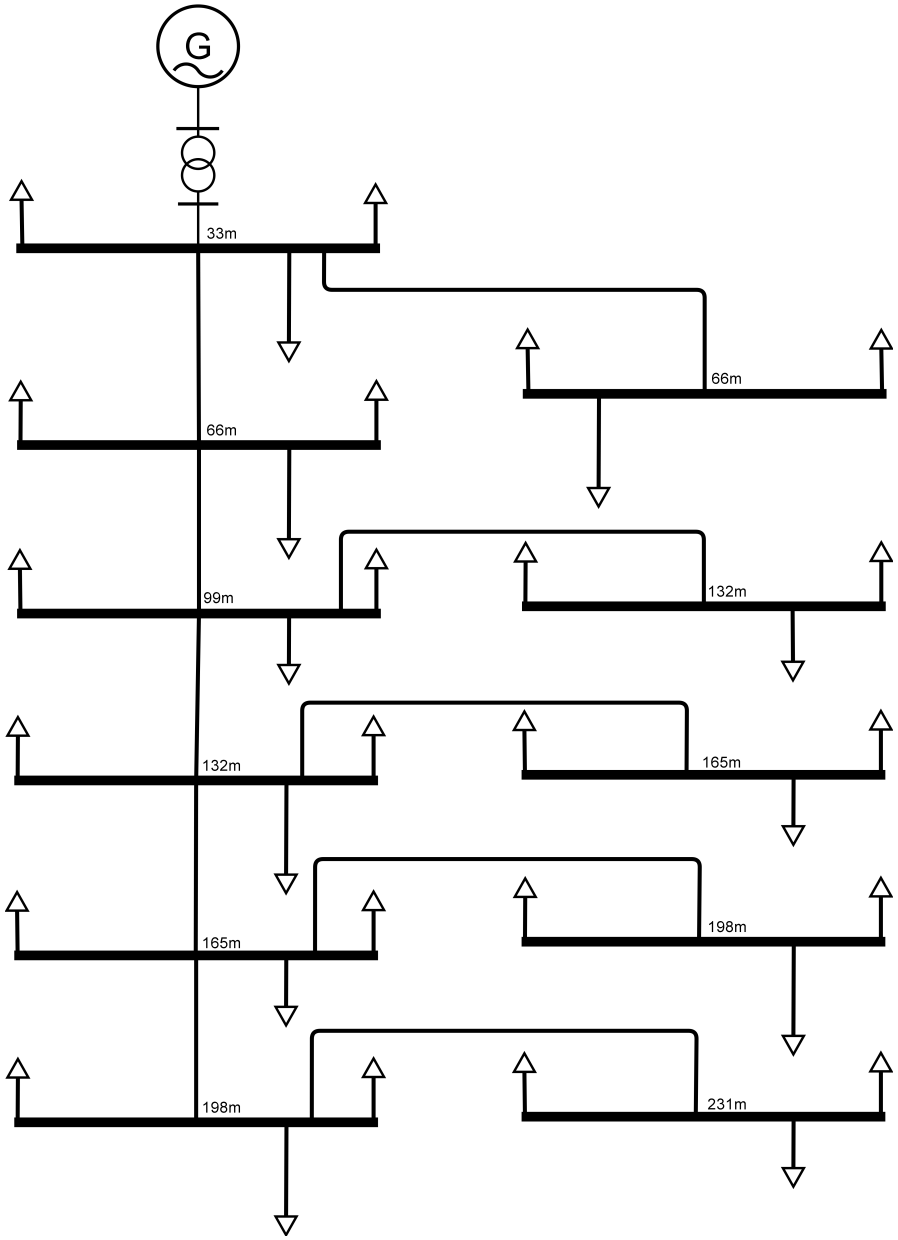

Figure 3.7: Single feeder network with branches at each bus

The single line diagram displayed in figure 3.8 represents a feeder with two branches, with one of the branches situated close to the front of the feeder and the other branches situated at the end of the feeder. The first branch has three nodes connected to it and the second branches has four nodes connected to it. This design aims to determine the effect of high loaded branches at opposing ends of the network and how randomly placed DERs affect the line voltages.

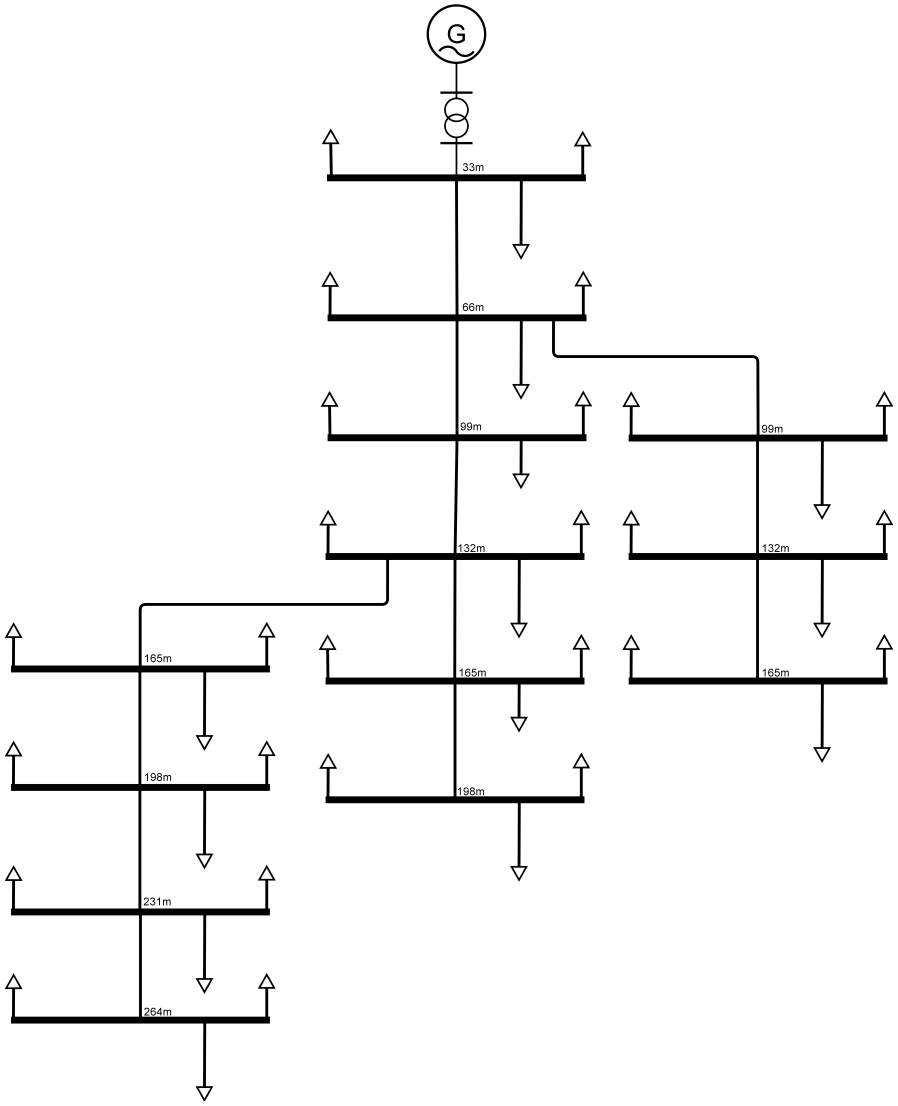

Figure 3.8: Single feeder with high load branches at different sections of the main feeder

The line diagram displayed in figure 3.9 below exhibits a reticulation feeder containing loads distributed across the feeder. The network is composed of three branches, with two branches branching off down the line from the first branches. This is assumed to decrease the line impedance whilst increasing the line loading at the respective points within the network. Of the four high load units, one is situated at the start of the network, whereas the other three units are situated at the end of two of the three branches. Two of the high load feeders will share the same node. This will indicate the effects of extremely high loading at specific points within a feeder. The consumption from these loads will be balanced across the three phases since the heavy loads are represented as three-phase loads.

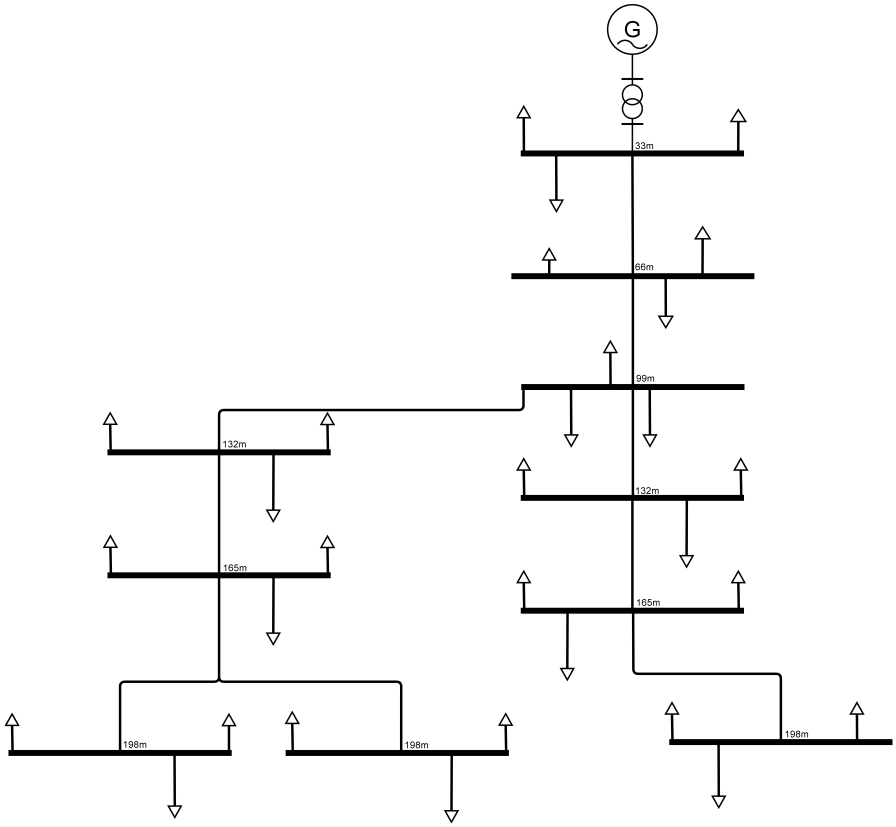

Figure 3.9: Single feeder network with a dual branch split

The line diagram displayed in figure 3.10 represents a spider network with longer reticulation lines on each branch. The maximum line length of any given branch is 80 m long. This network aims to determine the effect of a high branch concentration in combination with medium length reticulation lines. The assumption is that if the renewable energy sources (RES) are added to the ends of the various branches with different line lengths, then the voltage rise in the network will be unique on every endpoint in the feeder. The prediction is that the transformer will trip due to overloading before the line voltage exceeds the predefined bounds.

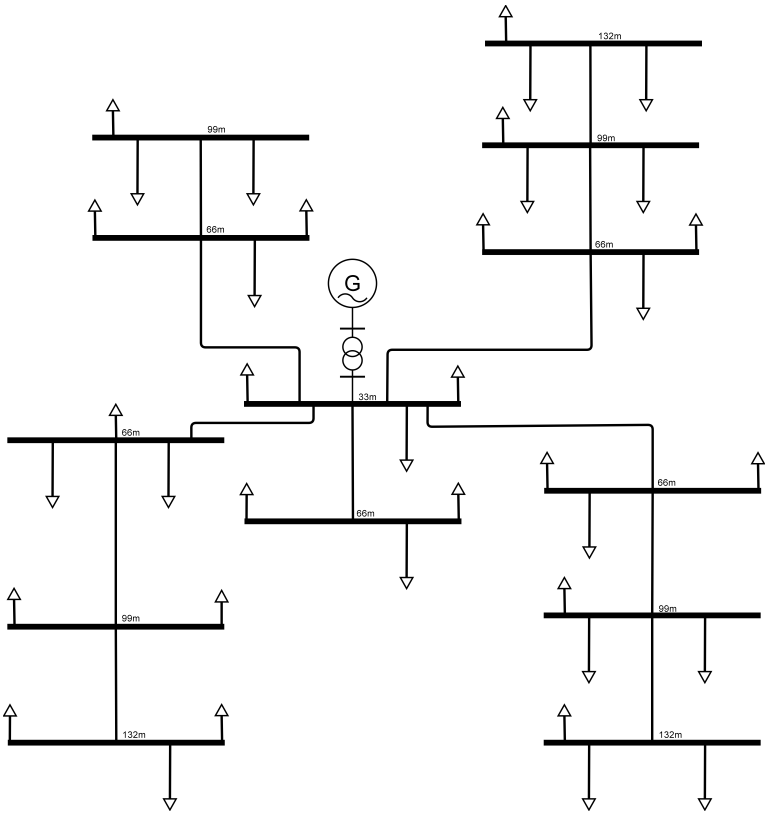

Figure 3.10: Radial branch network with extentions on four of the five feeders

3.9 Conclusion

The aim of this chapter was to determine what the network would look like based on the specifications found in the NRS 034-1. The network is deemed to be that of a three-phase network that operates on a voltage of 400 V rms. The network has a full load capacity of 315 kVA with a range of users from 20 to 40 units per network. The reticulation line lengths between each node within the network are calculated to be a length of 40 meters which is represented by the resistance and inductance values that characterise the transmission lines. Each node within the system is limited to three units to determine which network configuration is best suited for the implementation of intelligent control in the sense of that network being the network with the most to gain from intelligent control. A set of nine randomised networks have been designed based on the predetermined network parameters. The next chapter will discuss the simulation environment and the results obtained from simulating each of the nine networks at different renewable energy penetration implementations ranging from balanced to unbalanced generation implementation and creating worst-case scenarios in terms of load implementation.

Chapter 4

Simulation environment

4.1 Introduction

The contents of this chapter revolve around the computer-aided mathematical model of a low voltage distribution network. The mathematical model presented in chapter three will be implemented in MATLAB Simulink®. This chapter serves as the development phase of the digital wireframe for determining the optimal control to maximally increase the renewable energy penetration. The simulation will consist of all the mathematically modelled components in chapter three and the data-driven simulation components obtained from real-world implementations, including the predetermined SSEG components. The contents of this chapter will revolve around the simulated network characteristics of a low voltage residential energy network. The purpose is to develop a robust simulation model on which an intelligent computing algorithm can be implemented to simulate the prospective positive effects of an intelligent control scheme on the renewable energy penetration levels when paired with decentralised storage. The addition of aggregation is predicted to further the efficiency of the control scheme in terms of renewable energy penetration. This is due to the energy sharing capabilities that go along with it. The chapter will discuss the workings of the following systems within the network:

- Substation
- Reticulation lines
- Behind the meter microgrid
- The local control system
- The global control system

4.2 Simulation design

The simulation is divided into five defining components. The components are the power source, which represents the national grid. The reticulation lines transfer power over the reticulation lines from the substation to the PCC. The prosumers will be responsible for the consumption and generation of energy. The network is developed to simulate the effect of the energy production supplied by the grid in conjunction with the SSEG. The line loading effects, the effects of the reticulation line lengths at the various nodes on the network and the load on the network induced by residential consumers all affect the feeder voltage and, in turn, the level of safe renewable energy penetration. The critical component in this study is to evaluate voltage deviations at the various nodes within the network and the effect of both the positive and negative loading effects on the network induced by residential consumers.

4.2.1 National grid

The national grid consists of a three-phase power source configured in a delta configuration with a delta three-phase connection leading to the transformer. The three-phase source function block supplies power to a step-down transformer function block with the internal windings made up in a Dyn 11 configuration. The Dyn means that the high voltage side of the transformer is wired in a delta configuration, and the low side is connected in a star configuration with a neutral point. The 11 of Dyn 11 indicates that the secondary winding voltage leads the primary winding voltage by 30 degrees. This function block converts the medium three-phase voltage of 11 kV rms to a three-phase voltage of 400 V rms through three single-phase cores[35].The three phases will individually be used in the LV network to service the single-phase loads. The single-phase loads will be connected between the respective phase and neutral. All voltages measured between the phase and the neutral should read a nominal voltage of 230 V rms. The previous chapter specifies that the transformer's power capacity equals 315 kVA. The transformer is oversized for mitigating overloading in the system. The power source layout is evident in figure 4.2.

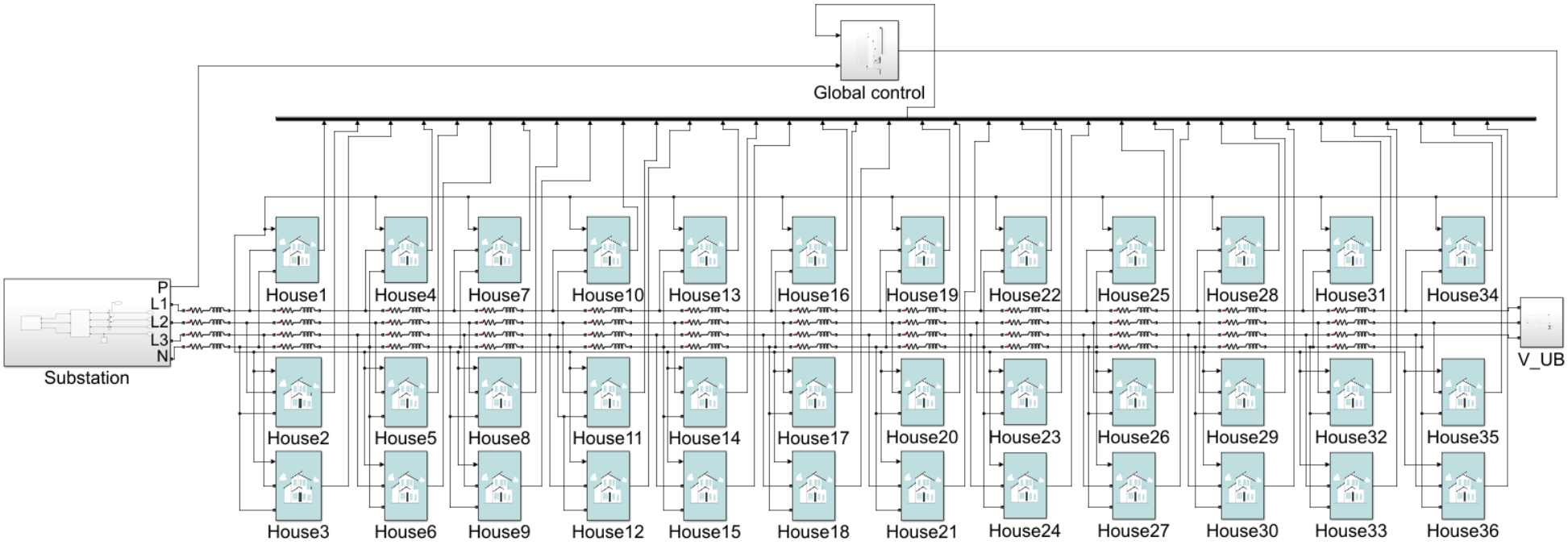

Figure 4.1: Single feeder network Simulink® model

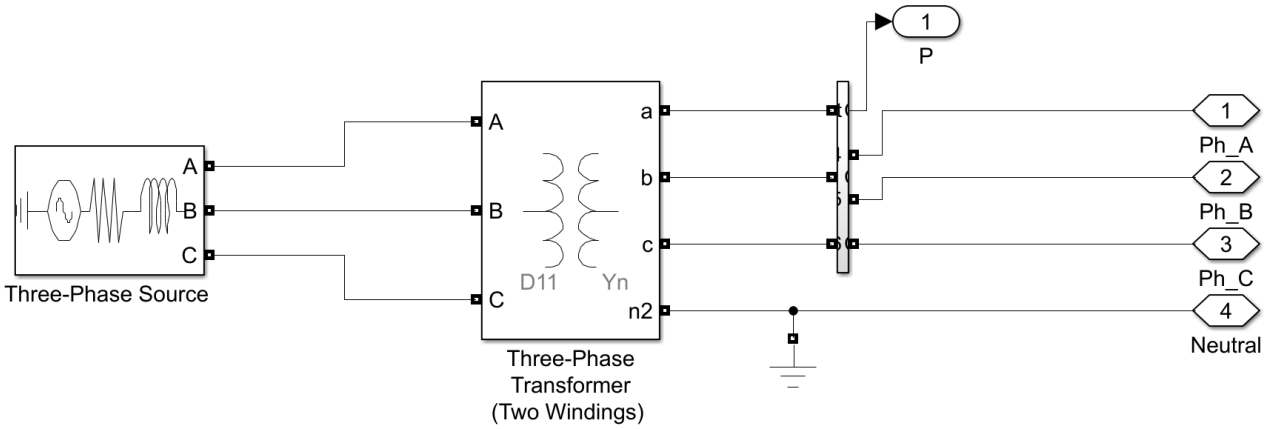

Figure 4.2: National grid model (power source)

The transformer parameters are obtained from the manufacturer's datasheet [36]. The primary winding has a per unit resistance of 0.000585 p.u. and an inductance of 0.017366 p.u. The secondary winding has a resistance of 0.002014 p.u. and an inductance of 0.017366p.u, whereas the magnetising impedance and inductance are equal to 108.47 p.u. The image displayed in figure 4.3 exhibits the internal workings of the power measurement bus.

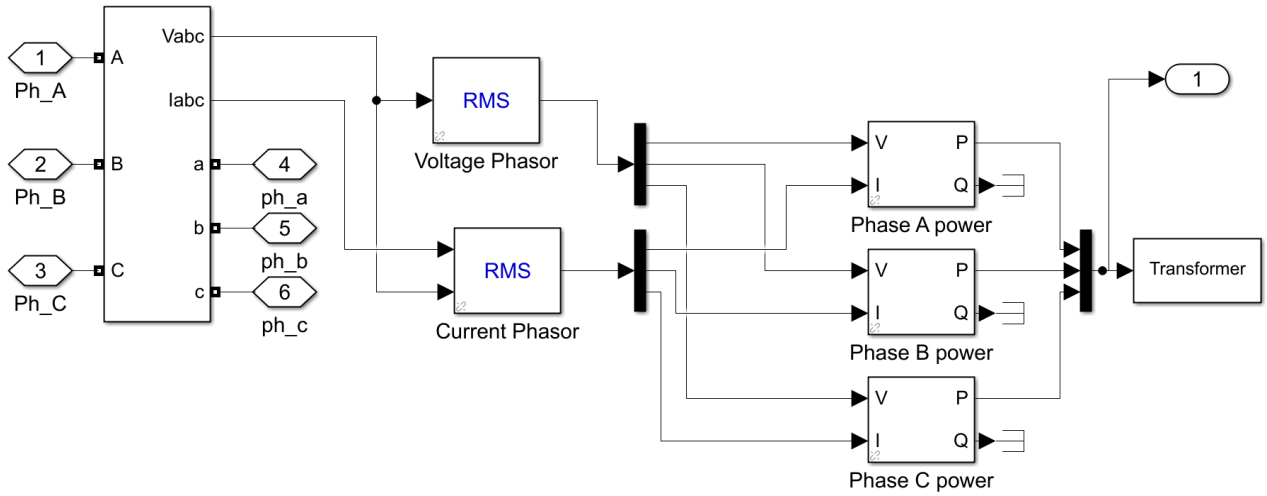

Figure 4.3: Power measurement bus model

The power-measurement bus function block utilises a three-phase IV measuring function block to measure the voltage relative to ground and the current at the transformer's LV side. The voltage is measured from phase to ground to determine the single-phase voltage. The voltage and current values are extracted from the function block in peak values. They must first be reduced to their respective rms values and converted to phasors to only work with their amplitude. In order to convert the Peak-to-Peak line voltage and current to true rms values, they first need to be fed into an rms function block, which then produces the respective rms

values.

The current rms function block had to be modified in order to display negative current values when energy is flowing in the reverse direction, from the LV network to the MV network. The reverse flow detection was implemented by means of measuring the phase angle of the single-phase currents. A 180-degree change in phase angle will indicate that the current flows in reverse. This phase shift will cause the rms current value to be multiplied by -1 to indicate negative current flow. After the true rms values are obtained, the signal is sent to a demultiplexer to split the voltage and current values into the three single-phase voltages and their accompanied current values. The values are then fed into a power conversion block converting the voltage and current values into active and reactive power values. For this thesis, the active power will be the only component analysed due to the assumption that the residential network is functioning at the unity power factor. The model is designed in such a manner that future tests can be conducted on the effects of reactive power control on the voltage levels and how it could improve the renewable energy penetration when all the units on the feeder are collectively controlled. The reason for measuring the power on the individual phases is to determine the loading on the transformer and the balancing between the phases. The different power components which collectively make up the apparent power is then sent to two locations. The first is to the global controller for data interpretation and decision making to control the units on the feeder partly based on the energy measurements at the transformer. The second location is the workspace for further possible data processing, and data visualisation will be done. The control implementation will utilise the transformer data node to monitor the power flow between the MV and LV networks to assist in decision-making for control.

4.2.2 Reticulation lines

The reticulation lines within the simulation model serve two primary purposes. The first purpose is to connect the national grid function block and all the residential unit function blocks. The second fundamental purpose is to model the characteristics of real-world reticulation lines, which includes line losses and accurate voltage drops. Real-world reticulation lines are constructed from either an aluminium or copper conductor. All conductors have some form of resistance due to the electron scattering off the vibrating ions within the material. As the vibrating ions speed up or slow down, the resistance changes. Reticulation lines also possess an inductance value which is the propensity of a conductor to oppose a change in the electric current flowing through it[37]. This flow of electrical energy creates a magnetic field around the conductor. Therefore, the reticulation lines are characterised in terms of their resistance

and inductance per meter of conductor. The impedance of the conductor directly correlates to the voltage drop within the line. The reticulation lines are modelled by three basic series RL circuits for the three-phase system with a shared neutral to simulate the effect of high neutral currents caused by unbalance in the feeder. The RL components for each line varies depending on the line length. The line impedance is negligible due to the line voltage and frequency and the fact that we assume the network operates at a unity power factor. The test conductor of 50mm^2 has a resistance of 15.8 $m\Omega$ and 12.64 μH respectively for each 40 m conductor length. The effect of increasing the length of the reticulation lines will also be evaluated. The tests will utilise decreasing conductor thicknesses as the loads decrease. The conductor thickness depends on the total load on the specific section of the feeder, meaning that the conductor at the end of the feeder will be 35mm^2 thick, and the conductor size at the beginning will be sized to carry the total load of the feeder. The neutral conductor will be the same size as the other conductors.

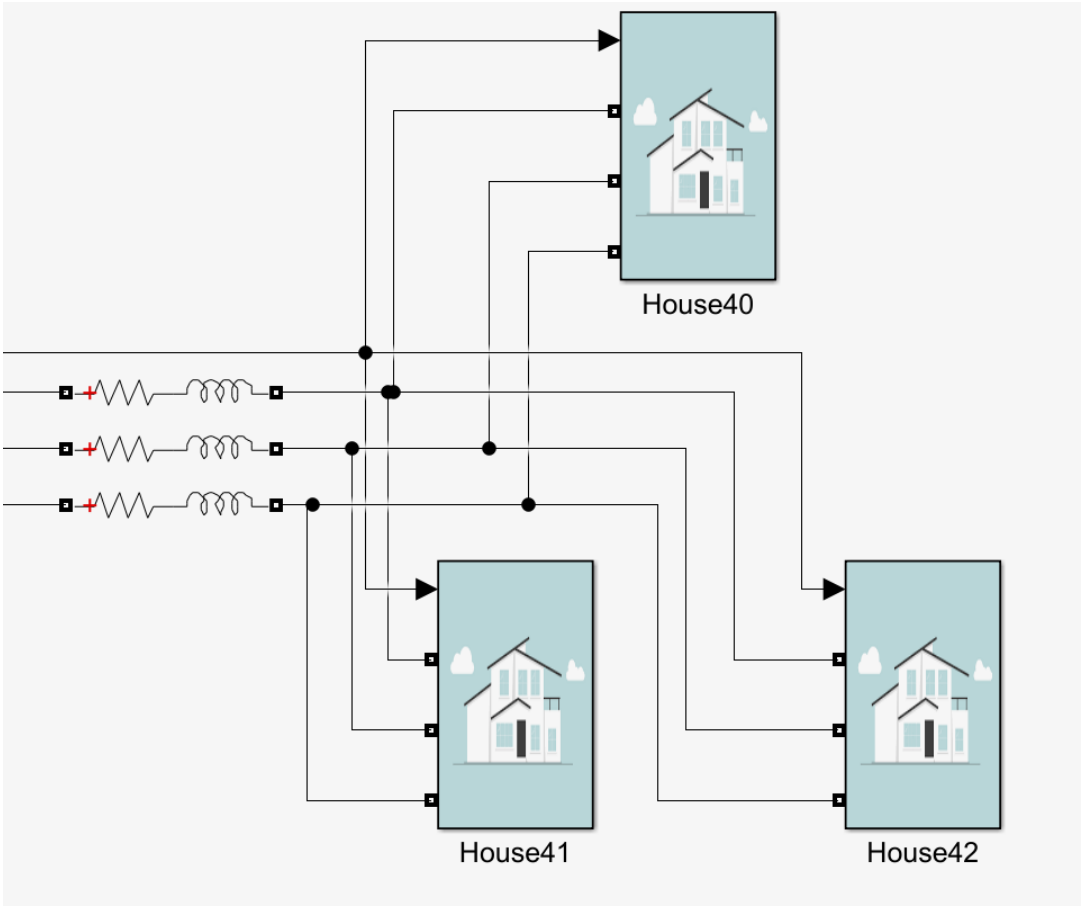

Figure 4.4: LV reticulation line model and unit masks

The reticulation lines in the various models will supply energy to both single-phase and three-phase loads. The presence of mutual inductance and coupling between phases will be neglected due to the infinitesimal. The reticulation lines will be joined by a communication line which

in this model is represented by two lines, one flowing into the unit providing information to the local system and one flowing out of the unit providing data to the global control system.

4.2.3 Microgrids

The microgrid consists of three components, the loads represented by real-world data, the distributed generation (DG) which is also represented by real-world generation curves and the ESS which is modelled by mathematical equations. Each microgrid receives its solar and load data from a lookup table synchronised with the simulation time to provide in-time data to be used in conjunction with the dynamic function blocks of the simulation environment. The microgrid will utilise the PV energy and the storage mediums to prioritise energy flow to the loads in normal operating conditions. The microgrid, also a house on the feeder, interconnects with a feeder live and neutral connection to a single-phase dynamic load. The single-phase dynamic has been modified from the three-phase dynamic load function block already available in Simulink®. The dynamic load is a current source that receives a current input value based on the value given to it by the synchronisation model. The synchronisation model accepts a reference input combination of active and reactive power. For this thesis, the active power is the only component utilised to indicate the load and generation. The active power reference provided to the single-phase dynamic load is the net power difference between the load, the PV and the ESS as indicated in (4.1):

$$P_{Grid} = P_{Load} - P_{PV} - P_{ESS} \tag{4.1}$$

Where P_{Grid} represents the power exchanged between the single-phase dynamic load(the house) and the grid. P_{load} represents the load over the 24 hours, and P_{PV} represents the energy generated by the local PV system. P_{ESS} represents the power exchange between the house and the ESS. This value can be positive or negative, depending on whether the system is charging or discharging. The ability of the ESS to charge or discharge is what makes it vital to the grid stability and power security since the ESS system can act as both a load and a generator when instructed to do so. It can also act as neither when required. The single-phase dynamic load is paralleled with a resistor to negate the discrepancies caused by connecting a current source in series with the reticulation line. The outputs of the single-phase dynamic load consist of the positive sequence voltage and the active power. The local controller will read the positive sequence voltage in the presence of SSEG to act according to the voltage on the node.

The local controller situated behind the meter at every unit on the feeder is responsible for

measuring the load data, the PV energy, the SOC of the battery, the active power exchanged between the unit and the network. The power reference from the global controller is also fed into the local controller. The microgrid architecture is displayed in figure 4.5

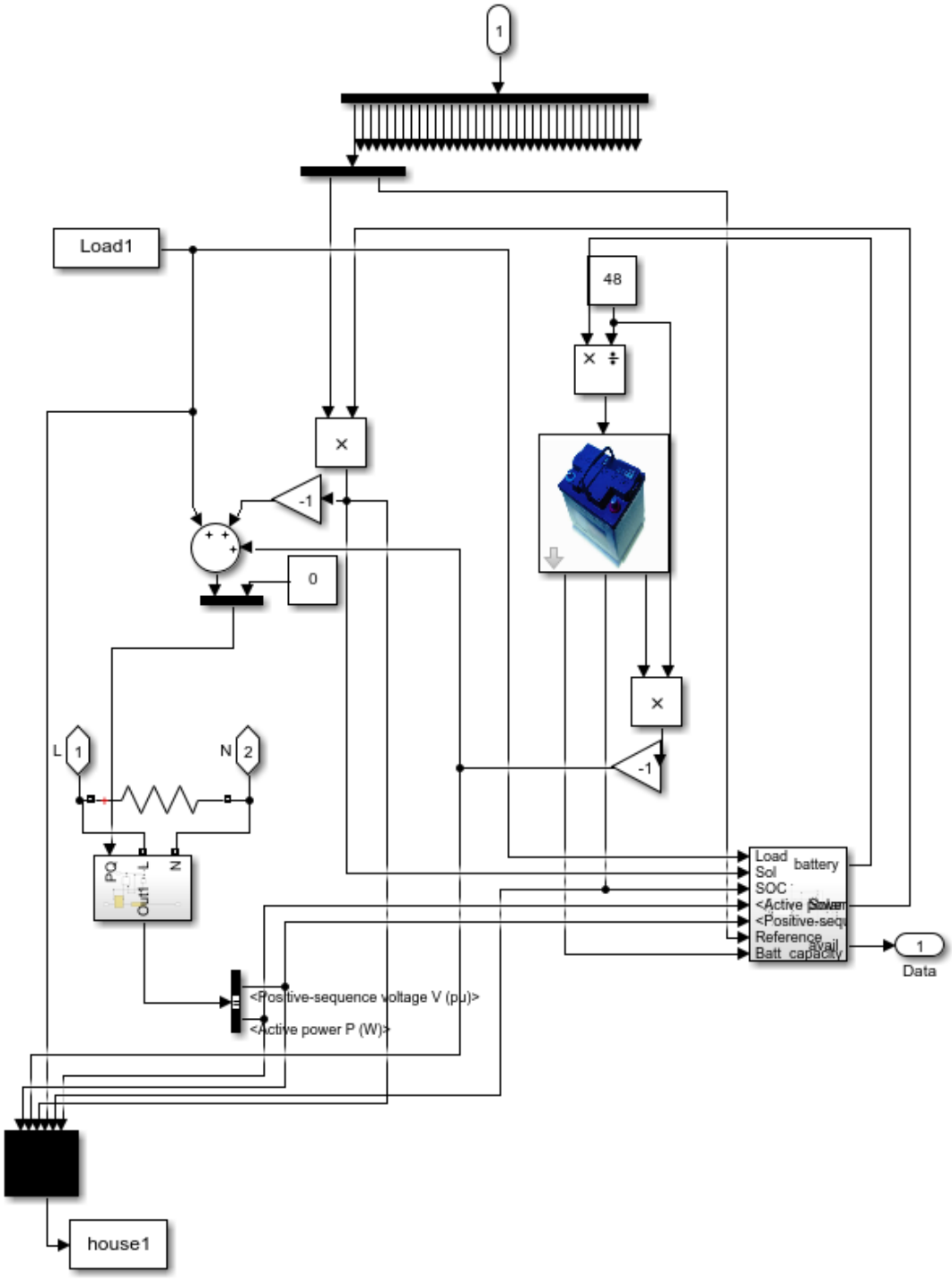

Figure 4.5: Generic household unit architecture (behind the meter)

4.2.3.1 Loads

Loads are at the centre of any power system, as there would be no generation in a system without loads. Loads affect the stability of a system and are at times unpredictable. However, we cannot live without loads since they form a vital part of our everyday life in the sense that every electrical appliance has a power draw and therefore serves as a load. The initial simulations will consist of the simulation of worst-case scenarios. These scenarios are divided into the four extremes of generation and consumption. The extreme conditions consist of maximum generation at minimum load, minimum generation at maximum load, maximum generation at maximum load and, lastly, minimum generation at minimum load. The extreme conditions will provide an understanding as to what affects the voltage levels across the network. Once the network has been characterised, the load and generation can be evaluated over 24 hours.

The accurate modelling of residential loads over a period of time requires real-world load data. In order to acquire a diversified load profile at the PCC originating from different usage profiles, it has been decided to assign a unique load profile to each house which will provide a better representation of real-world occurrences. This implementation method allows for a diverse load profile and adds to the uncertainty and unpredictability of the load at the PCC.

The use of the Herman-Beta method (HB method) will ensure that the loads are generated stochastically and with the proper dispersion according to the predetermined ADMD as specified in the NRS 034-1. The control can then be implemented along with incorporating the ESS to mitigate voltage deviations by controlling the PV curtailment and the power flow to and from the energy storage mediums. The loads are distributed so that a portion of the loads is more dominant in the early mornings and late afternoons. In contrast, the other load profiles resemble the consumption of a family working from home or a lot of residential activity during the day due to intelligent appliances. Certain users are switching specific loads during the day to optimally self-consume the PV energy produced.

The accurate modelling of residential loads requires the use of real-world load data. In order to acquire a diversified load profile at the transformer originating from different usage profiles, it has been decided to utilise eight different load profiles, which will be altered in terms of peaks and baseload to obtain the same ADMD. This implementation method allows for a diverse load profile and adds to the uncertainty and unpredictability of the load as reflected by the transformer.

4.2.3.2 PV system

As specified earlier in the chapter, the implementation of the PV system can be seen as a basic power equation where the amount of power generated is subtracted from the load. As in the real world, the PV system is modelled as a current source that is synchronised to the voltage waveform. The PV bell curve is obtained from power data generated by an existing system. The bell curve represents the optimal generation of the system under real-world conditions meaning that the bell curve is not perfectly symmetrical. Instead, it has a minor imperfection that gives it its authenticity. The generation profile can be altered in any way, shape, or form to provide the desired results. This could be beneficial if the effect of summer or winter load profiles needs to be evaluated by changing the generation duration or generation amplitude or uncertainty in the generation needs to be created to simulate generation during cloudy days. Altering the generation profile is beneficial if the effects of different renewable energy penetration levels need to be evaluated.

The PV generation curve is one part of the input to the power calculation of single-phase dynamic load. The generation profile is uniform to all the units on the feeder due to their proximity to one another. The only difference in each unit's generation output is that the local controller controls the generation intensity by curtailing the generation output when needed. This allows for improved energy management due to the fine energy control that is able to take place during the generation periods.

4.2.3.3 Energy storage system

The ESS is modelled by means of a combination of mathematical equations. The battery model is a basic model and does not account for derating due to temperature or high discharge currents. The model does not take into effect the ageing of the ESS. The non-linear voltage characteristics are also not taken into effect. The voltage effect will also be neglected, and the nominal voltage of the ESS will be utilised as the reference voltage. The battery takes an input value in the form of a current. The problem, however, is that the controller provides a reference value in the form of power. The power value is then divided by the nominal battery voltage in order to acquire the current reference. The current reference is then run through a saturation block which represents the battery management system (BMS) of the lithium battery. This saturation block will prohibit the battery from exceeding the current limit. The battery, in this case, is limited to a 0.5C rating which limits the battery's maximum demand to half of its capacity. The current value then proceeds from the saturation block to three sections within the battery. The first section is the output current section. The output

current section equates to the input current while the input current adheres to the saturation limits. The output current is only allowed through when the SOC is situated between 99% and 5%. If the SOC values violate the SOC limits, the ESS will put out a zero current. The second section is the amp-hour determination section. The system uses the input current to calculate the energy in amp-hours passed through the battery. The integrator function block integrates the current in order to acquire the current over time. The issue, however, is that the simulation iterates every minute, and the value needs to be converted to amp-hours which is why the integrated value is divided by sixty, which is the equivalent minutes in one hour. The amp-hour formula is displayed in (4.2).

$$Ah(t) = \frac{\int_0^t I\, dt}{60} \tag{4.2}$$

The third and final section is the section utilised to determine the SOC of the ESS. The SOC is determined by means of taking the input current and derating it in order to represent the charging and discharging efficiency of the ESS. The derated current is then integrated concerning time and compared to the initial state of the ESS. The available Ah value is then divided by the product of 60 minutes and the total capacity of the ESS. This provides the difference in SOC between the current battery state and the full battery state. The fraction is then subtracted from 1 and multiplied by 100 in order to obtain the ESS SOC. The formula for determining the SOC is displayed in (4.3).

$$f(t) = \begin{cases} \dot{x}(t) = u(t) \\ y(t) = x(t) \end{cases} \qquad x(t_0) = Ah * SoC * 60 \tag{4.3}$$

Where the $u(t)$ represents the block input and $y(t)$ represents the block output and $x(t)$ is the block state and $x(t_0)$ represents the initial condition of the function block. The output of the function block is then divided by the battery's capacity and time constant, which yields the SOC difference as a fraction of one. The value is then subtracted from one to obtain the true SOC value and subsequently multiplied by 100 to obtain the SOC value as a percentage. The process is exhibited in (4.4):

$$SOC(t) = 100(1 - (\frac{y(t)}{Ah * 60})) \tag{4.4}$$

The complete working of the ESS model is exhibited in figure 4.6

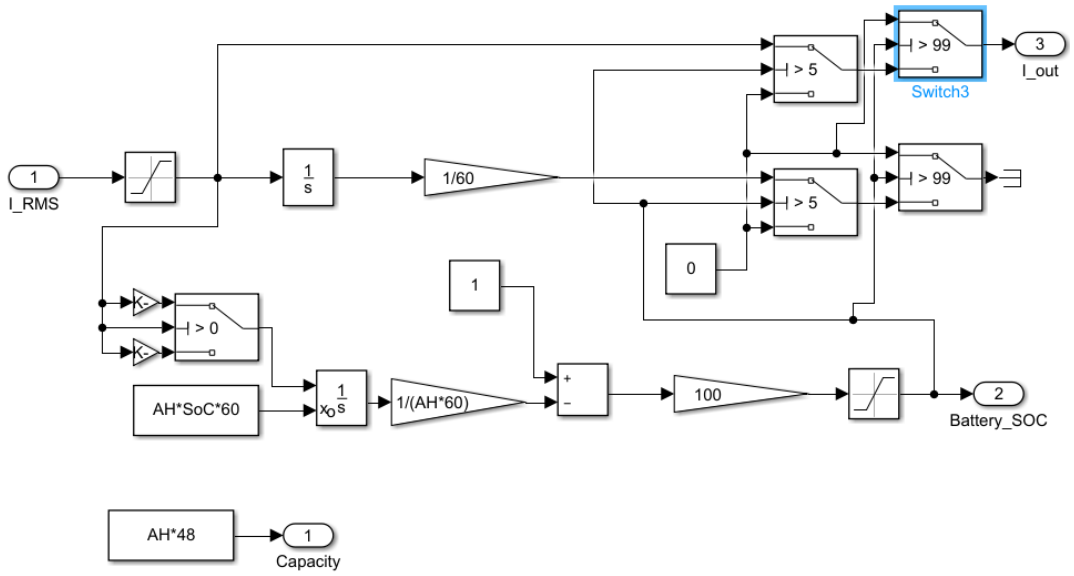

Figure 4.6: Simulink® ESS model

4.2.3.4 Local control

The PV system and ESS on their own or collectively need some form of supervisory control that can efficiently manage the energy behind the meter as efficiently as possible. The idea was to create a controller situated behind the meter, which would be henceforth called a local controller. The local controller would be responsible for controlling the energy flow favouring optimal self-consumption if there is no instruction from the global controller. The local controller would also be responsible for adhering to the immediate regulatory conditions, which are pre-programmed into the hardware within the system. The inverters come pre-programmed from the manufacturers with the grid codes of the specific country in which they will be utilised. The local controller will look at the load, the SOC, the instantaneous solar production, the node voltage, the battery capacity, and the global controller's reference power if there is one. The local controller interprets the local data available to it and provides three outputs. The first output is the power of the PV inverter to provide a power reference. The second output will be to the battery inverter to provide a power reference and energy state, meaning whether the power reference is a charging reference or a discharging reference. The third output will be the data output that relays data back to the global controller in order for the global controller to know what is happening at that specific node and the available resources at that node. The architecture is displayed in figure 4.7. The layout and architecture are complete. The method for how the local controller will manage the energy will be discussed in the control development chapter.

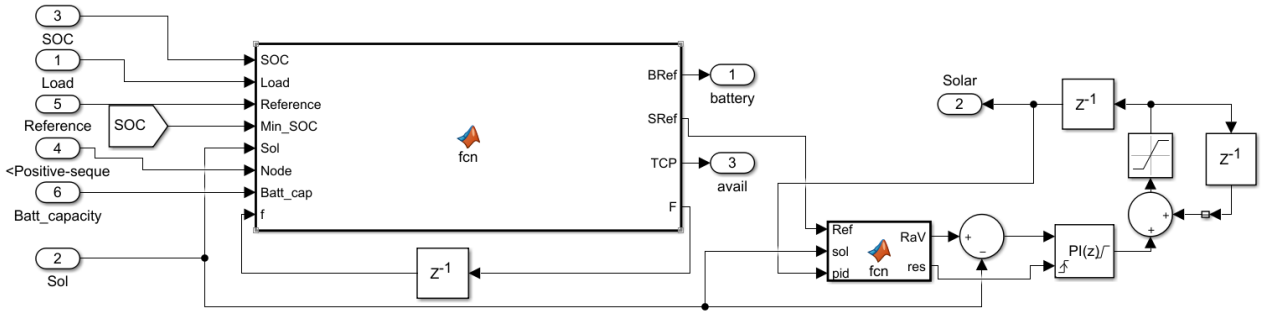

Figure 4.7: Local controller Simulink® block diagram

4.2.4 Global control

This thesis aims to increase renewable energy penetration by means of implementing virtual power plants. A virtual power plant requires a global control infrastructure to measure and control energy resources collectively. The control architecture is more complex than the local control architecture because the controller is working with units on different phases, and all the units have unique load and generation profiles that affect the capacity level of their ESS. For this purpose, the global controller needs to aggregate all the data it receives and categorise the aggregated data to determine the total aggregated energy and the energy available on individual units. The global controller will receive all the essential data from all the units in its portfolio. The data will then be sorted and aggregated, and decisions will be made as to how the reference energy for each unit in the portfolio needs to be in order for the energy to be maximally utilised and efficiently distributed on the feeder. The global controller architecture is evident in figure 4.8.

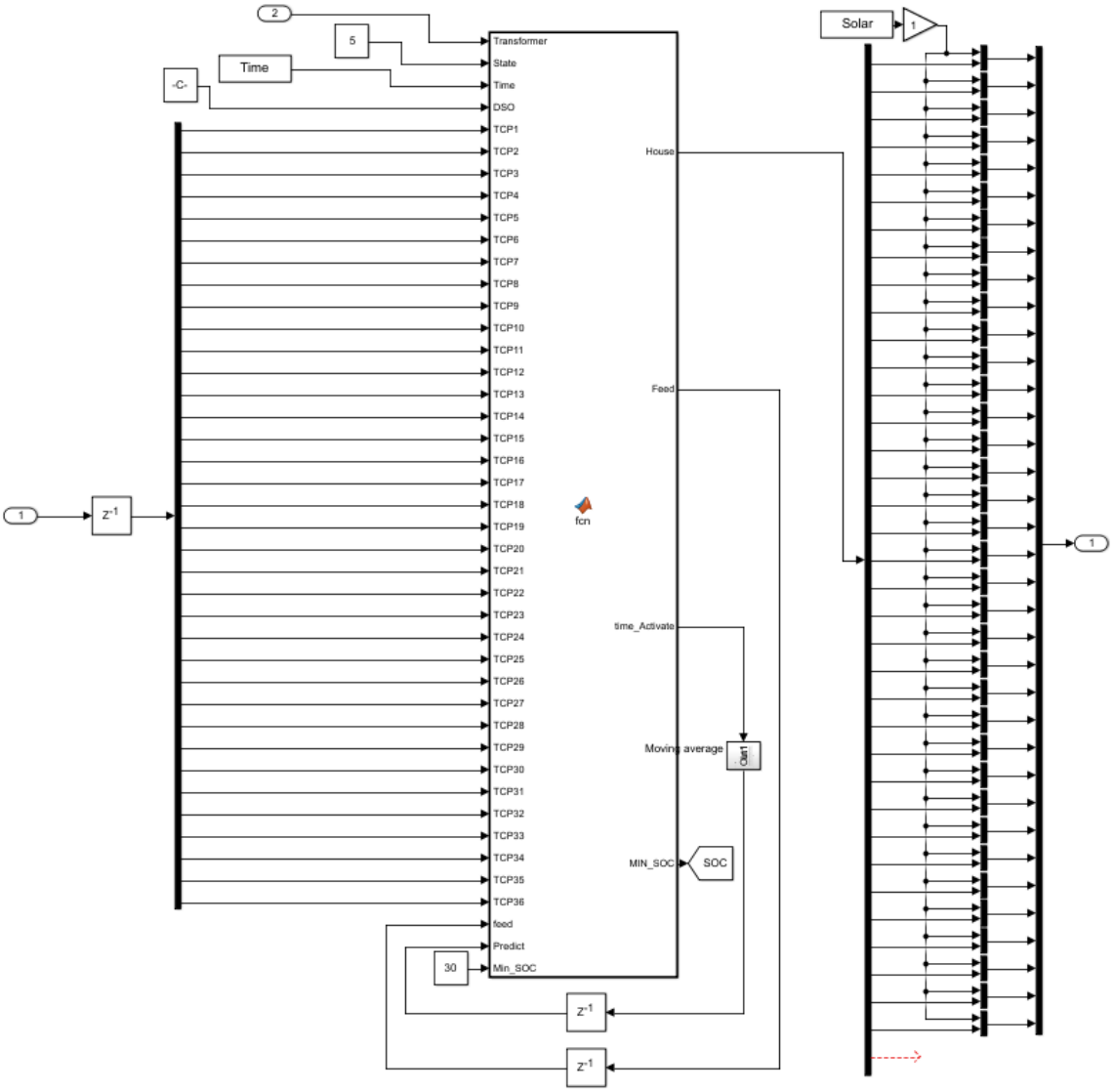

Figure 4.8: Global (VPP) controller Simulink® block diagram

4.3 Conclusion

The results in this chapter conclude that the appropriate steps were followed to create a simulation model on which the model workings can be verified and validated. Once the model has been validated, the control development and analysis can commence determining if the proposed method of control can improve the safety and surety that is typically lacking with the increase of renewable energy penetration levels. The model also must regulate the voltage to remain within the limits while the penetration levels are incrementally increased. The next chapter will characterise the models and conduct a validation experiment on the chosen model to determine if the data produced by the model is trustworthy enough to deem it valid.

Chapter 5

Model finalization and validation

5.1 Introduction

This chapter provides the necessary information and techniques to accurately model a low voltage distribution network capable of simulating the effects of renewable energy penetration on the feeder voltage on each phase of the feeder. The chapter will contain the assumptions made and the methodologies used in order to accurately design the active LV network in order to mimic the characteristics of a real-world active LV feeder.

An accurate LV feeder design ensures an acceptable voltage quality at the various nodes across the feeder. The standardised approach utilised to design LV feeders based on worst-case scenarios in South Africa is the HB method. The HB method is the recommended and the nationally accepted method used for voltage drop calculations LV as per the SANS 507, and NRS 034 [31].

The HB method is viewed as a probabilistic voltage drop calculation tool utilised to transform current values, assumed to be beta distributed, into beta-distributed voltage drops. A definite indication that the algorithm is considered a transformation based on analytical statistics should be made. Transformation based on analytical statistics axiomatically indicates that it includes the effects of diversity. The HB method is designed to calculate the voltage drop for three different networks, of which only the three-phase and single-phase typologies will be evaluated.

5.2 Model classification

Developing a simulation model to mimic the characteristics of a real-world implementation is not always as straightforward as it seems since all the variables are unknown to the designer. A set of assumptions will thus be made under which the model will be developed when the real-world data are unavailable to the designer.

The assumptions that form the basis for both this model and the adjusted HB method for the active LV feeder design as stated by [38] are as follows:

1. The maximum voltage drop occurs at the point of highest unbalance between phases at the interval of maximum demand for the selected consumers.
2. Current sources represent the loads at unity power factor synchronizing to the voltages since the loads tend to unity power factor at the maximum demand.
3. At any specified point in time, the cumulative loads may be modelled statistically to represent a beta probability density function (PDF).
4. At a specific instance in time, the load currents are assumed to be independently distributed. This is valid if the statistic is considered at a single time interval.
5. LV feeder impedance is viewed as predominantly resistive at a specified temperature. The feeders in question typically have small reactances (phase spacing about 200 m for bare conductors and less than 20 mm for aerial bundled conductors and underground conductors).
6. DG is represented in the network as negative loads by drawing negative power.

Now that awareness has been generated of the assumptions, the construction of the three-phase LV feeder can commence. This experiment will be conducted on a base-case calibration network example provided in the NRS 034. The accurate modelling of the distribution network is represented as a three-phase four-wire LV distribution feeder. The simple electric circuit diagram of a single section of the three-phase feeder is displayed in 5.1. The simplified three-phase four-wire LV network will be used as a building block for the network to be utilised for this experiment. The simplified circuit diagram indicates that four components make up the feeder.

The MV/LV transformer connects to four feeder conductors, consisting of the three main phases and a single neutral line connected to ground, and at the end of the line, the consumer loads are situated. The transformer sizing will be equivalent to the collective ADMD of all loads on the network. The reticulation lines are represented as resistance sources. The reticulation line's resistance depends on the conductor's size and the length of the conductor.

The loads and generators will be represented by current sources drawing or injecting the net power difference between the generation and consumption of the prosumers concerning the network.

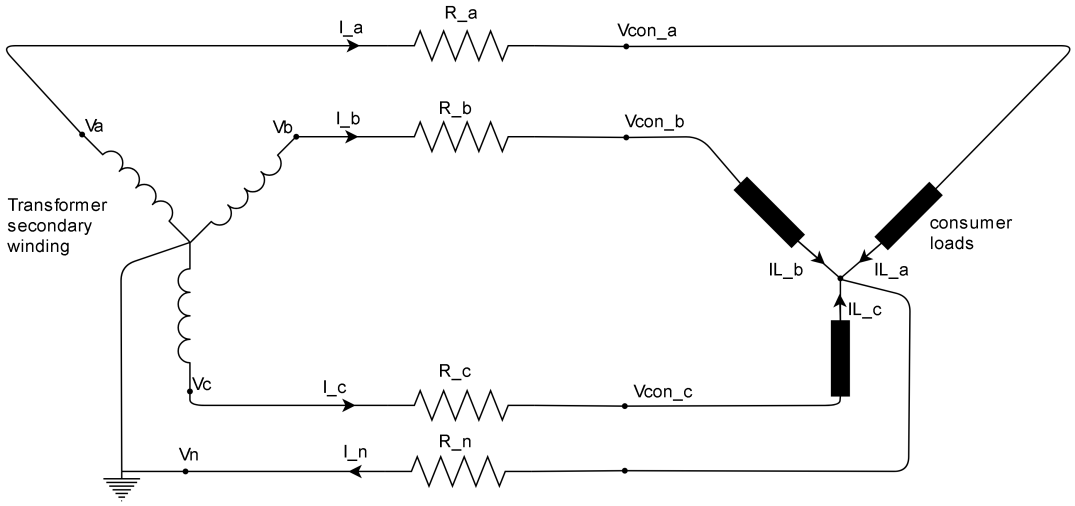

Figure 5.1: 3-phase 4 wire simplified LV network derived from [38]

The model verification will be conducted by means of comparing the results obtained from the same feeder model simulated in two different simulation methods. The first method is the basic HB method for calculating the voltage drop on an active LV feeder with renewable energy present. The second method is to evaluate the effects of the same conditions on the feeder voltage by actively simulating the LV network in Simulink®.

The purpose of this test is to conduct a worst-case scenario test concerning the PV penetration and voltage drop testing. The base-case model found in [39] represents that of the example networks provided by the NRS 034 to be used for data validation and verification. The representative feeder displayed in figure 5.2 has been adjusted from the NRS model in order to evaluate the effect that DER might have on the feeder voltage and power.

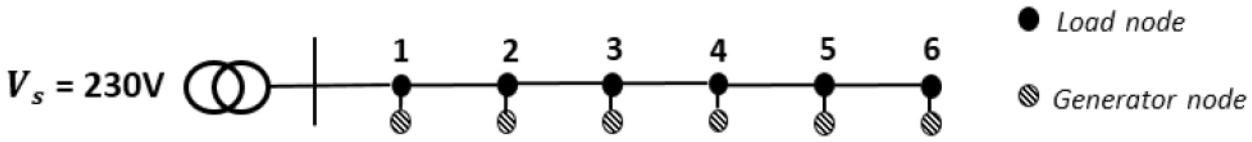

Figure 5.2: Verification feeder [39]

This radial feeder network is 360 m long with a node separation length of 60 m. The feeder is a three-phase feeder with an rms voltage of 230 V from phase to ground, with the reticulation

line being a 35 mm^2 underground copper conductor. Each node constitutes three customers, with the total number of customers being 18. The generalised consumer profile for this test will be generated from a Beta PDF. The Beta PDF is generated from the data accumulated in the NRS load research project. The load data are based upon residential consumers living in South Africa accumulated over several years.

Previously, the DG data were not readily available, which resulted in the reference case utilizing a beta PDF in order to model the generation in the worst-case, meaning maximum generation at minimum consumption. Today, however, the data has become more readily available due to irradiation charts and renewable energy becoming a force for change. This enables researchers to utilise real-world PV generation curves to conduct data-driven simulations to simulate different scenarios effectively.

5.2.1 PV and load variation

Real-world situations dictate that the PV generation is stochastic, and the same can be said for the demand. The certainty of PV generation has improved over the years due to intelligent forecasting techniques reaching a prediction certainty of 90% [40]. For this test, however, the photovoltaic distributed generation (PV-DG) limit is determined by the lowest aggregated consumption and the highest amount of aggregated PV production.

The advantage of conducting a worst-case scenario test is that it will confidently indicate that the odds of landing in these scenarios are small. When the odds are satisfied, it would be apparent if the network would handle the levels of renewable energy occupying the network. When conducted incorrectly, the disadvantage of conducting the worst-case scenario test (minimum load - maximum DG) is that it would typically lead to under design of the DG penetration limit. Under designing is caused by the fact that minimum load and maximum generation are not concurrent [41]. The stochastic nature of PV-DG has a significant impact on the voltage level of the residential feeder. The adverse effect on the voltage regulation is caused by the fact that the load profile is typically inversely proportional to the generation, meaning that at times of zero generation, the load is high. At noon, the consumption is typically low due to the lack of consumers while the generation is at its peak [42]. There is, however, speculation in the industry that when PV-DG is installed, consumers tend to alter their consumption patterns by employing intelligent energy control devices. The latter would optimise their consumption to coincide with the generation, which, in turn, allows for efficient energy consumption. [43] Indicates that the improvement in the energy efficiency of certain appliances leads to an alteration in the shape of the load profiles. For example, lighting tech-

nology has improved from incandescent technology to efficient LED technology over the past ten years, replacing conventional stoves with gas-powered stovetops.

The improvement in energy efficiency means that the weighting effect of the relevant appliances on the load profile has decreased and even changed the profile completely. There are, however, still appliances that have high energy consumption profiles both during the night and daytime. The importance, therefore, lies in conducting a test at the four worst scenarios, zero-generation at low-load, zero-generation at high-load, high-generation at high-load, and finally high-generation at low-load. These four points are depicted in figure 5.3.

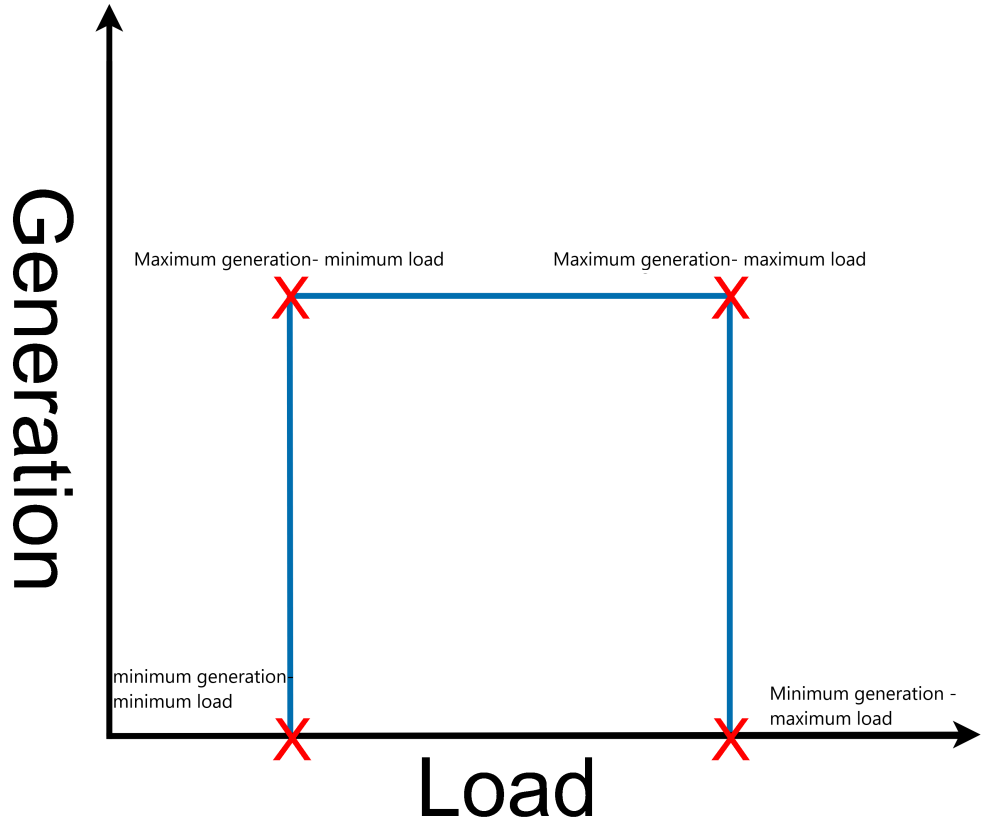

Figure 5.3: Illustration of the four worst-case load-generation scenarios

The worst-case scenario MATLAB simulations will be conducted on the physical model simulated in Simulink® by means of taking data snapshots at different penetration levels and then monitoring the voltage drop at these different levels of renewable energy penetration as opposed to the mathematical method utilised in [39].

When comparing the implementation of the DG sources in both models, it is evident that even though the generation in both models are represented as negative loads to be deducted from the positive loads. The Simulink® model does basic power calculations by subtracting

the generated power from the load power and injecting or extracting the net power difference with regards to the network. The reason is that the losses between the DER and the loads are ignored due to their proximity to one another. Power loss will only come into effect when the generators and loads are situated further than 100m apart.

The sole use of the HB method requires the PV generation curve to be converted into a Beta distribution in order to obtain the α, β, and C value. The C value, in this case, is considered to be the maximum current rating of the main circuit breaker. These values will then be used as a representation of the DER in the HB method in the same manner as in the Simulink® LV feeder simulation where the DER is considered to be a negative load.

5.2.1.1 Power factor

The base case simulations are conducted assuming that the load is at a unity power factor. It is stated in the research conducted by R. Herman and C.T. Gaunt in 2008 that the reason for the unity power factor is due to the fact that the majority of the high load appliances are resistive. The assumption was validated by data supplied by the South African utilities during times of peak loading. Times have changed, and with the implementation of inverter-based heating and cooling systems and LP gas-powered cooking systems, the use of purely resistive appliances consuming the majority of the energy at times of high load has decreased.

The increase in inverter-based heat pumps has resulted in a study evaluating the effect of these appliances on the power factor in the LV network [44]. The study conducted power quality tests on six different heat pumps. Among the heat pumps, some functioned on the conventional direct online method, and others utilised inverter-based Power Factor correction (PFC) technology to increase the efficiency of the system. The inverter-based heat pumps ranged from low-cost systems to high-grade systems. The results obtained indicated that the conventional heat pump has a high lagging power factor, as expected. However, due to the modern technological advancements in power electronics, the assumption can be made that these heat pumps are phased out, and that only inverter-based heat pumps remain available to purchase.

The tests conducted on the inverter-based heat pumps indicated that at low loads, the low-cost heat pumps have a high lagging power factor which, however, does not have a substantial effect on the general power factor of the consumer. In contrast, the low-cost inverter heat pumps have a low capacitive power factor at high loads, meaning that the general power factor also tends to unity. The tests conducted on the top of the range heat pump indicate that at low load, the heat pump has a low lagging power factor, and with the increase in load, the

power factor tends to unity.

The fact that heat pumps are used for water heating and air conditioning applications indicate that the results also apply to airconditioning units. The tests, therefore, conclude that the assumption still stands that at maximum load, the power factor tends to unity regardless of the implementation of new or old technology.

The power factor in the modern era is not only affected by the load anymore but the generation as well or, to be more specific, the DG. The implemented technology in conjunction with the operating conditions affects the power factor. The various generators consist of synchronous and asynchronous machines, whereas static generators are inverter-based generators consisting of power electronic technology. Inertial energy generators tend to deliver active power while absorbing reactive power, whereas static generators generate power at unity power factor but are likely to induce harmonics in the network. The research will be conducted on PV based generation and will utilise inverters as the interface between the generator and the network [45].

Modern inverter technology can run at a leading or lagging power factor. Some inverters can even operate at a zero power factor, be it leading or lagging. These functionalities can increase the effectiveness of voltage regulation, reduce energy losses and result in a near unity power factor. The improvements on the LV networks are, however, not spectacular since the control of active power has a more noticeable effect on the voltage regulation than reactive power control has on the voltage regulation [46]. The assumption, therefore, still stands that the network operates at unity power factor (pf) provided that the DG implemented is that of PV.

5.2.1.2 Renewable energy penetration

RS097-2-3 stipulates that each consumer's specified PV-DG capacity is restricted to a pre-determined percentage of the consumer's NMD depending on the configuration of the LV network on which the consumer is situated. This is due to the adverse effects that renewable energy penetration might have on the distribution grid when left ungoverned. The restrictions may be waived in particular cases with the necessary approval. Approval, however, is only possible after a grid impact study has deemed it to be safe to install additional PV-DG. The purpose of a grid impact study is to establish whether the network can handle the additional renewable energy generation or if the grid needs reinforcement before any additional renewable energy may be added to the existing infrastructure.

When simulating the effects of renewable energy penetration over 24 hours, the typical PV power production curve would resemble that of a bell curve as displayed in figure 5.4. The

PV penetration will, however, be simulated at the DG systems maximum power production interval. For this test, it is assumed that the PV-DG system has an efficiency of 80% concerning the total installed capacity. The 20% efficiency loss is due to conversion losses induced by the power electronics and external environmental factors such as deviating from Standard Test Conditions (STC). Therefore, it is evident that renewable energy production is not equal to the installed generation capacity. This, in turn, means that the renewable energy penetration capacity and the installed RES capacity are not the same. Therefore, it is assumed that the renewable energy penetration is directly equivalent to the maximum power rating of the inverter, and the installed generation potential is equal to 120% of the inverters power rating.

This verification simulation will be conducted to take data snapshots at different penetration levels. Therefore, it is evident that the PV power curve is unnecessary when taking data snapshots due to the lack of variation in power.

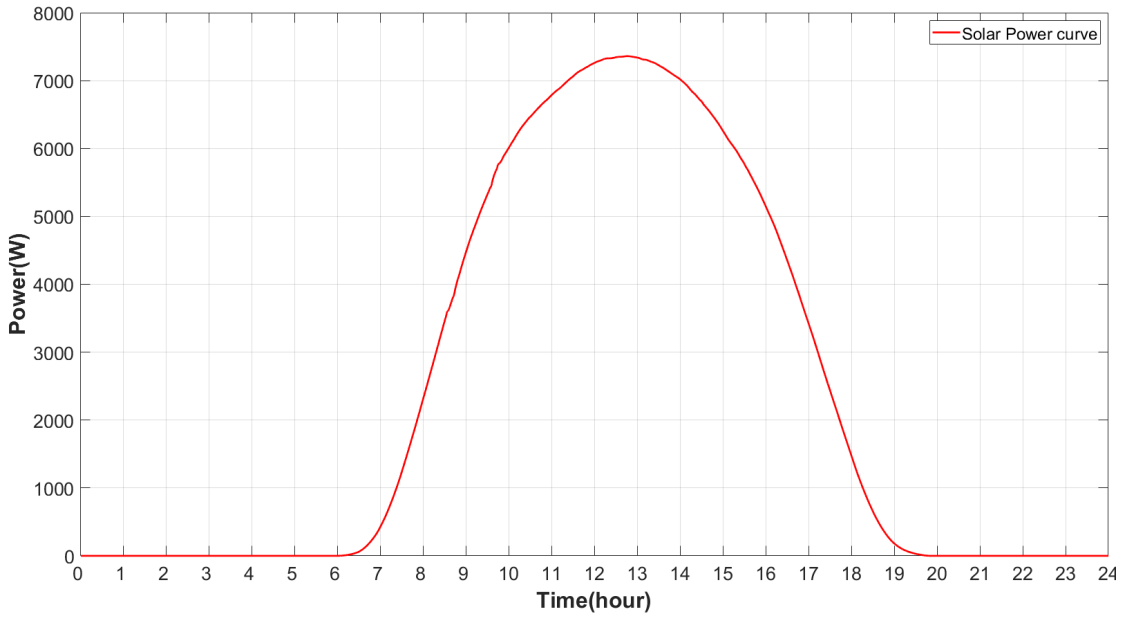

Figure 5.4: Ideal PV generation curve for worst case simulations

The maximum size definitions for LV feeder PV-DG capacity integration is stipulated as follows:

- **Shared LV feeder**(typical in normal residential areas)
  The maximum generation capacity should be equal to or less than 25% of the consumer's NMD
- **Dedicated LV feeders** (typical in light commercial, industrial and agricultural areas)
  The maximum generation capacity should be no greater than 75% of the consumer's

NMD

The difference between the base case simulation in [39] and the base case simulation in Simulink® is that the original base case is modelled solely by the Herman beta method, which is a form of deterministic LV feeder design through mathematical calculations. The HB method utilises a beta PDF that is considered the best fit for load data obtained from 10 years of load data acquired during the NRS load research project. The load data in question are based on residential energy consumption profiles in South Africa. The Simulink® model, on the other hand, is constructed from individual network components represented by their independent mathematical models. These components include a simulated energy source, a simulated MV/LV power transformer with a capacity equal to the ADMD of the consumers on the LV network, transmission lines modelled by resistors, and lastly, the prosumers modelled by single-phase dynamic loads as described in the model development chapter. The mathematical model in [39] only utilises the Herman beta method to accurately simulate the effects of renewable energy penetration and loads on the LV network.

Figure 5.5 illustrates a prediction of what is to be expected when the renewable energy penetration on a feeder increases. The increase in photovoltaic embedded generation (PV-EG) increases the feeder voltage. The increase in voltage is due to the fact that the positive energy flow decreases, ultimately resulting in negative energy, which leads to a rise in the feeder voltage.

Renewable energy penetration is represented as %EG/ADMD. This is due to the scalability of the feeder capacity, commonly referred to as the ADMD. The reason for this being is due to the utilised ratio being dependent upon two values. The values in question are:

- embedded generation (EG) – the aggregation of the rated capacity of the grid-tied PV-EG units.
- ADMD – After Diversity Maximum Demand is the average aggregated load of all the consumers situated on the feeder, usually the winter load demand is utilised to design the LV feeder.

The utilization of the %EG/ADMD as the determining variable simplifies the process of evaluating the effect of voltage deviation at different ratios as the ratio is adapted as the ADMD changes or the EG changes meaning that the results can be scaled accordingly. Variation in ADMD and EG can mean many different possible generation, load, and positioning combinations that generate similar results. For this reason, it is of vital importance to simulate the worst possible conditions in order to form an envelope in which any possible results might fall.

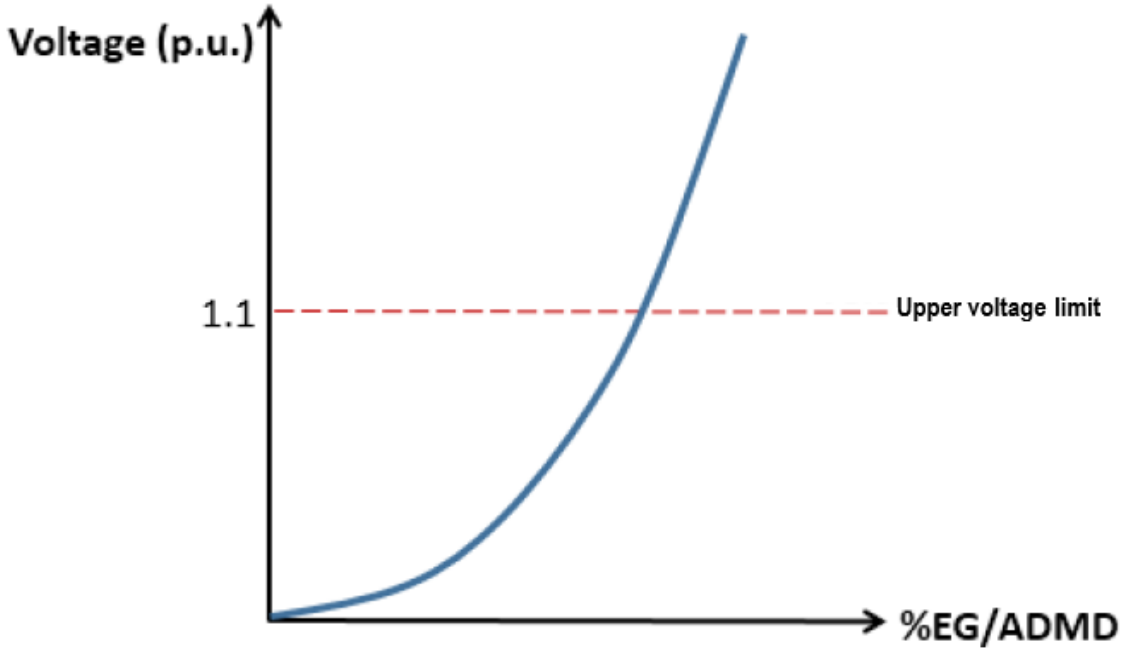

Figure 5.5: A representation of the correlation between the renewable energy penetration and feeder voltage [39]

In order to obtain maximally accurate, reliable and reproducible results that can serve as an extension of a real-world LV distribution system, the following assumptions and considerations are made:

1. The maximum installable generation capacity a prosumer may install at their residence is restricted to 50% of the nominal connection capacity of the residence. The nominal connection capacity is represented by the current rating of the main circuit breaker. This restriction is only valid for the validation tests, after which the restriction will be raised to 100%. The existing guideline is as stated in the NRS 097-2.
2. All PV systems are located in an optimal position to allow for maximum energy generation.
3. At the period of maximum energy generation, the PV systems provide 100% of the rated output power at ideal operating conditions. This is due to the 80% efficiency rule, which accounts for the conversion inefficiencies when converting from direct current (DC) to AC in the inverter. The DC generation is sized up to 120% of the inverter capacity by design.

These assumptions are in addition to those that underlie the HB method for active and passive LV feeders.

The reference model that will be mimicked in this section is acquired from the example models

set out by the NRS 034 as validation models. The model is useless if not populated with data representing a real-life feeder network. It is of vital importance to design the network for the desired scenario, and in order to do this, Emanual utilised the process as stated :

- Step 1: Design the desired passive LV feeder, utilising the winter load ADMD Beta parameters (α, β and c), for the maximum voltage drop (10%) for the required test scenario.
- Step 2: Locate the interval of maximum excess generation from the summer load and PV data. Obtain the beta parameters for this interval – summer load beta parameters. Replace the winter load beta parameters with the summer beta parameters on the feeder to generate a more significant delta between the load and generation.
- Step 3: Calculate the maximum PV generation capacity that a household can install by utilising the following formula: $\frac{0.5\times\text{Circuit breaker size}}{\text{rated PV output current}}$. The total aggregated PV capacity is calculated as the product of the total number of customers and the maximum generation capacity per customer.
- Step 4: At increasing penetration level :
  Calculate the total ADMD value of the feeder using $ADMD = \frac{\alpha\times\text{number of customers }\times V_s\times c}{(\alpha+\beta)}$ and calculate the %EG/ADMD = $\frac{\text{Power rating of connected PV}\times 100}{ADMD}$.
- Step 5: Plot the results as a scatter plot on Voltage (p.u.) vs %EG/ADMD graph.

The worst-case scenario MATLAB simulations will be conducted on the physical model simulated in Simulink® by means of taking data snapshots at various penetration levels and then monitoring the voltage drop at these different levels of renewable energy penetration as opposed to the mathematical method utilised in [39].

The similarity between the two different environments is that both these models utilise the same Beta probability distribution to model random loads that together equal the predetermined winter ADMD as displayed in 5.1. The data evident in 5.1 is a representation of the Beta probability distribution that represents the worst-case and best-case load profiles of the base case simulation. The best-case load profile matches that of a typical summer load profile and the worst-case load profile on which the average ADMD has based a winter load profile. The PV-DG beta parameters are also evident. These beta parameters will be utilised to represent a 1 kW single-phase PV-DG unit with the maximum PV capacity limit situated at 7 kW per consumer.

Table 5.1: Base case LV feeder parameters [39]

FEEDER PARAMETERS	VALUE		
Winter load ADMD beta parameters	$\alpha = 0.8625$	β=0.8625	c = 50.01270
Summer load beta parameters	$\alpha = 0.4366$	$\beta = 1.2877$	c = 24.8680
1-kW 1-phase PV unit beta parameters	$\alpha = 255.50$	β =255.50	c = 6.8696
Maximum number of PV units (per customer)	7		

5.3 Model validation

The base case, a simple 6-node radial feeder with 18 customers, is designed utilizing the winter load ADMD. The feeder conductor used is a 35 mm^2 4-core copper conductor, with the thermal limit of 143A considered to design the passive LV feeder. In order to carry out the voltage analysis of the active feeder with DG, the feeder load will be represented by the summer load beta parameters, particularly at the interval of maximum generation and minimum load. The feeder will be designed based on the total winter load, which is calculated as the total design feeder ADMD = $\mu_{\text{winter load}}$ $\times$ no. of customers = (15.677 $\times$ 0.23) $\times$ 18 = 64.90 kW. The feeder, designed for the winter load, will utilise the summer loading for worst-case scenario testing. The active feeder load will be calculated as total load (active feeder) = $\mu_{\text{summer load}}$ $\times$ no. of customers = (6.297 $\times$ 0.23) $\times$ 18 = 26.07 kW

The increase in PV penetration on a passive LV feeder results in a proportional increase in feeder voltage. This is because the active feeder load is exceeded at a PV generation capacity of 26.07 kW (approximately 40% EG/ADMD), which, at this point, results in reverse power flow on the feeder. The rise in feeder voltage at a penetration level below 40% EG/ADMD is due to the dispersion in demand between different consumers. The dispersion equals a standard deviation of 6.55 A at a mean of 6.30 A. One should also note that the random dispersion is implemented over the three different phases and will cause an unbalance on the feeder. The unbalance will cause a voltage rise on lightly loaded phases and a voltage drop on heavily loaded phases.

Exceeding the 40% EG/ADMD penetration point causes the feeder voltage to increase due to the reverse current flow with respect to the PCC as a result of the surplus energy generated. It is also important to note that the effect of dispersion in the load diminishes, as stated in the central limit theorem. This is as a result of the increasing ratio of generation to load. The feeder is considered full when each customer has installed the legal maximum PV capacity – 50% of their NMD. The full feeder indicates no unbalance meaning that all voltages across the phases and along the length of the feeder are balanced.

The randomised allocation of PV based generation is critical to the study's outcome as the nominal capacity and operation time are predetermined. The Monte Carlo simulation (MCS) test conducted in [39] used for voltage analysis of the active LV feeder with the random allocation of DG generated a scatter plot of possible maximum voltages on the feeder. The iterative random allocation generated a copious amount of data from a large number of runs. However, the data are unlikely to produce all the possible outcomes of PV-based Generation allocation combinations since the probability of successfully obtaining the correct allocation of both load and generation on the nodes and phases is minuscule. The maximal effect of unbalance in the voltage across the phases and the feeder length can be illustrated by means of deterministically allocating the PV-based generation to create the two extreme conditions consisting of voltage balance and unbalance.

The voltage unbalance in the LV feeder caused by the uncertainty in the allocation of PV-based generation is caused by the random allocation of said generation on:

- Different nodes along the feeder – Same phase
- Different nodes along the feeder – Different phases
- Corresponding nodes on the feeder – Different phases

The validation test is carried out on the Simulink® model in the same order as the reference model. The test will be carried out in the order as follows :

- The active LV feeder is configured with the betarnd function according to the summer beta parameters. The randomised load data are generated and implemented in a balanced fashion across the phases on the feeder.
- With a comprehension of the maximum generation capacity that a consumer can install on their household, the EG is incremented in 7 kW increments per phase. The PV is allocated in such a way as to establish an envelope to show the extreme limits of the most balanced allocations and the most unbalanced allocation.
- For the most unbalanced allocations, the procedure is as follows:
  - 7 units are placed on the red phase on the feeder's last node (node 6), and the maximum voltage on the feeder profile is recorded. The red phase is filled progressively with 7 kW each time from node 6 to node 1. For every 7 kW fill on the phase, the maximum voltage on the feeder profile is recorded.
  - Once the red phase is fully loaded with PV units, PV units are added to the white and blue phases progressively from the start of the feeder (node 1) to the end of the feeder (node 6), alternating EG allocation between the two phases with each iteration.
  - When every unit of every node on the feeder is assigned 7 kW of generation, the

feeder is considered full. The maximum voltage recordings are plotted on the graph to form the upper limit of the deterministic envelope.

This allocation is viewed as the most unbalanced allocation since each allocation of 7 kW of generation ensures that the most significant possible difference exists between the loaded and unloaded phases (in terms of voltage unbalance along the feeder length) as well as ensures the most significant difference in the amount of PV-based generation between the phases (for voltage unbalance across the phases).

- For the most balanced PV allocations, the allocation is as follows:
  - 7 kW of EG is placed on each phase (red, white and blue phases) at node 1 (start of the feeder). The total generation added to each node per iteration equals 21 kW, and the maximum voltage on the feeder profile is recorded. The nodes are loaded progressively from node 1 to node 6.
  - When 7 kW of generation is assigned to each node on every phase on the feeder, the feeder is then considered full and the maximum recorded voltage is plotted on the graph, which forms the lower limit of the deterministic envelope. This allocation method is the most balanced allocation because each 7 kW of generation allocation per phase maintains the balance between the phases and the implementation direction.

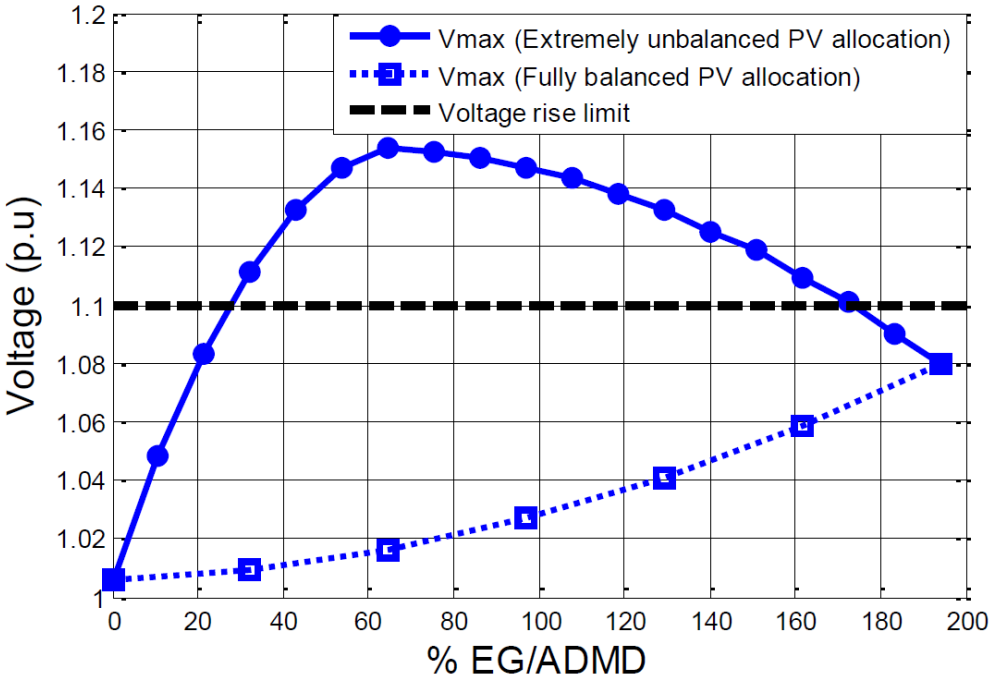

Figure 5.6: Reference worst-case voltage envelope from literature [39]

Both the maximum balance and unbalance of the reference study is displayed in figure 5.6.

It is evident from the graph that the unbalance on the feeder causes the phase voltage to significantly rise above the 1.1 p.u. limit compared to the balanced feeder. The voltage rise is mainly due to the unbalance in the network, causing high neutral currents, which increases the voltage delta across the phases.

The increase in renewable energy penetration causes the two plots to converge to a single point due to the PV capacity constraint (50% of the nominal household capacity). The diminishing effect of the random PV allocations on the feeder indicates the increased likelihood of the generation being more balanced across the phases and length of the feeder.

After conducting the test in the Simulink® environment with the summer load beta parameters and a transformer ADMD of 64.90 kW, the following worst-case voltage envelopes can be obtained under the same conditions as the reference experiment. The worst-case voltage envelope generated by the Simulink® model can be viewed in figure 5.7.

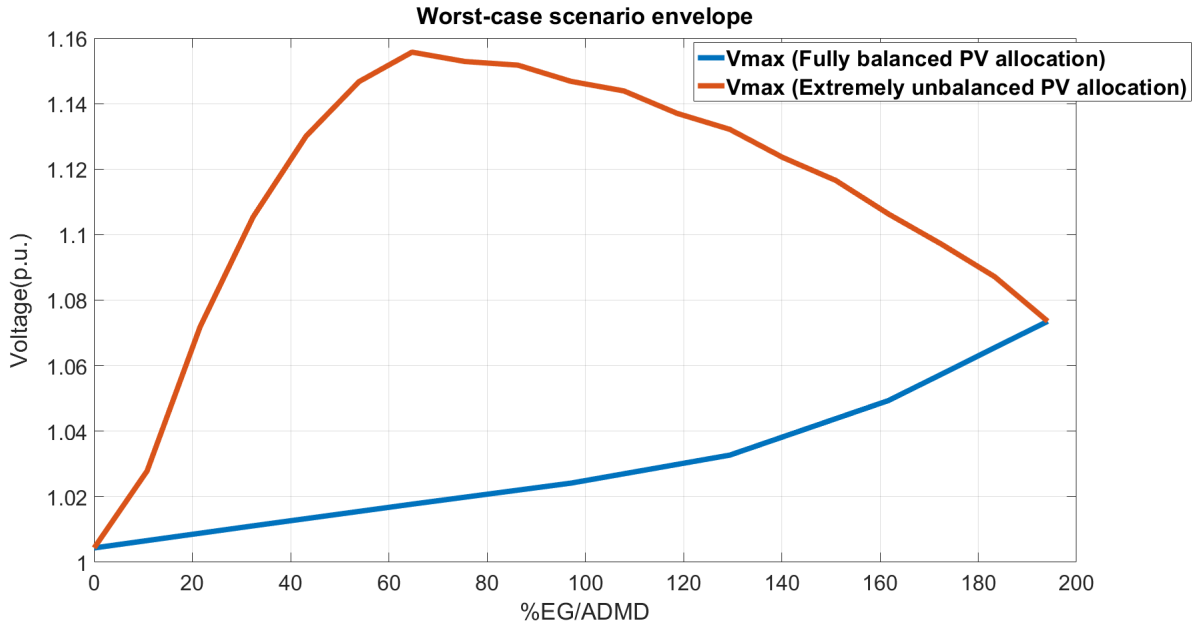

Figure 5.7: Simulink® model worst-case voltage envelope

Now that the reference envelope and model envelope has been established, they can be plotted over one another to ensure that the results correlate. With this, the results can be validated and, in turn, validate the correctness of the Simulink® model. The data displayed in figure 5.8 indicates the correlation between the reference data and the model obtained data. It is evident that the general shape of the two figures is a close match. However, there exists a slight offset in the data. The random load allocation causes this offset along the feeder generated by the *betarnd* MATLAB function and the effect of negating the effect of the distance between the EG and the loads at each unit on the LV feeder.

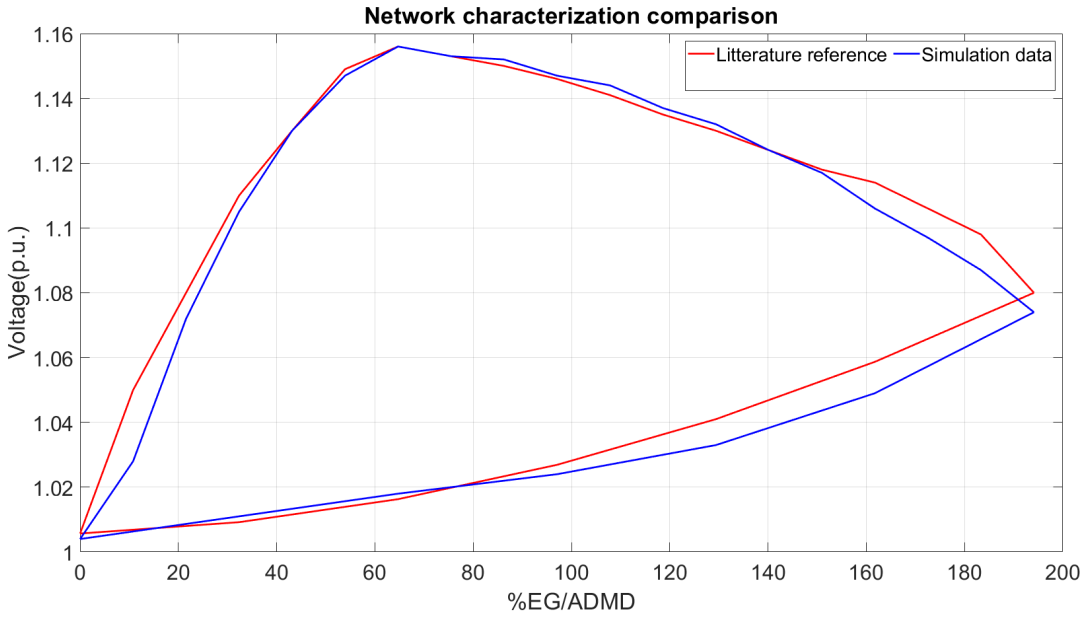

Figure 5.8: Worst-case voltage envelope comparison (literature vs simulated data)

The numerical comparison between the reference data and the simulation data at different renewable energy penetration levels for the balanced PV allocation can be obtained in table 5.2.

Table 5.2: Balanced PV allocation result comparison

PV generation on feeder [kW]	Penetration level [%EG/ADMD]	Reference maximum voltage on feeder profile [p.u.]	Maximum voltage on feeder profile [p.u.]
0	0.00	1.0057	1.0044
21	32.36	1.0092	1.0111
42	64.71	1.0163	1.0177
63	97.06	1.0269	1.0241
84	129.42	1.0410	1.0327
105	161.77	1.0587	1.0494
126	194.13	1.0799	1.0735

The numerical comparison between the reference data and the simulation data at different renewable energy penetration levels for the unbalanced PV allocation can be obtained in table 5.3

Table 5.3: Unbalanced PV allocation result comparison

PV generation on feeder [kW]	Penetration level [%EG/ADMD]	Reference maximum voltage on feeder profile [p.u.]	Maximum voltage on feeder profile [p.u.]
0	0.00	1.01	1.01
7	10.78	1.05	1.03
14	21.57	1.08	1.07
21	32.35	1.11	1.11
28	43.14	1.13	1.13
35	53.92	1.15	1.15
42	64.71	1.15	1.15
49	75.49	1.15	1.15
56	86.28	1.15	1.15
63	97.06	1.15	1.15
70	107.85	1.14	1.14
77	118.63	1.14	1.14
84	129.42	1.13	1.13
91	140.20	1.13	1.12
98	150.99	1.12	1.12
105	161.77	1.11	1.11
112	172.56	1.10	1.10
119	183.34	1.09	1.09
126	194.13	1.08	1.07

The work conducted in [39] and the data present in the NRS 034 played a crucial role in developing a validated dynamic Simulink® model. The validation of this model also symbolises the verification of this model due to the fact that the data obtained from the Simulink® model coincides with the data obtained from the Herman beta model in [39], which has been validated by real-world data and has been verified with the example models present in the NRS 034. This LV network model can be utilised to accurately model the effects of renewable energy penetration on LV networks. The model can be utilised to experiment with different network configurations and evaluate the effect of these configurations on the network. The list of potential experiments conducted on the network is endless due to many component parameters that can be altered to suit any application. Incorporating control functionalities opens up a list of possibilities, pushing for more intelligent networks and the transition to decentralised energy generation.

It is important to note that even though the base case simulation was conducted with only six nodes and 18 customers with a conductor thickness of 35 mm^2 and the ADMD of each customer was not equal to 4.5 kW, and the core fundamentals still apply as with any other network. When converting a network from a small conductor thickness to one with a larger conductor sizing, the correct line resistance value for the specific conductor thickness and length should be applied.

5.4 Network characterization

The model validation represents a crucial step in the research process, which indicates that the model is viewed as a tool that mimics the behaviour of a real-world LV network. However, the issue is that there is a variety of network topologies which in its self can be random. Defining specific parameters and assumptions is critical when characterizing different network topologies. To understand these parameters, an electrical network's workings first need to be defined and understood. A network is defined by specific characteristics such as the feeder type, the number of T-offs, the line length, the number of customers, and the conductor thickness. The network characterization will determine the effect of these parameters on the network voltage in both balanced and unbalanced generation conditions.

The list of assumptions made in the network characterization is that the total network length is limited to a maximum length of 500 meters from the point of connection to the furthest node on the feeder. The maximum number of T-offs per network is limited to five. The transformer size remains constant at 315 kVA with a feeder voltage of 241.5 V, translating to 1.05 p.u. The conductor thickness remains constant at 50 mm^2, and the consumers with an LSM of 8 will have an ADMD of 4.5 kW. The Beta parameters according to the NRS 034 for an ADMD of 4.5 kW are α=1.43, β=4,41 with a main circuit breaker capacity of 80 A. The beta parameters have to be adjusted due to the commonly implemented circuit breaker size of 60A. The adjustment conducted according to the NRS 034 yields new beta parameters of α=1.17, β=2.41 at 4.5 kW ADMD. The mean value of 19.57 A and the standard deviation of 13.15 A remain constant.

The network characterization procedure for characterizing the nine different predetermined networks are as follows:

1. The 4.5 kW adjusted beta parameters serve as inputs for the *betarnd* MATLAB function along with the number of units present on the feeder. The function generates an array of random current values between zero the main circuit breaker (MCB) size. This step is repeated until both the array mean and standard deviation is within 5% of the reference mean and standard deviation
2. The data in the array are arranged from low to high and allocated to the units in chronological order whilst the PV penetration remains zero
3. The simulation is initialised, and the three-phase feeder voltage profile is recorded.
4. PV based generation capacity of 7.36 kW (50% of NMD) is added to each unit on the feeder resulting in a balanced PV allocation. The simulation is initiated, and the three-phase feeder voltage profile is recorded

5. PV based generation capacity of 7.36 kW (50% of NMD) is added to each unit on the red phase of the feeder resulting in an unbalanced PV allocation. The simulation is initiated, and the three-phase feeder voltage profile is recorded
6. The load data is then re-arranged from low to high and implemented in chronological order across the feeder. The change in load position on the feeder will indicate the effect of the load on the feeder voltage in each network.
7. PV based generation capacity of 7.36 kW (50% of NMD) is added to each unit on the feeder resulting in a balanced PV allocation. The simulation is initiated, and the three-phase feeder voltage profile is recorded
8. PV based generation capacity of 7.36 kW (50% of NMD) is added to each unit on the red phase of the feeder resulting in an unbalanced PV allocation. The simulation is initiated, and the three-phase feeder voltage profile is recorded.
9. The six different feeder voltage profiles obtained are now plotted over each other in order to generate a worst-case voltage graph for each network typology. This graph aims to indicate the scenario at which the voltage deviation is highest and the magnitude of the voltage deviation.

The legend for each graph will remain constant for each network topology. The general graph legend will identify the different phases of each scenario generated by the different topologies. The general legend can be viewed in figure 5.9.

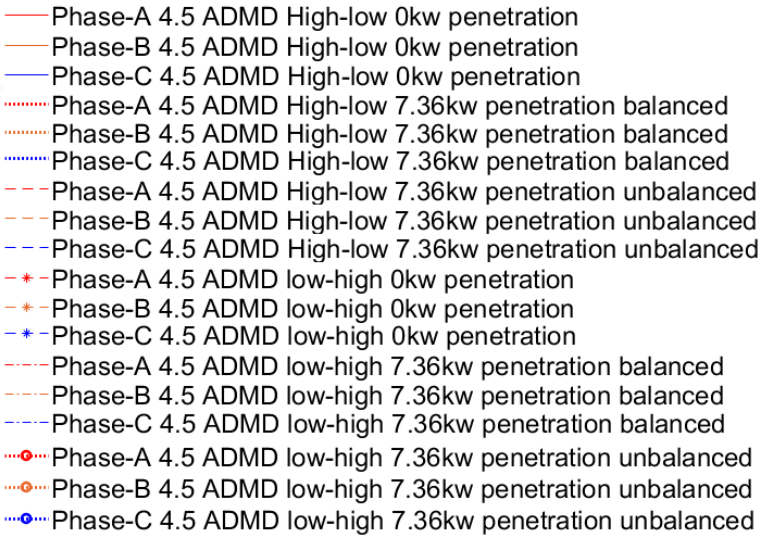

Figure 5.9: Generic legend denoting the test and phase data on the 9 test topologies

The initial network design will consist of 21 users and a single T-off. The units will be divided up that 15 users will be situated on the main radial feeder, and six users will be situated

on the T-off radial feeder. This feeder aims to evaluate if a single T-off feeder with minimal consumers alters the effect of renewable energy penetration on the Voltage regulation of said network. The distance between nodes remains constant at 40 meters resulting in a maximum feeder length of 200 meters and a collective ADMD of 94.5 kW, drawing on average 30% of the transformer capacity meaning that the approximate load factor is equal to that of the low consumption class.

The results obtained from the worst-case scenario test are displayed in figure 5.10. The data indicates that the upper voltage limit is violated at node three caused by the unbalance in the network. The data also indicates that the short T-off feeder has a minor voltage deviation compared to the long T-off feeder. The worst voltage deviations occur at both the low to high and high to low load allocation orders. The balanced PV allocation results in a significant voltage rise on the feeder, and the maximum voltage drop on the feeder in the absence of renewable energy drops below 1.02 p.u..

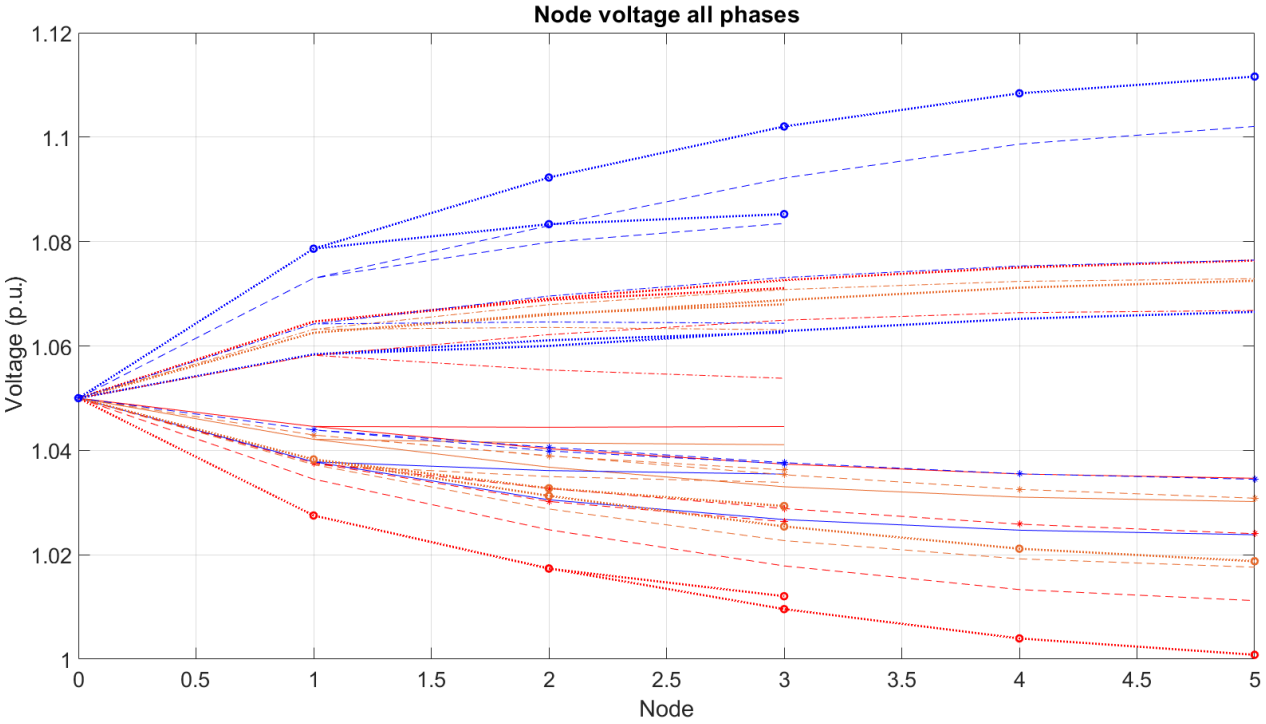

Figure 5.10: Single feeder dual branch network worst-case voltage deviation

The Spider feeder network evaluates the sole effects of T-offs on the network without altering the line length. The worst-case voltage graph displayed in figure 5.11 indicates that the increase in T-offs decreases the voltage variation due to the added reduction in the Thevenin equivalent resistance. The short feeder with the five T-offs does not violate the voltage limits of the feeder nor the feeder current limits due to the load dispersion on the feeder. The voltage

variations at the single node T-offs are within 1% of one another. This variation is mainly due to the load dispersion between the nodes on the feeders.

The worst-case voltage variations are once again generated at the interval of unbalanced PV allocation. The maxima and minima are present where the load allocation is arranged on the feeder in chronological order from low to high. These extremes are also evident in figure 5.11, which serves as a preliminary indicator that one of the worst-case conditions that the feeder may experience is the heavy unbalance in terms of PV allocation, and the load concentration being situated towards the rear of the feeder.

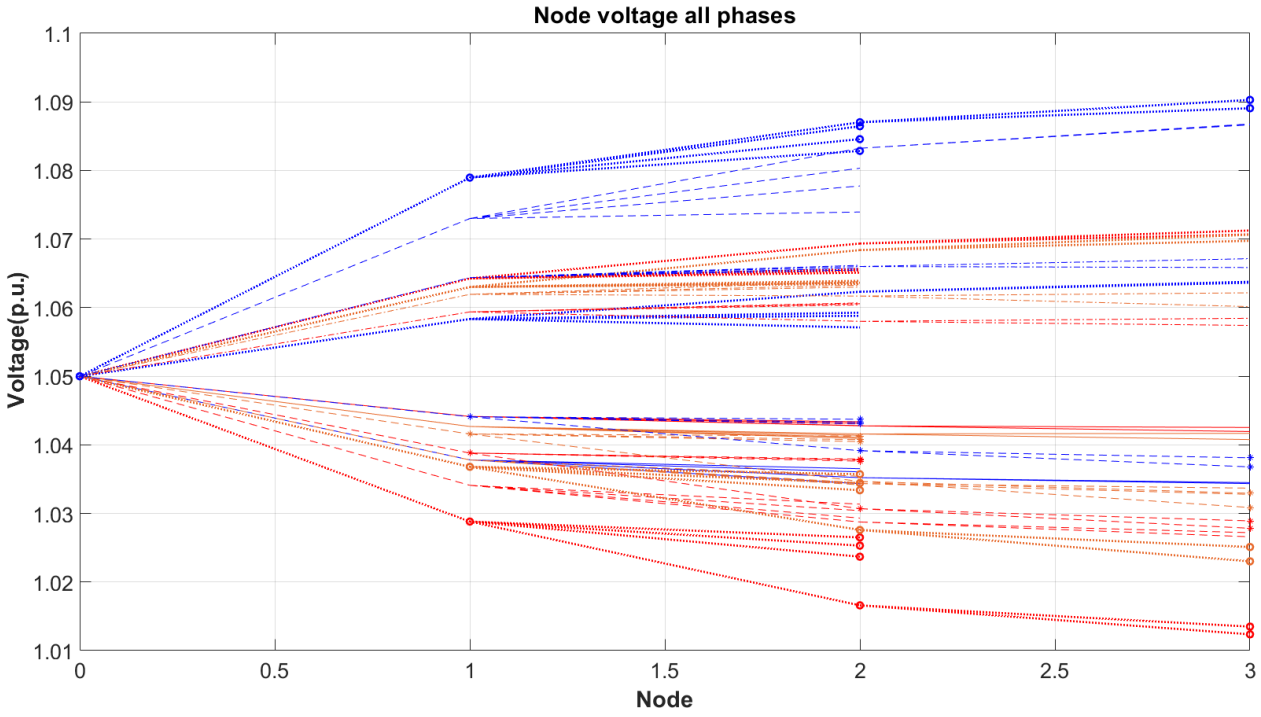

Figure 5.11: Spider feeder network worst-case voltage deviation

The spider feeder network with an extended shared feeder evaluates the effect of increasing the feeder length on a single T-off while the other feeders remain unchanged. The total number of units on the feeder increased from 21 to 39 units due to the addition of 18 units on the main radial feeder. The increase in units also increases the collective ADMD in the feeder to 175.5 kW resulting in a load factor of 55,7%. The increased load factor indicates that the feeder has moved up to a high consumption class. The data exhibited in figure 5.12 denotes a rise in feeder voltage is due to the increase in line length. The increase in line length increases the feeder's Thevenin equivalent resistance. A change in network resistance directly correlates to a change in the deviation amplitude of the feeder voltage. The change is due to the effect of the resistance within the network. The voltage deviations on the short T-offs remain within

the voltage limits.

On the other hand, the lengthened feeder violates the top voltage limits at both balanced and unbalanced PV allocation implementations. The balanced PV implementation only violates the upper voltage limit on phase C when the loads are arranged from low to high on the feeder. The unbalanced generation allocation violates the upper voltage limit for both the low to high and high to low load allocations. The low to high load allocation results in the highest voltage deviation. The low to high load allocation paired with unbalanced renewable energy penetration leads to the worst-case conditions. The voltage violations indicate that this network is deemed suitable for control implementation.

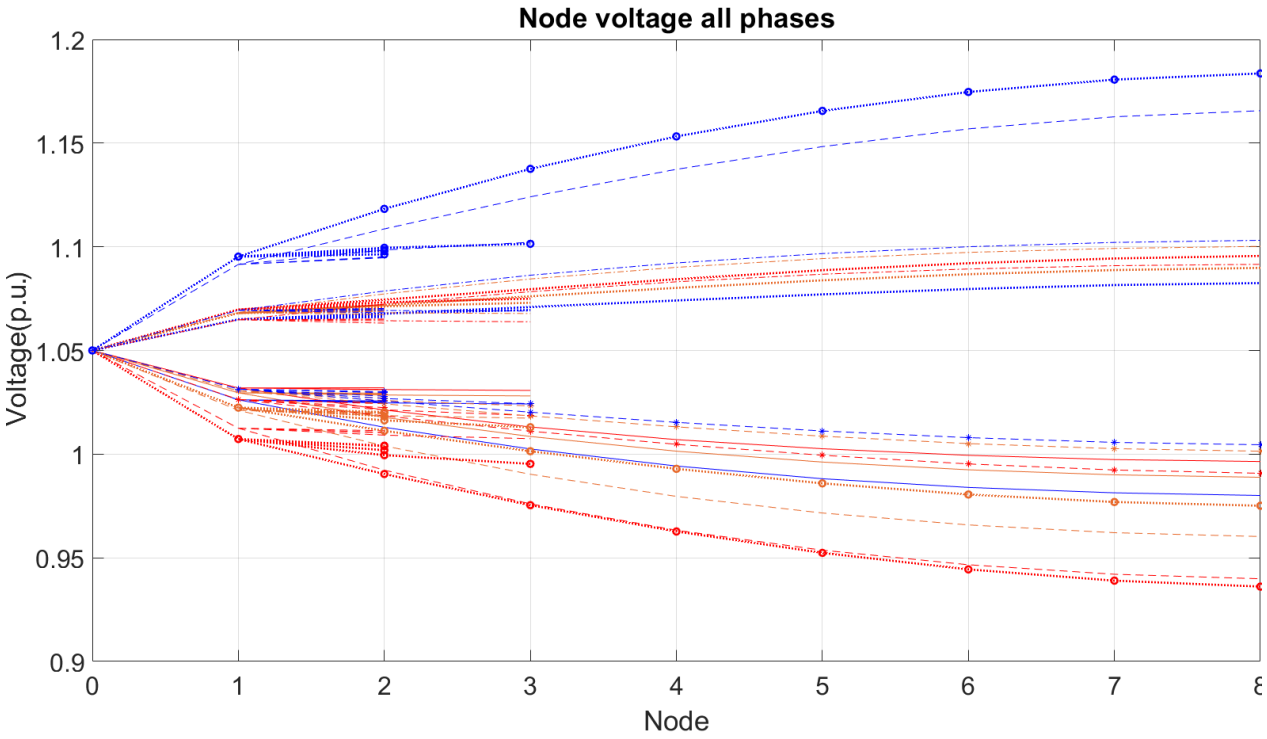

Figure 5.12: Spider feeder network with an extended shared feeder worst-case voltage deviation

The three feeder network with varying unit quantities evaluates the effect of T-offs positioned at different nodes along the length of the feeder while not exceeding the T-off limit of five T-offs. The feeder length of this network is situated at 280 m with a total number of 33 units. The data exhibited in figure 5.13 denotes the effect of T-offs on the feeder voltage profile. The results indicate that the feeder voltage violates the upper voltage limit in the balanced and unbalanced generation allocation scenario. The data indicates that the position of the T-off on the feeder affects the voltage level of the T-offs. The T-off, however, does not affect the voltage of the node that it is connected to.

Interestingly, the T-off feeder voltage on a phase with a rising voltage profile is always lower than the feeder it is connected to, and the T-off voltage on a phase with a decreasing voltage profile is always higher than the feeder it is connected to. The unbalanced generation allocation with a low to high load allocation yields a maximum voltage level of 1.174 p.u. exceeding the upper voltage limit by 7.4%. The results, therefore, indicate that this network can be categorised as a suitable network for control implementation.

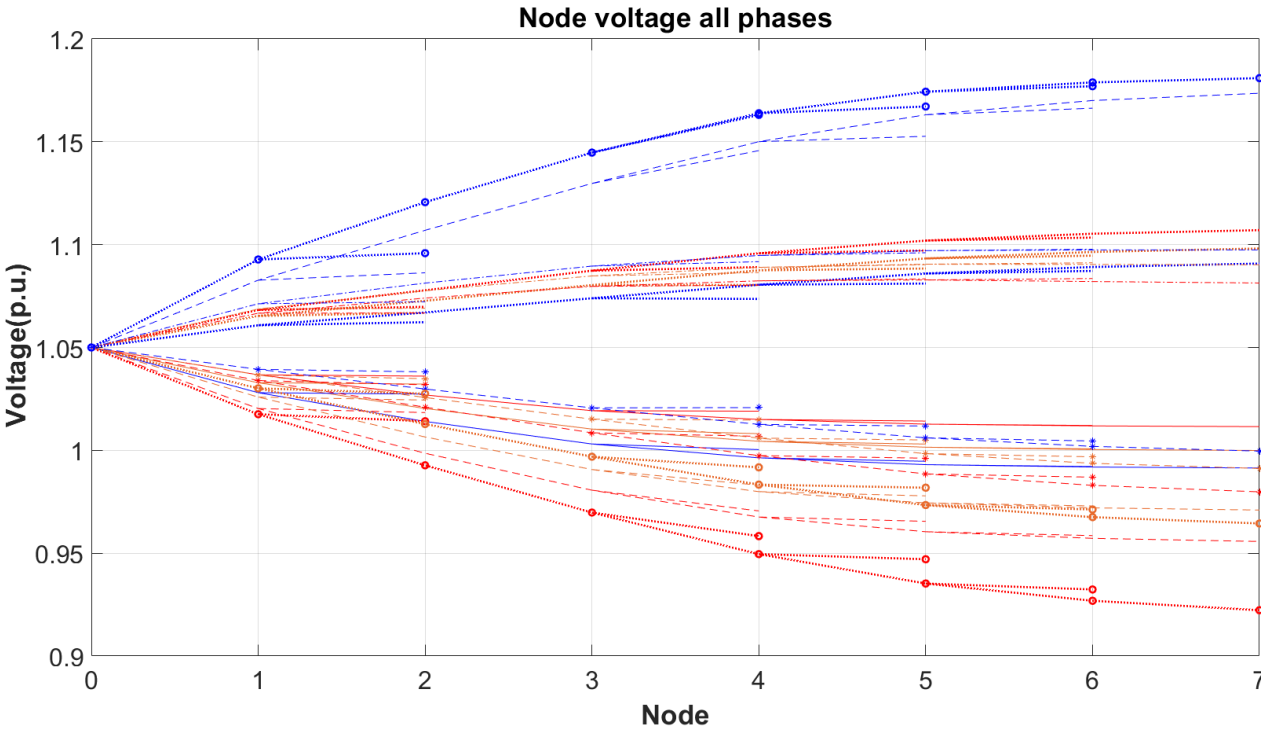

Figure 5.13: Three feeder network with varying unit quantities worst-case voltage deviation

The Single feeder network with branches at each bus is utilised to evaluate the effect of multiple T-offs at a higher line loading, each with an extended feeder of its own. With one of the T-offs shorter than the rest, the aim is to establish if the network length has a higher impact on the voltage than the number of T-offs have on the voltage. The feeder consists of 42 units reaching the feeder occupation limit, which means that a feeder of this magnitude is the largest feeder in this test series. The longest single feeder is composed of 12 nodes with a total feeder length of 240 m. The allocation of 2 units means that the total ADMD has shifted to 189 kW resulting in a load factor of 60%. The Results exhibited in figure 5.14 denotes that the voltage remains within limits at zero generation and balanced generation implementations. However, the voltage on the unbalanced network violates the upper voltage limit by an excess of 5.5%. This network is also suitable for control implementation due to the upper voltage violations in worst-case conditions.

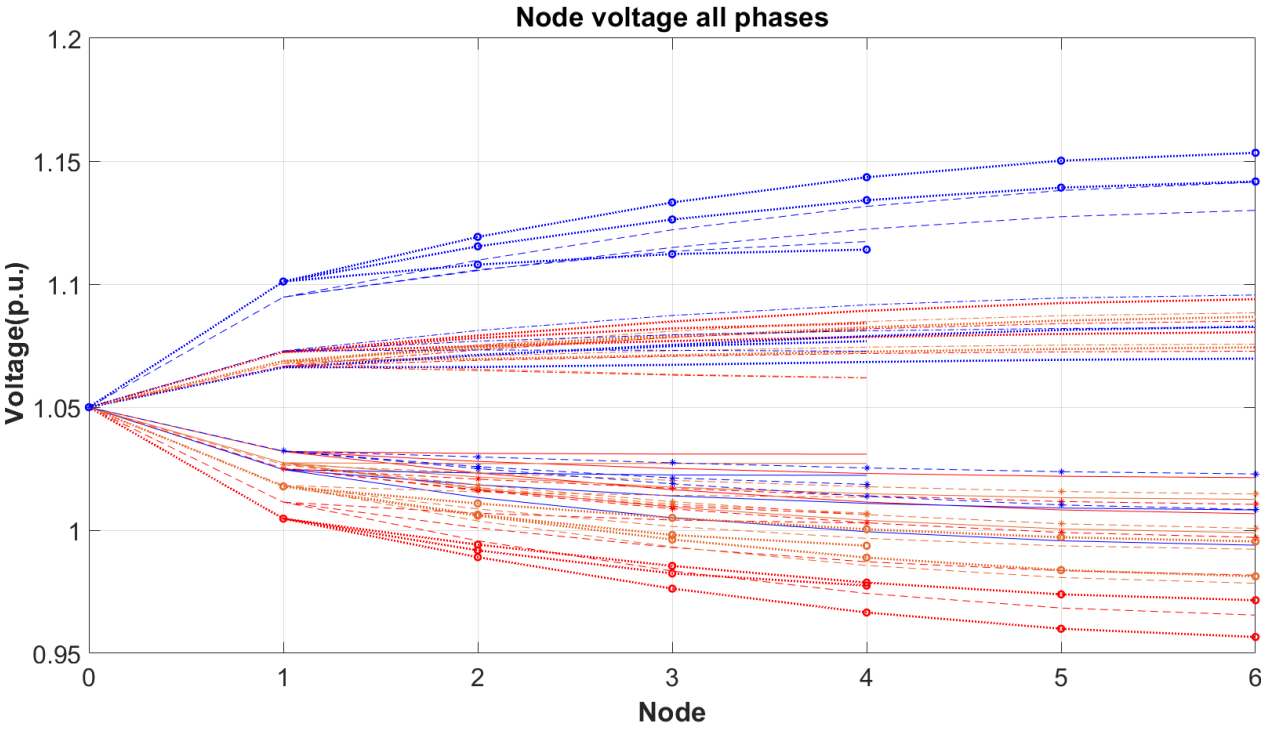

Figure 5.14: Single feeder network with branches at each bus worst-case voltage deviation

The Single feeder with high load branches at different sections of the main feeder is utilised to evaluate the effect that the multi-node T-off feeders positioned at different positions on the main feeder have on the feeder voltage. The worst-case voltage graph exhibited in figure 5.15 indicates that the feeder positioned close to the front of the feeder does not experience a voltage rise higher than the T-off situated close to the end of the network. This results from the collective line impedance between the transformer and the respective nodes on the network. An indicator would be that the T-off feeder has a lower resistance path to the transformer at the beginning of the feeder than the T-off feeder at the end of the network. This assumption is evident in the voltage profiles of the two T-off positions where the first T-off experiences a lower voltage rise than the second T-off in the presence of SSEG and a smaller voltage drop without the presence of SSEG on the feeder. Positioning the second feeder close to the end of the network results in the T-off feeder extending the network to a total of 320 m. The extension resulted in a voltage rise of 10.5% above the upper voltage limit at the instance of maximum generation unbalance. The network is a good candidate for control implementation due to its upper voltage limit violations at times of high renewable energy penetration.

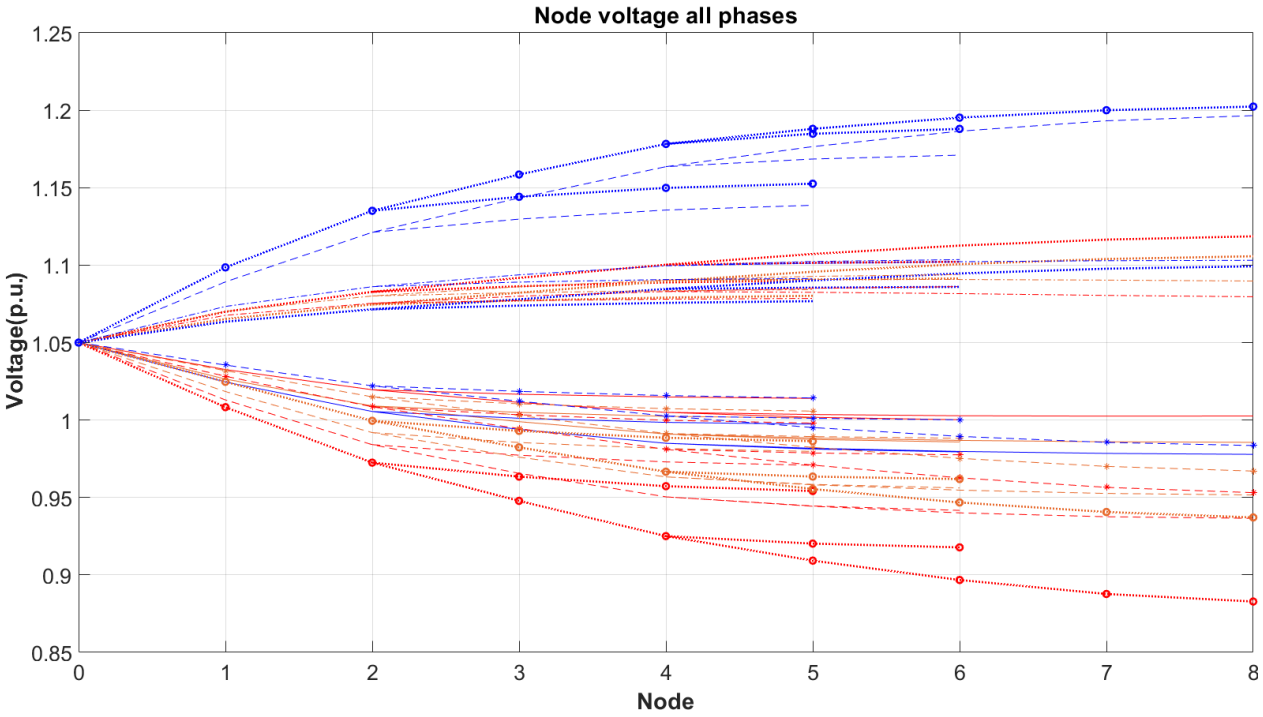

Figure 5.15: Single feeder with high load branches at different sections of the main feeder worst-case voltage deviation

The Single feeder network with a dual T-off split evaluates the effect of branchings on an already branched network. The branched feeder originating from the centre of the main feeder has another branch located at the end of the feeder. The worst-case voltage graph displayed in figure 5.16 denotes the effects of the multiple branches on the feeder. The results indicate that both the upper and lower voltage limits are violated. The upper voltage level excess equals 7.6% above the 110% upper deviation limit, and the voltage drops 2.1% below the 90% lower voltage limit. The feeder violates the upper voltage limit in the balanced and unbalanced generation implementation. It is evident that the nodes situated on the two branches at the end of the feeder induce a heavy load concentration at the end of the network, which results in a significant voltage rise when the load is lightened due to the implementation of renewable energy. The load concentration can also cause a significant voltage drop in cases of maximum unbalance. This feeder network serves as a good candidate for control implementation due to its voltage violation on both sides of the voltage spectrum. The Voltage violations encountered in this network can provide good data for the control development phase of this study.

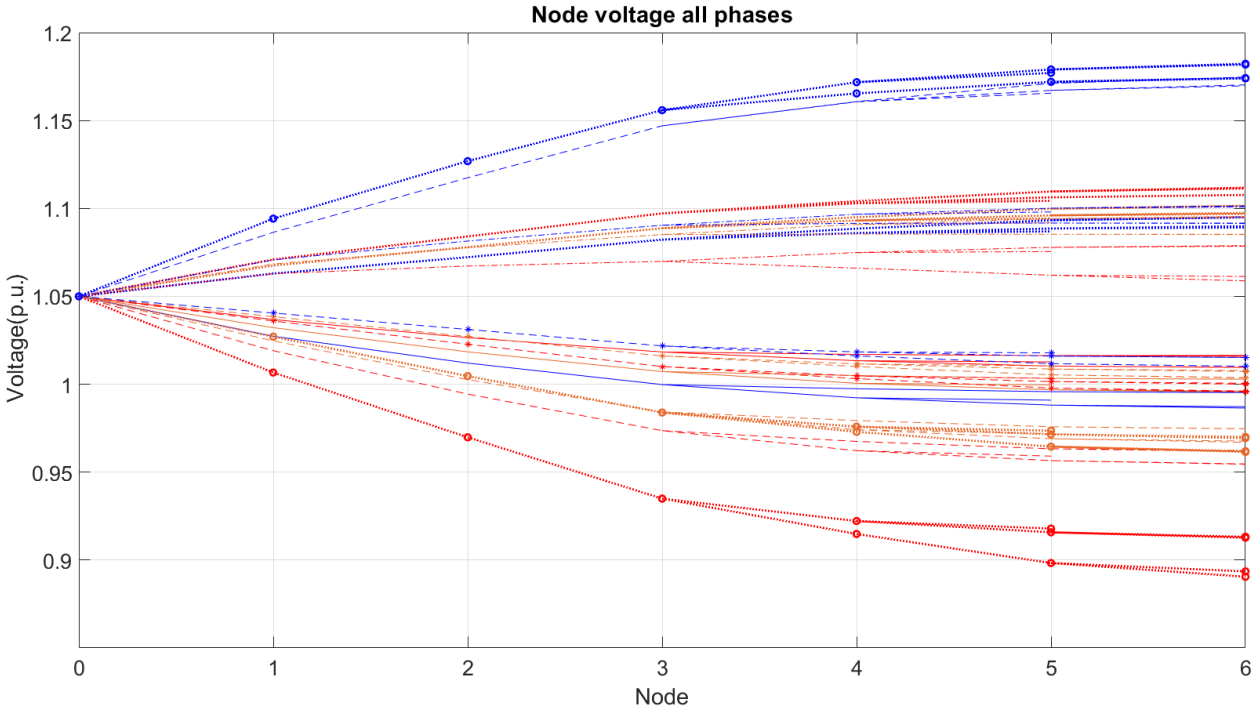

Figure 5.16: Single feeder network with a dual branch split worst-case voltage deviation

The Spider branch network with extentions on four of the five feeders is a modified spider network where the T-off feeders are extended to evaluate the effect of increasing the number of consumers and the line length of the feeder on the voltage profile. The worst-case voltage profile exhibited in figure 5.17 denotes the voltage profile of the different scenarios. It becomes evident when comparing the data obtained from figure 5.11 with the data in figure 5.17 that an increase in the line length has resulted in an immediate increase in the feeder voltage variation. The increase in line length has also led to an increase in the number of occupants on the network. The renewable energy penetration per customer equals 7.36 kW at a load ADMD of 4.5 kW. The average power difference between load and generation is 2.86 kW fed back into the grid. The increase in consumers leads to an increase in the net negative energy flow resulting in a higher voltage deviation on the feeder. This feeder is a good candidate for control implementation due to the upper voltage limit violation by 2% at the interval of maximum unbalance.

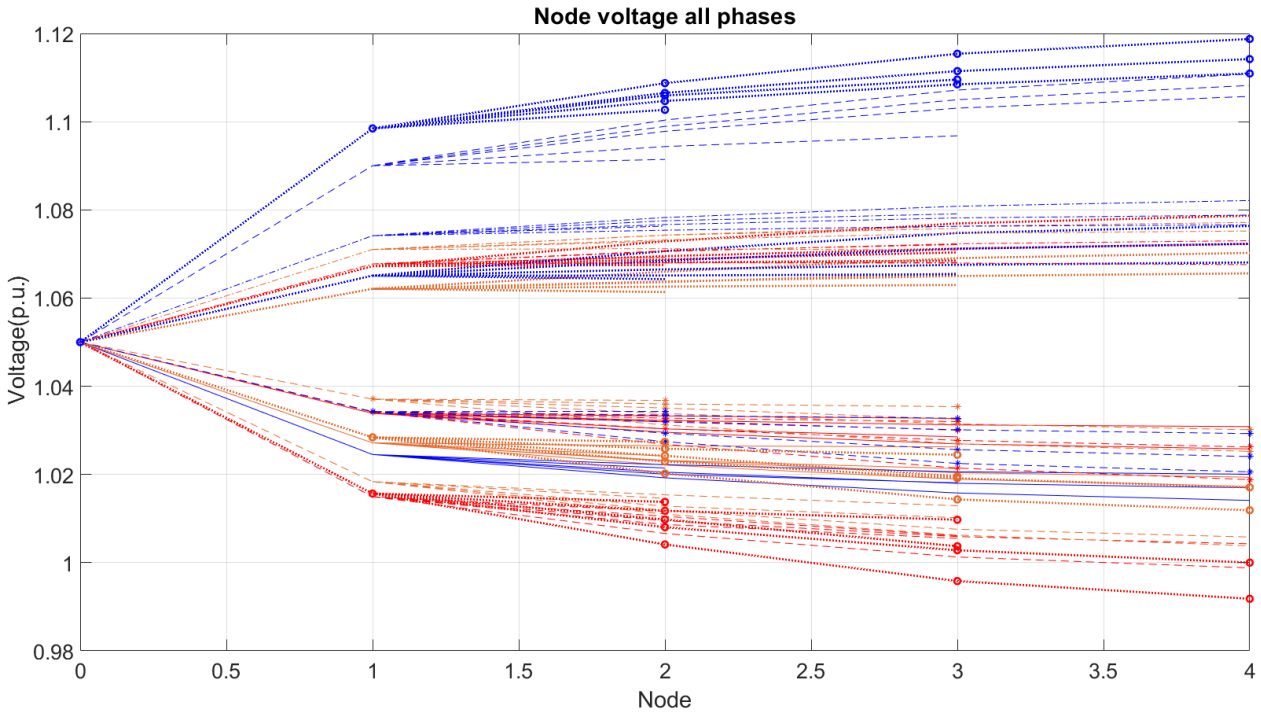

Figure 5.17: Spider branch network with extentions on four of the five feeders worst-case voltage deviation

The final network is a basic 12 node radial network without any T-offs. This network aims to evaluate the sole effect of an extended network on the feeder voltage profile based on the culmination of knowledge obtained from the previous feeder network tests. The worst-case data obtained from the network simulation is exhibited in figure 5.18. The feeder voltage profile indicates that the network violates the upper and lower voltage limits at times of maximum generation unbalance as well as times of balanced generation when the loads are ordered from high to low on the feeder. The excess voltage rise above the upper voltage limit of 110% is 18.9%, whereas the maximum voltage drop is 17% below 90%. The extreme voltage deviations are caused by the collective Thevenin equivalent resistance of the feeder line with a length of 320 m. The total number of consumers on the feeder equals 36, equating to a total ADMD of 162 kW with a load factor of 51.4%. The data indicates that the single-line feeder produces the best worst-case results of all the network typologies and has the highest voltage deviations. For this reason, the single line feeder will be utilised for the control development chapter and further control experimentation and performance analysis.

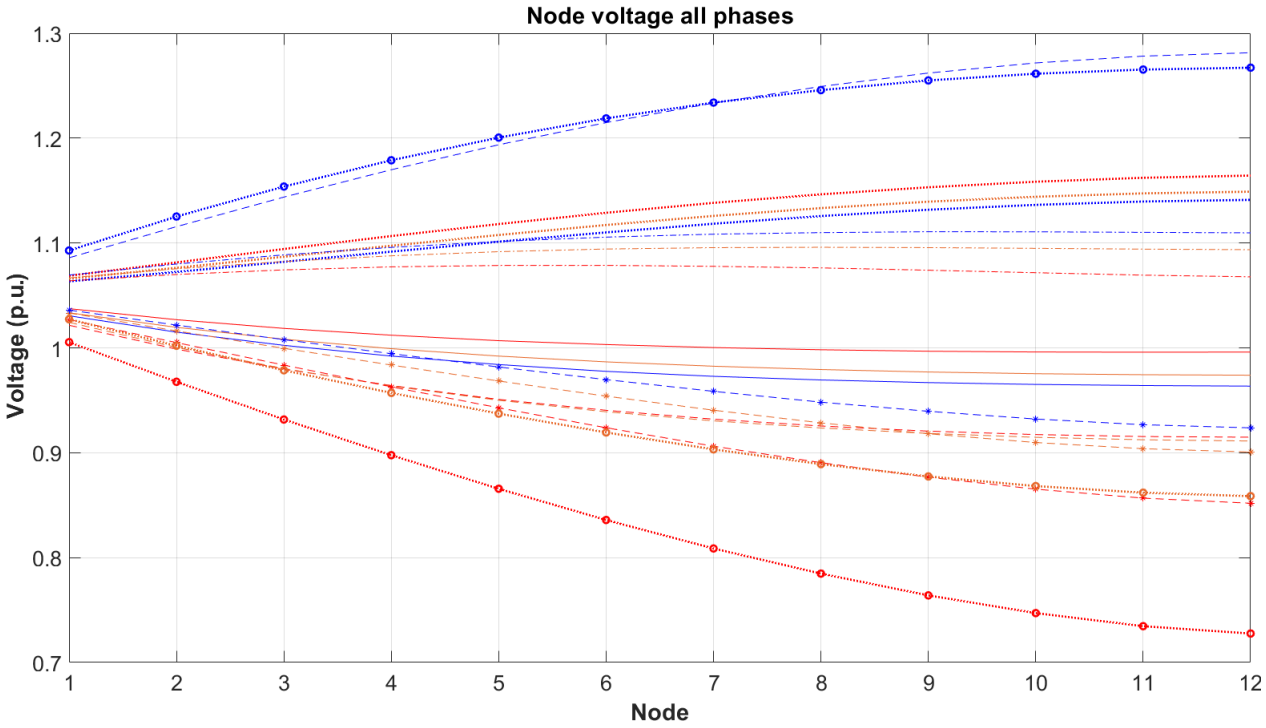

Figure 5.18: Single feeder extended three phase network worst-case voltage deviation

5.5 Conclusion

The beginning of this chapter focused on the validation and verification of the Simulink® model. The results indicated that the validation and verification phase went off without a hitch providing the desired results in terms of voltage profile generation under the same conditions generated in the reference study. The worst-case scenario voltage profile was a close mimic of the data validated in [39]. The results indicated that the model functions as intended. It can be implemented on a wide array of network scenarios if the parameters are correctly adjusted to portray a specific component.

The completion of the model validation resulted in the analysis of nine different random networks to evaluate the network typology's effect on the feeder voltage. The data obtained from the model characterization brought the following observations to light:

- An increase in the line length leads to an increase in the voltage deviation if the loads remain constant.
- An increase in feeder branches(T-offs) leads to a decrease in the magnitude of the feeder voltage deviation while the number of consumers remains constant.
- An increase in the number of units on the network has led to an increase in both power

consumption and voltage deviation amplitude. This voltage rise is due to the increase in energy that flows back into the grid and reduces the power strain on the transformer and, in effect, the MV network, therefore, increasing the voltage

The 12 node feeder will be utilised in the next phase of this study due to the extreme voltage deviations on the feeder encountered in worst-case conditions. The next phase of the study will be the control design and implementation phase. The control development and implementation phase will test the effectiveness of control on the feeder. This test will be carried out over 24 hours with real-world load profiles.

Chapter 6

Regulatory control analysis

6.1 Introduction

This chapter evaluates the effects of the current NRS 097-2-3 regulatory control structures and possible modified versions of the regulatory control implemented on the validated LV network as chosen in the previous chapter. The effectiveness of the voltage regulation managed by the regulatory controller will determine the maximum level of safe renewable energy penetration. The test will be carried out in 25% increments from 25% to 100% renewable energy penetration. Once a controller cannot safely manage the energy and regulate the voltage to remain within the regulatory limits, the test will be stopped and continued on the following control variation.

6.2 Base-case characteristics

The consumption profile of each household in the world is unique in such a way that no two load profiles are the same as no two people are the same. However, there is a correlation between the peak power consumption periods and the minimum consumption periods. In order to accurately represent the generalised consumption profile of the average household, an array of real-world consumption data was recorded at 5-minute intervals from the national residential load research project. These data were obtained by S Heunis and M Dekenah [47]. The dataset was filtered according to time of day, season, presence and absence of sunlight. The filtered data would then be compared to each other and sorted by day of the week, and if a certain profile were evident for three iterations out of four for that specific day, then the profile would be deemed acceptable. The load model is then generated from the

accumulated data through filtering the data according to temperature, daylight and average annual consumption. From this process, a generalised addative model (GAM) is obtained. The model, together with standard deviations accounting for variations in the general load profile, is depicted in figure 6.1.

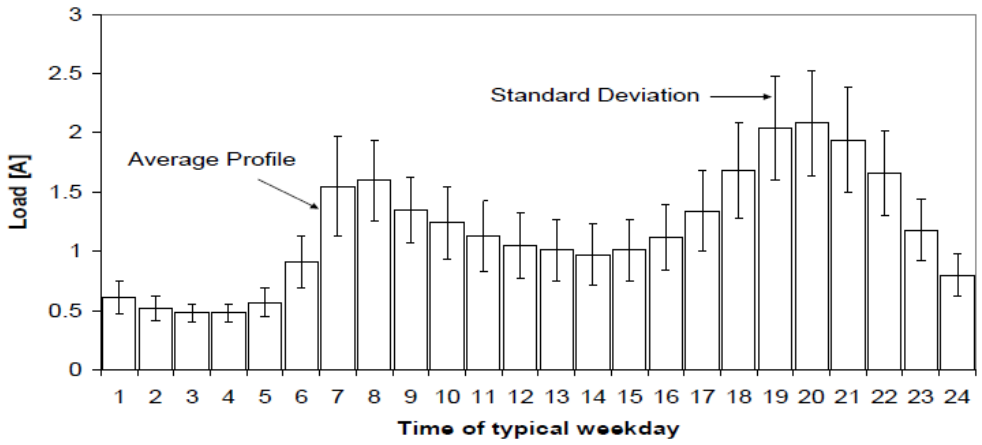

Figure 6.1: General residential load profile example generated from the NRS 034 load research project [47]

Therefore, the base case feeder load profile needs to mimic the generalised load profile to be deemed an accurate representation of a real-life residential feeder load. This comparison will verify the load profile accuracy.

The base case will indicate the voltage profile to be expected on a passive feeder with only stochastic loads. The voltage profile measurements will take place at the point of maximum deviation. The point of furthest deviation has been identified as the node the farthest distance from the transformer due to the topology of the feeder being a shared radial feeder with no T-offs. The units on the farthest node of each phase will indicate the maximum deviation from the reference feeder voltage.

The data exhibited in figure 6.2 show the load profile on the three phases measured at the transformer over 24 hours. The balancing between the phases is within 10 kW of one another at the baseload. The maximum demand of the feeder is situated on phase three and is achieved at 20:00 when everyone is home. The maximum demand exceeds the thermal limit at both the morning and the evening peak. The morning peak momentarily exceeds and quickly drops back under the feeder thermal limit indicated by the red reference line. The thermal limit violation is not a significant concern when violated for a short period since the thermal limit depends on environmental factors. If the thermal limit is violated, the side effects are not imminent. The violation of the thermal limit of the transmission line will cause the conductor

material to soften and sag towards the ground, possibly nearing structures and running the risk of electrocutions. The thermal limit increases in the early mornings and evenings due to the low environmental temperature exhibiting a cooling effect on the conductor[48]. The red line displayed on the load graph indicates the thermal limit of the conductor. Any value above the red line violates the conductor thermal limit. The maximum demand on the feeder is equal to 217.48 KW. This load profile resembles the shape of an aggregated version of the average residential load profile, which indicates that the base-case load profile has been verified with the literature.

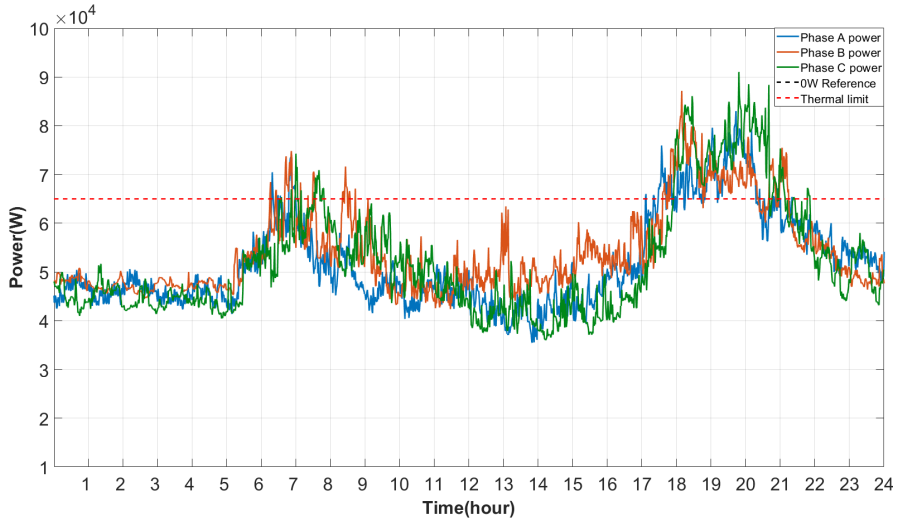

Figure 6.2: 24-hour reference load profile as measured transformer without SSEG presence

The data displayed in figure 6.3 denote the voltage profile that corresponds to the load profile of the base case. The data indicates that the voltage levels are lowest when the load is highest. This means that there is an indirect correlation between the voltage level and the energy exchange at the PCC. The voltage deviates from the source voltage as the phases' unbalance increases.

The voltage limit violation of the base case is evident at times of maximum unbalance, as can be seen during the middle of the day or by maximum loading. The base case exceeds the lower voltage limit on two separate occasions. The first occasion was at midday due to phase B experiencing a rapid rise in load. This unbalance causes the voltage to drop disproportionally to the other phases and violate the lower voltage limit indicated by the bottom red line on the graph. The second occurrence occurs at the maximum evening load causing the highest loaded phase to violate the lower voltage limit as it also violates the conductor thermal limit.

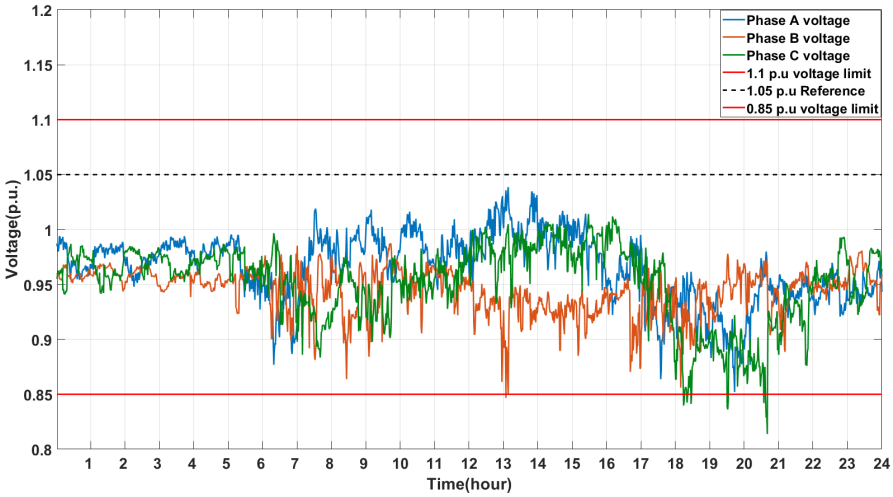

Figure 6.3: 24-hour reference voltage profile measured at the most volatile node on the feeder

6.3 Renewable energy implemetation

The specifications and regulations are implemented in order to protect consumer electronics as well as electrical infrastructure. The regulatory standards ensure that a feeder voltage between 85% and 110% is maintained. If the feeder voltage is not regulated to remain within this limit, the abnormality could cause damage to power electronic appliances, which are extremely sensitive to overvoltage. The lack of control can also cause the power on the feeder to exceed the thermal limit of the conductor or overload the transformer. Therefore, the power levels can cause an insurmountable amount of damage to the electrical infrastructure, leading to long-term blackouts.

To prove that renewable energy without control is detrimental to the state of the network, the incorporation of renewable energy has first to be tested without the assistance of a control mechanism. The initial of three 24 hour PV tests will be conducted at a renewable energy penetration level equal to 25% of the consumers NMD and increase in 25% increments. The voltage and load profiles unique to this test are exhibited in figure 6.4 and figure 6.5.

The data obtained from the initial test indicates that the demand still exceeds the upper thermal limits. In addition, the renewable energy penetration matches the load at the time of maximum generation. The generation to load ratio at maximum generation and minimum load is equal, as can be seen where the load curve reaches the black zero watt reference line. The maximum generation capacity on the feeder is equal to 137.16 kW at 25% renewable energy penetration.

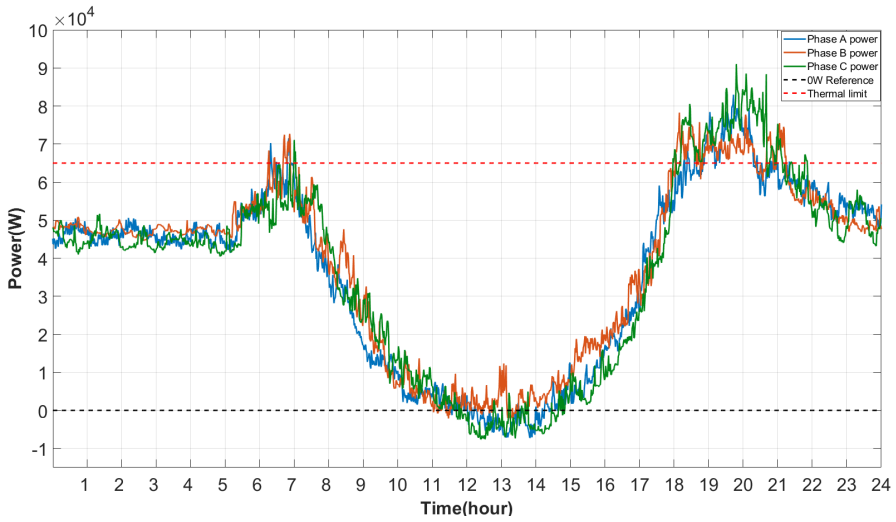

Figure 6.4: 24-hour transformer load profile with unregulated PV generation at 25% renewable energy penetration

The voltage profile at the 25% renewable energy penetration test indicates that when the generation exceeds the consumption, the highest node on the feeder tends to violate the upper voltage limit by 1% for an instant.

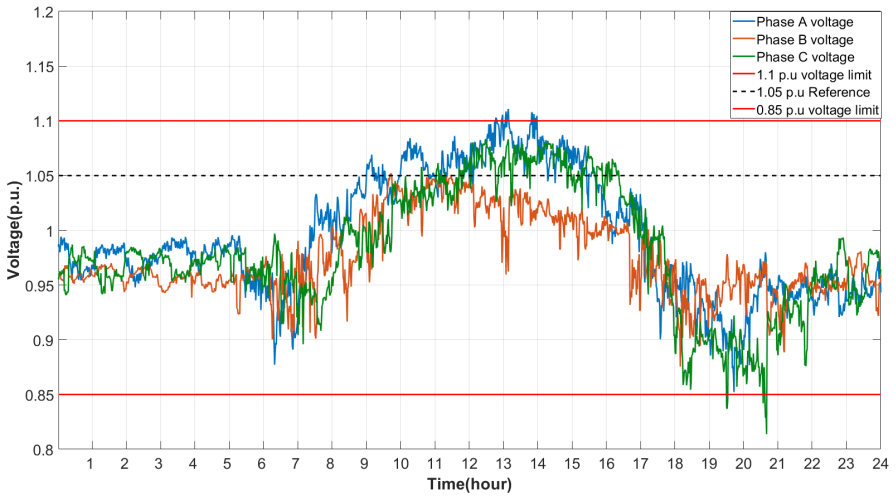

Figure 6.5: 24-hour worst-case voltage profile with unregulated PV generation at 25% renewable energy penetration

The increase in renewable energy penetration from 25% of the units NMD to 50% results in an increase in the amount of energy fed back into the MV network by 40 kW per phase at the period of maximum generation. The total renewable energy penetration on the feeder is now equal to 274,32 kW. The increase in renewable energy penetration on its own has not improved conditions on the network in the absence of control or regulation. The conditions have worsened from the basic network conditions.

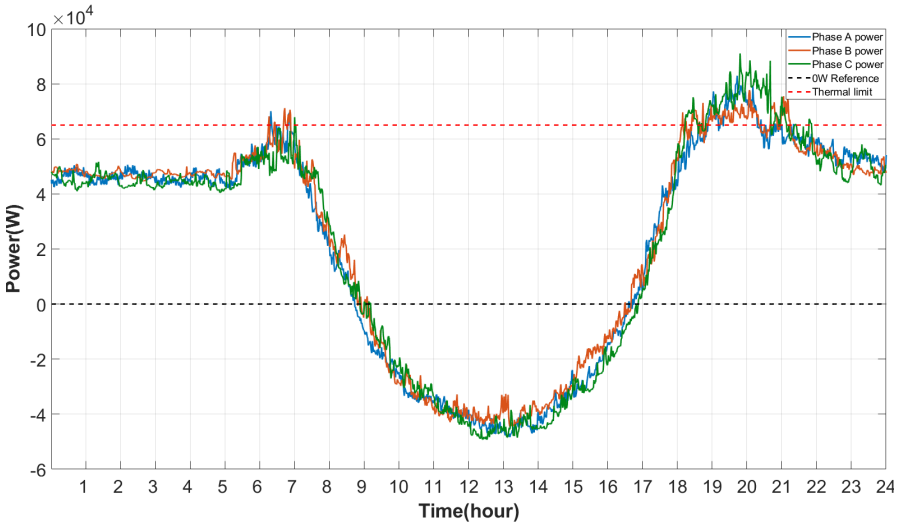

Figure 6.6: 24-hour transformer load profile with unregulated PV generation at 50% renewable energy penetration

The increase in renewable energy penetration has resulted in both the upper and lower voltage limits being violated, with the upper voltage limit being violated by all three phases at the point of greatest influence. The maximum voltage rise is evident on phase A with a magnitude equal to 8% above the upper voltage limit.

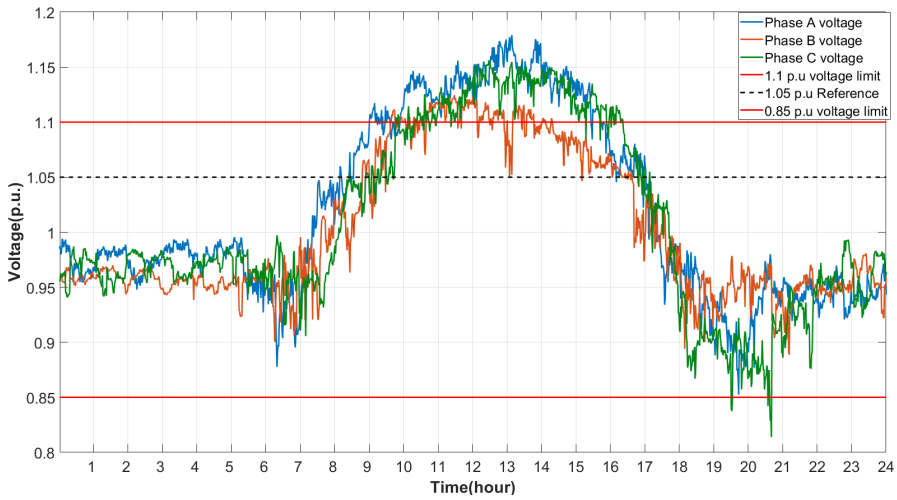

Figure 6.7: 24-hour worst-case voltage profile with unregulated PV generation at 50% renewable energy penetration

The increase in renewable energy penetration from 50% to 75% has exceeded both the upper and lower conductor thermal limits. This, due to the aggregated renewable generation capacity of 411.48 kW, which also exceeds the transformer capacity, which could result in the transformer being damaged when no load is drawn. The only reason for not overloading the

transformer is that the baseload on the feeder equates to a total of 153.7 kW. Therefore, the net energy difference equals 257.78 kW flowing into the MV network maximum generation and minimum load.

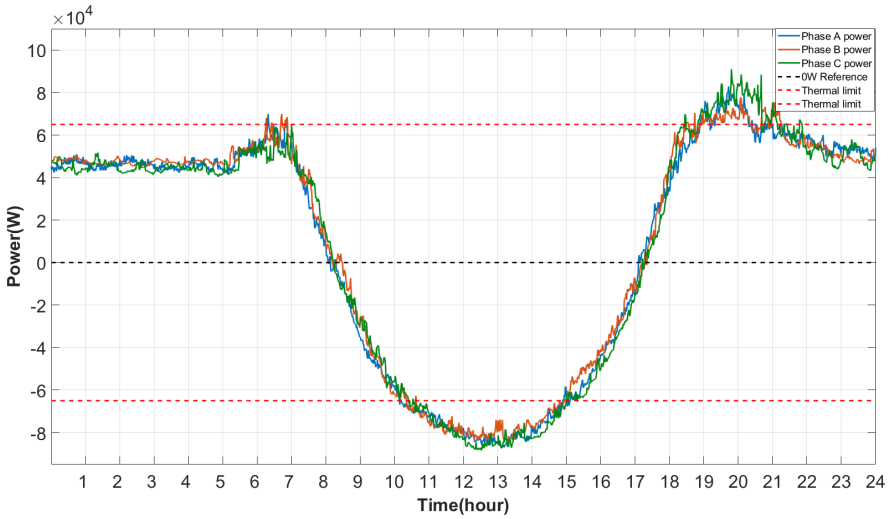

Figure 6.8: 24-hour transformer load profile with unregulated PV generation at 75% renewable energy penetration

The corresponding voltage profile indicates that the voltage rise as a result of the 75% renewable energy penetration level amounts to 15% above the upper voltage limit. A voltage deviation of this magnitude can cause network protection equipment to trip and cause a blackout in the absence of regulatory control.

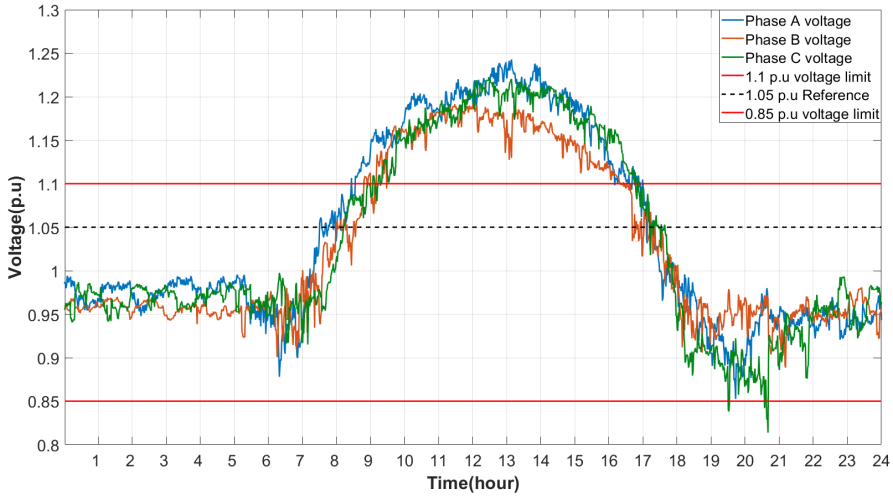

Figure 6.9: 24-hour worst-case voltage profile with unregulated PV generation at 75% renewable energy penetration

The results at different levels of renewable energy penetration have indicated that it is dangerous and inefficient to exceed the specified maximum renewable energy penetration level

without any form of control. The implementation of basic control can assist in efficient SSEG utilisation and higher levels of safety and predictability.

6.4 Regulatory control

6.4.1 NRS 097 control

The data acquired from previous chapters indicate that voltage regulation is a pressing concern with the implementation of renewable energy. The industry is aware of the so-called abnormal conditions when implementing renewable energy. The abnormal conditions are as follows:

- Network voltage or frequency out of bounds conditions
- Loss of grid conditions
- Exceeded d.c. current injection threshold
- Residual d.c. current

The focus lies on the voltage out-of-bound conditions due to the mutually exclusive relationship between the voltage level and the renewable energy penetration. Being aware of the abnormal conditions regulatory bodies indicated that all legal grid-tied inverters should possess a disconnection device capable of automatically and safely isolating the inverter from the grid in an anomaly called anti-islanding. These specifications are in accordance with the IEC 62109.

The regulations have forced inverter manufacturers to implement disconnect devices into their inverters. The quick disconnect regulations are only applicable to SSEG in sub-categories A1 and A2 as sub-category A3 has adjusted regulations because the system size is greater than 100 kW. The disconnect serves as a form of passive voltage regulation due to its reliance on passive control instead of active control. Passive control dictates that the system control is reactive, meaning that the system only acts on a value when it has violated its limit and does not alter the course of the parameter not to violate the voltage limit.

The regulations state that the embedded generator shall cease to energise the utility distributions system if the network voltage deviates outside the voltage limits specified in figure 6.10. The standard operating voltage range is between 85% and 110%. The likelihood that a voltage level of 85% is reached under normal conditions is relatively low. The data indicates that the inverter should isolate itself when the voltage deviates above 110% but remains below 115% for longer than 40 seconds. If the voltage level deviates to the 5% band above the 115%

limit, then the inverter should isolate from the grid within 2 seconds. Suppose a parameter is violated and the delay time is exceeded. In that case, the inverter will disconnect from the network for a minimum of 60 seconds, reconnect to the network and start to produce power considering the feeder parameters are respected.

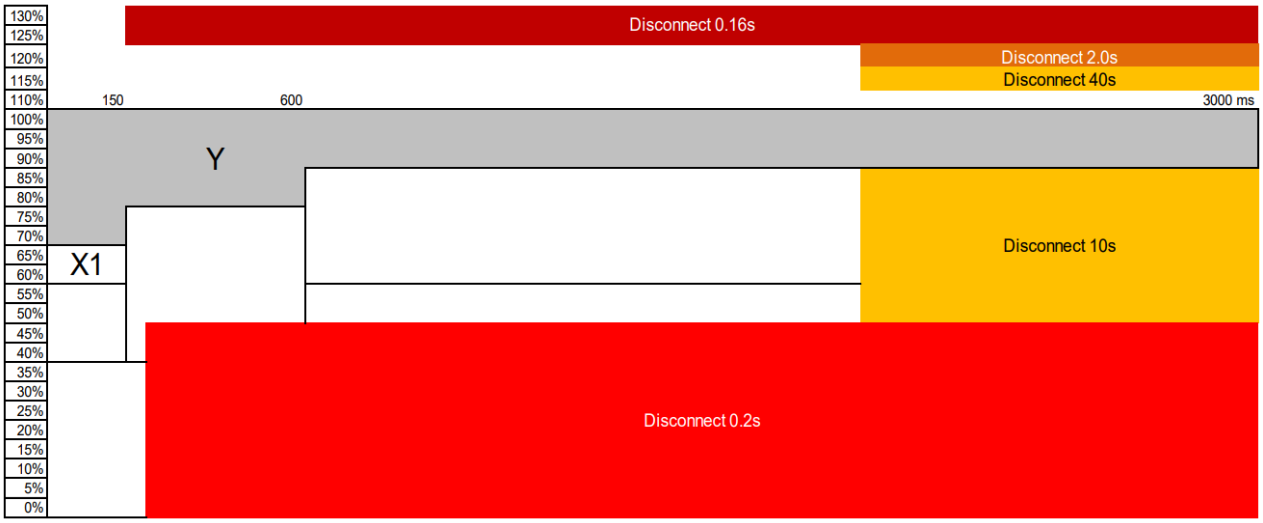

Figure 6.10: Graphical representation of NRS 097-2-1 voltage-ride-through and voltage disconnect requirements for SSEG

The regulations state that the purpose of the permitted time delay is to ride through short term disturbances to avoid any excessive nuisance tripping. The other reason for the time delay is to provide an opportunity for the voltage to return to normal operating conditions before the need for a trip occurs. The over frequency regulations and anti-islanding requirements are not vital to the objective of this study, which means that the detailed role and workings of these functions will not be explored. The regulations state that the time delays are implemented to minimise nuisance tripping. The notion is that with the increase in renewable energy penetration, the frequency of the violation of voltage levels will increase. The frequency of violations will likely increase because the limited renewable energy penetration is exceeded. The excessive tripping will most likely cause a cascading effect down the feeder resulting in further voltage deviations.

The Simulink® model will utilise a local regulatory controller situated on the Grid-tie inverter only to control the PV based generation in the case of a voltage limit violation. The controller will continuously monitor the node voltage at each house. The node voltage indicates the voltage at that specific point in a particular phase on the feeder. The controller will measure the node voltage. If the voltage exceeds the pre-programmed limit for a specific period, the controller will terminate the generation on the relevant node. This termination is a representation of the inverter disconnecting from the utility grid. The termination effect is

predicted to cause the node voltage to drop due to the instantaneous change in the direction of power flow.

6.4.1.1 25% Renewable energy penetration

The load profile displayed in figure 6.11 denotes the effect of regulatory passive voltage regulation at a renewable energy penetration equal to 25% of the MCB size. The feeder does not possess any form of energy storage. The data indicate that the phase with the smallest loading is the first to experience an overvoltage. The overvoltage, however, remains within the time and amplitude parameters of inverter disconnection. This means that the voltage drops below the upper voltage limit within the first time delay of 40 seconds, indicating no action is needed by the regulatory control. The load data at the 25% renewable energy penetration test follows the same trajectory as the unregulated PV test because the generated power rarely exceeds the load at each unit on the feeder. This allows the voltage to remain within limits for a majority of the test.

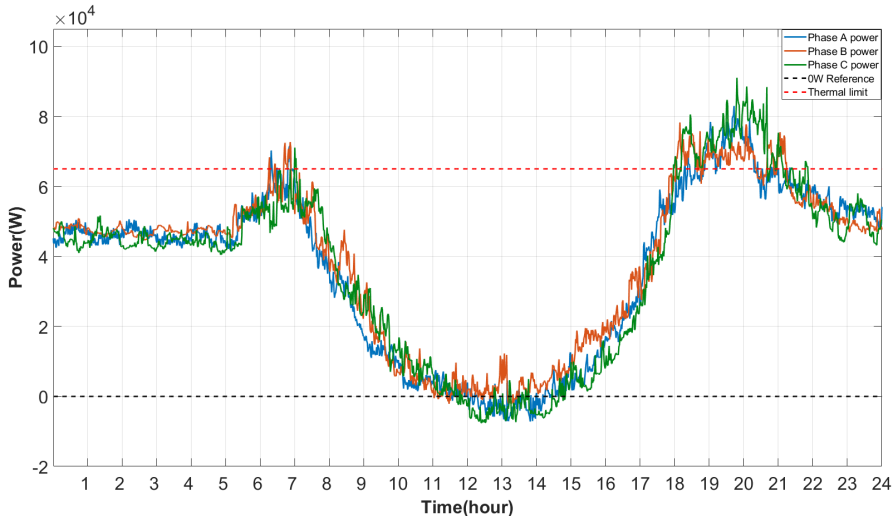

Figure 6.11: 24-hour worst-case load profile with NRS 097-2-1 regulation at 25% renewable energy penetration

The voltage profile displayed in figure 6.12 indicates that the voltage profile reaches a peak at 1.12 p.u. on phase A. This is due to Phase A having the lightest load while possessing the same generation as the other phases. The NRS 097-2 control effects are not evident in the voltage profile. Suppose the test was conducted at a lower ADMD while maintaining the current generation capacity. In that case, the voltage might violate the limits due to the fact that the generation to load ratio would be higher in favour of the generation.

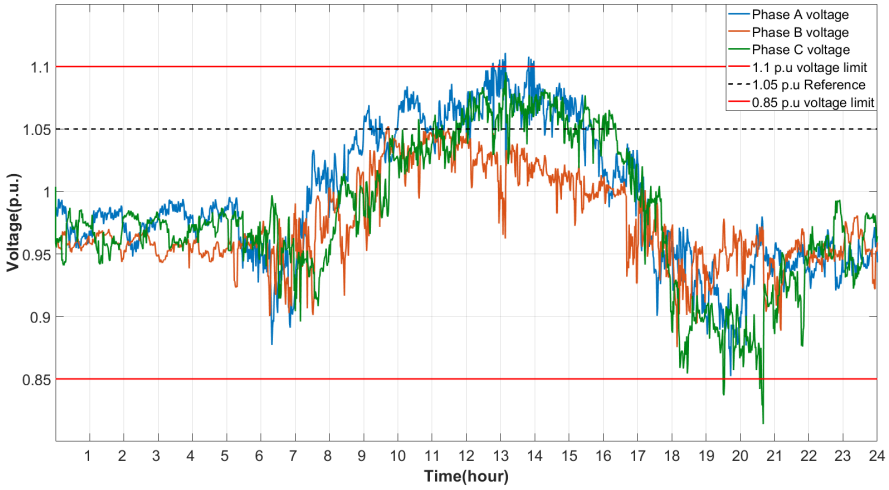

Figure 6.12: 24-hour worst-case voltage profile with NRS 097-2-1 regulation at 25% renewable energy penetration

The data analysis has concluded that the standard regulatory voltage regulation control scheme does not do the network justice due to the lack of positive results at an ADMD of 4.5 kW. This indicates that the regulatory requirements would only play an increasing role in lower ADMD residences. To determine the effect of the regulatory control on the feeder, the test will be conducted once more at a renewable energy penetration level of 50% of the MCS in order to determine whether the increase in renewable energy penetration leads to a deterioration in grid stability.

6.4.1.2 50% Renewable energy penetration

The renewable energy penetration will now be increased to 50% of the household NMD. The load profile displayed in figure 6.13 exhibits the effect of passive regulatory control on a feeder with only energy generation. At first glance, it becomes clear that the voltage regulation has not improved grid stability and smoothly reduced power to bring the voltage back within limits, instead the abrupt change caused by the first inverter tripping off. The regulatory control starts to take effect when the general power flow at the transformer begins to flow in the direction of the MV network.

The regulatory control generates a violent oscillation which causes deterioration in the network stability. This oscillation causes the voltage to vary chaotically and could lead to voltage harmonics. The oscillation is induced by the crude control shutting off the generator when the voltage limit is violated. This causes a sudden change in the power flow on the network. When the generator comes back online, it immediately throttles back up, causing another instantaneous shift in the energy flow. This energy shift is most devastating at the moment

of maximum generation. In addition to the negative energy flow, the unbalance between the phases also contributes to the variation in voltage levels on the feeder, resulting in the inverters tripping off earlier than they would on a balanced network. The dominance of the generators energy capacity also leads to an unbalance between phases due to not constant tripping. The network's energy oscillations are not independent of one another since the level of unbalance constantly changes. When an inverter on the one phase trips off, it causes a high unbalance between the phases, increasing the voltage level on the other phases. This increase in voltage, in turn, leads to the inverters on those phases tripping off. The tripping of inverters with a high renewable energy presence increases the likelihood of nuisance tripping on all phases.

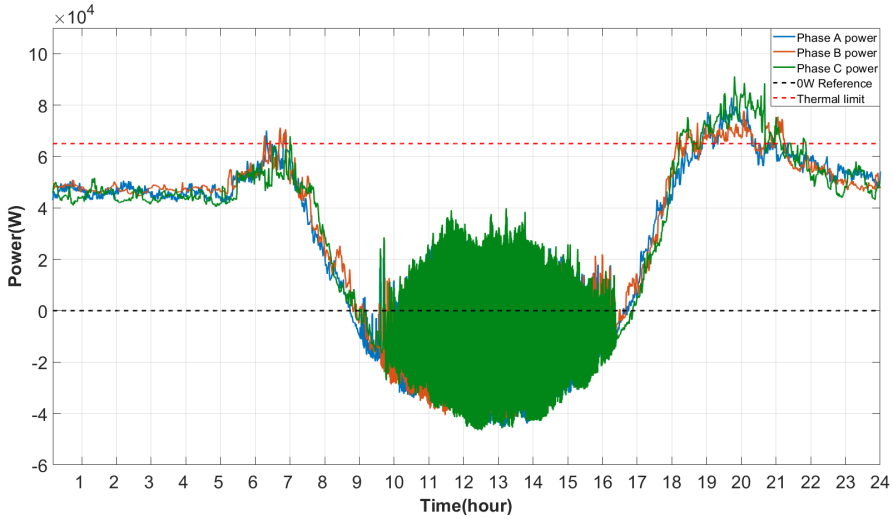

Figure 6.13: 24-hour worst-case load profile with NRS 097-2-1 regulation at 50% renewable energy penetration

The voltage profile of the feeder with 50% renewable energy penetration is displayed in figure 6.14. The data indicate that the maximum voltage level is 1.34 p.u. which is 24% higher than the upper voltage limit of 1.1 p.u. as stipulated in the NRS 097-2-1. The voltage profile is inversely proportional to the power curve. The energy oscillations caused by the inverters constantly tripping off and re-synchronising to the network causes the voltage on all phases to fluctuate in such a manner that both the upper and lower voltage limits are violated during times of maximum generation, which is likely caused by maximum unbalance on the feeder.

The variation in power causes the voltage curve to oscillate between 0.8 p.u. and 1.34 p.u. at times of maximum energy generation. This voltage deviation will cause permanent damage to electrical components on the network and might even cause the network protection equipment to trip prematurely under fault conditions.

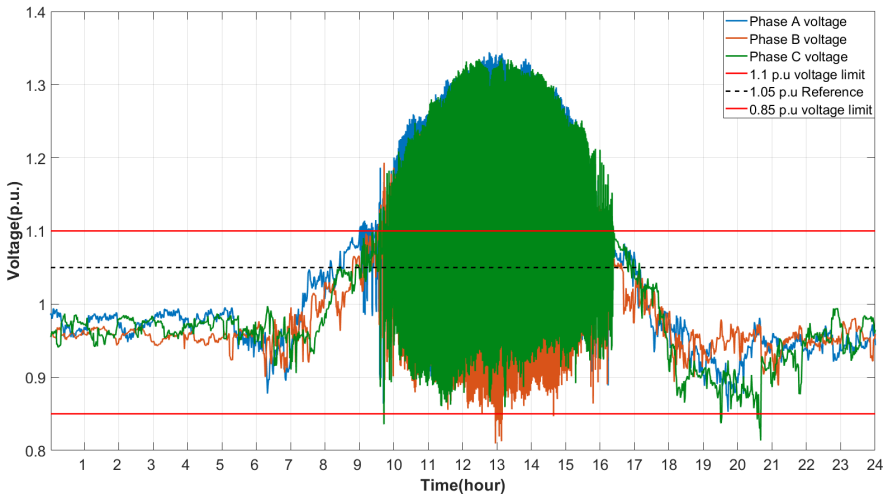

Figure 6.14: 24-hour worst-case voltage profile with NRS 097-2-1 regulation at 50% renewable energy penetration

The comparison between the test with 50% renewable energy and the test with the 25% renewable energy penetration indicates that with the current regulatory voltage regulation infrastructure inside the inverters, the voltage oscillations increase as the renewable energy penetration increases. The renewable energy increase also leads to a violation of the feeder thermal limits. A clear indicator of when the voltage regulation starts to take effect is when the transformer's energy flow turns negative irrespective of the renewable energy penetration. Therefore, this could also occur when large loads like a water heater instantaneously disconnect from the network and energy is fed back into the grid.

The NRS097-2 currently does not stipulate the maximum number of trips before the inverter should switch off indefinitely, which could help increase the voltage regulation by setting a limit on the number of re-synchronisation before a cooldown period is implemented. Implementing a soft start might also improve the voltage regulation by decreasing the voltage variations with a slow power ramp-up. The IEEE 1547 states that new regulations allow for the local implementation of power-based voltage regulation.

The proof that current local specifications on voltage regulation are not delivering favourable results indicates that the effectiveness of voltage regulation practices as defined by the IEEE 1547 needs to be re-evaluated.

6.4.2 Soft start test

The second test will be the soft-start method utilised when the grid-tie inverter re-synchronises to the grid. The incorporation of a soft starter is believed to improve the effectiveness of the

voltage regulation by allowing the feeder voltage to settle by slowly increasing the generation on the network after synchronisation. The inverter will still follow the disconnect protocol based on the voltage amplitude and time delay. The only addition will be that the inverter will, after 60 seconds, re-synchronise to the grid. Once the re-synchronisation is completed, the inverter will ramp up the power production at a rate of 10% of the inverter's rated output per minute until maximum capacity is reached or the voltage regulation parameters are violated.

6.4.2.1 25% Renewable energy penetration

The soft starter test will initially be conducted at the NRS 097-2-3 renewable energy penetration level of 25% of the NMD, equating to 3.81 kW of generation per consumer. The test will determine whether implementing a soft starter will improve the voltage regulation capability at a local level of control compared to the basic voltage regulation methods currently being implemented on an active LV network. The load profile displayed in figure 6.15 denotes that the variation in load as measured at the transformer is significantly smaller when compared to the primitive reactive voltage regulation load profile. The variations in load are also less frequent on the 25% renewable energy penetration soft started test than on the primitive voltage regulation test.

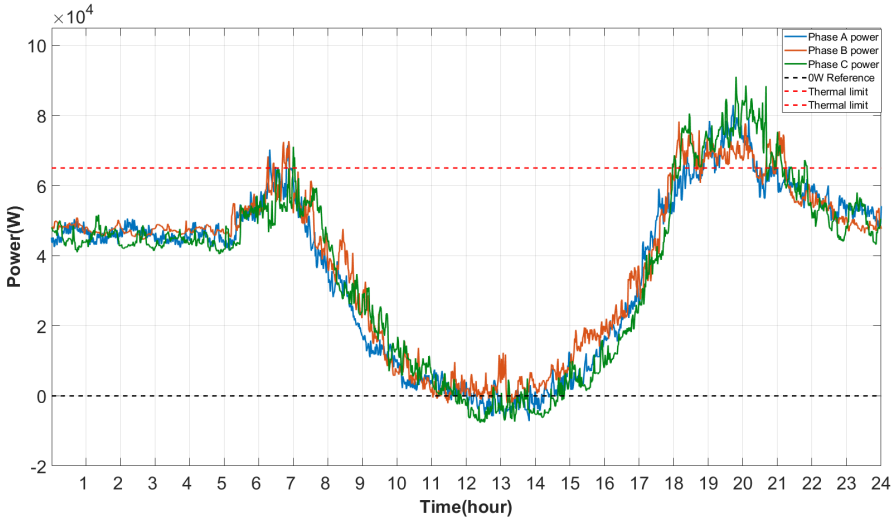

Figure 6.15: 24-hour worst-case load profile with future NRS 097-2-1 regulation at 25% renewable energy penetration

The load profile of the soft-start test looks the same as that of the regulatory control test and unregulated PV test. In terms of power draw, there are no visible discrepancies between the various load profiles. All the phases are relatively balanced, and the energy flow only veers negative for a short while before drawing energy from the MV network again.

The voltage profile exhibited in figure 6.16 indicated that the maximum voltage level reached during the 24 hours is 1.105 p.u. The voltage violation only occurs on phase A because it is the lightest loaded phase at the moment of maximum generation. The voltage profile indicates that the soft starter algorithm minimises the frequency of overvoltage on the feeder. The voltage only violated the upper limit on four occasions in a time span of an hour. However, it does not inhibit the voltage from exceeding the upper voltage limit, indicating that there is still work to be done to identify methods for further improving voltage regulation the desired efficiency.

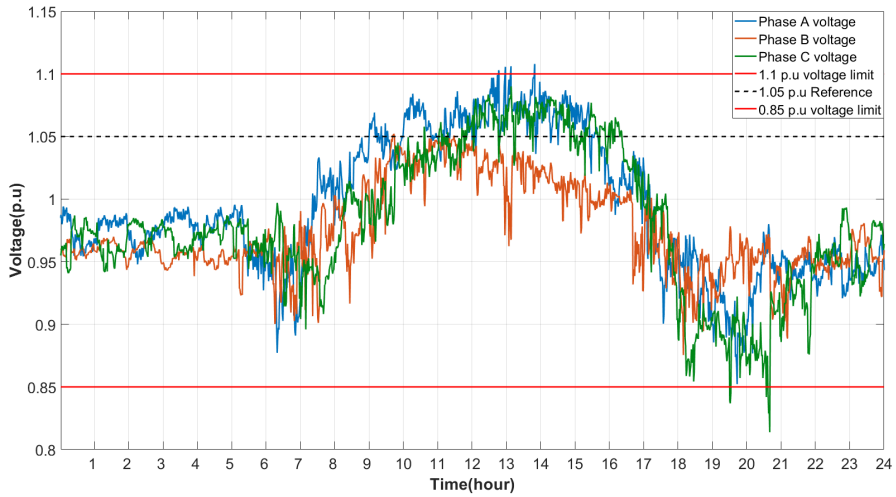

Figure 6.16: 24-hour worst-case voltage profile with future NRS 097-2-1 regulation at 25% renewable energy penetration

Nonetheless, the voltage variations are not as frequent and violent with a soft-starter implemented as they are without a soft-starting algorithm. The phase voltage dependencies are not as high as in the basic voltage regulation method. This is due to the slow power ramp rate minimising the voltage transients that would typically be present when constantly removing and then re-introducing energy generation every minute to two minutes.

6.4.2.2 50% Renewable energy penetration

The results of the soft starter test at a 25% renewable energy penetration are an improvement compared to the basic voltage regulation present in the industry at the time. To evaluate the efficiency of the soft-starter voltage regulation method, the performance has to be assessed at different renewable energy penetration levels. The verification test will be conducted at 50% renewable energy penetration. The purpose of this test is to identify if the results are similar in form to the 25% test and evaluate the degradation of results as the renewable energy penetration is increased.

The soft starter test at 50% renewable energy penetration generated the load profile displayed in figure 6.17. The graph denotes that when compared to the 25% renewable energy penetration soft starter test, the oscillation in load has increased in frequency, which is to be expected when increasing the generation capacity on the feeder. The power oscillation starts to occur above the 20 kW mark per phase, as seen in the regulatory voltage control test at the same renewable energy penetration level. The load profile on its own already indicates a significant improvement when implementing the soft starting voltage regulation in conjunction with current industry practices. This improvement indicates that the renewable energy generated came closer to the daily generation capacity of the system than in the basic voltage regulation test, meaning that the energy generated could be better utilised. The average negative power flow at the interval of maximum generation was equal to 19 kW per phase.

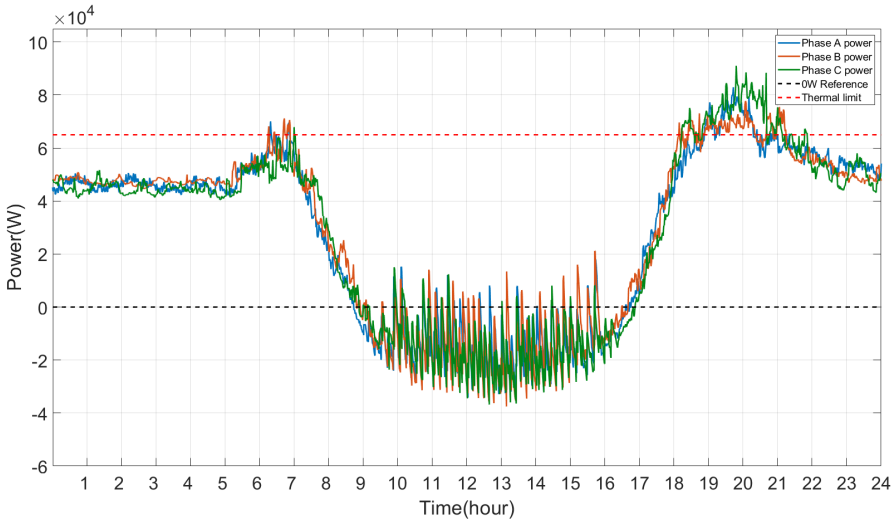

Figure 6.17: 24-hour worst-case load profile with future NRS 097-2-1 regulation at 50% renewable energy penetration

The increase in renewable energy did not cause a significant change in the expected results. At times of negative power flow, power level had only risen above the 0w reference line 16 times collectively across all phases. The average negative power flow at times of maximum generation is equal to 25 kW per phase. The maximum reverse power flow of 40.12 kW per phase was 25 kW shy of exceeding the negative thermal limit.

The voltage profile corresponding to the 50% renewable energy penetration load profile with the soft-start algorithm implementation is exhibited in figure 6.18. The profile indicates that the maximum voltage level equals 1.18 p.u, which is 8% higher than the 25% test. The voltage oscillations are inherently indirectly equivalent to the power oscillations. This relationship indicates that with the increase in power oscillations caused by the rise in renewable energy penetration, the voltage oscillations also increases. The number of upper voltage limit vio-

lations have increased dramatically with the increase in renewable energy penetration, even though the increase in maximum voltage deviation is only marginal.

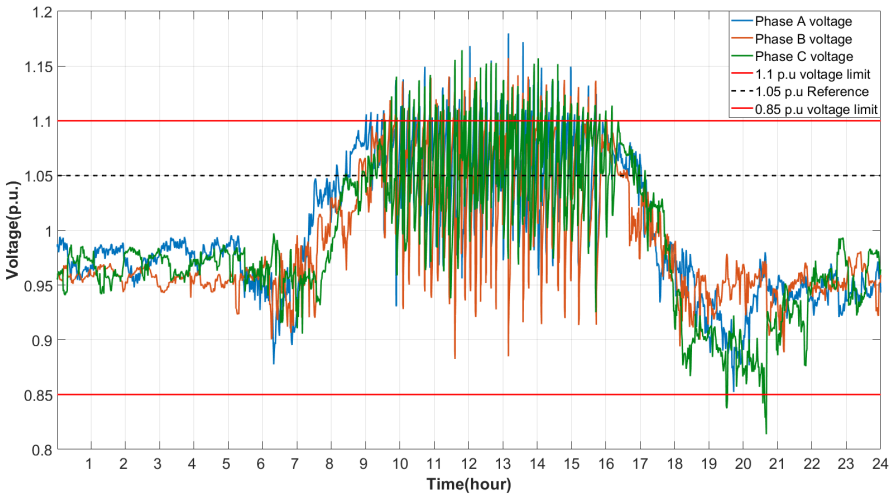

Figure 6.18: 24-hour worst-case voltage profile with future NRS 097-2-1 regulation at 50% renewable energy penetration

Comparing the two tests at different voltage levels denotes that the soft starter method improves the effectiveness of a single inverters' voltage regulation concerning the LV feeder voltage. The various tests indicated that this method is more effective at different levels of renewable energy penetration than the current voltage regulation practices present in the NRS 097-2. The soft starter voltage regulation method has thus far produced favourable results in terms of voltage regulation without the use of energy storage.

6.4.3 Power-voltage test

The third test will evaluate the effectiveness of power-based voltage regulation. The IEEE 1547 indicates that the inverter can curtail its power generation when the voltage at the PCC violates the upper voltage limit. The voltage-power scale operates similarly to the power-frequency scale found in the NRS097-2-1. The relationship between the voltage level and the power draw is indirectly proportional to one another. The voltage-power relationship is indicated in figure 6.19 displayed below. The graph shows that the power starts to curtail at 250 V and should reach 20% power output at a voltage of 260 V. If the voltage exceeds 260V, then the inverter should disconnect from the grid. The power curtailment would possibly allow the voltage levels to dip back under the voltage limit. This minimises the possibility of disconnecting from the network and discarding the clean power that could be generated. The case still exists that voltage levels can remain high for long periods at a time. Continuously

high voltage levels will result in the inverters curtailing their power output for longer periods and, in effect, throwing away clean energy and increasing the payback time on these systems by increasing the system LCOE.

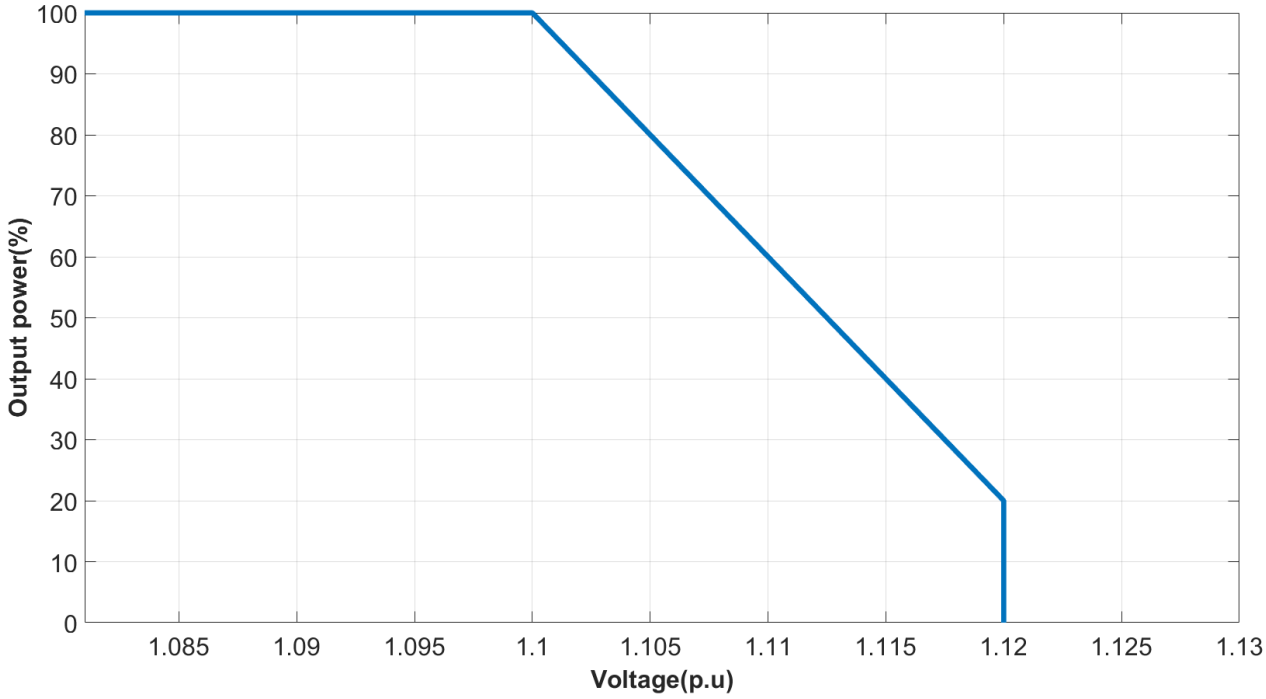

Figure 6.19: The voltage-power curve to determine the power output at specific voltages

6.4.3.1 50% Renewable energy penetration

The previous three tests have indicated that due to the generation and load balancing each other out at a renewable energy penetration level of 25%, the voltage does not typically exceed the upper voltage limit for the time required to activate the different voltage regulation control schemes. The increase in renewable energy typically brings the flaws of a regulatory method to the surface due to the tolerance changes and weight changes in the ratio between feeder load and generation. The power oscillation tends to increase due to the higher renewable energy penetration level due to the difference in the curtailment weight with each renewable energy penetration iteration. The 50% renewable energy penetration test with the power-voltage regulation implementation will evaluate the effect of doubling the allowed renewable energy penetration level has on the effectiveness of the voltage regulation scheme.

The feeder power curve measured at the transformer follows a similar profile to the power curve in the 25% renewable energy penetration test. The power curve displayed in figure 6.20 exhibits how the increase in generation causes the effect of unbalanced loads on the respective

phases to disappear. Interestingly, as the generation uniformly converges to the point of maximum generation, the generators at the end of the feeder start to trip off, inadvertently causing a voltage drop. The voltage drop causes the still active generators to increase their generation output whilst the tripped generators remain off due to the curtailment level being below 20% even though the voltage level at the PCC is within limits. The generators at the end of the feeder waste more energy than the rest of the feeder.

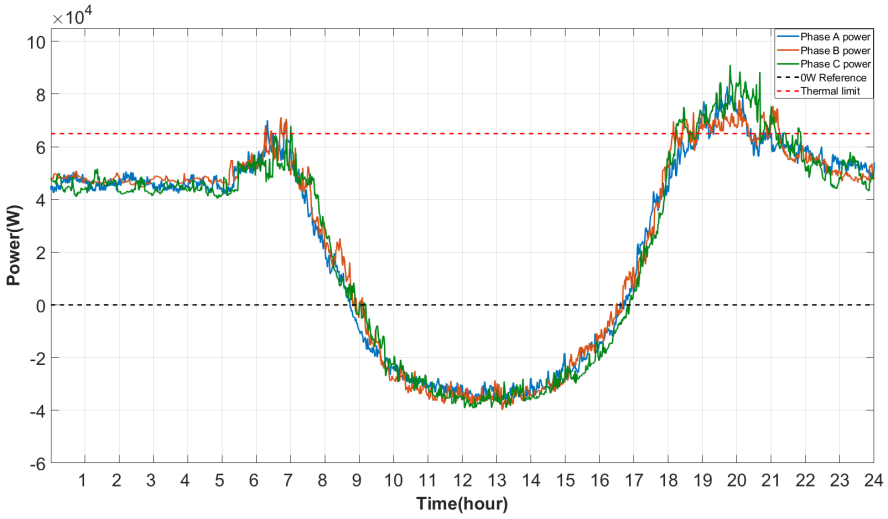

Figure 6.20: 24-hour worst-case load profile with active voltage regulation at 50% renewable energy penetration

The voltage profile indicates a minimal difference between the 25% renewable energy penetration maximum voltage and the 50% renewable energy penetration test maximum voltage. The voltage profile in figure 6.21 shows that the voltage regulation has improved with the increase in renewable energy penetration due to the lack of prominent voltage spikes. The majority of the nodes are net producers at times of high generation.

The balancing effect of renewable energy generation on the network minimises the sensitivity of the voltage deviations and, in turn, decreases the amplitude of the voltage oscillations around the 1.1 p.u. mark. However, the higher renewable energy penetration automatically means that a large amount of green energy is wasted in the energy curtailment process. The less green energy utilised means, the higher the reliance on fossil fuel-based energy generation. The power curtailment also increases the LCOE and the payback period of the system.

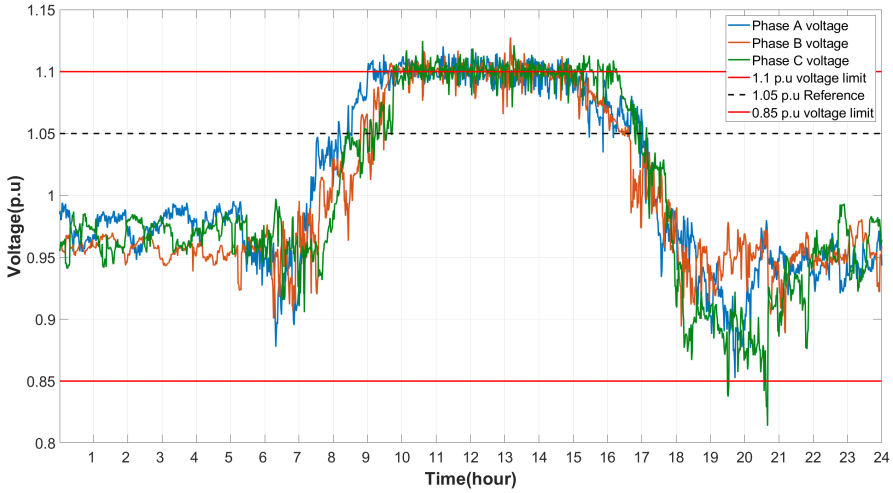

Figure 6.21: 24-hour worst-case voltage profile with active voltage regulation regulation at 50% renewable energy penetration

The power-voltage interdependent voltage regulation method is the most promising method of this chapter's three evaluated voltage regulation methods. It is important to note that the discussed voltage regulation methodologies are only relevant to grid-tie inverter technologies. This means that voltage regulation techniques with storage incorporated may require additional forms of control, and DC-coupled systems do not possess the regulatory control implementations.

6.5 Conclusion

The purpose of this chapter was to indicate that the NRS 097-2 regulations are outdated and need to change. The layout of this chapter was to initially test out current regulatory implementations and possible future regulatory deployments that can be implemented using new cost-effective technologies currently available on the market to allow for increased renewable energy usability and penetration.

The initial NRS 097-2-3 test indicated that the reactive nature of the voltage regulation method causes voltage spikes and drops due to the oscillation in renewable energy presence every minute. The flux is caused by voltage limit violations resulting in the inverters tripping off. When comparing the current regulatory test to a possible future regulatory standard where the generation ramps up at 10% per minute until the maximum generation is reached after synchronisation, it is evident that the oscillations have significantly decreased. The voltage fluctuation decreased due to the slower ramp rate, and the number of trips is also

substantially less than the regulatory voltage regulation test.

The active voltage regulation method, which regulates the voltage through regulating the power, yields favourable results due to the controller keeping the voltage constant. This allows for better energy usage induced by curtaining the power output and not regularly disconnecting for 60 seconds which yields control superiority above the other regulatory control techniques. The following chapter will focus on the effects of implementing ESS and energy aggregation to further improve renewable energy penetration.

Chapter 7

Intelligent controller development

7.1 Introduction

This chapter aims to develop and implement an intelligent VPP control structure on the validated residential LV network to showcase how renewable energy penetration can safely be increased to a higher tolerable limit without the need for grid impact studies. The intelligent control architecture can now be developed since the functionality and effect of all existing regulatory control structures have been evaluated. These tests include voltage and power regulation and network unbalance tests since these factors are predominantly the cause for the imposed renewable energy penetration limits.

The controller development will indicate the effects of the localised unit control with storage and the intelligent VPP control structure. The decision to utilise the active power flow to control the voltage on the feeder is warranted based on the work done in [49]. The effectiveness of the voltage regulation will determine the maximum level of renewable energy penetration. Additional features will provide ancillary services to the network in the form of active power support and voltage regulation. The system should also maintain a power balance between phases on the feeder network and maintain energy flow within the LV network parameters.

7.2 Local control

Grid-tie PV EG is the most cost-effective method for generating energy and becoming more self-sufficient by being less reliant on the grid. The dilemma, however, is that, as previously mentioned, the consumption profile and generation profiles do not continuously coincide, and

SSEG owners do not want to throw away any generated power.

The advancements in manufacturing technologies and improved electrochemical technology of chemical batteries to store energy have allowed the general homeowner to own an energy storage system. The ESS has made it possible for homeowners to store energy at times of maximum generation and effectively shift this generation to periods when power is most needed, typically at night or early morning. Another vital function of a residential ESS in South Africa is to keep the lights on during mandatory load shedding as a result of grid constraints.

The addition of ESS to SSEG opens up a whole new realm of possibilities. One example of this is that ESS can act as both a load and a generator and can swiftly ramp generation up or down to offset network disturbances. ESS can act as a buffer at periods when variation in generation occurs due to weather conditions. ESS enables SSEG to participate in ancillary services such as voltage regulation, upwards frequency regulation and downwards frequency regulation. ESS improves the dependability of environmentally dependent RES. The aforementioned functionalities assist with grid operations and improve grid stability.

The addition of ESS to a grid with renewable energy generation is a given in today's society. Still, before ESS may be incorporated into the SSEG of each unit on the feeder, the workings and composition of the ESS need to first be defined and clarified. The operations of the ESS will be described by the following assumptions:

- The battery chemistry to be mimicked will be lithium-ion Phosphate. LiFePo4 has a high current rating and a high depth of discharge.
- LiFePo4 batteries have a depth of discharge (DOD) of 90% with a lifetime of 6000 cycles
- The battery system will be represented as an AC battery, meaning that the conversion between DC and AC will not be taken into account within the Simulink® model.
- The batteries will have an overall energy conversion efficiency of 85%, according to the manufacturer datasheet.
- The battery capacity will be indicated in kilowatt-hour (kWh). kWh is easily interchangeable between the DC and AC energy criteria and will avoid any confusion.
- All the batteries in the feeder will start with a SOC of 20% at the simulation start. The 20% SOC will be viewed as the minimum SOC limit and will indicate a depleted battery.
- The battery will be limited to a maximum SOC of 99% since all ESS owners attempt to maximise the LCOE of the hybrid system and to overcharge an ESS exponentially shortens its lifetime.
- The battery is modelled as an ideal battery regarding the thermal characteristics. The

battery will not increase or decrease its inefficiencies as the temperature varies.

- The batteries are limited to 0.5C, meaning that the batteries have a maximum demand equal to half the battery's capacity.

The ESS capacity can differ between consumers depending on their needs. The problem with the randomisation of storage capacity allocation on the feeder is that the number of different allocation combinations is endless. It is assumed that due to the state of the country and the dislike for the current energy provider, high earning households who are financially capable of procuring a significant ESS capacity to decrease their dependence on the grid to zero will do so. A rule of thumb in the industry when designing a system to be off-grid in ideal conditions is that the ESS should be four times larger in capacity than the maximum installed capacity of the solar array. An example of this will be that if the PV array is sized at one kilowatt peak (kWp), the ESS capacity will be equal to 4 kWh. For this study, the battery system is designed so that total grid independence is impossible. The ESS will be sized to a capacity equal to three times that of the RES. This sizing method will cause the batteries to charge to maximum capacity with the ideal generation. The system is required to curtail its generation or feed energy back into the grid, depending on the grid state. The ESS sizing will induce the need for intelligent control to better manage the energy flow on the feeder when all resources are aggregated.

The assumptions mentioned are only pertaining to the chemical and physical aspects of the ESS. The ESS can not function without following a particular set of rules, otherwise known as a protocol or algorithm. The ESS requires an energy management algorithm to correctly adhere to the system's limitations and determine when and how much energy should flow between the ESS and grid. The algorithm in question will reside on an energy controller situated behind the meter of every unit on the feeder. From this point forward, the control scheme will be referred to as the local controller.

The local control scheme monitors seven different system parameters, namely the load, local PV generation, ESS SOC, active power flow at the PCC, the positive sequence node voltage, the grid setpoint and the battery capacity constant. The local hybrid controller's purpose is to effectively manage the energy distribution behind the meter as well as between the SSEG and the network based on the inputs received from the user or an external controller.

The local hybrid controller will process all the incoming data with the local control algorithm, which will yield the required outputs. These outputs will be transmitted to both the battery inverter and PV inverter. The battery inverter value can be positive or negative. The polarity of the value will indicate whether the ESS should be drawing power from the household network or injecting power into the household network. The value will indicate the amount of

power to be exchanged between the ESS and the household network. Suppose the controller instructs the ESS to absorb more energy or deliver more energy than it is capable of doing. In that case, it will restrict the energy exchange between the ESS and the network. The ESS will also deactivate its charging function if the ESS SOC reaches 99%. The same can be said for when the ESS reaches an SOC of 5%. However, the local controller is programmed to restrict the SOC to between 97% and 20% under normal operating conditions. A safety zone is built in to accommodate for any unforeseen condition changes.

The data transmitted to the PV inverter will indicate whether the inverter should operate at maximum capacity or if the inverter should curtail its output. The data sent from the local controller to the PV inverter will also dictate the amount of power by which the inverter should reduce its output. Once the ESS is charged to the desired SOC, the local controller will instruct the PV inverter to curtail the generation output to match the load that is currently being drawn. The load-generation matching results in the ESS going into stasis. The ESS will only react in the event of an instantaneous change in load or generation to counteract the change if it is within the capacity of the ESS.

The benefit of the local controller is that it enables two independent systems to work in unison. The advantage of working in unison is that the energy flow can be precisely controlled during variations in load and generation. The accurate control and ESS allow for energy stability during times of uncertainty.

The local controller algorithm is exhibited in figure 7.1. The flow diagram follows the decision process of the local controller to manage the energy flow within the system. The algorithm receives the reference power value from the global controller. The reference is assumed to be zero in the absence of the global controller since there is generally no incentive to feed energy back into South Africa's grid. If there is an incentive, it generally does not make financial sense. The algorithm determines if the energy generation is greater than the difference between the load and the reference. If the energy generation is higher than the difference between the load and the reference, this means that there is excess energy available to charge the ESS. Once it is determined that extra energy is available, the algorithm will evaluate whether the ESS SOC is within the preset bounds. If the SOC is below the upper limit, the ESS will absorb the excess energy. If the current SOC is equal to or above the upper bound, the ESS will not charge, and the controller will instruct the PV inverter to power match the difference between the load and the reference.

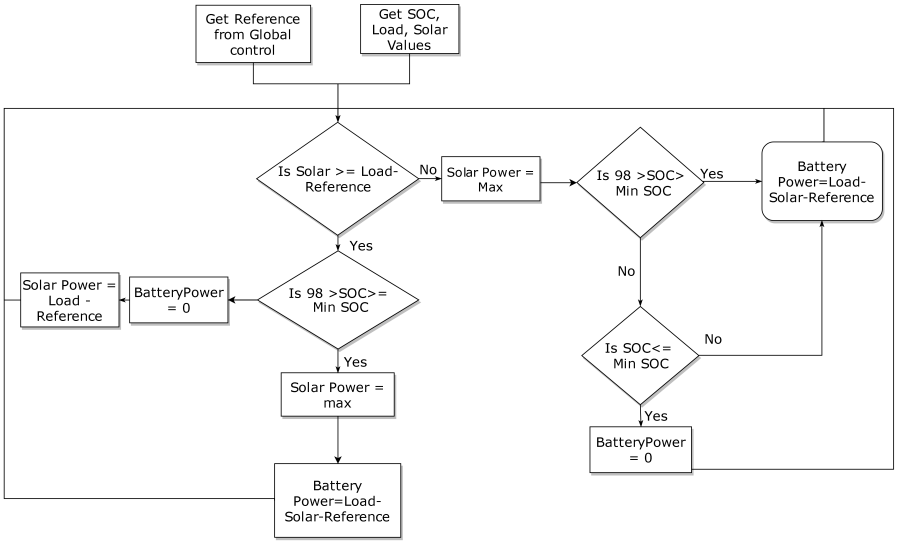

Figure 7.1: Local control decision process flow diagram

The reason for utilising the delta between the load and reference is that when the reference is positive, the difference between the load and reference is smaller than the load. This indicates that when the ESS is sufficiently charged, the PV inverter will match the delta to not produce or absorb power unnecessarily. The reference also allows for a predetermined amount of power to be exchanged with the grid if required.

If the energy generation drops below the delta, the ESS will start to discharge energy equal to the difference between the generation and the delta. As the generation decreases, the discharge power of the ESS increases until no more generation remains, and the ESS discharge power is now equal to the delta. The algorithm will monitor and cease to discharge the ESS if the SOC drops to 20%. The energy flow management system will automatically draw energy from the grid if the ESS is drained to its limit.

The voltage regulation protocols are still in place with the local hybrid controller. The goal of the control scheme is to evaluate the effect of energy storage and energy management on the voltage profiles within the network and network stability. The purpose of the ESS is to determine if the renewable energy penetration can increase and power curtailment can be mitigated with ESS implementation. The benefits that would originate from these goals are improving energy management and the efficient utilisation of clean energy. The test procedure will be similar to the tests conducted without ESS.

7.2.0.1 25% Renewable energy penetration

The first evaluation is at 25% renewable energy penetration with 13.8 kWh ESS at each unit. The ESS capacity is calculated as a function of the PV array size. The array size is 20% larger than the renewable energy penetration. This results in an ESS capacity equal to three times the PV array size. The total aggregated generation capacity on the feeder is equal to 137.16 kW. The generation is complemented by an aggregated storage capacity of 498 kWh.

The load profile displayed in figure 7.2 exhibits the load profile of the feeder with ESS and local control present. The data indicates that when the batteries are depleted in the early morning, the early morning peak still prevails. However, as the generation starts to pick up, the load at the transformer decreases. The moment the generation equals or exceeds the loads, the net energy flow on the feeder tends to zero and never goes negative due to the ESS absorbing any excess energy generation. This allows for optimal self-consumption. It is evident from the load profile that the load at the transformer never drops to 0 W due to the dispersion on the network. This is caused by specific units having excess energy to charge their ESS. Other units utilise all the generated energy to service their loads while drawing the difference from the grid. This restricts any negative energy flow, which results in effective voltage regulation.

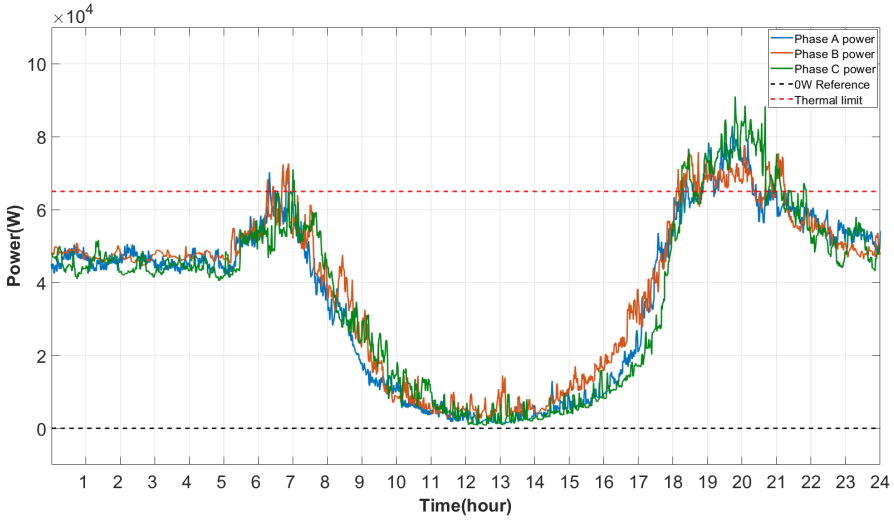

Figure 7.2: 24-hour worst-case load profile with local control at 25% renewable energy penetration

The improved energy management becomes clear when inspecting the worst-case voltage profile where the maximum voltage deviation occurs. It is clear that the implementation of ESS has flattened the voltage curve during times of high generation and has improved the energy efficiency of the feeder by minimising the amount of green energy wasted. Even though the ESS implementation has increased the overall self-consumption of users, it still leaves wanting

for a balanced feeder. The variation in load resulting from the SOC difference between the different ESS has caused an imbalance in the grid energy between the phases measured at the transformer at times of discharging and stochastically depleting the ESS. The voltage profile displayed in figure 7.3 shows the significant difference between a grid with ESS vs without ESS when compared to figure 6.11. The difference in voltage levels is remarkable. The voltage level remains around 1.05 p.u., rarely nearing the 1.1 p.u. limit. However, the lower voltage limit is violated by the maximum demand because the system cannot fully charge the ESS, and the capacity of the ESS can only sustain the load for 2.4 hours if fully charged.

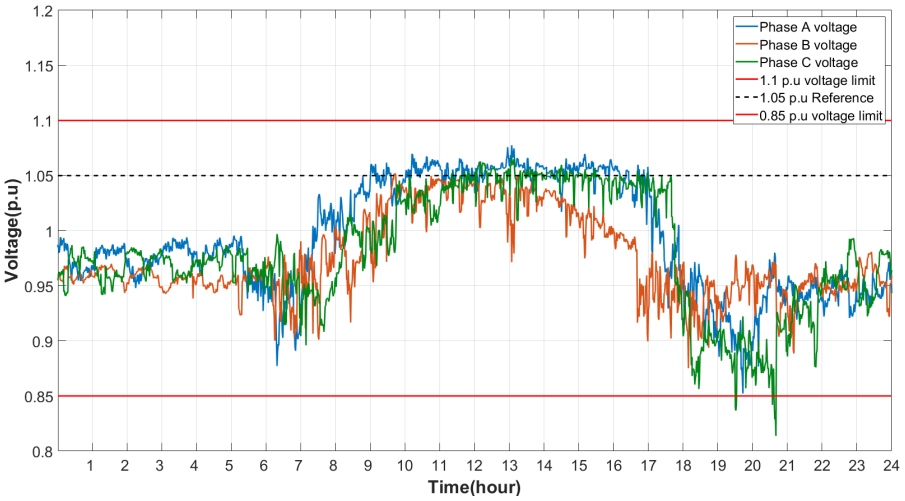

Figure 7.3: 24-hour worst-case voltage profile with local control at 25% renewable energy penetration

7.2.0.2 50% Renewable energy penetration

Following the 25% renewable energy penetration test, the 50% renewable energy penetration test will see the renewable energy penetration double from 25% of the household NMD to 50%. With an increase in the generation capacity, the ESS capacity also increases proportionally from 13.8 kWh of storage capacity to 27.6 kWh per household. The 1 - 3 generation to storage ratio for the renewable energy penetration test is constantly maintained. The total aggregated renewable energy present on the feeder at times of maximum generation in ideal conditions is equal to 274.32 kW of generation complemented by an aggregated ESS capacity of 995.328 kWh. The generation and storage will serve an average aggregated load of 162 kW. The aggregated values indicate that there might be a possibility of specific systems curtailing their output due to excess generation and ESS systems at maximum capacity. The goal of this test is to evaluate two predominant factors. The first is the voltage regulation improvement in the presence of ESS and the second is the efficient use of all generated energy within the feeder.

The power curve analysis indicates that at a renewable energy penetration of 50%, the negative slope of the power curve induced by the increase in the generation is significantly steeper than at 25% renewable energy penetration, which is to be expected. The increase in generation at sunrise has resulted in a smaller morning peak, which is also evident in the morning voltage drop indicated on the feeder voltage profile exhibited in figure 7.5. The feeder load profile in figure 7.4 indicates that generation exceeded the load at all units due to the increase in irradiation. This causes the ESS to absorb the excess energy generation. The loads being exceeded by the generation is evident where the loads tend to zero and remain at zero for most of the day. The energy absorption by the ESS allows for better grid stability and improved voltage regulation in the presence of excess generation. The absorption of energy in the event of excess generation is critical as this is one of the leading causes of voltage rise on the feeder, the other cause being unbalanced loading on the feeder. The feeder voltage profile serves as a testament to the improved voltage regulation indicating that at times of energy exchange between the grid and the ESS, the voltage at each node on the feeder tends to the feeder source voltage at 1.05 p.u. Once the generation decreases, due to the decrease in irradiation, the ESS takes over and services the loads up to the point of total energy depletion. The EMS then draws energy from the grid to service the loads; as more units drain their reserve energy, the load on the transformer increases. This can be seen in the load profile, where the load rises from zero to full load in a matter of minutes.

Figure 7.4: 24-hour worst-case load profile with local control at 50% renewable energy penetration

The increase in renewable energy penetration and ESS capacity in relation to the load has allowed for a larger portion of the generated capacity to flow to the ESS after serving the loads. This means that the ESS reaches a higher state of charge due to the increased ratio of

generation to load. The addition of ESS has also resulted in a drop in the feeder's maximum demand from 80 kW per phase to 70 kW per phase. The decrease in maximum demand increases the longevity of network components and reduces the strain on centralised power plants or the need for natural gas peaking power plants to operate. Reducing the need for peaking power plants could decrease capital expenditure to maintain these power plants when needed.

However, the drawbacks of ESS are that the load's stochastic nature and the high nighttime peaks cause the ESS to charge and discharge unevenly, resulting in certain ESS depleting before others on the network. The uneven charging and discharging can be solved by minor adjustments in the energy control algorithm, which would increase the balance in the network. However, it would lower the effective utilisation and storage of the generated energy within the network. The ESS depletion results in the system drawing energy from the network while other SSEG's on the network remain self-sufficient and causes an unbalance between the phases. The unbalance in phases leads to a deviation in the feeder voltage.

The voltage profile in figure 7.5 indicates that the maximum voltage does not approach the 1.1 p.u. upper voltage limit with an increased ESS capacity and increased renewable energy penetration levels at times of maximum generation. The maximum voltage does not exceed 1.1 p.u., and the minimum voltage does not vier below 0.86 p.u., indicating that ESS is a viable option in aiding the improvement of voltage regulation to increase renewable energy penetration.

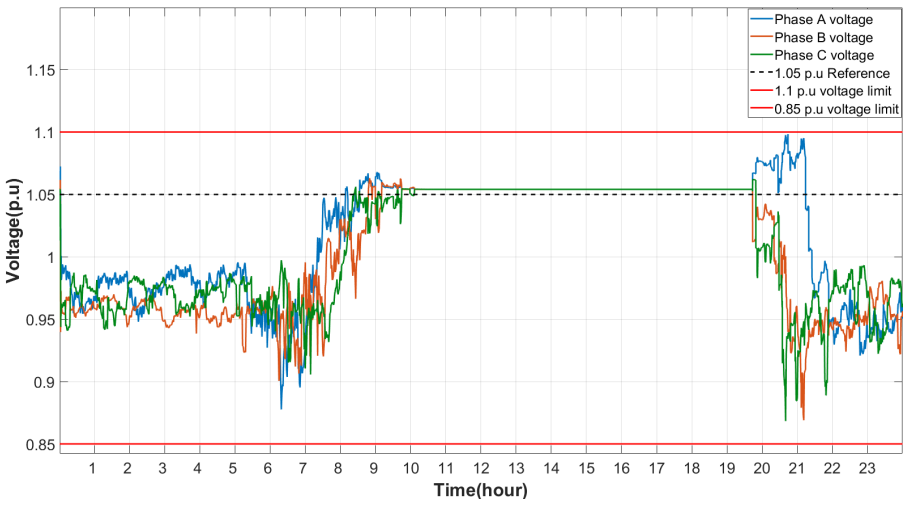

Figure 7.5: 24-hour worst-case voltage profile with local control at 50% renewable energy penetration

The utilisation of local energy control has automatically improved the voltage regulation on the feeder at high renewable energy penetration levels. However, the downside of local control

is that when an ESS reaches maximum capacity resulting in the throttling of the power generation. The curtailed generation can be efficiently utilised in other parts of the feeder to support the nodes most in need of energy, assuming the necessary incentive is in place for assisting in network operations. Feeding energy to other nodes could be achieved by means of energy exportation. The only hurdle is that the local controller cannot identify the amount of energy needed to be fed into the network to service other loads on the feeder in the event of excess generation.

On the other hand, the nodes that could use the excess energy on the feeder would not know how much energy to draw from the grid to maintain a net-zero power balance at the transformer. This has to be done while maintaining the voltage within regulatory limits. A centralised controller capable of monitoring the conditions on the entire feeder is needed to make intelligent decisions based on a set of rules in order to optimally utilise the energy generated by the various SSEG whilst remaining within the voltage limits.

7.3 Virtual power plant

The local controller has shown how effective the combination of local energy management in conjunction with ESS can be to improve the voltage regulation on the network and, in turn, increase the renewable energy penetration level. The voltage regulation methodology is still left wanting since the voltage is regulated correctly, but no energy generated is fed back into the grid. This is where the use of a T-VPP will become evident.

The purpose of a centralised controller that aggregates and manages all of the resources on the feeder is to distribute energy as effectively as possible at any renewable energy penetration level while still regulating the voltage within the upper and lower voltage limits.

The global controller is a centralised controller with the role of controlling all the decentralised local controllers. In addition to receiving data from the local controllers, the global controller also measures the energy interchange between the MV and LV networks. The global controller requires information from the local controller to determine the system's capabilities. The local controller of each of the 36 units will send seven parameters to the global controller. These parameters are as follows:

- A binary variable indicating the presence and combination of generation and ESS.
- The storage capacity of the ESS.
- The amount of energy being generated at the specific unit.
- The load being drawn.

- The node voltage on the connected phase.
- The state of charge of the battery.
- The energy flow to and from the ESS.

The influx of 255 data points every second results in high data traffic. The variables need to be processed, after which the algorithm needs to make decisions based on the different inputs. The decisions will then be translated into reference power values sent to the relevant units. The power reference indicates to the controller the desired power draw based on the current local variables and the overall energy flow on the entire feeder. The reference value can be positive or negative depending on whether the unit needs to draw energy from the grid or inject energy into the grid. The algorithm responsible for interpreting the data and assigning the reference power values to each unit on the feeder has been designed based on the data accumulated from the characterisation tests and the regulatory and local control tests. Integrating different algorithms into one super algorithm will pose some challenges as specific algorithms could clash when transitioning between states.

The data transmitted from the local controllers are sorted by the algorithm and assigned to a phase based on the classification variable. (The global controller has two main functions: keeping the voltage within the limits as specified by the GCRPP and controlling the energy flow for optimal energy distribution. The two algorithms regulate the flow of energy for both voltage regulation and energy optimisation and are not mutually exclusive from one another).

The main priority is to maintain voltage regulation. The voltage regulation algorithm of the global controller scans through all the data and then compares the node voltages on each phase along the feeder. The algorithm then identifies the unit with the highest voltage and registers the phase on which it is located. The voltage regulation (VR) algorithm will then identify the node with the lowest voltage level and determine the phase it is on by means of allocating the node with the lowest voltage to the phase with the highest current draw. The extreme node voltages will then be compared to the regulatory limits to determine if the extreme values lie between the boundaries. If the upper voltage limit is violated in the absence of generation, the algorithm will then determine if there is any energy available in the ESS of units on other feeders in order to feed energy back into the grid and lower the maximum voltage on the network. If there is no form of ESS available on the other phases, the algorithm will increase the power draw on the phase with the higher voltage in order to bring the maximum voltage back under the limit. The presence of solar changes the operating conditions of the algorithm. A renewable energy presence will cause the algorithm to throttle the generation on the phase containing the node that violates the upper voltage limit. This is done by reducing the power feed-in to zero or changing the power reference positive such that

the unit draws power from the feeder to lower the voltage and, in effect, throttle the energy generation or redirect it to the ESS.

The occurrence of both the upper and lower voltage limits being simultaneously violated at moments of no generation results in the algorithm increasing energy draw to 115% of the instantaneous aggregated load of the feeder. The power draw helps restore balance to the feeder and mitigate both the upper and lower voltage violation. In the event of maximum unbalance in the feeder due to DG allocation, the VR algorithm will throttle the feeder with the DG to the point where both the voltage limits are satisfied.

Two proportional controllers control the power flow. The central controller regulates power flow based on the upper voltage limit. In contrast, the secondary controller changes the reference value of the first controller based on the lower voltage limit. The first controller is active in all voltage level violation scenarios. The second P controller is only active if the feeder voltage violates the lower voltage limit. The reason for selective use of the secondary controller is that in the event of voltage limit violations of both the upper and lower voltage limits, the 2 P controllers will work together to lower the upper voltage level in order to raise the lower voltage level by means of rebalancing the power consumption across the phases.

In addition to voltage regulation, the T-VPP will also attempt to optimise the available green energy on the feeder while not violating the voltage limits. The initial step in controlling the energy flow is to first predict the energy available at certain times within the system. The prediction is made based upon the availability of stored energy and not generated energy due to the consistency and reliability of the stored energy. The availability period of the stored energy will be predicted based upon the average amount of energy that is flowing into the ESS. The average hourly energy is determined by means of a moving average filter that averages the hourly energy fed into the ESS. The time-based prediction of when the batteries will be fully charged is calculated as portrayed in (7.1).

$$time_{Activate}(t) = \frac{\frac{65 - SOC(t)}{100} * ESS_{cap}(t))}{0.85 * \frac{-BP(t)}{60}} + Time(t) \tag{7.1}$$

The predicted time $time_{Activate}(t)$ is calculated by utilizing the percentage difference between the desired SOC of 65% and the current SOC $SOC(t)$ of each unit within the feeder. The SOC difference is then multiplied by the battery capacity $ESS_{cap}(t)$ in order to calculate the capacity difference between the desired capacity and the current capacity of the ESS. The capacity difference is divided by the product of the average energy $BP(t)$ flowing into the ESS and the efficiency of the ESS. Based on the predicted time that the ESS will reach the preset

SOC level and the capacity of the ESS, the algorithm can determine when the feeder can view a unit as a load and when the unit can be viewed as a generator. The calculation is made for every phase on the feeder. Once a unit is identified as a load, it will draw a maximum of 6 kW from the network to help charge the batteries. The same goes for a generator being able to feed a maximum of 6 kW into the network. The problem, however, is that the ratio between the aggregated load and aggregated generation is seldomly balanced. The unbalance can cause unwanted voltage deviations. Maintaining the balance between the load and generation will be done by utilising the ratio between the load and generation to balance the load and generation. The load on a specific phase will be decreased to equate to the generation in the event that the load is greater than the generation. The generation will be decreased to equate the load in the event that the generation is higher than the load.

Load-generation balancing occurs in the initial stages of the self-consumption cycle when the load exceeds the generation as the aggregated generation increases and exceeds the aggregated load on all three phases. The algorithm will determine which phase has the least excess generation and set the aggregated generation reference equal to the phase with the lowest generation. As generation increases on the lowest phase, so does the amount of energy exported to the MV network. The energy exportation is limited to the thermal limit of the reticulation lines on this specific feeder. The energy export limitation of the VPP can be set to either the reticulation thermal limits or 75% of the transformer capacity, depending on which one is the lowest. The reason for this is not to damage the network infrastructure when feeding energy into the MV grid.

The final two algorithms are the balancing algorithm and peak shaving. This balancing algorithm comes into play when the ESS discharges in order to service the load. Certain ESS drains faster than others resulting in an unbalance when certain ESS are depleted and others not. The balancing algorithm then allocates more energy from the ESS system to the feeder. The reason for this is to ensure that the unbalance is minimised between phases while not drawing current from the MV grid. The overall goal of the algorithm is to improve balance while maintaining optimal self-consumption. The balancing algorithm determines whether it should engage or not by determining which ESS's are at the minimum SOC. The algorithm then divides the units up into consumers and self consumers. The load drawn by the consumers are aggregated. The aggregated load profile indicates the total amount of load that the system needs to minimise. The aggregated SOC capacity is then used in order to determine the ratio between the power available and the power required. The ratio is then utilised to determine the amount of power that each unit has to feed into the grid from the ESS to overcome the load. The feed-in value is then halved to ensure that the support time is prolonged.

All algorithm functions are combined in the flow chart displayed in figure 7.6 and figure 7.7. This indicates the thought process of designing the algorithm used in the global controller to increase renewable energy penetration. The flow diagram of how the controller interprets and sorts the data is displayed in figure 7.6.

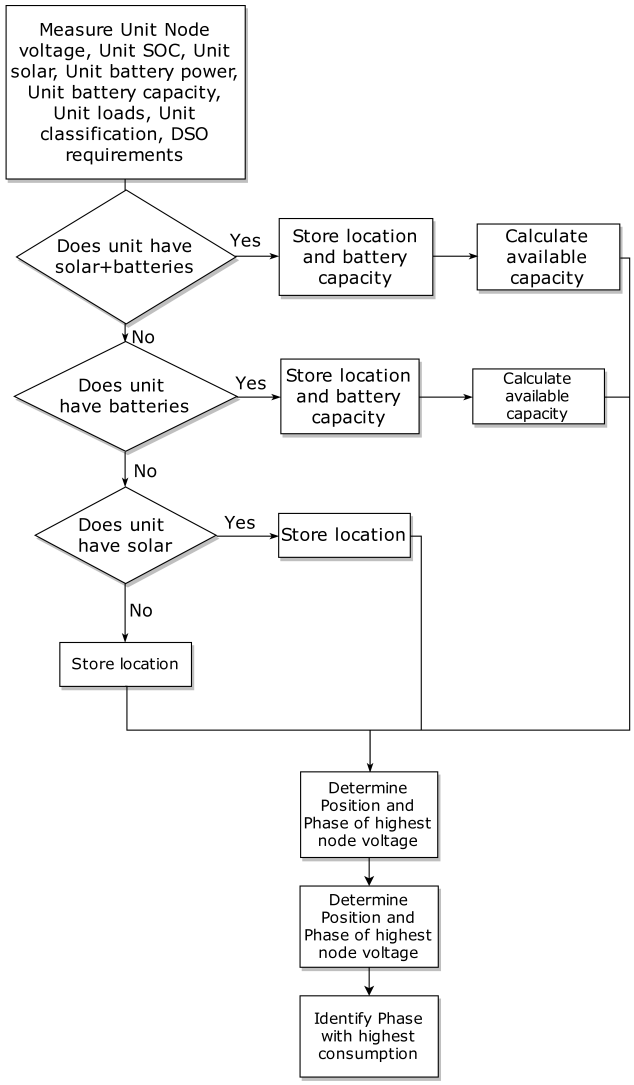

Figure 7.6: Flow diagram for global control sorting and identification algorithm

The interpretation and dispatch algorithm responsible for determining the power reference for each unit based on the identification algorithm is displayed in figure 7.7.

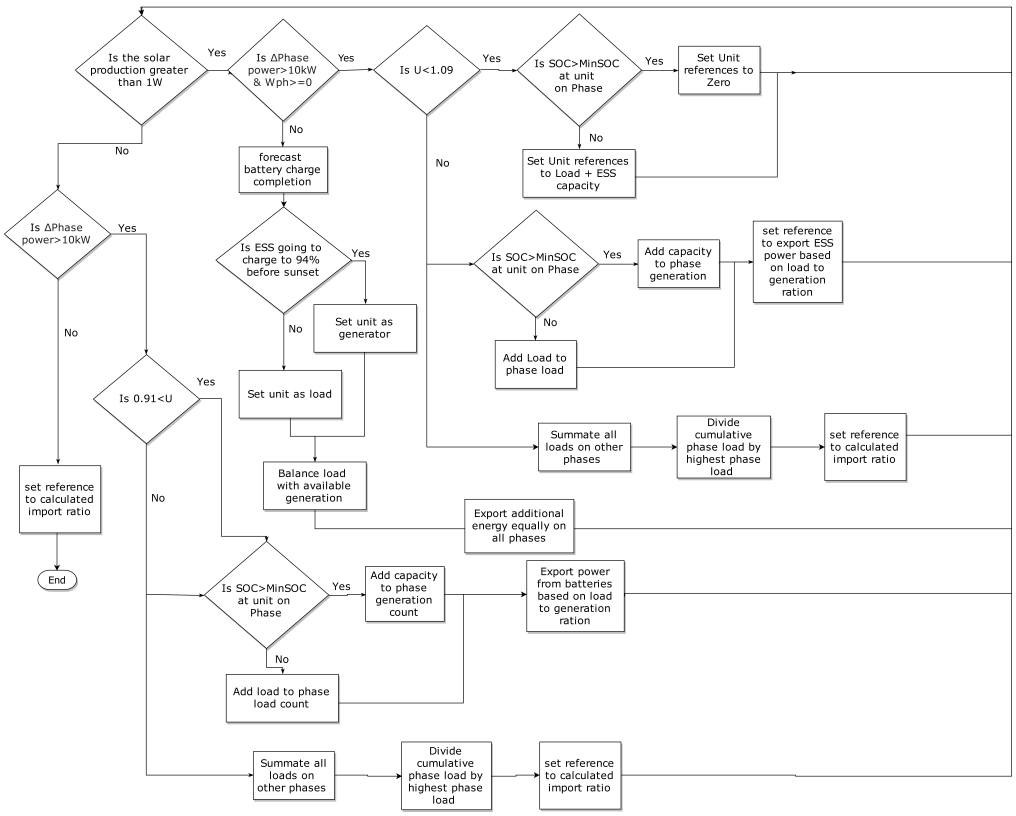

Figure 7.7: Flow diagram for global control interpretation and implementation algorithm

7.3.1 50% Renewable energy penetration

The test of the virtual power plant will initially be conducted at a 50% renewable energy penetration level due to the fact that the maximum generation at a renewable energy penetration level of 25% does not exceed the average load value. The 50% level comfortably exceeds the ADMD of each unit on the feeder, indicating that the power is high enough to charge the battery at maximum generation. The purpose of the test is to evaluate if there is any improvement in voltage regulation between the local control test and the global control test. The global controller, as previously mentioned, is tasked with the responsibility of safely increasing the renewable energy penetration from the regulatory 25% to possibly double that while remaining within the voltage limits and minimising the curtailment of the DG systems. The regulatory control is still active in each unit on the feeder.

The test conditions for the global control are similar to the local control. The ESS is still sized three times larger than the installed capacity of the PV system. The ratio remains the same as the renewable energy increases meaning that when the renewable energy penetration doubles, so do the ESS capacity. The ESS of each unit starts each test at the minimum SOC.

The drained battery ensures that the test is unbiased instead of beginning with a full ESS and providing ancillary services when the ESS should be depleted. The test is supposed to represent real-world conditions and results, and for this reason, the starting parameters should be as accurate as possible.

The power as measured at the transformer can be viewed in figure 7.8. The graph indicates that the loads are relatively stable and balanced since everyone sleeps in the early morning. The effect of the aggregated ESS is not yet visible as no storage system houses any residual energy. The beginning of rush hour induces a spike in load as everyone is preparing to travel to work. As rush hour starts, so does the generation causing a slight reduction in the maximum morning peak due to the light presence of generation.

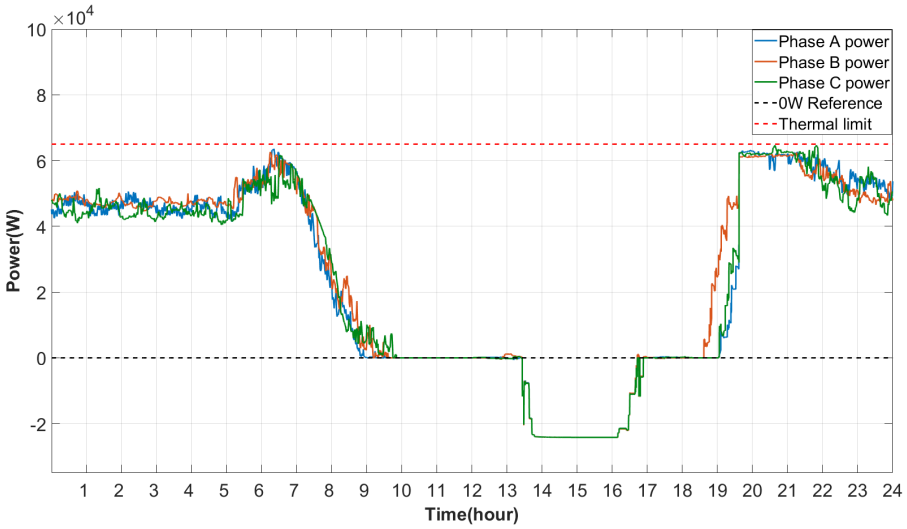

Figure 7.8: 24-hour worst-case voltage profile with VPP control at 50% renewable energy penetration

The peak shaving algorithm effectively keeps the load below the conductor thermal limit by lowering the minimum SOC and partially discharging the ESS on each unit in order to fill the power required above the thermal limit at both the morning and evening peak. The increase in generation induces a decrease in effective load, alleviating the peak shaving algorithm. The late rise in load caused by the rise in demand from the feeder due to more people waking up induces an unbalance on certain phases. The unbalance is still within the tolerable range to not cause the voltage to violate the voltage limits. The increase in the slope of the generation curve increases the slope angle of the load decrementation. Once the load reaches the zero mark, the ESS begins to charge by absorbing the excess energy generated. The charging is indicated by the power curve maintaining a straight line at zero. The prediction algorithm then determines when the batteries will reach an SOC level of 65%. Once the first unit reaches 65% SOC, the control algorithm separates the units that require additional power and the

units that can deliver extra power. This internodal power transference can be seen where all three phases have a slight offset from one another in terms of power drawn from the grid. Once all three phases can deliver the same amount of minimum excess power, the controller will regulate the power flow on all three phases to export energy in a balanced fashion to the MV network. As more power is readily available on the feeder, the controller will increase the amount of energy exported to the MV network until the thermal line limit, transformer limit or upper voltage limit is reached. The export regulation is evident on the power graph, where the energy flow turns negative and increases to 21.1 kW per phase. The 21.1 kW per phase export mark sets the voltage at the 1.1 p.u. limits. Any higher voltage will violate the upper voltage limit, which defies the controller's purpose. This limit is automatically set by the controller based on the feeder voltage.

The decrease in renewable energy generation leads to the ESS taking over as the primary power provider. Once this occurs, the SOC of specific units will fall below 60%, causing the controller to put the specific units in self-consumption mode by setting their reference power draw to zero. The effective aggregated energy is lower as the sun starts to set, resulting in the controller throttling the energy fed into the grid in order to conserve the energy stored in the ESS for nightly consumption.

The ESS SOC of the various units starts to reach the minimum SOC resulting in an increase in power draw from the network. The stochastic nature of the loads causes the ESS to discharge unevenly, resulting in a variable load incrementation at the end of the day. This, in turn, leads to an unbalance in the loading, causing a significant voltage deviation.

The voltage profile of the 50% renewable energy penetration test with global control is displayed in figure 7.9. The graph indicates a stable voltage in the early morning hours due to minimal variations in the load. The increase in morning load due to rush hour results in a 10% voltage drop. The voltage drops significantly without the aid of local generation. However, the peak shaving function allows the ESS to assist, so the voltage drop remains within respectable limits. The increase in generation leads to a voltage rise up to the point where the generation exceeds the load. The voltage oscillates around the source voltage during the transitioning period until all phases reach an equilibrium at 0W. The voltage remains constant as the network is in a state of self-consumption where the generation is only responsible for charging the ESS and servicing the load. The voltage rises and remains between the 1.05 p.u. and 1.1 p.u. voltage bands, indicating that energy is exchanged between units on the feeder.

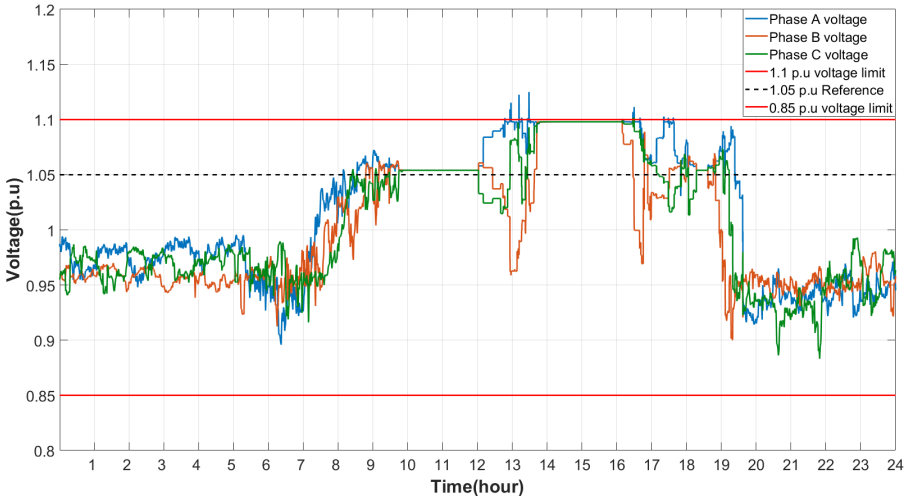

Figure 7.9: 24-hour worst-case voltage profile with VPP control at 50% renewable energy penetration

The moment the ratio of generation units to load units increase above the 1-to-1 ratio, energy is fed back into the grid as indicated by the voltage rising to 1.1 p.u. where the proportional controller regulates the power in such a way that the voltage remains at the limit of 1.1 p.u. with the exception of a random spike due to change in energy availability altering the balance and in turn the voltage balance. The decrease in generation causes the ratio of generation to load units to change back in favour of the load units resulting in the controller terminating the exportation procedure, favouring self-consumption and conserving energy for the nighttime peak.

The effect of the export limitation on the voltage is evident in the voltage decrease from 1.1 p.u. back to 1.05 p.u.. The voltage is regulated during the entire process by the power, which is controlled to limit the voltage from exceeding the upper and lower voltage limits. The events where the voltage limit is exceeded is allowed. However, the upper voltage limit may not be exceeded for longer than 40 seconds while the voltage remains below 1.15 p.u.. The controller adheres to the regulations by throttling the power when the voltage exceeds the upper voltage limit and increasing the energy draw from the ESS when the voltage drops below the 0.85 p.u. voltage limit.

When the ESS discharges all available energy under normal conditions and reaches its minimum SOC, the voltage drops back below the source voltage of 1.05 p.u. with a trajectory towards the minimum voltage limit as the demand on the network increases. The maximum peak load usually occurs at night. When the peak load occurred at 8 PM, and the voltage dropped below 0.85 p.u., the controller evaluated the unbalance and determined that the best method of lifting the voltage level is to increase the power draw on the other two phases.

This increased the voltage levels to a safe level. Another method of minimising the maximum demand on the feeder is to discharge the ESS for a short time while the load is at its peak and then afterwards recharge the ESS exceptionally slowly so as not to shift the peak from one point to another.

7.3.2 75% Renewable energy penetration

The 50% renewable energy penetration test yielded favourable results, and the global control algorithm regulated the voltage efficiently to remain within the limits while at the same time optimally utilising every ounce of energy produced by the SSEG on the feeder. The system did not curtail any generation, meaning no energy went to waste. The resulting data indicated that a 50% renewable energy penetration for each house on a feeder is possible when utilised in a VPP scheme. The total aggregated PV-DG is equivalent to 265 kW, which makes up 84% of the capacity of the transformer. The penetration exceeds the allowed generation capacity on an LV network since the total generation is limited to 75% of the transformer's capacity. The results prove that a larger renewable energy presence is possible if correctly managed.

The following test will be carried out at a renewable energy penetration level of 75%, equating to a maximum generation capacity of 11.43 kW per unit. The aggregated generation capacity is equal to 411.48 kW, which is equivalent to 1.3 times the capacity of the LV transformer, meaning that if something goes wrong and the control does not isolate or incapacitate the generation correctly, it will overload and eventually damage the transformer. The increased ESS may assist in absorbing most of the energy because it also receives a capacity increase as the renewable energy penetration level increases.

This test will start in the same manner as the 50% renewable energy penetration test. The ESS will begin at an SOC of 20%, indicating a discharged storage system. The ESS will have to further utilise the remaining critical capacity to provide grid support when the local generation is unavailable. The ESS can otherwise wait until generation increases and charge up with the excess energy generation.

The graph displayed in figure 7.10 indicates that the early morning profile represents that of the 50% renewable energy penetration level test. The load remains relatively stable on all phases due to the baseload of all units on the feeder. The morning peak is significantly shorter due to the increased effect of the generation due to the higher renewable energy penetration level. The increased renewable energy penetration generates a steep downwards slope and results in the generation exceeding the loads at an earlier stage. As the number of units where the generation exceeds the load increases, the power curve tends to zero. The ESS then

absorbs the excess generation while all units are in a local self-consumption state until the first ESS of each phase reaches an SOC of 65. The controller then instructs all other units on that phase to increase the power draw from the feeder until the exportation and power draw match. This is evident from the slight power deviation that occurs at noon.

Once the number of generators exceeds the number of energy users, the controller will allow the phases to feed energy back into the grid synchronously. The energy being fed back is controlled to regulate the voltage level and at the same time feed energy back into the grid, as seen by the negative power block evident on the power graph. The increased generation has allowed the feed-in function to start earlier because the excess generation is more readily available earlier in the day than the generation in the 50% renewable energy penetration test.

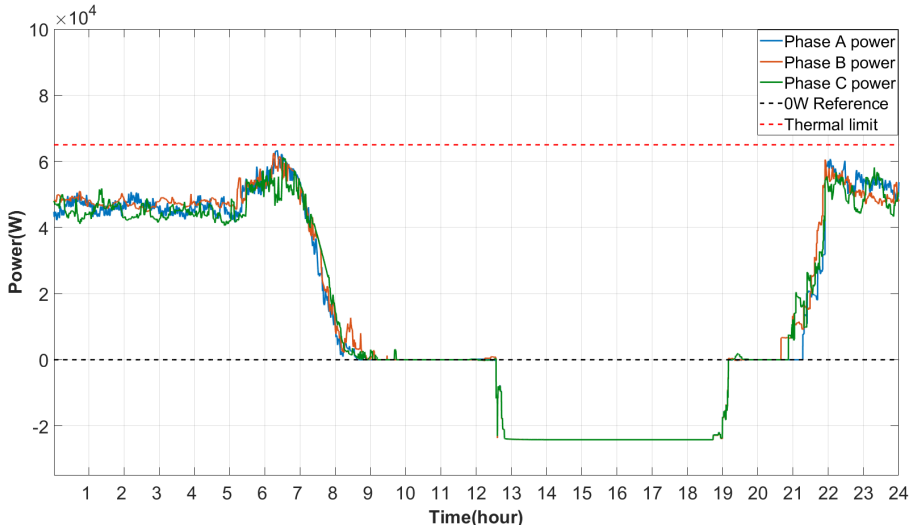

Figure 7.10: 24-hour worst-case voltage profile with VPP control at 75% renewable energy penetration

The decrease in generated energy on the feeder due to a reduction in irradiance late in the day causes the algorithm to revert to phase-based self-consumption at 19:00 as the nighttime peak starts. The nighttime peak is serviced by the ESS due to the increased storage capacity of the ESS at 75% renewable energy penetration when compared to the 50% renewable energy penetration test. The ESS capacity starts to run out at 21:00 and is fully depleted at 23:00 after the peak has passed.

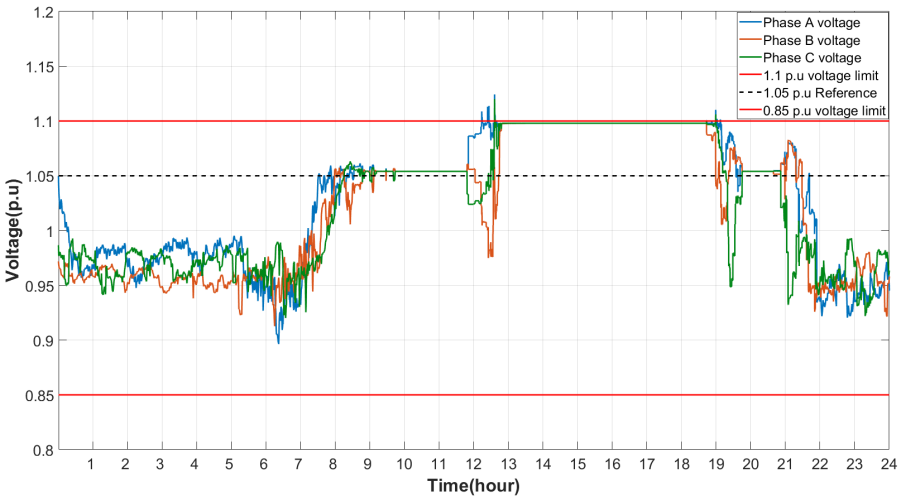

Figure 7.11: 24-hour worst-case voltage profile with VPP control at 75% renewable energy penetration

The voltage profile analysis at the 75% renewable energy penetration level displayed in figure 7.11 denotes the voltage profiles across all three phases. The voltage profile indicates that in the absence of generation and with the ESS being depleted, the slight load distribution causes a variation in the feeder voltage across all phases. Once all feeder units possess excess generation to charge the ESS, the voltage settles at 1.05 p.u. for the while in which the local self-consumption occurs. When the algorithm switches to feeder self-consumption, the position of specific units on the feeder dictates the voltage drop or voltage rise when energy is shared between generator units and load units. The voltage variates in the same manner as with the 50% renewable energy penetration test. The only difference is that the feeder voltage reaches 1.1 p.u. faster due to the increased penetration level and the increased generation to load ratio. Once all the load units have converted to generator units, the voltage starts to level out at 1.1 p.u. due to the balanced energy discharge from all units on the feeder. Small voltage spikes exceeding the 1.1 p.u. limit are evident on the graph. Once the voltage exceeds the limit, the controller immediately reduces the power output to bring the voltage back into bounds. The improved voltage regulation leads to an increase in effective green energy utilisation and renewable energy penetration.

The trend of voltage regulation then starts to run in reverse order due to the reduction in energy generation as the sun begins to set. The controller reverts to the feeder self-consumption as the generation decreases and then furthermore reverts to local self-consumption to optimally utilise the remaining energy in the ESS to service the unit's loads. This can be identified on the graph from the consistent voltage of 1.05 p.u. The depletion of the ESS results in the units drawing energy from the network resulting in voltage deviations on the voltage profile.

7.4 Conclusion

This chapter set out to develop and implement an intelligent control algorithm capable of safely increasing renewable energy penetration by means of accurate voltage regulation. This was accomplished through energy and power aggregation. The results indicated that all the objectives were met, and the renewable energy penetration could successfully be increased to 81% of the transformer capacity while not posing any threat to the network integrity.

The incorporation of ESS has allowed the control system to safely increase the renewable energy penetration on the LV feeder. The effect of ESS incorporation in SSEG was evaluated and compared to the tests without ESS, and the results are opposite extremes. The feeder with an ESS presence can finely regulate the voltage level as opposed to the SSEG without ESS. The system can store excess energy in the ESS and curtail any additional power. The implementation has increased the effective use of energy at an increased renewable energy penetration level and improved voltage regulation.

The incorporation of global control has resulted in increased energy exchange between units on the grid to optimise the use of SSEG at incremental renewable energy penetration levels while maintaining voltage regulation. The VPP has been able to allocate energy to parts of the feeder where it is most needed while regulating the voltage on the limit. The VPP has also provided ancillary services such as peak shaving and generation support during critical periods. The results indicate that with an intelligent control scheme, the increase in renewable energy penetration is possible, as the control will regulate energy effectively while maintaining voltage regulation and safeguarding network integrity.

Chapter 8

Performance analysis

8.1 Introduction

The various control implementations have proved to be successful in safely increasing the amount of renewable energy penetration on the feeder. The controller effectiveness is, however, still to be determined. The performance analysis chapter evaluates each control algorithm's effectiveness under different conditions to determine which algorithms deliver the best overall results. The performance analysis is required to determine where the control algorithms become ineffective. The effectiveness of the control algorithm, both in terms of effective energy utilization and voltage regulation and unbalance mitigation, will serve as a testament to the effort and thought that went into the design and development process of the energy controllers.

8.2 Test parameters

The performance analysis of the different control methodologies will be conducted by means of measuring and comparing the set of parameters critical to the succession of the control scheme. The parameters in question will be compared across the control structures to classify the control structures from worst to best. The parameters form a critical part of the controller's performance due to the fact that the parameters in question are affected by the manner in which the controller controls the units on the feeder and, in turn, the energy. The parameters that need to be evaluated are as follows:

- The net energy consumption from the MV feeder as measured at the transformer over

24 hours.

- The net feeder energy consumption will provide insight into the feeder's energy self-sufficiency during the 24 hours.
- The net energy exchange between each unit and the feeder will also be measured and compared with the other units and other controllers to determine the participation of units in grid activity on the feeder.
- The total generated energy from the PV system of every unit will be measured to evaluate how much of the system's capacity is utilised instead of being curtailed due to a lack of load.
- The voltage regulation on the feeder will be evaluated to determine whether the controller keeps the voltage within the necessary limits.
- The unbalance on the feeder will indicate how the variation in energy is managed and the voltage regulated to maintain a balance below 3%

The base-case scenario established the reference load energy in the absence of any form of SSEG to which the test results can be compared. (The tests can be conducted at low ADMD levels as well in order to indicate whether changes in the ADMD makes the control algorithms more sensitive or less sensitive). The reference generation can be determined from the reference power curve of the SSEG. The energy efficiency will be tested at renewable energy penetration levels of 25% to 75%, mimicking ideal and weather-dependent generation profiles at every 25% renewable energy penetration increment. The reason for testing in ideal generation and non-ideal generation conditions is to view the effect of the weather on the efficiency of the controllers.

The energy consumed in the base case equals 3.8 MWh across the entire feeder, with each unit drawing an average of 108 kWh over 24 hours, while the generation is equal to zero. The base case has identified that the cumulative 3 phase energy drawn from the MV grid over 24 hours should be less than 3.8 MWh in the presence of SSEG. The self-sufficiency of the feeder is measured by how low the feeders with SSEG are below the base-case load. It is expected that feeders with ESS present will have higher self-sufficiency than those without ESS, and feeders with the largest ESS capacity will have the highest level of self-sufficiency. This is valid under the assumption that the control scheme is the same for the different situations. The voltage values of the test in the absence of SSEG also serve as the reference voltage regulation.

Table 8.1: Unregulated PV energy performance

Unit identifier	Load(kWh)	Renewable energy penetration level					
		25%		50%		75%	
		Net load	Generated energy	Net load	Generated energy	Net load	Generated energy
Transformer	3800	2681	**NA**	1647	**NA**	438.195	**NA**
Unit 1	104.17	75.135	100%	46.090	100%	17.044	100%
Unit 2	102.09	73.049	100%	44.003	100%	14.958	100%
Unit 3	88.553	59.508	100%	30.463	100%	1.418	100%
Unit 4	93.256	64.211	100%	35.166	100%	6.120	100%
Unit 5	99.607	70.562	100%	41.517	100%	12.472	100%
Unit 6	97.023	67.978	100%	38.933	100%	9.888	100%
Unit 7	103.47	74.428	100%	45.383	100%	16.337	100%
Unit 8	98.479	69.435	100%	40.389	100%	11.344	100%
Unit 9	99.177	70.133	100%	41.087	100%	12.042	100%
Unit 10	98.141	69.098	100%	40.052	100%	11.007	100%
Unit 11	104.10	75.051	100%	46.006	100%	16.960	100%
Unit 12	92.524	63.474	100%	34.429	100%	5.384	100%
Unit 13	100.43	71.392	100%	42.347	100%	13.302	100%
Unit 14	91.453	62.405	100%	33.360	100%	4.315	100%
Unit 15	87.459	58.407	100%	29.362	100%	0.317	100%
Unit 16	95.432	66.383	100%	37.337	100%	8.292	100%
Unit 17	91.070	62.024	100%	32.979	100%	3.933	100%
Unit 18	98.042	68.994	100%	39.949	100%	10.904	100%
Unit 19	103.46	74.425	100%	45.380	100%	16.334	100%
Unit 20	101.60	72.555	100%	43.510	100%	14.464	100%
Unit 21	105.85	76.802	100%	47.756	100%	18.711	100%
Unit 22	100.50	71.456	100%	42.411	100%	13.365	100%
Unit 23	107.78	78.735	100%	49.690	100%	20.645	100%
Unit 24	106.67	77.620	100%	48.575	100%	19.530	100%
Unit 25	99.721	70.676	100%	41.631	100%	12.586	100%
Unit 26	105.00	75.958	100%	46.913	100%	17.867	100%
Unit 27	94.302	65.256	100%	36.212	100%	7.166	100%
Unit 28	103.72	74.679	100%	45.634	100%	16.588	100%
Unit 29	106.61	77.570	100%	48.525	100%	19.479	100%
Unit 30	103.87	74.830	100%	45.785	100%	16.739	100%
Unit 31	97.826	68.772	100%	39.727	100%	10.681	100%
Unit 32	105.50	76.458	100%	47.413	100%	18.368	100%
Unit 33	100.69	71.643	100%	42.598	100%	13.553	100%
Unit 34	78.351	49.308	100%	20.263	100%	-8.781	100%
Unit 35	107.80	78.757	100%	49.713	100%	20.667	100%
Unit 36	101.33	72.287	100%	43.242	100%	14.196	100%

The reference energy consumption with maximum PV-DG effect without any curtailment is obtained from the base case with the PV-DG test conducted in chapter six. The results con-

clude that the maximum individual efficiency without storage and regulatory control equals 100%. The energy consumption at the different renewable energy penetration levels is displayed in table 8.1. The table will consist of the feeder energy consumption, the PV system's performance at every node on the feeder and the net energy flow at the PCC. The unregulated test will indicate that the PV performance is at its maximum due to the lack of control. The results with regulatory control should be situated between the maximum load at no generation and the maximum generation at maximum load.

The load data exhibited in the far left column of table 8.1 indicate that the feeder has a total energy consumption of 3.8 MWh. In contrast, the energy drawn from the units varies between 78.531 kWh and 107.80 kWh, evident at units 34 and 35, respectively. The fact that the units with both the highest and the lowest energy consumption are situated close to one another is a testament to the dispersion and random allocation of loads on the feeder.

The effect of unregulated PV penetration at a renewable energy penetration level of 25% has induced a reduction of 1.12 MWh in feeder load over the 24 hours to 2.68 MWh. Each unit on the feeder is generating energy at maximum capacity resulting in an average load decrease of 29 kWh at each unit. The purpose of gathering generation data without any control is to establish a criterion to which the other tests can be compared. The 50% renewable energy penetration test data indicates a sliding scale with the incrementation from 25% to 50% renewable energy penetration. The sliding scale will ease the data validation process due to the identifiable patterns in the energy production at different renewable energy penetration levels. The 50% level indicates a further reduction in the feeder load. The net feeder load is reduced to 1.65 MWh, with the maximum load on any unit equating to 49.71 kWh.

The 75% reference indicates that the amount of energy fed back into the grid almost cancels out the amount of energy drawn over 24 hours. The energy difference equates to 438.2 kWh with unit 32, which is established to be the lowest consumer turning into a prosumer with a net energy production of 8 kWh. Notably, the generated energy at all renewable energy penetration levels indicates a production value of 100% of the rated energy output due to the lack of energy curtailment induced by control.

8.3 Voltage unbalance comparison

The evaluation of energy flow in the feeder is one method of determining the efficiency of the different control structures. Another method is to study the worst-case voltage profiles on the feeder with the different control structures. Unbalance in a feeder can increase energy losses.

This indicates that the rise in unbalance is directly equivalent to the rise in energy losses on the feeder causing green renewable energy to be spent. There is currently no indication of the maximum allowable percentage unbalance on a feeder. However, the NRS 048-2 has stipulated that the aim is to limit the level of unbalance to 3% in the future.

Unbalance is calculated from the voltage on the feeder. The NRS 048-2 indicates two different ways to calculate the unbalance of a feeder. The first one is to divide the negative sequence voltage by the positive sequence voltage. The ratio of negative sequence voltage to positive sequence voltage represents the level of unbalance.

$$UB = \frac{Vn}{Vu} * 100 \tag{8.1}$$

The second method for determining the unbalance in the feeder and the preferred method for this chapter is by calculating the unbalance from the r.m.s line-to-line voltages. The reason for utilizing this method for conducting the tests is due to the fact that the rms line-to-line voltages are readily available. The formula for calculating the unbalance is divided into two sections, with the first being the beta calculation displayed in (8.1) and the second being the unbalance calculation in (8.2) and (8.3).

$$UB = \sqrt{\frac{1 - \sqrt{3 - 6\beta}}{1 + \sqrt{3 - 6\beta}}} * 100 \tag{8.2}$$

$$\beta = \frac{V_{12}^4 + V_{23}^4 + V_{31}^4}{(V_{12}^2 + V_{23}^2 + V_{31}^2)^2} \tag{8.3}$$

For example, V12 represents the line-to-line voltage at the fundamental frequency between phases 1 and 2.

The measured unbalance over the 24 hours will be utilised to determine the effectiveness of control in terms of balance on the network between the different voltage regulation methodologies. The initial voltage regulation efficiency comparison will be conducted on the Voltage regulation methodologies without ESS. The Control methodology with the best results will then be compared to the two methodologies incorporating ESS with local and global control. The controller with the smallest unbalance will be the victor of the unbalance test.

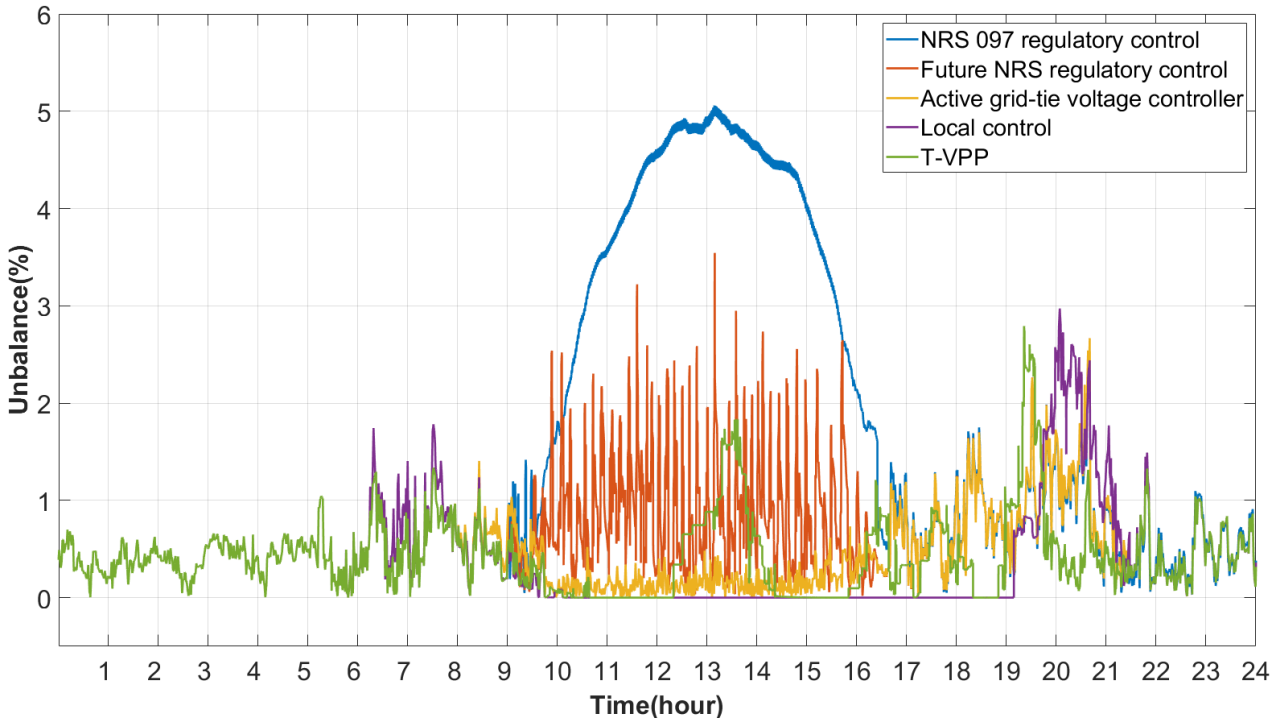

Figure 8.1: Network unbalance mitigation comparison of different controllers at 50% renewable energy penetration

The comparison of voltage unbalance between the different voltage control structures are evident in figure 8.1. The graph indicates that all control structures coincide during the initial testing stage due to the lack of generation acting upon the feeder. At the same time, no conditions are violated, as indicated in the voltage profiles in chapter six, meaning that any form of control would be irrelevant at that stage in time. The data suggests that as the early morning peak arrises, a dissolution occurs between the T-VPP and the other control structures. The diminishing unbalance is due to the peak shaving algorithm balancing and limiting the power draw on the feeder, resulting in the phase voltages being less unbalanced. From this point forward, the T-VPP follows the unbalance of the other controllers at a marginal offset due to the increasing generation presence. At 9:00, the voltage unbalance of each controller follows its path onwards.

The controller with the highest unbalance is the controller that utilises the current NRS 097-2 voltage regulation techniques of isolating the inverter from the grid in the event of a voltage violation. This voltage regulation method proves to be lacking due to the voltage unbalance exceeding the unofficial unbalance limit of 3%. The maximum unbalance reaches a level of 5.1%. The shape of the unbalance curve on the NRS 097-2 regulatory control seems to mimic the generation curve of the SSEG. An explanation is that the generators start to trip-off non uniformly across the phases resulting in an increase in unbalance on the feeder.

The mix of unbalance and increasing renewable energy generation causes the frequency of the trips to increase, as previously stated. This results in the unbalance curve in the presence of renewable generation resembling the SSEG curve. The decrease in generation indirectly leads to a reduction of unbalance due to the decrease in the frequency of the inverters tripping off, after which the unbalance curve synchronises to the grid-tie unbalance curves.

The future NRS 097-2 regulatory controller generates the second-highest voltage unbalance of all the controllers, with a peak unbalance of 3.5% still above the unofficial unbalance limit of 3%. The generated voltage unbalance due to the soft starting protocol leads to a decrease in frequency and amplitude of the unbalance spikes. The trip-off of the inverters induces the spikes evident in the graph. The most significant spike occurs at the moment of maximum generation due to the amount of power being removed from the grid instantly. The slow ramp rate reduces the unbalance on the feeder and helps delay voltage deviations caused by nuisance trips.

The active grid-tie voltage controller has the best results in the presence of SSEG with an average voltage unbalance of 0.5%. The increase in generation results in an apparent decrease in unbalance on the feeder. The unbalance graph for the active voltage regulation can be interpreted from the feeder voltage graph. The voltage data indicates that the inverter curtails its energy once a node reaches the upper voltage limit. As the number of inverters that reach the upper voltage limit increase, the voltage unbalance decreases due to the difference in phase voltages decreasing. The percentage unbalance not equating to zero is due to the minute voltage oscillations around the upper voltage limit. The low unbalance levels during energy generation are due to the voltage convergence towards the upper voltage limit.

The previous control structures all managed the voltage levels purely through SSEG energy curtailment. The local control and T-VPP both utilise ESS to assist with smoother voltage regulation. The local control complemented by ESS has the lowest constant voltage unbalance at an unbalance level of 0% during the day. The low and uniform straight line is induced by the zero energy exchange between the feeder and the units on the feeder. Once all the generators exceed the load and the ESS supplies the power deficit, the feeder becomes a synchronization source. Once the generation subsides, the ESS services the load until all storage units are depleted. The non-uniform depletion of the energy stores causes an unbalance on the feeder resulting in an unbalance increase of 2.9%, after which the unbalance subsides.

The T-VPP has the capability of sharing power between units in order to regulate the voltage on the feeder. The issue is that voltage can only be efficiently regulated in the event of energy balance induced by sufficient energy availability. The graph indicates that the voltage unbalance is mitigated as the generation increases due to the unit self-consumption stage. The

changeover between unit self-consumption and feeder self-consumption increases unbalance due to the energy exchange between units on the same phase. The unbalance is caused by an imbalance in energy availability between the phases. This imbalance subsides, as does the unbalance as more ESS reach the desired SOC for energy feed-in. The unbalance remains zero as energy is fed into the MV grid in a balanced fashion. The transition back to feeder self-consumption sees a rise in unbalance once again, followed by a short stint in the unit self-consumption stage. Then the algorithm increases consumption from the grid to prepare for the evening peak shaving. This is evident in the peak unbalance of the T-VPP followed by a drop in unbalancing considerably below the unbalance levels of the other controllers during peak load.

The best controller in terms of daytime unbalance minimization is considered the local controller due to the constant low unbalance level during the day. The T-VPP controller is on a broader spectrum, the better controller due to its high all result and low average daily unbalance maintaining an unbalance level below 3% for the entire duration.

8.4 Envelope determination

The data collected over the 24 hours have been on randomly allocated consumption profiles while the feeder performance favours certain conditions over others. For example, when the highest loads are assigned to the front of the feeder and the lowest loads are allocated to the back of the feeder. This method of load distribution is indicative of best-case conditions. On the other hand, as shown in chapter five of this study, an indication of worst-case conditions is when the load allocation is switched around.

The positioning of a high load determines the intensity of the effect on the voltage on the feeder. The issue, however, is that the loading oscillates from front to back, dependent on the units that utilise the highest amount of energy at that specific point in time. This makes it difficult to determine which consumption profiles can be classified as the largest loads on the feeder. Therefore, the plan is to categorise the highest loads in two different ways, meaning the envelope determination will be carried out two times. The first method of load classification will be conducted by means of categorizing the units in terms of their daily energy draw. The units with the highest energy consumption are predicted to have the highest effect on the feeder voltage and, in turn, on the effectiveness of the control structure. The second method for classifying the highest loads are by means of decerning the maximum demand of each unit on the feeder. The prediction is that the maximum demand might correlate to the maximum energy consumption in most cases, but the prediction is yet to be proven.

The initial test is conducted with the loads being arranged from low to high in terms of total daily energy consumption. The lowest energy consumption equates to 62.1 kWh, and the highest equates to 107.8 kWh. This load shuffling has caused certain days with similar load profiles to occupy adjacent units on the feeder leading to low dispersion between adjoining units.

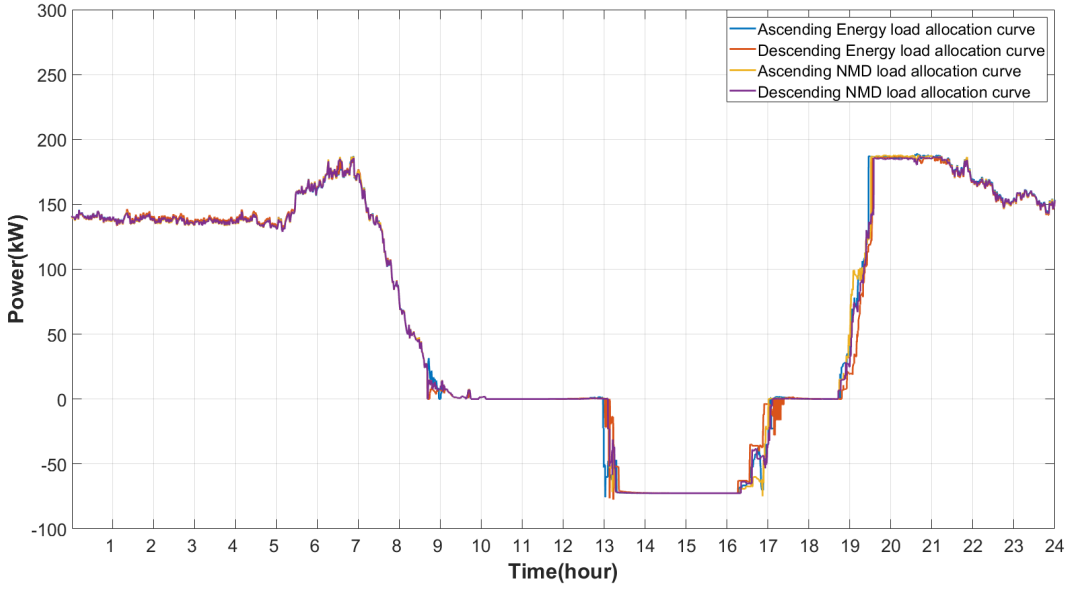

Figure 8.2: Feeder load profile comparison graph demonstating the effect of alternating load allocation

The load profile shuffling has caused certain loads with similar consumption patterns to be pared with each other, which means that most of the load profiles that resemble one another are situated close together on the feeder. The profile grouping means that the dispersion on certain zones within the feeder is minimal. The lack of dispersion means that the feeder load profiles line up and cause a maximum balanced load. The collective power profile plotted in figure 8.2 exhibits the difference between the four different power profiles. The voltage unbalance of the four different tests will also be compared to one another to indicate the worst and best load allocation by means of evaluating the controller's performance on the different allocation combinations.

The cumulative load profile of the ascending load order indicates that there occur spikes in the early mornings due to the lack of dispersion on the feeder. This peak could be due to a water heater turning on at that stage. The unexpected peaks drain the ESS unnecessarily due to the peak shaving algorithm being active on more occasions than is needed. The drained ESS also results in the Feed-in algorithm taking over later than it usually does due to the spent energy that needs to be recuperated, causing an energy deficit. The slight 5 kW deviation

from zero is the feeder self-consumption algorithm exchanging energy between the units on the feeder. The initial stages of the energy feed-in show how the energy reaches the set limit and then curtails the feed-in energy due to the upper voltage limit being reached if any more energy becomes available. The overall load profile provides overall good results. The energy is optimally utilised, the power is within the thermal limits at all times, and the excess energy is fed back as efficiently as possible. The voltage unbalance of the ascending energy ordered graph in figure 8.3 indicates that the maximum unbalances on the feeder equates to an unbalance of 2.7% with an average unbalance lower than the conventional reference test carried out earlier in this chapter.

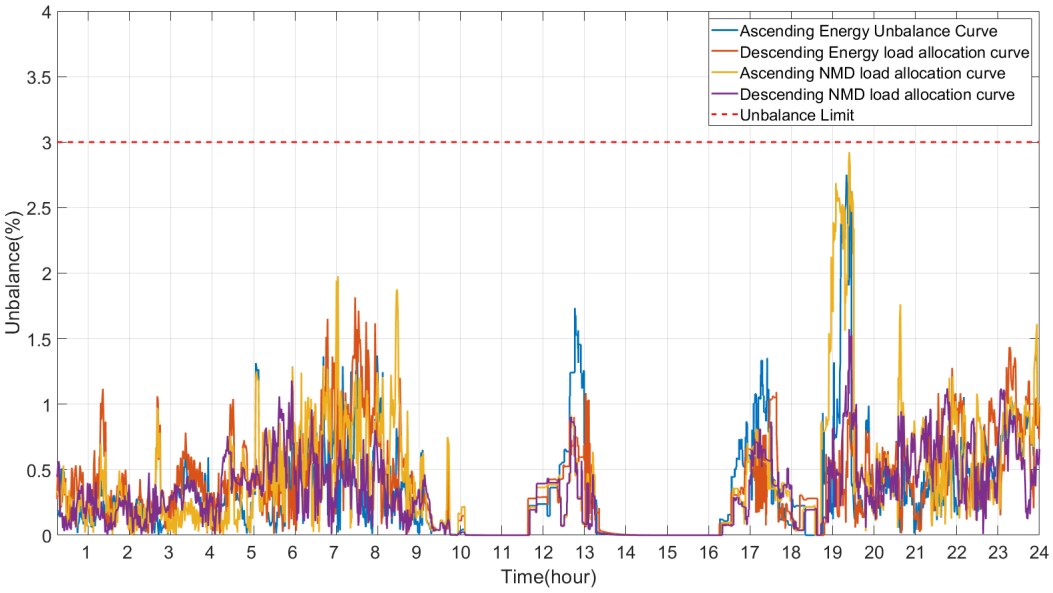

Figure 8.3: Voltage unbalance comparison graph demonstrating the unbalance effect at alternating load allocations

The descending energy-based load implementation order indicates more peaks unnecessarily draining the ESS due to unexpected peaks with a higher load than the network can handle. The energy flow, when compared to the ascending load implementation, is significantly smoother al be it higher than the ascending energy graph. The deviations due to energy availability are also fewer than before. This is mainly due to high loads at the front of the feeder, resulting in a declined effect of the energy exchange on the feeder losses. A decrease in load dispersion can also lead to the SSEG on the feeder synchronizing and better resource management. The energy feed-in is also significantly more stable than before, evident from the gradual increase and decrease in energy fed back to the MV network. The low dispersion causes more frequent peaks in the early mornings and late afternoon, with the peaks also being more prominent and continuing for longer. The same can be said for the low demand

regions. The energy consumption during low demand is also significantly less due to the energy feed-in starting earlier in the day and continuing for far longer than the other allocation combinations. The high nighttime demand causes the system's ESS to drain faster than it usually would. The frequency of these peaks is evident in the peak shaving section of the load profile.

The unbalance graph of the descending energy-based allocation indicates that the total unbalance on the feeder throughout the test is minimal, with the maximum unbalance never exceeding 1% as opposed to the other load allocation tests. The maximum unbalance only occurred momentarily and was an outlier compared to the average unbalance of this test. The absence of generation sees the unbalance oscillating minimally, whereas during times of peak shaving, the unbalance on the feeder oscillates violently due to the peak shaving algorithms task of individually controlling the power on the different phases and not collectively. In the presence of renewable energy generation, a slight level of unbalance occurs during midday due to the transition from self-consumption to feeding in excess energy. The overall smoothness and consistency that the data exhibits indicates that arranging the loads from high to low in terms of the daily energy consumption of each unit generates a best-case scenario. The descending energy-based load implementation also has the lowest feeder energy consumption at 50% renewable energy penetration with a daily energy consumption of 1.36 MWh while at the same time maintaining an average unbalance of 0.1%.

The loads are now to be ordered in terms of the maximum demand of each unit over the day. The first ordering will be low to high in terms of the maximum demand. The ascending maximum demand (MD) power curve exhibits a higher dispersion in the early stages of the test. This is evident in the lower base load during the early morning hours, which is also the cause for the smaller morning peaks. The increased dispersion also results in smaller peaks occurring before the high morning peak. The morning peak rarely exceeds the 185 kW mark. This combination of load implementation also sees that the generation starts to fully transcend the loads the latest of all the implementations. The feed-in power experiences small energy fluctuations during the reserve energy ramp-up, where it stabilises at negative 72 kW due to the upper voltage limit. The energy reserves are the fastest to deplete of all the combinations due to the positioning of the load on the feeder and has a similar peak time as most of the other implementations.

The unbalance chart indicates that the general unbalance of the ascending MD based load implementation is the highest of all the combinations, with an average voltage, unbalance of 0.26% and a maximum unbalance of 2.97%, which is also the highest peak unbalance of all the implementations. The total energy drawn from the MV network equates to 1.67 MWh,

which is lower than the Ascending energy load implementation. The feeder has a standard performance in terms of energy management. However, the same could not be said about the voltage unbalance resulting in the worst-case implementation in terms of voltage unbalance.

The descending MD load allocation power curve has a load profile that closely follows that of the ascending energy-based load profile. The load profile is the second to last load profile where the solar transcends the loads, and the self-consumption can commence. The maximum feed-in power is immediately available at full capacity and reduces gradually before the nighttime peak arrives. The current load allocation sees the ESS deplete gradually before the peak shaving algorithm activates for a short while before the load reduces to below 185 kW. The total energy consumption of the descending MD load allocation equates to 1.78 MWh, which can rank the descending MD load allocation as the second-worst situation to be in terms of load allocation.

The unbalance chart indicates that the descending MD load allocation produces the second-best level of unbalance with an average unbalance of 0.1% and a maximum unbalance of 1.93%.

8.5 48 hour test

The 24-hour time frame in which the conventional test is conducted provides limited diversity and does not truly occur randomly. The 24-hour test does not take the stochastic states of the ESS into account when the control ends, meaning that as a new test starts, the ESS parameters are reset to the start parameters. The goal of the 48-hour test is to determine the effect of varying daily conditions on the control structure. The main reason for this is that when a 24-hour test is conducted, the end variables are not the same as the start variables going into the next day. The randomness of the ESS SOC could cause the controller to operate inefficiently since all avenues might not have been explored in the design of the VPP controller. The 48-hour test could shed light on the controller's functionality over a multi-day period where no two days have the same conditions and the variables get carried over from day to day, indicating that the system will have to adapt to the changes.

The load data will differ slightly between the first and second days to maintain load randomness. The 48-hour load profiles of each unit will be generated by means of taking a random number generator to generate a list of randomised numbers between 1 and 36. The number allocation will then indicate which daily load profiles will be added as second-day load profiles to other units on the feeder. At the same time, the ESS SOC of each unit is situated at a

possible different level going into the next day. The energy implementation is likely to differ between the first day and the second day due to load variation and energy levels of the ESS.

The data obtained from the 48- hour test indicates that the energy is well managed and efficiently allocated as none of the units was required to throttle their energy generation during any of the two days. This is due to the ESS capacity being more than enough to absorb the excess energy generated each day at a renewable energy penetration level of 50% of the NMD. The ESS provided the capability of feeding power into the MV network at a constant rate due to the ESS filling the gaps between the generation and consumption. The power fed into the MV network is controlled as not to violate the upper voltage limit on the feeder on both days. The control of power to remain within the voltage limits can be seen in figure 8.5, where the voltage on all three phases remain within the voltage limits for a significant duration of the test. The voltage violations over the 48 hours occurred within the 40-second trip delay before returning to acceptable voltage levels.

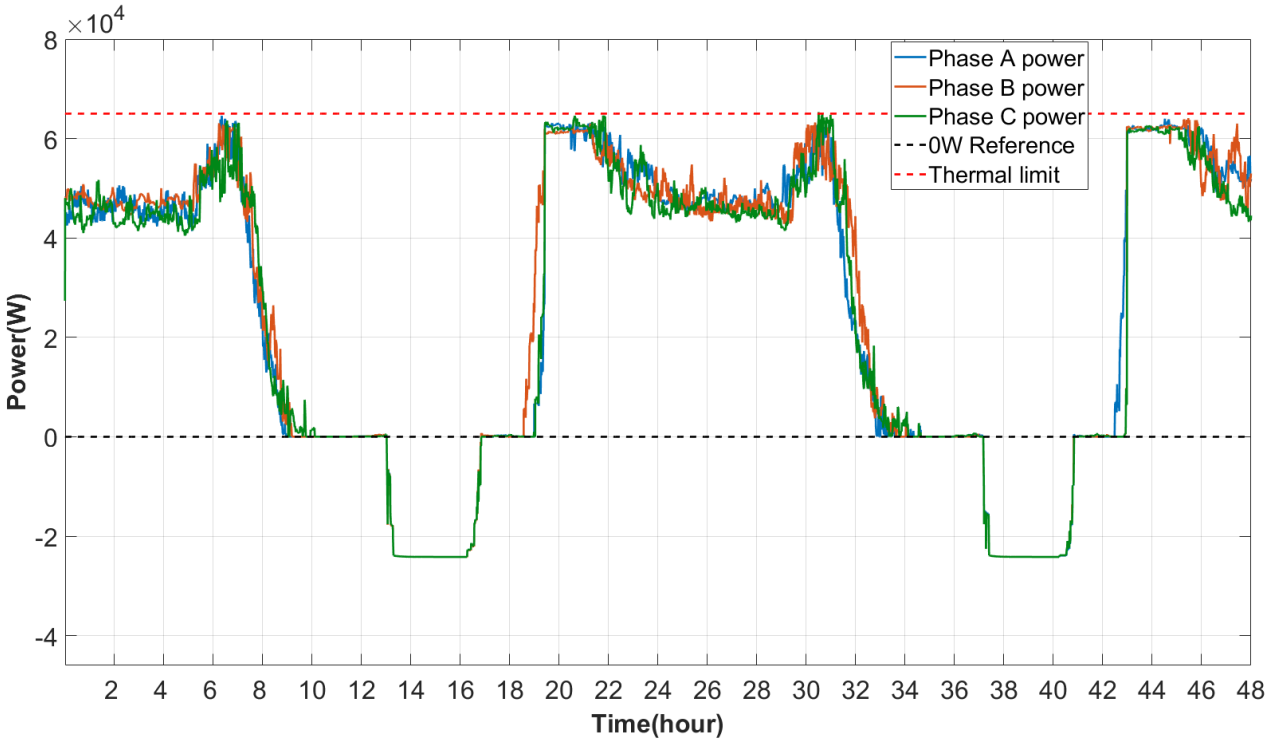

Figure 8.4: 48 hour worst-case load profile with VPP control as measured at the transformer

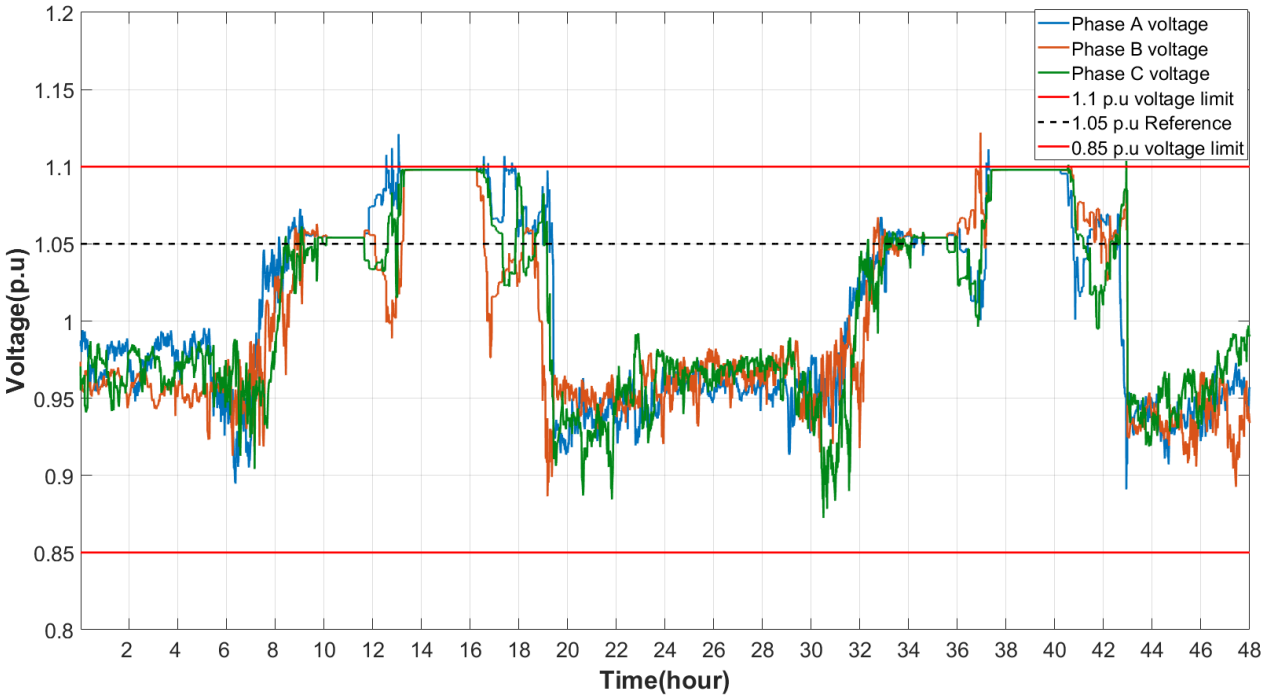

Figure 8.5: 48 hour worst-case voltage profile with VPP control indicating the effect of parameter variation

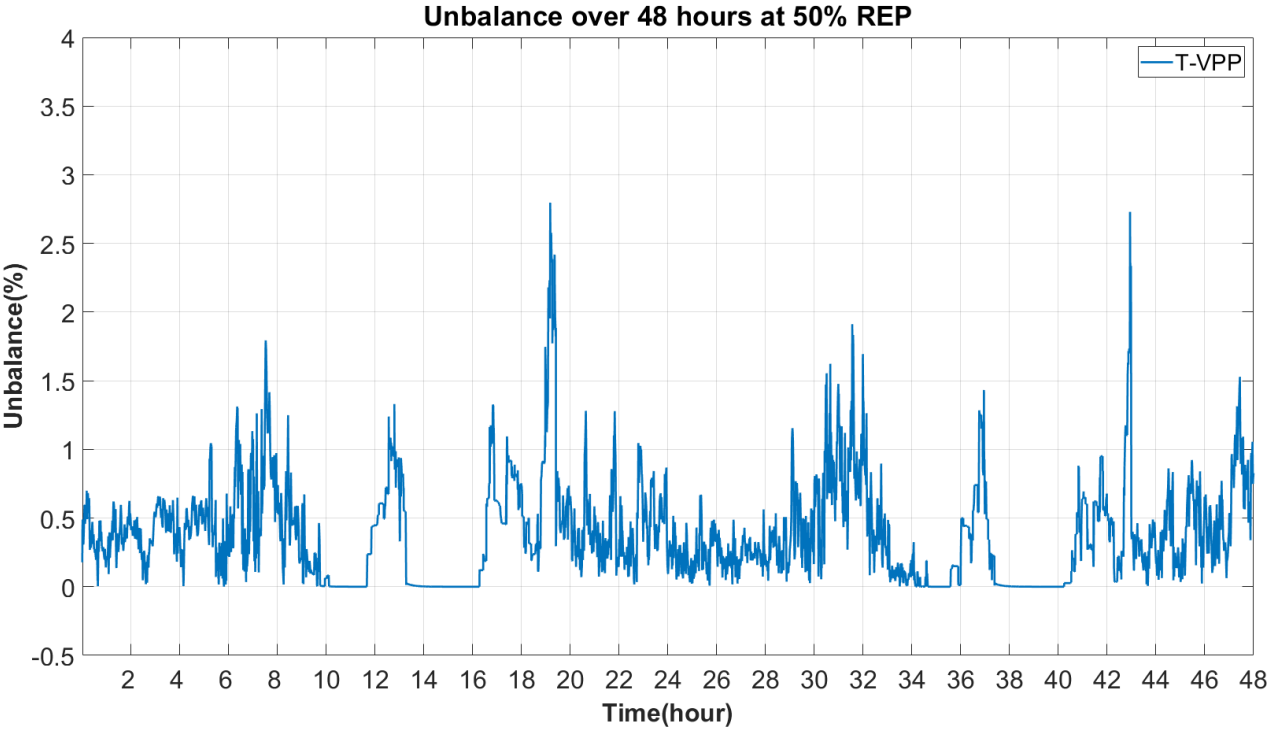

Figure 8.6: 48 hour unbalance profile with VPP control

8.6 Alternative network test

Completing all the performance tests on the current feeder topology for the VPP control algorithm warrants a final examination to evaluate if the VPP algorithm is genuinely diverse. The diversity of the VPP will be determined by evaluating if it is capable of increasing the renewable energy penetration on any feeder while maintaining voltage regulation on said feeder.

The critical component to evaluating the control structure on the different feeders is that most fundamental elements need to remain the same. The fundamental elements include the transformer size, the number of units on the feeder, the test penetration level and the load values of all the feeder units. The differences between the feeders will reside in the reticulation lines specifications due to the shift in the location of the units and loads due to the additional feeder T-offs. Based on newfound experience, the change in the layout of the feeder will likely affect the voltage characteristics of the feeder, possibly causing the algorithm efficiency to improve or deteriorate depending on the voltage variation sensitivity on the feeder.

The validation network to be utilised is chosen from the nine variations of feeder topologies presented in chapter five. The validation network in question is the triple T-off network. The reason for selecting this network is the multiple shared feeders connecting to the single 315 kVA transformer. The network characterization in chapter five has proven that with this network, the possibility of grossly exceeding the thermal limits on the feeder is higher than exceeding the voltage limits. The feeders are shorter, while the total load on the feeder remains the same, meaning that the individual feeders are less likely to experience high voltage rises due to the length of the reticulation lines. The shared feeder will test the VPP's energy aggregation capabilities due to the possible increased energy management constraints that the multi feeder network brings to the table. For the test, the conductor sizing of the feeders will be reduced since each feeder on the network possesses a smaller amount of units than the original feeder meaning that the conductor of each feeder does not need to carry a large amount of current.

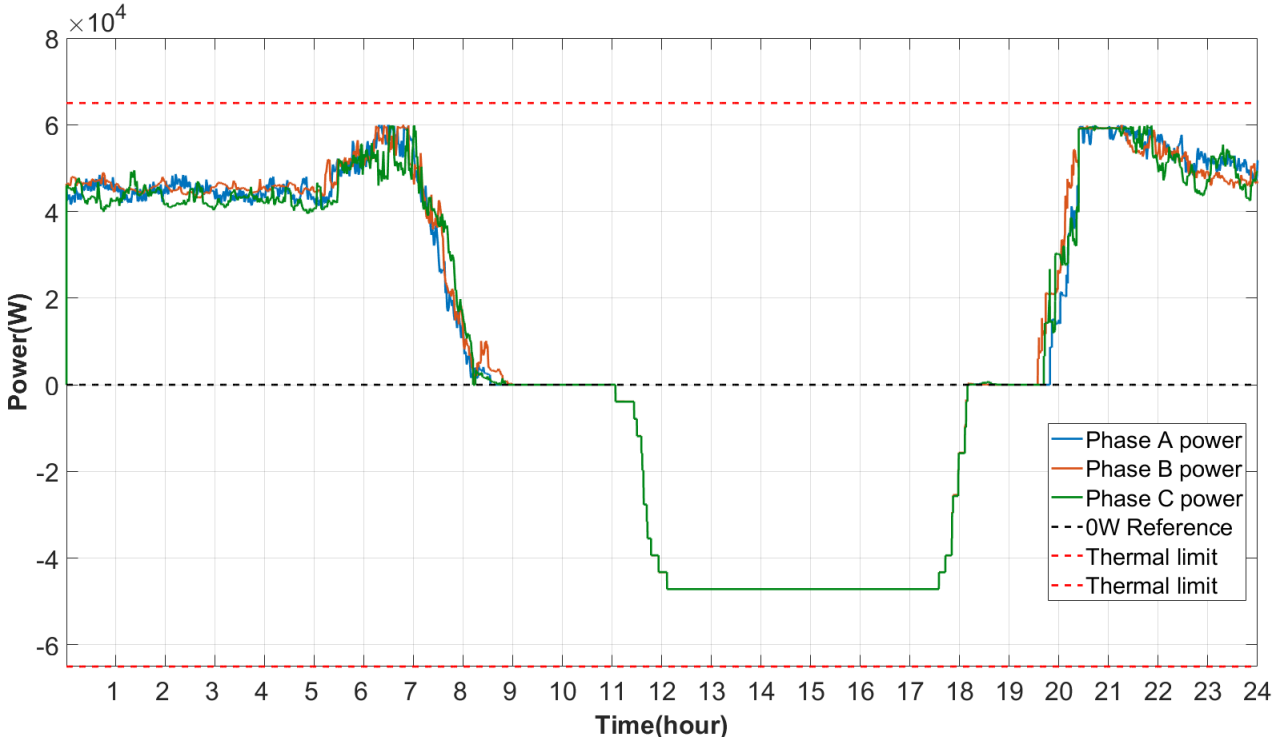

Figure 8.7: Validation load profile as measured at the transformer of the multi feeder network

The data displayed in figure 8.7 exhibits the power curve of the multi feeder compatibility test over the 24 hour test period. At initial inspection, it is notable that there is no difference in the power curve at the early stages of the test compared to the original single feeder power curve. The approach of the early morning peak sees the peak shaving algorithm activate to shave the peaks as to not exceed the thermal limits. The controller effectively manages the power to remain well under the feeder thermal limit as the sun starts to rise and irradiance starts to increase. The effective feeder load tends to zero with the increase in irradiation, where the local self-consumption protocol is set to take over. The self-consumption phase sees the overall feeder power remaining at zero.

The ESS charge up from the excess solar until the 65% SOC mark is reached before the feeder self-consumption period commences. The feeder self-consumption phase starts at 12:09, as indicated by the minor power deviations evident between 12:09 and 13:33 at 13:33. In conjunction with the feeder self-consumption algorithm, the feed-in algorithm ensures that excess renewable energy is fed back into the MV grid while remaining within the voltage and thermal limits. The architecture of the multi feeder network allows for more energy to be fed back to the MV grid as opposed to the single feeder due to the ratio of voltage rise to power exportation being lower on the multi feeder network. This is due to the closer proximity of the units on the feeder to the transformer resulting in lower voltage deviations for the same

renewable energy penetration. The maximum power fed back into the grid while maintaining a voltage below 1.1 p.u. is equal to 53 kW per phase(hierdie waarde moet nog verander soos die lyn diktes na die regte dikte verander word) momentarily. At the same time, the energy availability fluctuated due to the high feedback demand from 13:40 to 16:05. The reason for not reaching the 1.1 p.u. voltage limit is that the feeder thermal limit is reached before the voltage limit is reached, which is caused by the power feed in which is almost three times more than in the single extended feeder test. The inability to reach the upper voltage limit on the multi feeder network in balanced conditions indicates that the only possible moment the upper voltage limit can be violated is when maximum unbalance occurs. The unbalance can either be a generation or load unbalance.

The energy management order then happens in reverse as the irradiance decreases and the ESS starts to discharge. The ESS exchanges energy between the consumers who have an abundance and those who need it the most before isolating all the units to self-consume their remaining energy. The late-night peak commonly being the largest peak, the algorithm successfully shaves the peak under the feeder thermal limit for the entire duration of the peak on a feeder with a different topology.

The voltage profile displayed in figure 8.8 indicates the change in architecture from the extended feeder to a multi feeder network constituting the same number of units sees an adjustment in the feeder voltage sensitivity at the same load. The minimum voltage on the feeder is situated at one p.u. The peak shaving algorithm assists in limiting the voltage drop at times of maximum demand. The increase in generation induces an increase in the feeder voltage, which is expected. The feeder voltage tends to 1.05 p.u. as the aggregated feeder load tends to zero. This phenomenon can be encountered in the extended feeder test as well. The general assumption is that when the transformer sees no load on the feeder, the feeder voltage becomes equal to the source voltage. The feeder voltage at the time of maximum energy feed-in reaches a maximum voltage level of 1.09 p.u. The voltage oscillation be it below 1.1 p.u, follows the power oscillation induced by the lack of adequate energy generation from the SSEG. However, the energy oscillation is not a bad situation, especially if the voltage is within regulatory limits and the power is below the thermal limits of the feeder. This indicates that more SSEG capacity can be added to the feeder if more energy is required. The end of the feed-in period sees the voltage fall back to around 1.06 p.u. across the phases. The evening peak induces a further voltage drop down to 1.01 p.u. with the assistance of the ESS to implement peak shaving.

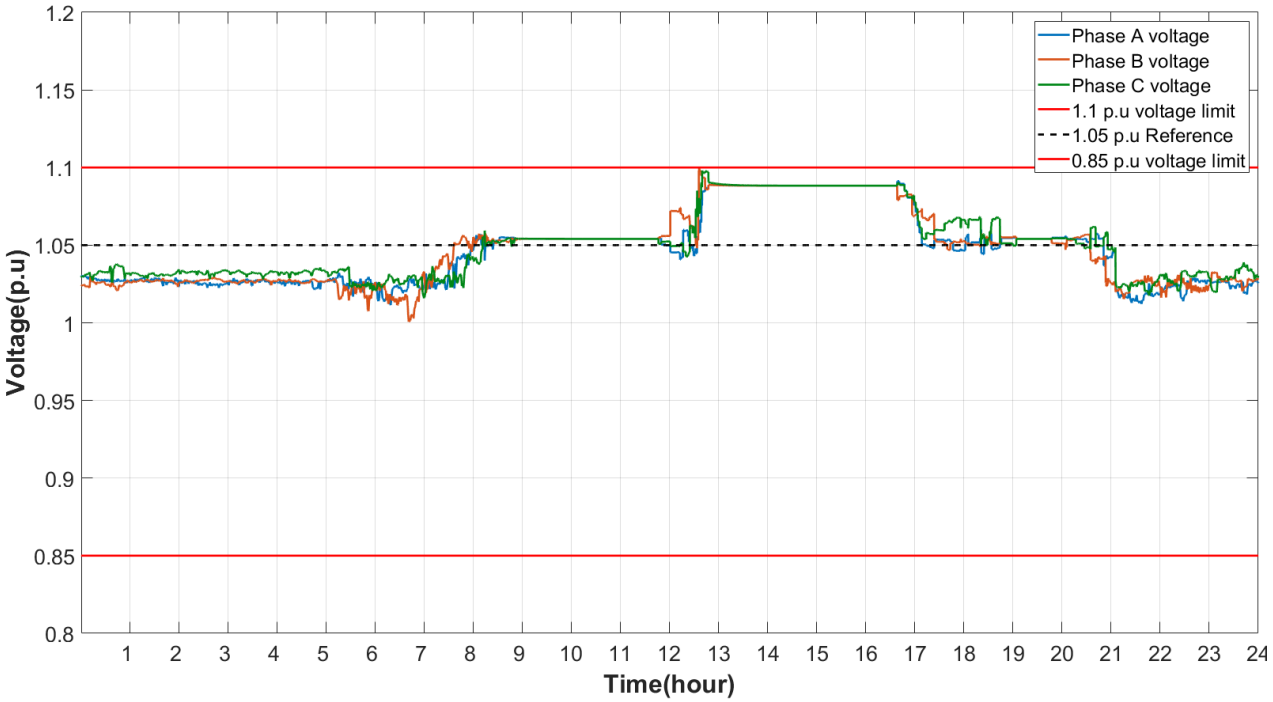

Figure 8.8: Multi-feeder voltage profile

The similarity in the power curve of the extended single feeder network and the multi feeder network indicates that the controller is dynamic in the sense that it can successfully and effectively control the energy flow and voltage levels on any feeder topology in order to increase the renewable energy penetration level on, said network.

The different control methodologies can be categorised according to their services. The data in table 8.2 indicates what the different voltage regulation control schemes are capable of and if they satisfy the objective of the thesis in being able to increase the renewable energy penetration.

Table 8.2: Control capability rating

	Capabilities				
Controller	Voltage regulation	Energy efficient	Power support	Peak shaving	Functions under higher renewable energy penetration
NRS-097	X				
NRS-097 + Soft Start	X	X			
Power based voltage regulation	X	X			X
Local controller	X	X		X	X
VPP Controller	X	X	X	X	X

The data indicate that the prevailing voltage regulation standard set out in the NRS 097-2 can only regulate the voltage. The current voltage regulation method struggles with this task as the voltage rise inertia increases as the renewable energy penetration level increases. The current voltage regulation method is seen as a temporary fix to an endearing problem

and cannot actively regulate the voltage at increasing renewable energy penetration levels. The constant nuisance tripping decreases the energy efficiency of the feeder due to the time which the system is unable to generate green energy. A functional addition to the current regulatory standards in the form of a soft start function has increased the effectiveness of energy management during times of voltage regulation. The soft starter has reduced the frequency of nuisance trips caused by constant voltage violations at higher levels of renewable energy penetration. This has reduced the amount of energy lost due to inverter isolations, increasing the control algorithm's energy efficiency.

The active power-based voltage regulation took a different approach to how the voltage can efficiently be regulated without sacrificing a large amount of generated energy. The active voltage regulation controller can limit the energy output of SSEG based on the voltage at the residing node. The power of the SSEG can be curtailed to zero at the worst point on the system while other SSEG on the feeder generate energy based on their relative voltage level. This allows for higher energy efficiency on the network while remaining within the voltage limits. The active voltage regulation controller cannot share energy or conduct peak shaving. However, the controller can regulate the voltage at any level of renewable energy penetration. The only limiting factor will be the amount of energy that the network can handle.

The local control based voltage regulation is complemented by ESS and can store any excess energy. If the ESS reaches maximum capacity, the system will curtail the generation in order to only service the loads. The system, therefore, maximises the use of clean energy while remaining within the voltage limits. The system can also raise the voltage level away from the minimum voltage limit at times of maximum demand by servicing a portion of the load. However, the local controller cannot share energy with other units on the grid due to the absence of a local controller. This positions the local controller second in the rankings of the best control schemes for efficiently and safely increasing the renewable energy penetration level on the network. Tests have proven that the Local control can increase the potential renewable energy penetration to 100% of the NMD of each unit on the feeder.

The final control scheme, the T-VPP controller, is regarded as the best control scheme of the evaluated control schemes within this thesis. The results obtained in the controller design and performance analysis phase indicate that the T-VPP has successfully increased the renewable energy penetration to 100% of the household NMD while regulating the voltage to remain within normal operating conditions without fail. This all while efficiently distributing the green energy where it is most needed. The T-VPP provides accurate voltage regulation while maintaining the highest level of energy efficiency. The T-VPP also provides balanced energy feed into the MV network at times of excess generation while maintaining a voltage level of 1.1

p.u. At times of zero generation or in conditions of generation uncertainty, the T-VPP utilises the reserve power in the ESS to diminish any peaks and reduce the need for expensive peaking power plants. The T-VPP assumes that the incentive to be part of the scheme is adequate and that all users fund their systems without the need for government intervention. Government subsidization is welcomed to streamline the process. The use of T-VPPs eliminate the need for CAPEX on peaking power plants and, if rolled out correctly, could in its entirety eradicate the need for peaking power plants with the implementation of grid-scale storage brought forth by the aggregation of thousands of SSEG. This makes the VPP the apex of implementations to shift energy from a centralised generation structure to a decentralised structure with the assistance of modern technological advancements.

8.7 Conclusion

The results obtained by conducting a performance analysis on the VPP control structure prove that the VPP algorithm for aggregating decentralised SSEG to act as a single power plant is achievable. This is done by means of regulating energy between units as well as between the LV and MV network, all while remaining within the voltage limits set out in the SAGC. The results also indicate that when comparing the different voltage regulation algorithms to one another, the VPP algorithm is the most effective method of voltage regulation while efficiently managing the energy flow on the feeder for optimal consumption and providing ancillary services. The local control algorithm purely meant for optimal self-consumption follows closely in second place.

The T-VPP is also tested on different network topologies to validate that the control algorithm is implementable on all network structures as a generic solution. This is because the measured values change with the change in network topologies. However, the operating parameters remain the same irrespective of the topological changes. This created a form of stability when developing the algorithm because specific parameters had to remain constant regardless of the network layout. The controller was also subjected to multiple day simulations to evaluate the controller's performance under changing conditions. At the beginning of this chapter, the test set out has all delivered favourable results. Therefore, the T-VPP control method is a generic method for safely increasing renewable energy penetration with excellent efficiency. The following chapter will summate the work done in the thesis and then discuss possible future work to be conducted for further improvement on the research conducted to date.

Chapter 9

Recommendations and conclusion

This chapter aims to conclude the document by referring to chapter one, re-evaluating the objective, and confirming whether the results meet the requirements. This chapter, at the outset, reflects on the research objectives as outlined in chapter 1, followed by a detailed discussion on the further refinement of the MATLAB model and additional capability that the model could present. Future work on the model's improvement and the exact algorithm control structure will also be discussed. Subsequently, additional recommendations are made to further improve the quality of work and capabilities of the system. This chapter will end with a conclusion.

9.1 Re-evaluation of objectives

The problem statement in chapter one stated that the purpose of the research is to safely increase the renewable energy penetration within a low voltage network by applying an intelligent control algorithm implemented on a T-VPP to maintain voltage regulation within regulatory limits. The main objective was identified as voltage regulation through energy and power management. The main objective's achievability was determined by breaking the problem into smaller manageable secondary objectives, also defined in chapter one. The objectives were reviewed and discussed as follows:

- *Research the workings of an LV network model and develop a mathematical model of a representative network on which the control algorithms can be implemented.*
  The fundamental characteristics of the popular LV network were evaluated, and different LV network topologies were generated from the acquired knowledge for simulation and data acquisition.

- *Research how the mathematical network models can be transferred to the simulation environment.*

  The MATLAB Simulink® mathematical modelling and simulation environment proved to be a suitable and effective option for constructing a working LV network model.
- *Develop the final model through characterising the chosen models according to the effect that the renewable energy generation has on the voltage of the different network topologies and select a suitable network for validation.*

  The simulations effectively identified the similarities and differences between the different topologies. The simulation environment also allowed for the validation of the chosen LV network model.
- *Incrementational control development for the increase of renewable energy penetration.*

  A set of crisp rule-based algorithms were developed for energy and voltage management. The algorithms were realised by means of manual coding and the MATLAB code function blocks. The algorithms were systematically implemented from the least to the most complex, and the voltage regulation improved with each implementation. The improved voltage regulation led to an increase in each unit's maximum allowable renewable energy penetration.
- *Performance analysis of the various control structures and validation of control.*

  The performance analysis of the various control techniques indicated that the active voltage regulation had the highest success rate of all the grid-tied implementations to regulate the voltage while simultaneously curtailing the minimum amount of renewable energy. Further investigation proved that theVPP control algorithm had the highest success rate of all the implementations due to the ability of the system to store energy and distribute energy within the network to optimise the use of renewable energy. The T-VPP also provided energy arbitrage to the MV network while constantly regulating the voltage within regulatory limits.

  The most promising algorithm was implemented on different network topology, and the controller without fail acted as it was intended to do, managing the energy flawlessly at different renewable energy penetration levels while at the same time remaining within the network parameter limits. The results of the two network implementations were compared, which validated that the T-VPP algorithm is a generic solution that shows great promise in safely increasing renewable energy penetration.

9.2 Simulation model improvement

A thorough analysis of the simulation data and model development indicated that specific components within the system required added functionality to reach a real-world simulation environment or otherwise known as a digital twin to a real-world network. The sections that require extra attention are, for a start, the ESS modelled component because it is evident that thermal inefficiencies and voltage level variations are not modelled in this simulation environment. Other inefficiencies include the modelling of the MV network and the effect that loads on the MV network have on the voltage levels of the LV network. The model is simulated under ideal conditions. More environmental factors need to be considered to generate data with higher accuracy to further improve the model's accuracy.

9.2.1 ESS inefficiencies

The ESS thermal inefficiencies could, when taken into account, lead to a more realistic SOC curve. The slight deviation in battery voltage at different load levels also plays a significant role in the battery's power output and the SOC curve. The internal battery resistance and self-discharge are also not taken into account. This would result in a more accurate representation of the energy flow in the system due to the energy losses being taken into account. This would allow the local and global controllers of the VPP to be aware of the inefficiencies when deciding how much energy to charge or discharge the ESS. The energy prediction algorithm would also increase its forecasting accuracy when taking the ESS inefficiencies into account.

The absorption state of a LiFePo4 battery is situated at a very high SOC (around 95% depending on the manufacturer). This means that the amount of energy with which the ESS charges decreases when the SOC exceeds 95%. The controller only charges the ESS up to a SOC of 97%, resulting in inaccurate energy absorption for the last 2% of the ESS capacity. If the absorption value is taken into account, the EMS can better manage the energy to more accurately reflect real-world scenarios.

9.2.2 System efficiency

The general system inefficiencies include the conversion inefficiencies in the system, such as the voltage transformation from the MV to LV network along with the line losses induced by possible reactive power present on the feeder, which is not taken into account. Incorporating reactive power control and the reactive power measurement is also a key aspect to look into

in the future due to reactive power's minimal yet noticeable effect on the feeder voltage. The voltage levels can also be affected by the loads induced by other networks on the MV side of the transformer. This can also alter the voltage level and affect the system's efficiency, which needs to be considered in the future. If the thermal line limits are not exceeded, the system's efficiency is predicted to increase as voltage decreases on the MV side.

9.3 Future work

9.3.1 STLF integration

The literature indicates that short term load forecasting will be beneficial to the resource management of the system, especially at times when peak shaving needs to be implemented. short term load forecasting (STLF) requires a form of Artificial Intelligence and can be implemented by combining fuzzy logic control with an ANN in order to mitigate uncertainty and identify patterns and trends in weather data. Short term load forecasting would also assist in bidding structures for the energy market participation.

9.3.2 Weather forecast integration

Weather forecasting works on the same basis as STLF in the sense that an ANN is utilised to predict the weather based on weather data from the past. Weather forecasting would add value to the control system. Weather forecasting can assist in predicting the generation output of the SSEG. The weather forecasting in conjunction with STLF would assist in correctly bidding in the energy market and decrease the LCOE of the portfolio. Forecasting of any kind increases the grid stability.

9.3.3 Energy market participation

In technical terms, the virtual power plant efficiently manages the energy in its portfolio and can support the larger grid with ancillary services. The evolutionary step is to utilise the virtual power plants in the energy market. The need for supply and demand to be balanced in real-time is critical, and the stochastic nature of renewable energy sources do not contribute to the energy balance. Energy markets are an economically efficient way to balance supply and demand by introducing a financial incentive for participation. The energy market allows

participants to bid on what they are willing to produce or consume at different price levels and time scales. The operator can activate the system of the participants who can provide the necessary services to balance the supply and demand in real-time. This could allow the smooth transition to 100% renewable energy penetration and increase control as more renewable energy units come online.

9.4 Recommendations

The experience generated throughout this process has exposed some places where improvements in the research methodology can be made to explore all possible avenues of this study. The variation in generation implementation across the feeder will increase the robustness of the control system as the variation in generation and storage capacity is something commonly found in real-world VPPs. The generation and storage dispersion results in variations in generation and causes limited certainty and storage capacity on the feeder. This leads to a decrease in error tolerance and will require prediction algorithms to be effective.

9.5 Conclusion and critical analysis

This study aimed to develop an intelligent algorithm capable of implementing rigid control that maintained grid stability irrespective of the renewable energy penetration on the low voltage network. The controller had to provide local grid ancillary services as well as limited ancillary services to the MV grid without sacrificing any green energy generation as far as possible. The critical objective of this study was first and foremost to regulate the voltage at all cost due to the voltage being the limiting factor to the increase in renewable energy penetration.

A verified model was developed in MATLAB Simulink® on which the various forms of control could be implemented as other simulation environments utilised for power systems simulations were not very user friendly and provided limited freedom in terms of control implementation.

Various voltage regulation schemes were studied and implemented to analyse the effect of the control implementation on both the feeder voltage and the energy management. The initial literature pointed to an exact rule-based logic controller being the optimal controller for the application due to the diversity and control precision. This form of control could only be executed with success due to the predetermined knowledge of the person developing the control algorithm. The aggregator controller was developed in Simulink®and was validated

as a generic control algorithm capable of safely increasing the renewable energy penetration irrespective of the network topology.

The control technique was iteratively tested and improved to account for various situations.

The implementation of VPPs warrants great potential to become a substitute for peaking power plants due to their low capital and operational expenditure. To abstain from a monopoly of the energy market can further increase the usefulness of VPP as a source of income to the community and increase grid security through incentives. The maintenance on a VPP is minimal because the public owns the majority of the infrastructure and the control structure is digital, which does not require high capital expenditure ether. The failure rate on VPPs is relatively low due to the redundancy of having thousands of small generators and storage units on a single control scheme. If one unit fails, it is barely noticeable in the aggregated energy value.

The work done in the past two years of this research process has time and time again provided technical insight as to why the way in which energy is generated needs to change and the regulation along with it. The data gathered and exhibited in this thesis proves that the current regulatory standards in terms of generation implementation are not up to standard due to the advancements in technology outrunning the regulation changes. The developed algorithm and implementation can improve energy security and increase a country's living standards since energy is a fundamental human right. Without energy, markets crash, and countries plunder into the darkness. The implementation of a VPP is simple and effective due to the pre-existing energy infrastructure, and the revelation of satellite internet such as Starlink has made it possible to control systems all over the world. The implementation of interconnections between continents will further the implementation of renewable energy due to the ability to transmit energy between continents, i.e. transmitting energy from a place where the sun shines to ones in total darkness.

Bibliography

[1] "Confronting the Duck Curve: How to Address Over-Generation of Solar Energy," https://www.energy.gov/eere/articles/confronting-duck-curve-how-address-over-generation-solar-energy.

[2] D. Akinyele, J. Belikov, and Y. Levron, "Challenges of Microgrids in Remote Communities: A STEEP Model Application," *Energies*, vol. 11, no. 2, p. 432, Feb. 2018.

[3] S. Bofinger and J. N. Stander, "LCOE estimation in aggregated wind/PV study," Nov. 2017.

[4] "NRS 097-2-1:2017 GRID INTERCONNECTION OF EMBEDDED GENERATION," Feb. 2019.

[5] "Third amendment to the Electricity Regulation Act in 2021 - Schedule 2 substituted again (5 October 2021)," https://cer.org.za/virtual-library/whats-new/electricity-regulation-act-increase-of-licensing-threshold-for-embedded-generation-projects-from-1mw-to-100mw, Oct. 2021.

[6] I. Kuzle, M. Zdrilić, and H. Pandžić, "Virtual power plant dispatch optimization using linear programming," in *2011 10th International Conference on Environment and Electrical Engineering*, May 2011, pp. 1–4.

[7] A. B. Jubarah, M. Al-Muhaini, and I. M. Elamin, "A MILP-Based Approach for Virtual Microgrid Restoration," *IEEE Access*, vol. 8, pp. 116 695–116 703, 2020.

[8] S. Porkar, P. Poure, A. Abbaspour-Tehrani-fard, and S. Saadate, "Optimal allocation of distributed generation using a two-stage multi-objective mixed-integer-nonlinear programming," *European Transactions on Electrical Power*, vol. 21, no. 1, pp. 1072–1087, 2011.

[9] M. Othman, Y. Hegazy, and A. Abdelaziz, "A Review of Virtual power plant Definitions, Components, Framework and Optimization," *International Electrical Engineering Journal (IEEJ)*, vol. 6, pp. 2010–2024, Nov. 2015.

[10] H. Pandžić, J. M. Morales, A. J. Conejo, and I. Kuzle, "Offering model for a virtual power plant based on stochastic programming," *Applied Energy*, vol. 105, pp. 282–292, May 2013.

[11] C. Hinrichs and M. Sonnenschein, "A distributed combinatorial optimisation heuristic for the scheduling of energy resources represented by self-interested agents," *International Journal of Bio-Inspired Computation*, vol. 10, p. 69, Jul. 2017.

[12] M. Arnold and G. Andersson, "Model predictive control of energy storage including uncertain forecasts," Jan. 2011.

[13] P. Stadler, A. Ashouri, and F. Maréchal, "Distributed model predictive control of energy systems in microgrids," in *2016 Annual IEEE Systems Conference (SysCon)*, Apr. 2016, pp. 1–6.

[14] E. De Santis, A. Rizzi, and A. Sadeghian, "Hierarchical genetic optimization of a fuzzy logic system for energy flows management in microgrids," *Applied Soft Computing*, vol. 60, pp. 135–149, Nov. 2017.

[15] Y. Zheng, Z. Y. Dong, F. J. Luo, K. Meng, J. Qiu, and K. P. Wong, "Optimal Allocation of Energy Storage System for Risk Mitigation of DISCOs With High Renewable Penetrations," *IEEE Transactions on Power Systems*, vol. 29, no. 1, pp. 212–220, Jan. 2014.

[16] S. Skarvelis-Kazakos, "Automating Virtual Power Plant Decision Making with Fuzzy Logic and Human Psychology," in *2018 53rd International Universities Power Engineering Conference (UPEC)*, Sep. 2018, pp. 1–6.

[17] M. H. Nehrir and B. J. LaMeres, "A multiple-block fuzzy logic-based electric water heater demand-side management strategy for leveling distribution feeder demand profile," *Electric Power Systems Research*, vol. 56, no. 3, pp. 225–230, Dec. 2000.

[18] O. Castillo and P. Melin, "3 Type-2 Fuzzy Logic," in *Type-2 Fuzzy Logic: Theory and Applications*, ser. Studies in Fuzziness and Soft Computing, O. Castillo and P. Melin, Eds. Berlin, Heidelberg: Springer, 2008, pp. 29–43.

[19] S. B. A. Bukhari, R. Haider, M. Saeed Uz Zaman, Y.-S. Oh, G.-J. Cho, and C.-H. Kim, "An interval type-2 fuzzy logic based strategy for microgrid protection," *International Journal of Electrical Power & Energy Systems*, vol. 98, pp. 209–218, Jun. 2018.

[20] Y.-Y. Chen, Y.-H. Lin, C.-C. Kung, M.-H. Chung, and I.-H. Yen, "Design and Implementation of Cloud Analytics-Assisted Smart Power Meters Considering Advanced Artificial

Intelligence as Edge Analytics in Demand-Side Management for Smart Homes," *Sensors*, vol. 19, p. 2047, May 2019.

[21] G. C. Swanepoel, "Microgrid energy management system based on artificial intelligence," Thesis, North-West University (South Africa), 2019.

[22] A. Rosato, M. Panella, R. Araneo, and A. Andreotti, "A Neural Network Based Prediction System of Distributed Generation for the Management of Microgrids," *IEEE Transactions on Industry Applications*, vol. 55, no. 6, pp. 7092–7102, Nov. 2019.

[23] Z. A. Vale, P. Faria, H. Morais, H. M. Khodr, M. Silva, and P. Kadar, "Scheduling distributed energy resources in an isolated grid — An artificial neural network approach," in *IEEE PES General Meeting*, Jul. 2010, pp. 1–7.

[24] S. X. Chen, H. B. Gooi, and M. Q. Wang, "Sizing of Energy Storage for Microgrids," *IEEE Transactions on Smart Grid*, vol. 3, no. 1, pp. 142–151, Mar. 2012.

[25] F. Alkhateeb, E. A. Maghayreh, and S. Aljawarneh, "A Multi Agent-Based System for Securing University Campus: Design and Architecture," in *Modelling and Simulation 2010 International Conference on Intelligent Systems*, Jan. 2010, pp. 75–79.

[26] R. Leo, K. Appaswamy, J. Vengatraman, and A. A. Morais, "Advanced energy management in virtual power plant using multi agent system," Mar. 2016, pp. 133–138.

[27] L. Oneto, F. Laureri, M. Robba, F. Delfino, and D. Anguita, "Data-Driven Photovoltaic Power Production Nowcasting and Forecasting for Polygeneration Microgrids," *IEEE Systems Journal*, vol. 12, no. 3, pp. 2842–2853, Sep. 2018.

[28] M. Pyne and S. Yurkovich, "Data driven modeling and simulation for energy storage systems," in *2016 IEEE Conference on Control Applications (CCA)*, Sep. 2016, pp. 1306–1311.

[29] J. Queiroz, P. Leitão, and A. Dias, "Predictive data analysis driven multi-agent system approach for electrical micro grids management," in *2016 IEEE 25th International Symposium on Industrial Electronics (ISIE)*, Jun. 2016, pp. 738–743.

[30] A. E. Thanos, M. Bastani, N. Celik, and C. Chen, "Dynamic Data Driven Adaptive Simulation Framework for Automated Control in Microgrids," *IEEE Transactions on Smart Grid*, vol. 8, no. 1, pp. 209–218, Jan. 2017.

[31] "NRS 034-1:2007," NRS, Standards 034-1:2007.

[32] SABS, "SANS 60076-1:2011," National Committee SABS, Standards, 2011.

[33] "Municipalities – Aberdare Cables."

[34] R. A. Serway, "Current and Direct Current Circuits," in *Principles of Physics*. New York, Fort Worth: Saunders College, 1998, p. 602.

[35] SABS, "SANS 1019:2014 (Ed. 2.06)," Mar. 2019.

[36] "Standard Mini Substations," https://www.actomep.co.za/standard-mini-substations.

[37] G. T. Meaden, *Electrical Resistance of Metals*. Springer, Dec. 2013.

[38] C. T. Gaunt and R. HERMAN, "VOLTAGE PROFILES ON LV RESIDENTIAL FEEDERS WITH PVEG USING A PRACTICAL, PROBABILISTIC APPROACH," p. 5, 2015.

[39] E. Namanya, "Voltage Calculation on Low Voltage Feeders with distributed generation," p. 168.

[40] I. K. Nti, M. Teimeh, O. Nyarko-Boateng, and A. F. Adekoya, "Electricity load forecasting: A systematic review," *Journal of Electrical Systems and Information Technology*, vol. 7, no. 1, p. 13, Dec. 2020.

[41] F. A. Viawan, "Steady State Operation and Control of Power Distribution Systems in the Presence of Distributed Generation," p. 185.

[42] R. Tonkoski, D. Turcotte, and T. H. M. EL-Fouly, "Impact of High PV Penetration on Voltage Profiles in Residential Neighborhoods," *IEEE Transactions on Sustainable Energy*, vol. 3, no. 3, pp. 518–527, Jul. 2012.

[43] S. P. Borg and N. Kelly, "The effect of appliance energy efficiency improvements on domestic electric loads in European households," *Energy and Buildings*, vol. 43, pp. 2240–2250, Sep. 2011.

[44] W. Heffernan, N. Watson, R. Buehler, and J. Watson, "Harmonic performance of heat-pumps," *The Journal of Engineering*, vol. 2013, no. 9, pp. 31–44, Sep. 2013.

[45] R. C. Bansal and A. F. Zobaa, *Handbook of Renewable Energy Technology & Systems*. WORLD SCIENTIFIC (EUROPE), Sep. 2021.

[46] "Active Power Injection - an overview — ScienceDirect Topics," https://www.sciencedirect.com/topics/engineering/active-power-injection.

[47] S. Heunis and M. Dekenah, "A load profile prediction model for residential consumers in South Africa," in *Twenty-Second Domestic Use of Energy*, Apr. 2014, pp. 1–6.

[48] I. A. Metwally, A. H. Al-Badi, and A. S. Al Farsi, "Factors influencing ampacity and temperature of underground power cables," *Electrical Engineering*, vol. 95, no. 4, pp. 383–392, Dec. 2013.

[49] A. Giannitrapani, S. Paoletti, A. Vicino, and D. Zarrilli, "Optimal Allocation of Energy Storage Systems for Voltage Control in LV Distribution Networks," *IEEE Transactions on Smart Grid*, vol. 8, no. 6, pp. 2859–2870, Nov. 2017.

Appendices

Appendix A

Implementation data and MATLAB® code used in this study

The data, simulation models and results folders of this study can be obtained from the various links listed below:

- Data processing code: This folder contains the data processing algorithms used to convert the raw obtained from the online microgrid monitoring platform into data usable in the MATLAB Simulink® model.
- Simulation data: This folder contains the processed data utilised in the MATLAB Simulink® model to generate the obtained results. The data represents different environmental conditions and daily load profiles to generate dispersion and stochastic conditions.
- Simulation models: This folder contains MATLAB Simulink® models of the different renewable energy implementation tests ranging from models without any form of control to models with ESS implemented and full aggregated control for maximum safe renewable energy penetration.
- Data processing code: The test results of the different models can be found in this folder. The results consist of balanced and unbalanced tests in ideal and cloudy weather conditions. The test results indicate the effects of the aforementioned conditions at renewable energy penetration levels ranging from 25% to 75%. The data also includes the results generated at each node on the feeder during the respective tests.

Appendix B

Additonal test for chapter 6

The contents of chapter 6 exhibited the results of the fundamental tests carried out on the different control structures. The data in this appendix shows how the control structures react to additional disturbances and unfavourable scenarios. The initial test is the reference test without any control implemented on the PV system.

B.1 Renewable energy without control

The additional tests consist of two variations. The first test is to evaluate the effects of cloudy weather on the control scheme. The second test is to assess the impact of maximum feeder unbalance on the control structure.

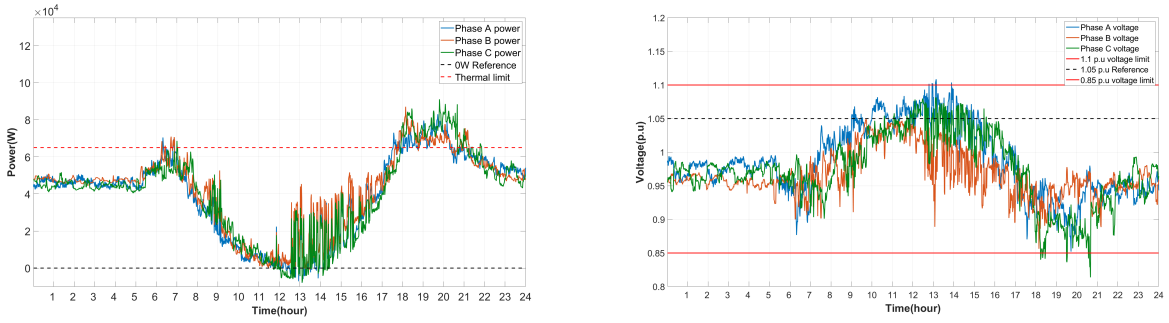

(a) (b)

Figure B.1: Power(a) and voltage(b) profile in cloudy weather conditions at 25% renewable energy penetration

The initial test at 25% renewable energy penetration level indicates that the cloudy weather

affects the power surety. This causes the collective power on the feeder to oscillate as the clouds pass over the neighbourhood. The oscillation in power dictates a corresponding fluctuation in voltage on the feeder. The feeder's balance is still maintained because the units are situated close to one another geologically and almost simultaneously affected by the cloudy weather. The network parameters are not violated unnaturally at the 25% renewable energy penetration level. The increase in renewable energy has a direct relation to network instability.

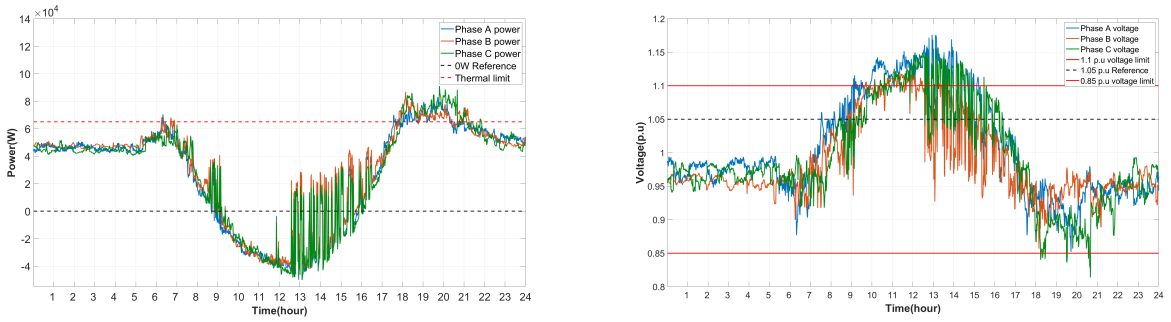

(a) (b)

Figure B.2: Power(a) and voltage(b) profile in cloudy weather conditions at 50% renewable energy penetration

The cloudy weather results at the 50% renewable energy penetration level indicate that the power and voltage profiles follow the same basic trajectory as the ideal profiles in chapter 6. The only difference is the oscillation induced by the variation in irradiance. Further than that, the upper and lower voltage limits are violated on both the ideal test and the cloudy weather test at the same positions.

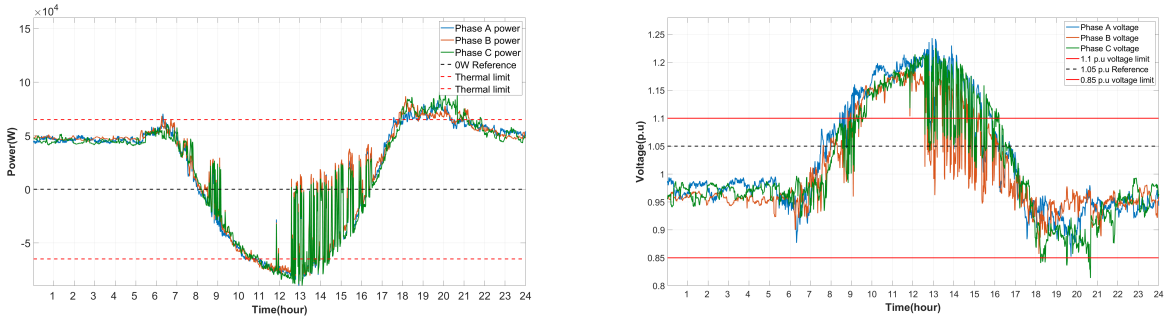

(a) (b)

Figure B.3: Power(a) and voltage(b) profile in cloudy weather conditions at 75% renewable energy penetration

The cloudy weather test at the 75% renewable energy penetration level exhibit similar char-

acteristics as the 50% test. Both the power and the voltage profiles yield similar results to the ideal test. The results only differ at times of weather condition changes causing the voltage and power uncertainty. The ideal and cloudy weather test violates the voltage and thermal line limits.

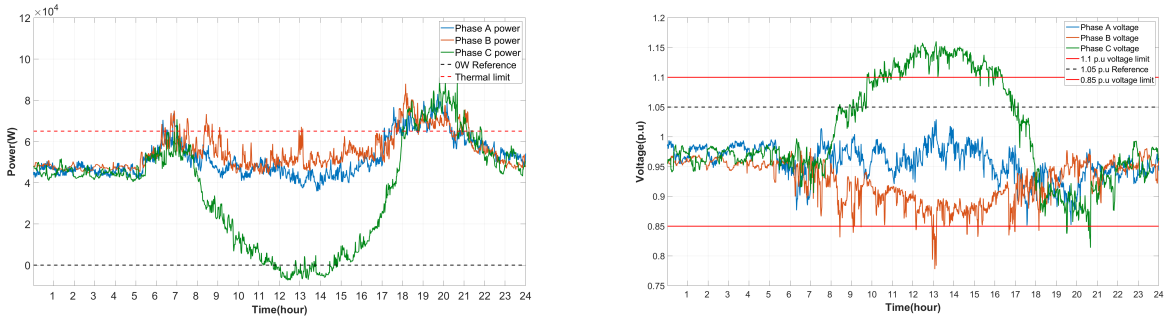

(a) **(b)**

Figure B.4: Power(a) and voltage(b) profile in unbalance test at 25% renewable energy penetration

The unbalance test evaluates the worst-case scenario that the feeder could experience by only exciting the least loaded phase with DG and ESS. The results obtained from the unbalanced test at 25% renewable energy penetration level indicate that as the generation increases during the day, so does the voltage on the excited phase. The unbalance causes the voltage to rise to a higher level than when the generation on the three phases is balanced. The upper voltage limit is exceeded by 5% on the excited phase, while voltage levels on the phase with the highest loading violates the lower voltage limit by 7% due to the maximum unbalance experienced on the feeder.

B.2 NRS regulatory control

The explanation in chapter 6 states that the NRS regulatory control limits the renewable energy penetration by instantaneously disconnecting the inverter from the network when the voltage limit is exceeded at that node.

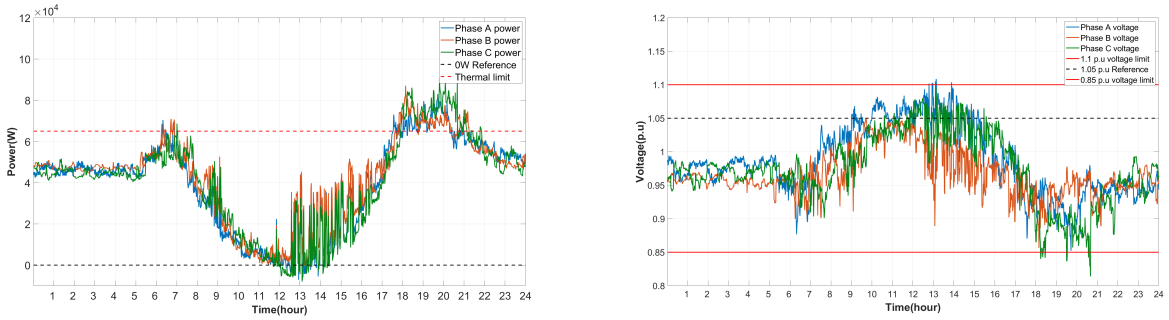

(a) (b)

Figure B.5: Power(a) and voltage(b) profile in cloudy weather conditions at 25% renewable energy penetration

The 25% renewable energy penetration test under cloudy weather conditions yield the same results as in the test without any control due to the voltage curve remaining below the upper bounds of the voltage limit at all times.

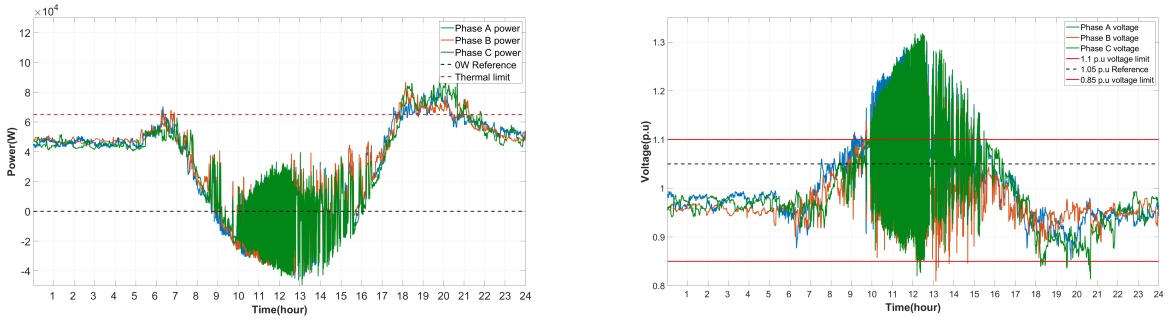

(a) (b)

Figure B.6: Power(a) and voltage(b) profile in cloudy weather conditions at 50% renewable energy penetration

Under the NRS regulatory control, the cloudy weather test indicates that both the power and voltage curves oscillate violently due to the DG disconnecting from and then reconnecting to the network and the irradiance fluctuation causing the power to fluctuate. The power fluctuation caused by the irradiation variance has a diminishing effect on the volatile fluctuations due to the clouds reducing the power output, which leads to the voltage dropping below the upper voltage level for extended periods of time. This leads to fewer oscillations. The oscillations cause the voltage to exceed the upper voltage limit by 20%.

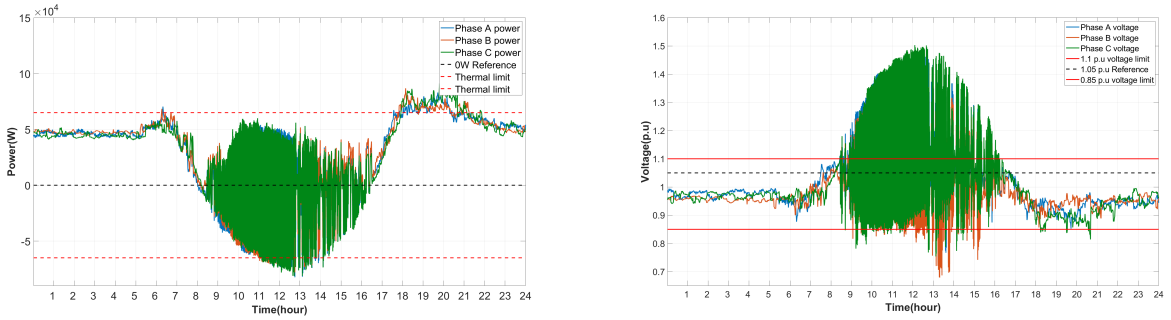

(a) (b)

Figure B.7: Power(a) and voltage(b) profile in cloudy weather conditions at 75% renewable energy penetration

The 75% renewable energy penetration test under cloudy weather conditions is similar to the same test data at 50% renewable energy penetration. The only difference is that the power curve exceeds both the positive and negative thermal line limit and the voltage level during times of maximum generation exceeds both the upper and lower voltage limit. The upper voltage limit is exceeded with 50%, and the lower voltage limit is exceeded with 17%.

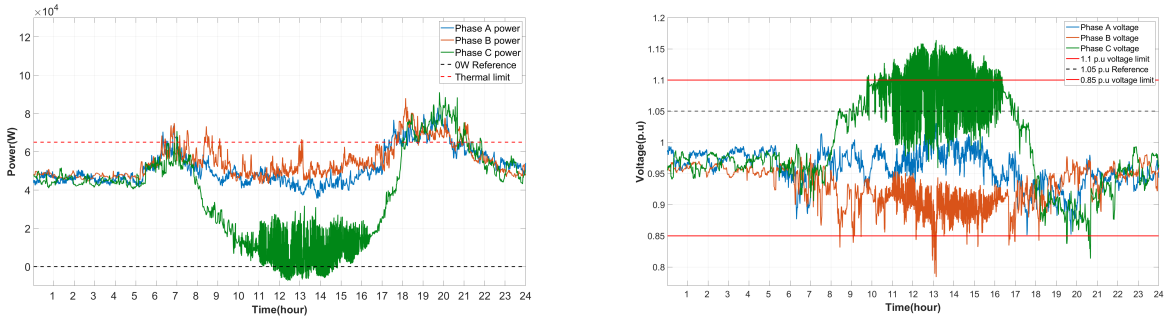

(a) (b)

Figure B.8: Power(a) and voltage(b) profile in unbalance test at 25% renewable energy penetration

The maximum unbalance at 25% renewable energy penetration level induces oscillations on the power profile of the excited phase. This is due to the voltage level of the excited phase exceeding the upper voltage limit at times of maximum generation, which causes the control to activate and disconnect the inverters. This disconnection causes the voltage to drop due to a decrease in generation. The reconnection causes the voltage to rise as a result of the increase in generation. The power curve indicates that only the phase with generation present oscillates violently while the other power profiles remain unscathed. However, the oscillation

in voltage on one phase causes a voltage oscillation on the other phases due to unbalance between the phases. Notably, the effective loading at maximum generation determines which phase is most affected by the oscillation.

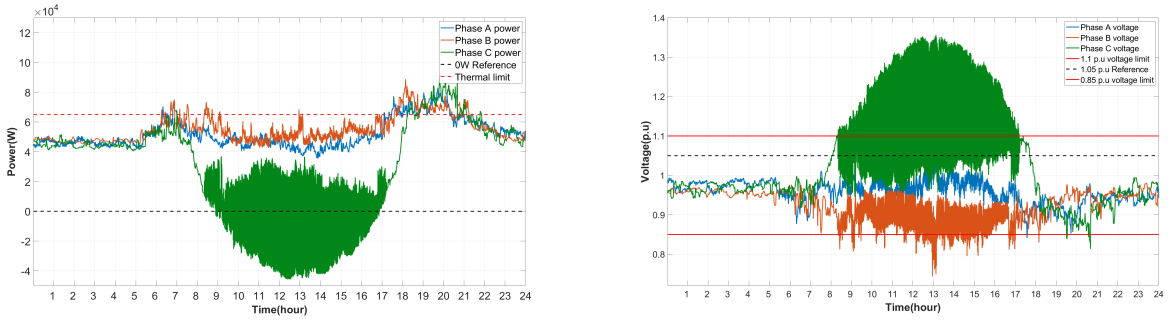

(a) **(b)**

Figure B.9: Power(a) and voltage(b) profile in unbalance test at 50% renewable energy penetration

The unbalanced results at a renewable energy penetration level of 50% indicate a similar pattern to the 25% unbalance test. The only difference is that the oscillation amplitude is higher due to the renewable energy penetration increase. The upper voltage limit is violated with 25%.

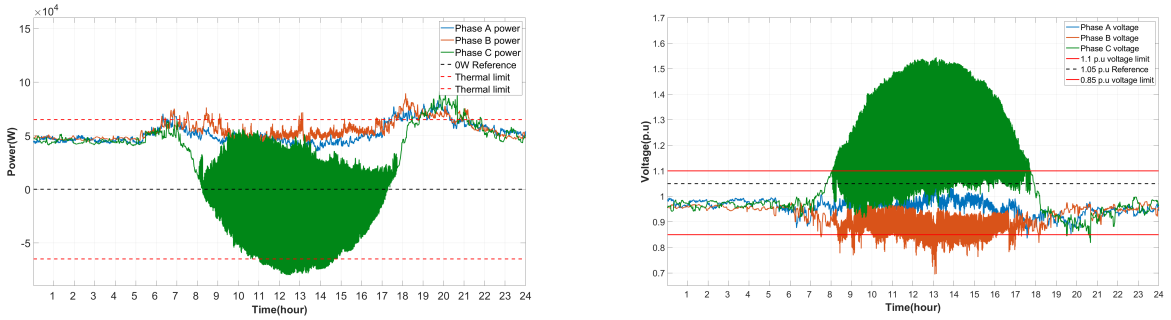

(a) **(b)**

Figure B.10: Power(a) and voltage(b) profile in unbalance test at 75% renewable energy penetration

The unbalanced results at 50% renewable energy penetration indicate a similar pattern to the 25% and the 50% renewable energy penetration unbalance test. The only difference is that the oscillation amplitude is higher due to the renewable energy penetration increase. The upper voltage limit is violated with 45%.

B.3 Future NRS regulatory control

AS previously stated, the future NRS regulatory control structure is an extension of the current NRS regulatory control structure. The future NRS Regulatory control differs from its predecessors in the sense that it ramps up the generation at a tempo of 10% of maximum capacity every minute to gradually re-introduce the generation to not increase instability on the grid.

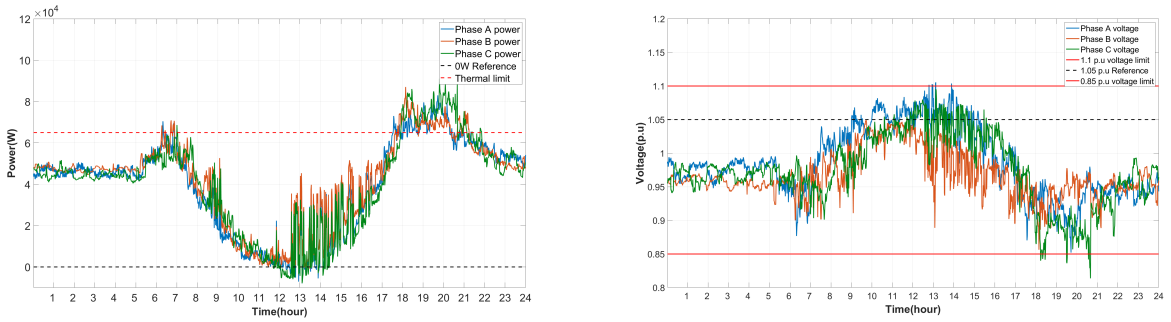

(a) (b)

Figure B.11: Power(a) and voltage(b) profile in cloudy weather conditions at 25% renewable energy penetration

The performance of the Future NRS regulatory controller under cloudy weather conditions yields the same results as all the previous tests conducted since none of the voltage parameters is violated. Both the voltage and power profiles are within acceptable limits.

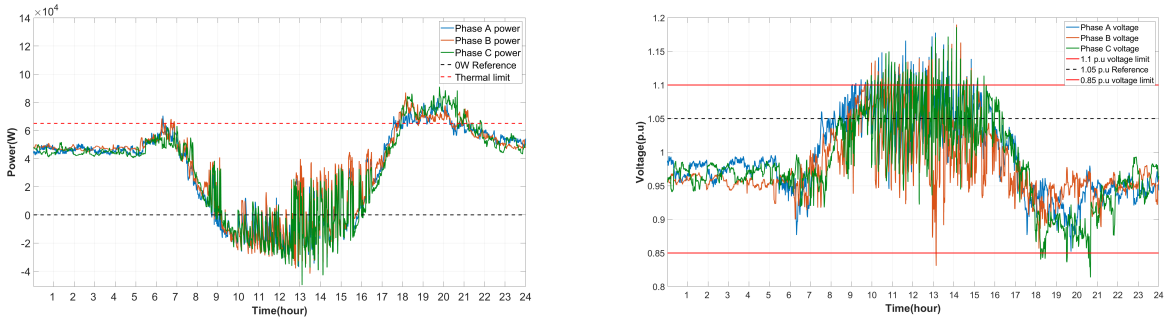

(a) (b)

Figure B.12: Power(a) and voltage(b) profile in cloudy weather conditions at 50% renewable energy penetration

The performance under cloudy weather conditions at a renewable energy penetration level of 50% is better when compared to the same test with the NRS Regulatory control. The

voltage and power oscillation frequency are lower than in previous trials, with higher energy stability caused by the soft-start implementation. It is constently evident that the oscillations are further reduced during times of alternating irradiance.

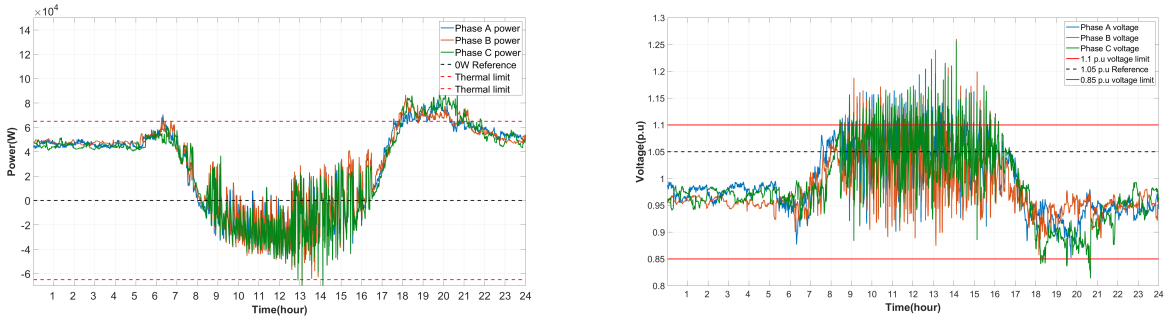

(a) (b)

Figure B.13: Power(a) and voltage(b) profile in cloudy weather conditions at 75% renewable energy penetration

The 75% renewable energy penetration naturally yields a higher power oscillation frequency. Still, the current control implementation reduces the frequency of voltage violations compared to the NRS test without the soft starter method. The voltage limit violations still occur, but more violations remain within the delay time before becoming an issue.

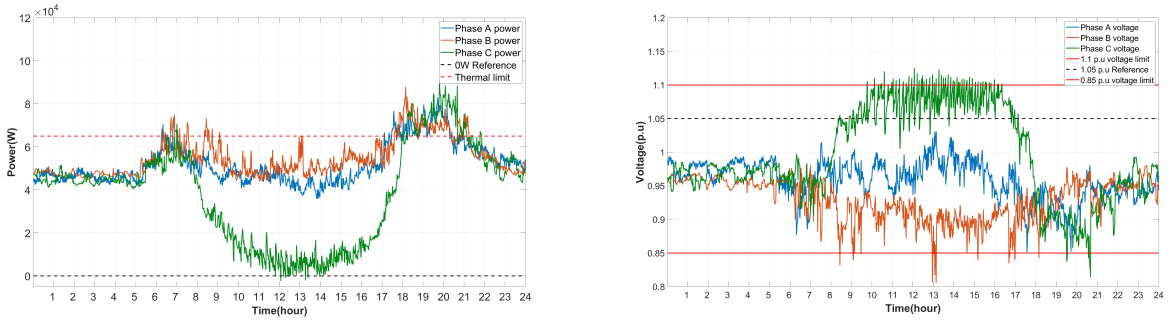

(a) (b)

Figure B.14: Power(a) and voltage(b) profile in unbalance test at 25% renewable energy penetration

The soft starter's true effect on the NRS regulatory control can be witnessed on the unbalance test starting at the 25% renewable energy penetration level. The power and voltage profiles indicate that the unbalance causes the voltage level to rise at a steeper angle than before, resulting in the upper voltage limit violation occurring significantly earlier than expected. This results in the power curve not deviating as far as it normally would in the test without

PV control. The voltage upper limit violation is notably reduced compared to the previous unbalance test at 25% renewable energy penetration.

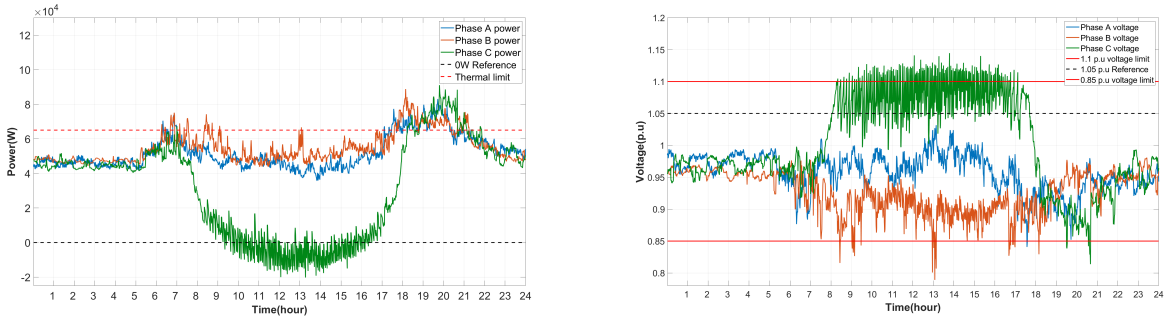

(a) **(b)**

Figure B.15: Power(a) and voltage(b) profile in unbalance test at 50% renewable energy penetration

The power and voltage profile indicates that the frequency of oscillation induced by the control has increased as the renewable energy penetration increased from 25% to 50%. However, the voltage violations remain within the required time limit even though the voltage level violates the limit. This all occurs at a higher renewable energy penetration level where it is notable from the power curve that the unbalanced phase minima are lower than the 25% renewable energy penetration test.

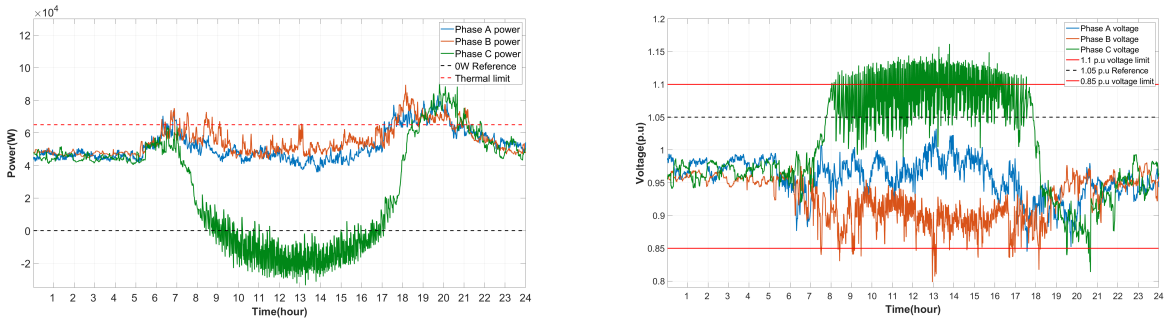

(a) **(b)**

Figure B.16: Power(a) and voltage(b) profile in unbalance test at 75% renewable energy penetration

Comparing results between the 50% and 75% unbalanced renewable energy penetration yields few different results. The voltage and power profiles all look similar, with minor differences in the oscillation frequency.

B.4 Active voltage regulation

The active voltage regulation, as previously stated, works on a voltage power curve to determine the energy output. The energy output, in turn, regulates the voltage level.

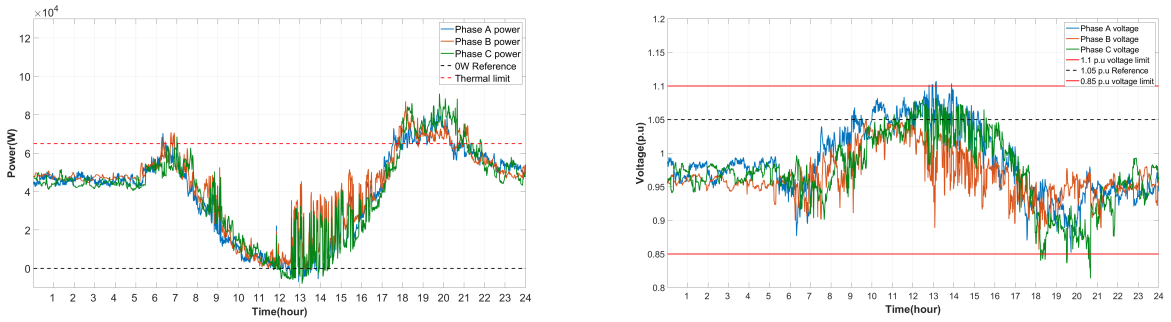

(a) (b)

Figure B.17: Power(a) and voltage(b) profile in cloudy weather conditions at 25% renewable energy penetration

Once again, the active voltage regulation control at 25% renewable energy penetration level in a cloudy weather environment yields the same result as the other test with the same conditions. This is due to the fact that no perimeters on the voltage profile have been violated.

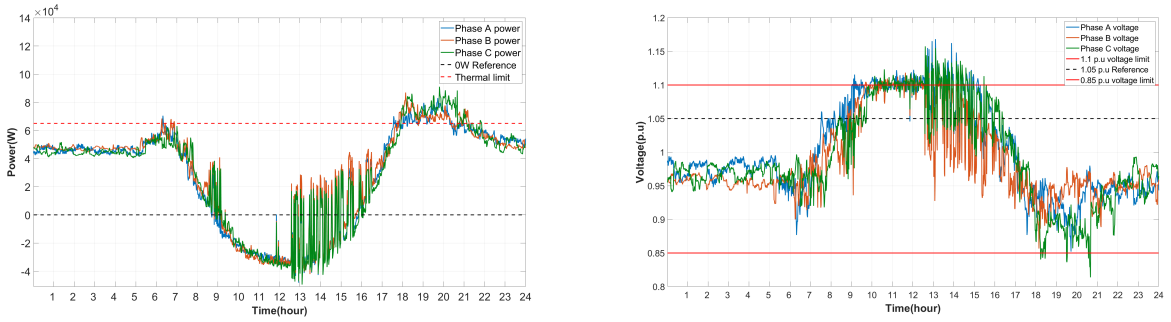

(a) (b)

Figure B.18: Power(a) and voltage(b) profile in cloudy weather conditions at 50% renewable energy penetration

The power and voltage curve show favourable results in the early morning hours due to the predictability of the DG production curve. As the afternoon period is reached, the variation in irradiance induces a hunting phenomenon due to the sudden changes.

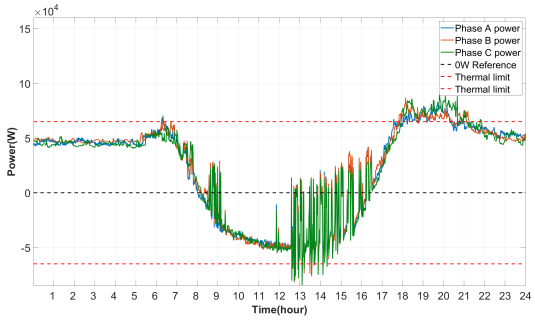

(a)

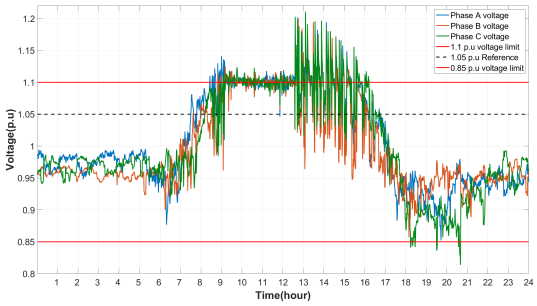

(b)

Figure B.19: Power(a) and voltage(b) profile in cloudy weather conditions at 75% renewable energy penetration

The cloudy weather test data at 75% renewable energy penetration indicates that the control algorithm reacts precisely like the 50% test. The only difference is that the oscillations in cloudy weather have a higher amplitude. On the power curve, the absolute minima violate the negative thermal line limits.

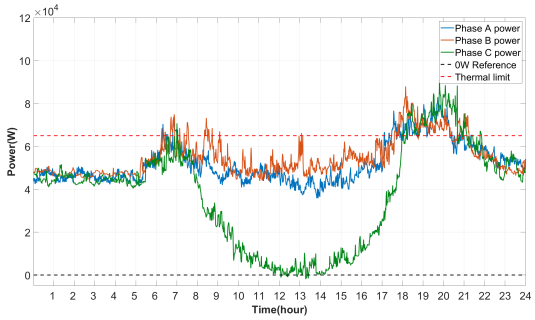

(a)

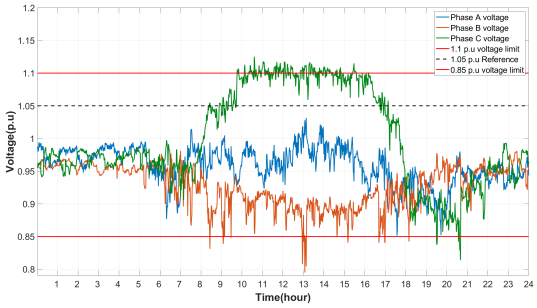

(b)

Figure B.20: Power(a) and voltage(b) profile in unbalance test at 25% renewable energy penetration

The worst-case unbalance at 25% indicates that the active voltage regulation technique regulates the power on the excited phase to regulate the voltage on said phase to remain within limits. The voltage of the excited phase oscillates around the upper voltage limits remaining within the time limit.

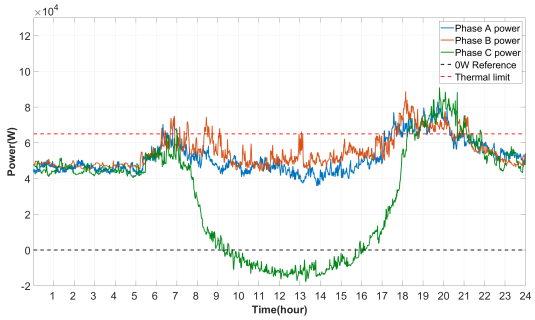

(a)

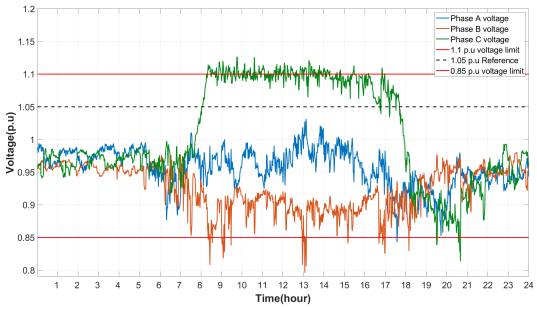

(b)

Figure B.21: Power(a) and voltage(b) profile in unbalance test at 50% renewable energy penetration

The 25% renewable energy penetration increase sees the power curve minima drop to below the 0W reference line while the voltage of the excited phase remains at the upper voltage limit. The voltage level of the unexcited phase with the highest loading exhibits an even lower voltage level than before due to the renewable energy penetration level.

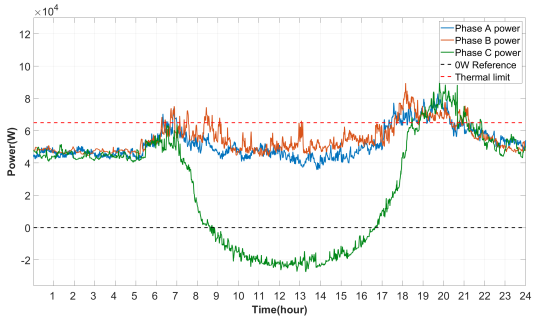

(a)

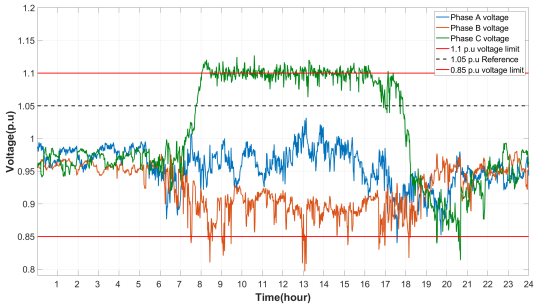

(b)

Figure B.22: Power(a) and voltage(b) profile in unbalance test at 75% renewable energy penetration

The active voltage regulation controller shows how efficient it can be without the help of any form of ESS. The effectiveness of control is evident at the 75% renewable energy penetration test due to the consistency between the 50% and the 75% renewable energy penetration test in unbalanced conditions. The data indicate that the control is effective for different renewable energy penetration levels.

B.5 Local control

The implementation of ESS and a localized control structure already brings more power stability with the capability of storing excess energy to utilize at a later stage. This is evident in the results in chapter 6.

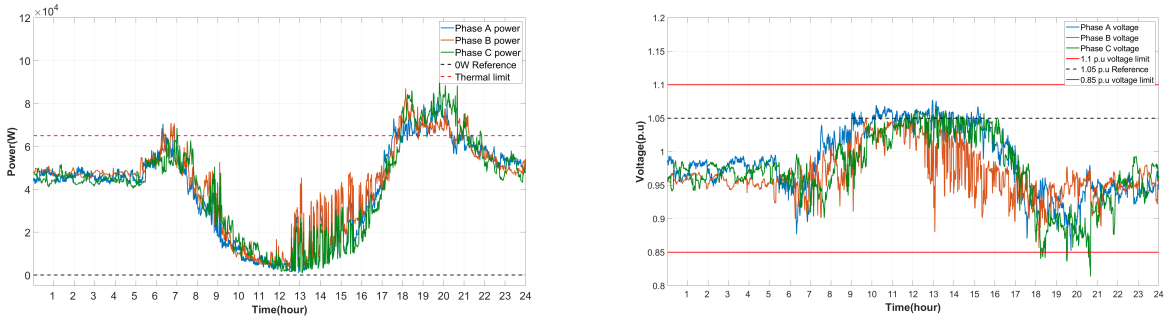

(a) (b)

Figure B.23: Power(a) and voltage(b) profile in cloudy weather conditions at 25% renewable energy penetration

The data in the power profile of the 25% cloudy weather test with local control indicates that the minima are situated above the 0 W reference line. This is due to the excess generation stored in an ESS at the relevant nodes. The energy storage is also evident in the voltage profile, with the maximum voltage oscillating around 1.05 p.u. mark and the lower voltage limit only exceeded at times of maximum loading on the feeder.

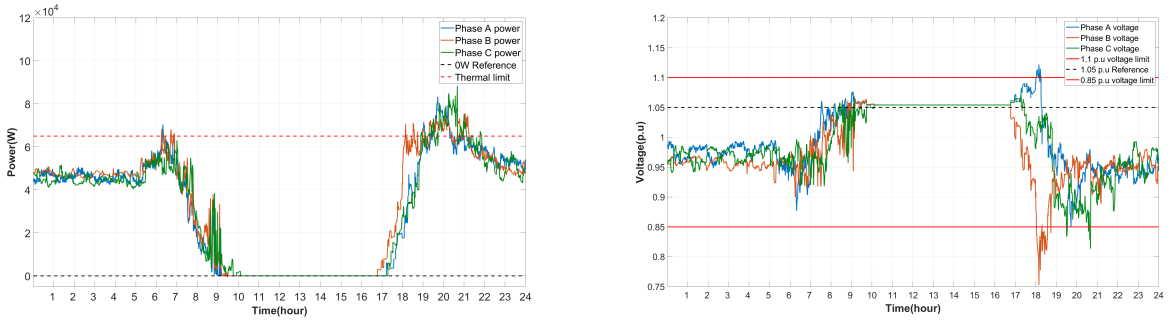

(a) (b)

Figure B.24: Power(a) and voltage(b) profile in cloudy weather conditions at 50% renewable energy penetration

The cloudy weather test at a 50% renewable energy penetration level exhibits the true potential of storage implementation that both the power and voltage can be controlled extremely

accurately if the storage level is above the minimum SOC. The voltage unbalance at high loads is induced by the difference in relative loads and SOC levels.

(a)

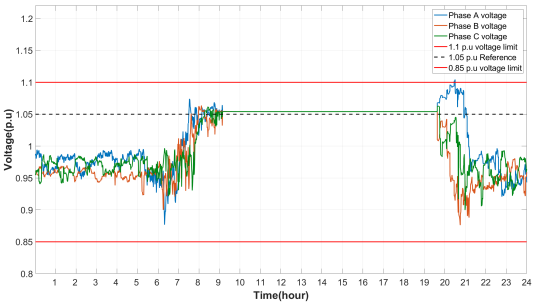

(b)

Figure B.25: Power(a) and voltage(b) profile in cloudy weather conditions at 75% renewable energy penetration

The increase in renewable energy penetration level from 50% to 75% diminishes the effect of cloudy weather on the feeder voltage and power security. The ESS absorbs all the excess energy and discharges it at times of no DG. The voltage level remains within the regulatory limits at all times.

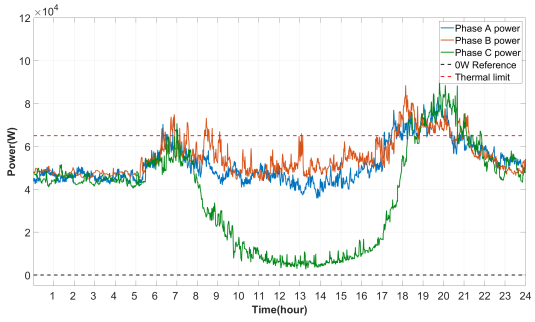

(a)

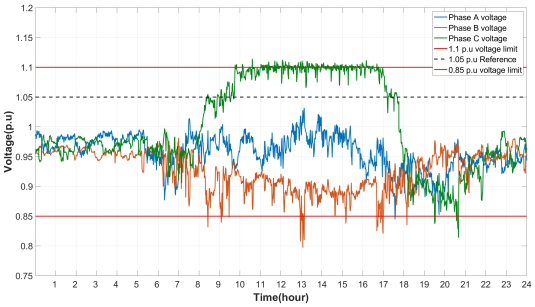

(b)

Figure B.26: Power(a) and voltage(b) profile in unbalance test at 25% renewable energy penetration

The unbalance test on the local control algorithm at a 25% renewable energy penetration level indicates that the voltage regulation control works as intended by keeping the voltage level within the upper and lower boundaries. The control attempts to maintain all voltage levels within the regulatory limits at all times.

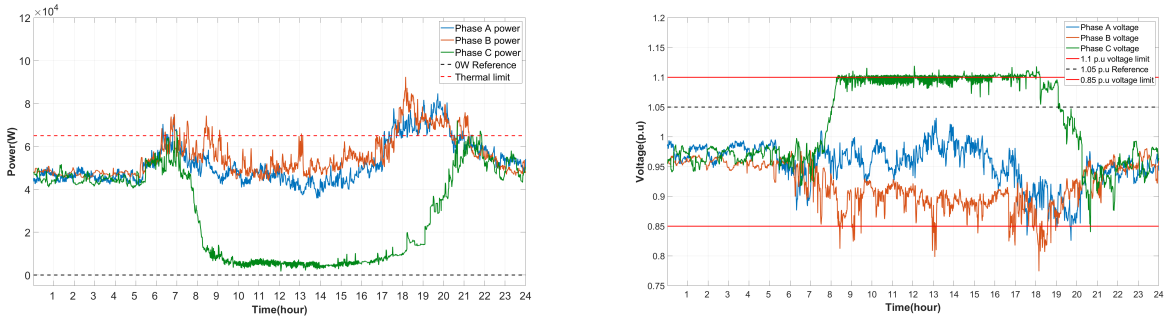

(a) (b)

Figure B.27: Power(a) and voltage(b) profile in unbalance test at 50% renewable energy penetration

The 50% renewable energy penetration unbalance test on the local control also indicates that the local controller can efficiently regulate the voltage to remain within the voltage limits. The only difference between the 25% test and the 50% test is that the upper voltage on the 50% test has a trip frequency, but the voltage remains within limits at all times.

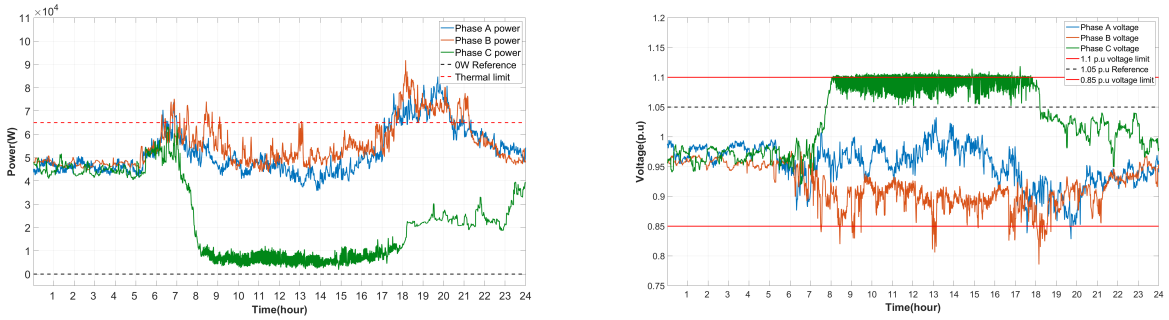

(a) (b)

Figure B.28: Power(a) and voltage(b) profile in unbalance conditions at 75% renewable energy penetration

The unbalance test with the local control structure yields the same basic results regardless of renewable energy penetration. This is confirmed by comparing the voltage and power profile at the 75% renewable energy penetration level with the previous tests. The results indicate that the general profile is the same, with the difference evident in the oscillation amplitude when the voltage level reaches the upper voltage limit.

B.6 Virtual power plant

The VPP control implementation mixes a range of control structures for voltage regulation, peak shaving, and optimal energy distribution.

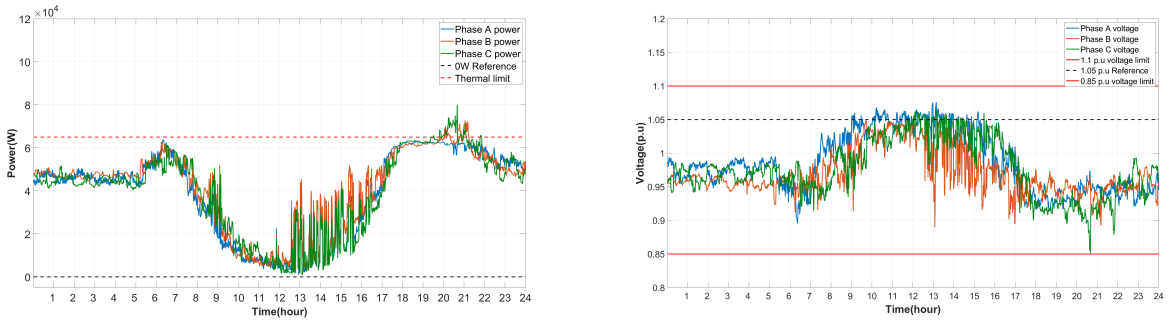

(a) (b)

Figure B.29: Power(a) and voltage(b) profile in cloudy weather conditions at 25% renewable energy penetration

The 25% renewable energy penetration cloudy weather test with a VPP controller yields similar results to the local control algorithm. However, the difference is that the VPP implements peak shaving to lower the strain on the network at times of high demand and fully maintains the voltage within the regulatory limits.

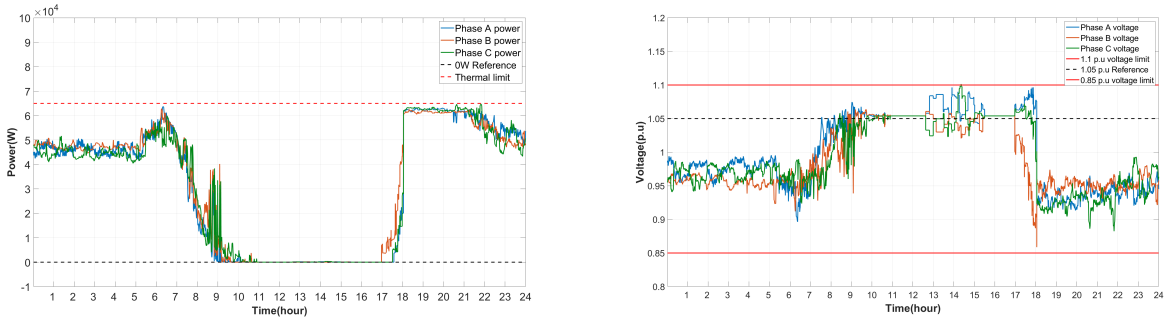

(a) (b)

Figure B.30: Power(a) and voltage(b) profile in cloudy weather conditions at 50% renewable energy penetration

The cloudy weather test at 50% renewable energy penetration yields better results due to the increased effect of storage as a result of the excess generation. While the voltage is regulated to remain within limits, nodes share energy to optimise energy utilization.

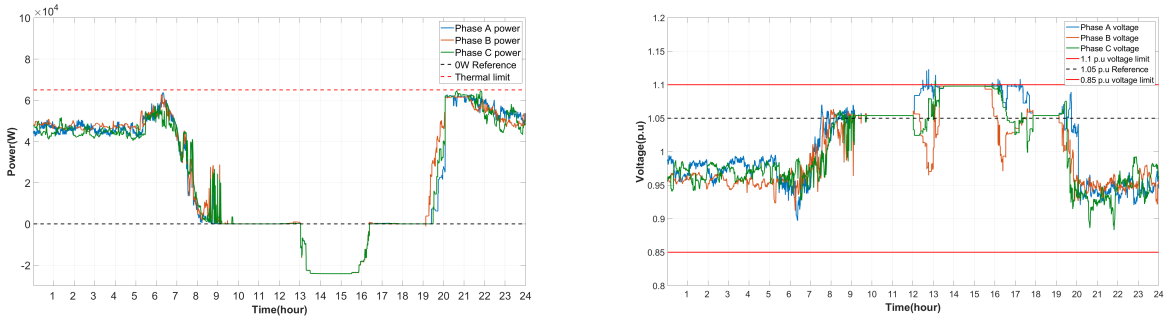

(a) (b)

Figure B.31: Power(a) and voltage(b) profile in cloudy weather conditions at 75% renewable energy penetration

The cloudy weather test at 75% renewable energy penetration denotes that there is enough energy available to service all loads on the feeder with an energy share algorithm and also feed the additional energy into the MV grid in a balanced fashion while remaining within the voltage limits.

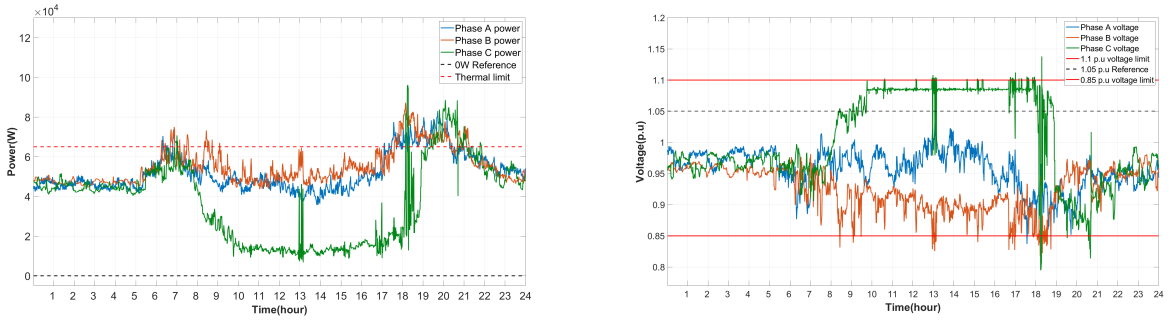

(a) (b)

Figure B.32: Power(a) and voltage(b) profile in unbalance conditions at 25% renewable energy penetration

The VPP controller is developed to be extra sensitive to voltage disturbances. If a voltage disturbance is detected, the controller adjusts the power to compensate for the disturbance. The 25% renewable energy penetration test with maximum unbalance indicates that the power is regulated in such a manner that the voltage remains within both the lower and upper voltage limits. A significant change in the exited phase's power is evident if one of the other phases violate any of the critical parameters.

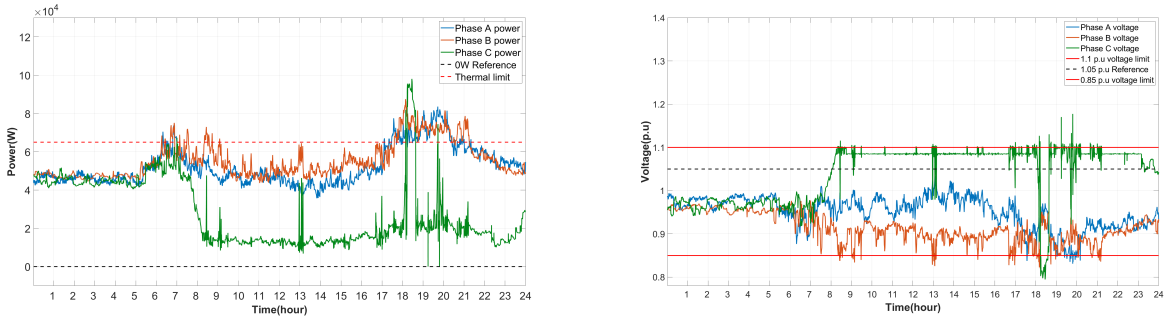

(a) (b)

Figure B.33: Power(a) and Voltage(b) profile in unbalance conditions at 50% renewable energy penetration

The unbalance test at 50% renewable energy penetration shows that the VPP controller has to better manage the energy with the larger amount of energy generated. The energy also lasts longer due to the larger batteries, which means the unbalance continues for extended periods. The controller violates the lower voltage limit with the excited phase in order to avoid the other two phases violating the voltage limits.

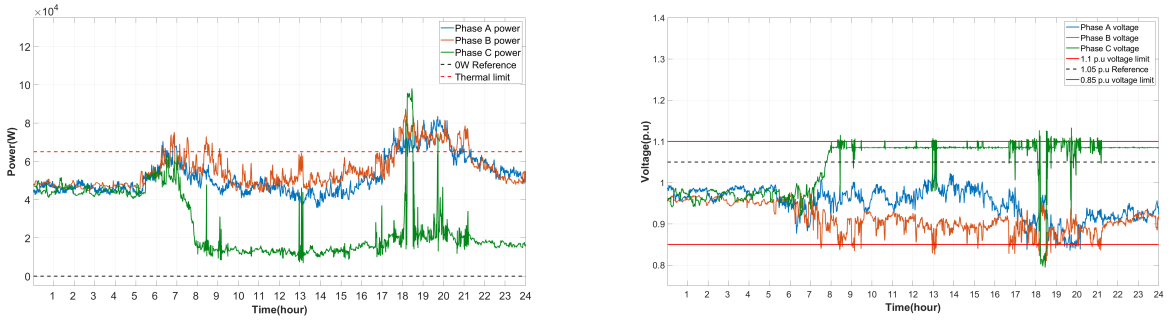

(a) (b)

Figure B.34: Power(a) and voltage(b) profile in unbalance conditions at 75% renewable energy penetration

The 75% renewable energy penetration level unbalance test exhibits similar results to the 50% renewable energy test. The only difference is that the controlled unbalance continues for longer than with the 50% renewable energy penetration test due to the loads remaining the same and the ESS capacity being increased.

B.7 Chapter 7 additional test

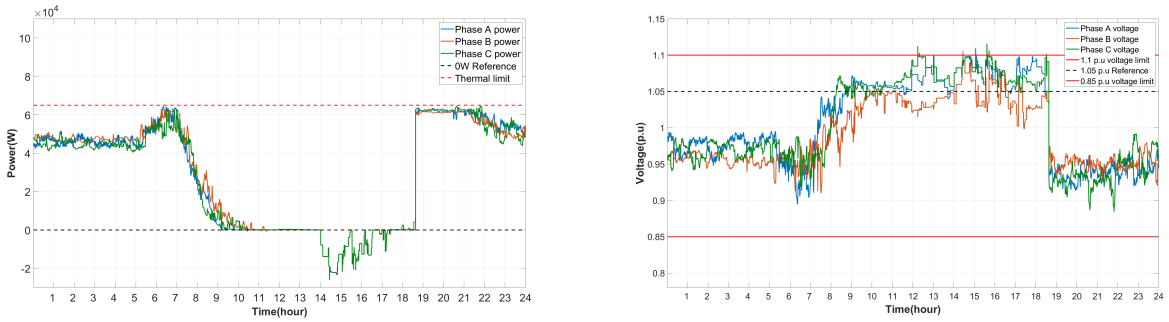

(a) (b)

Figure B.35: Power(a) and voltage(b) profile with randomised solar implementation

The controlled tests all indicate that the VPP control algorithm can manage energy flow efficiently irrespective of the conditions of the network. To prove that the controller is robust and can serve as a generic solution to increase the renewable energy penetration regardless of external factors, the VPP is exposed to the reference network with random storage and generation capacity on each node. The results indicate that the controller manages the energy efficiently while remaining within the voltage limits throughout the entire test. The maximum available energy is fed back into the network when the ESS reaches the set limit.